Pacific Northwest
NATIONAL LABORATORY

PNNL-35503, Rev. 0
EWG-RPT-044, Rev. 0

Direct Feed High-Level Waste APPS Model Glass Testing (DFHLW APPS) Matrix

June 2024

V Gervasio, X Lu, JT Reiser, M Peterson, NL Canfield, JB Lang, JC Rigby, JL George, DA Cutforth, JM Westman, R Brown, JM Oshiro, BT Boehnke, EA Cordova, JV Crum, NA Lumetta, JD Vienna

Pacific Northwest National Laboratory
Richland, Washington 99354

JW Amoroso, M Page, N Rod, MC Hsieh

Savannah River National Laboratory
Aiken, South Carolina 29808

U.S. DEPARTMENT OF ENERGY

Prepared for the U.S. Department of Energy
under Contract DE-AC05-76RL01830

DISCLAIMER

PACIFIC NORTHWEST NATIONAL LABORATORY
operated by
BATTELLE
for the
UNITED STATES DEPARTMENT OF ENERGY
under Contract DE-AC05-76RL01830

Printed in the United States of America

Available to DOE and DOE contractors from
the Office of Scientific and Technical Information,
P.O. Box 62, Oak Ridge, TN 37831-0062
www.osti.gov
ph: (865) 576-8401
fox: (865) 576-5728
email: reports@osti.gov

Available to the public from the National Technical Information Service
5301 Shawnee Rd., Alexandria, VA 22312
ph: (800) 553-NTIS (6847)
or (703) 605-6000
email: info@ntis.gov
Online ordering: http://www.ntis.gov

PNNL-35503, Rev. 0
EWG-RPT-044, Rev. 0

Direct Feed High-Level Waste APPS Model Glass Testing (DFHLW APPS) Matrix

June 2024

V Gervasio, X Lu, JT Reiser, M Peterson, NL Canfield, JB Lang, JC Rigby, JL George, DA Cutforth, JM Westman, R Brown, JM Oshiro, BT Boehnke, EA Cordova, JV Crum, NA Lumetta, JD Vienna

Pacific Northwest National Laboratory
Richland, Washington 99354

JW Amoroso, M Page, N Rod, MC Hsieh

Savannah River National Laboratory
Aiken, South Carolina 29808

Prepared for
the U.S. Department of Energy
under Contract DE-AC05-76RL01830

Summary

This report summarizes the data collected during the batching and melting of the Direct Feed High-Level Waste APPS Model Glass Matrix (DFHLW APPS) to serve as a quality-assured validation of the Aspen Process Performance Simulation (APPS) formulation method. Of 15 glasses tested, 12 satisfied all target property constraints. Two glasses, APPS-05 and -06, formed nepheline on canister centerline cooling heat-treatment and failed the Product Consistency Test response limits. Eight glasses failed the K-3 neck corrosion constraint. Glasses APPS-05 and 07-2 formed borderline high concentrations of phosphate crystals ($NaCaPO_4$ and $Na_3Nd(PO_4)_2$, respectively) when heat treated at 950 °C. All other glasses were found to be satisfactory.

The measured property values were compared to predicted values from a set of current models. In many cases the current models were found to be inadequate for design of DFHLW glasses. These models are being adjusted to correct for mispredictions. Other models, e.g., density, toxicity characteristic leaching procedure, and sulfur solubility, are adequate for formulation of DFHLW glasses.

Acknowledgments

The authors gratefully acknowledge the financial support provided by the U.S. Department of Energy Office of River Protection Waste Treatment and Immobilization Plant Project, with technical oversight by Albert Kruger. The following Pacific Northwest National Laboratory staff members are acknowledged for their contributions: Renee Russell, and Jose Marcial for technical help, David MacPherson for quality assurance, Chrissy Charron, and Cassie Martin for programmatic support during the conduct of this work, Will Eaton for project management, and Matt Wilburn for his editorial. Bechtel National Inc. staff supported glass selection and formulation methods including Bob Hanson, Michaela Trenidad, and John Julyk. We are grateful to Dr. David Kosson, Lisa Brown and Eva Nieto Burelos for collaboration on establishing the TCLP procedure under QA guidelines.

The refractory corrosion data is intended to be used in the development, validation, and implementation of enhanced property/composition models for waste glass vitrification at Hanford. Funding for this work by the U.S. Department of Energy Office of River Protection Waste Treatment & Immobilization Plant Project through Department of Energy Work Authorization M0SRV00101 managed by Albert A. Kruger is gratefully acknowledged.

Acronyms, Abbreviations, and Symbols

APPS	Aspen Process Performance Simulation (WTP steady-state flowsheet model)
ASTM	American Society for Testing Materials
BOF	balance of facilities
BS	blank spike
CaxP	$CaO \times P_2O_5$
CCC	canister centerline cooling
CF	crystal fraction
DFHLW	Direct Feed High-Level Waste
DL	detection limit
DOE	U.S. Department of Energy
DWPF	Defense Waste Processing Facility
EC	electrical conductivity
EDS	energy dispersive spectroscopy
EPMA	electron probe microanalysis
EWG	enhanced waste glass
EWG2	second iteration of enhanced waste glass
FIO	For Information Only
GFC	glass-forming chemical
HF	Hydrofluoric
HLW	high-level waste
HTWOS	Hanford Tank Waste Operations Simulator
ICP-MS	inductive coupled plasma-mass spectroscopy
ICP-OES	inductive coupled plasma-optical emission spectroscopy
INL	Idaho National Laboratory
LAB	WTP Laboratory
LAW	low-activity waste
LIBS	laser-induced breakdown spectroscopy
MS	matrix spike
MV	model validity
NL	normalized loss by 7-day PCT
NQAP	Nuclear Quality Assurance Program
ORP	Office of River Protection
p	probability of nepheline formation
PCT	product consistency test
PIBOD	Process Inputs Basis of Design
PNNL	Pacific Northwest National Laboratory

PT	Pretreatment Facility
Pt/Rh	platinum/rhodium
QC	quality control
r_a	product consistency test normalized element release
RCRA	Resource Conservation, and Recovery Act
RPD	relative percentage difference
SEM	scanning electron microscopy
SSM	sulfur-saturated melt
$T_{2\%}$	temperature at 2 vol% spinel
TCLP	toxicity characteristic leaching procedure
T_M	melting temperature
T_L	liquidus temperature
T_L-Zr	liquidus temperature for zirconium-containing phases
TSCR	Tank Side Cesium Removal
UTS	Universal Treatment Standards
WC	tungsten carbide
WDS	wavelength dispersive spectroscopy
WL	waste loading
wt%	weight percent
w_{SO3}	sulfur solubility
WTP	Waste Treatment and Immobilization Plant
XRD	X-ray diffraction
ε	electrical conductivity
η_{1150}	viscosity at 1150 °C
η_T	viscosity at temperature T
ρ	density
σ	standard deviation

Contents

Summary iii
Acknowledgments iv
Acronyms, Abbreviations, and Symbols v
1.0 Introduction 1.1
1.1 Quality Assurance 1.2
2.0 Test Methods 2.1
2.1 Matrix Design 2.1
2.1.1 Waste Composition Estimates 2.1
2.1.2 Enhanced Waste Glass Formulation Approach 2.2
2.1.3 Waste Composition Selection 2.6
2.1.4 Modification to Formulation Approach 2.7
2.1.5 Recommended Glass Compositions 2.9
2.2 Glass Fabrication 2.12
2.3 X-ray Diffraction and Scanning Electron Microscopy for Secondary Phase Investigation 2.13
2.4 Electron Probe Microanalysis/Wavelength Dispersive Spectroscopy for Chemical Composition Analysis 2.13
2.5 Canister Centerline Cooling 2.14
2.6 Isothermal Crystal Fraction and Liquidus Temperature 2.15
2.7 SO_3 Solubility 2.15
2.8 Density 2.16
2.9 Viscosity 2.17
2.10 Electrical Conductivity 2.17
2.11 Product Consistency Test 2.18
2.12 Toxicity Characteristic Leaching Procedure 2.19
2.13 Corrosion Testing of Refractory 2.20
3.0 Results and Discussion 3.1
3.1 Glass Composition 3.1
3.1.1 Secondary Phase Investigation in Quenched Glasses 3.3
3.2 Crystal Identification in Canister Centerline Cooling Glasses 3.5
3.3 Crystal Fraction and Liquidus Temperature 3.7
3.4 SO_3 Solubility 3.11
3.4.1 SSM SO_3 Concentrations 3.13
3.4.2 Comparisons to Predicted SO_3 Saturation Concentrations 3.15
3.5 Density 3.16
3.6 Viscosity 3.18
3.7 Electrical Conductivity 3.20

3.8 Product Consistency Test 3.23
3.9 Toxicity Characteristic Leaching Procedure 3.26
3.10 Corrosion Testing of Refractory 3.30
3.11 Future Modeling and Formulation Recommendations 3.34
4.0 Conclusions 4.1
5.0 Bibliography 5.1
Appendix A – Distribution of the 154 Glass Compositions A.1
Appendix B – Morphology/Color of Each Quenched Glass B.1
Appendix C – Comparison Measured and Target Chemical Compositions C.1
Appendix D – XRD Patterns of Samples With Crystalline Phases Present D.1
Appendix E – Morphology/Color of Each Glass after Canister Centerline Cooling E.1
Appendix F – Crystal Fraction of Heat-Treated Glasses F.1
Appendix G – Viscosity Data G.1
Appendix H – Electrical Conductivity Data H.1
Appendix I – Waste Compositions I.1

Figures

Figure 2.1. Distribution of non-volatile component concentrations in initial example of DFHLW blended feeds at four different target solids loadings. Mass fraction (mf) of calcined waste component basis. 2.2
Figure 2.2. Graphical representation of glass compositions for 154 DFHLW feed batches. 2.5
Figure 2.3. Within cluster sum of squares distance vs. number of clusters. 2.6
Figure 2.4. Waste loading comparison between EWG and EWG2 formulation approaches. 2.8
Figure 2.5. Comparison of component concentrations between EWG (▽) and EWG2 (△) formulation method for those glass components with significant differences. 2.9
Figure 2.6. Plot of target temperature schedule during CCC treatment. 2.14
Figure 2.7. Dried washed SSM glass powders mounted with epoxy in an aluminum puck for EPMA. 2.16
Figure 2.8. Schematic representation of the static crucible corrosion test configuration. 2.21
Figure 2.9. Schematic of refractory coupon position measurements before (left) and after (right) corrosion testing. 2.22
Figure 3.1. Surface of sample of HLW-APPS-01-1st melt that quenched in contact with the air (left) and platinum crucible wall (right). 3.3
Figure 3.2. SEM micrograph of the bottom (quench plate contact) surface at 4.3 K× magnification (left) and top phase separated region at 3.5 K× magnification (right) of HLW-APPS-07-2 sample. 3.5
Figure 3.3. SEM micrograph of the phase separated region at 4K× magnification (left) and at 9.5 K× magnification (right) of HLW-APPS-07-2 sample. 3.5
Figure 3.4. HLW-APPS-13-1 glass with large crystals after CCC. 3.7
Figure 3.5. HLW-APPS-07-2 SEM of crystal distribution across the sample width. 3.9
Figure 3.6. HLW-APPS-07-2 isothermally heat treated to 1150 °C SEM at 250×, 5K×, and 50K×. 3.10
Figure 3.7. HLW-APPS-07-2 900 °C original image (left) and with EDS locations overlaid (right). 3.10
Figure 3.8. Comparison of SO_3 solubility concentrations determined via ICP-OES and EPMA for select glasses from the first machine learning matrix. Uncertainties are represented by $SD_{pooled,SSM}$ for the ICP-OES data and SD_{EPMA} for the EPMA data. 3.12
Figure 3.9. Summary of historical and present SO_3 solubility procedures 3.13
Figure 3.10. Photos of the three melts (left to right: melts 1, 2, and 3, i.e., the SSM) for HLW-APPS-05 ..... 3.13
Figure 3.11. Measured SO_3 concentration in SSM and quenched glasses for the DFHLW APPS matrix. Uncertainties are represented by SD_{EPMA}. 3.14
Figure 3.12. Measured SO_3 saturation and predicted SO_3 saturation values for HLW-APPS glasses. Open symbols indicate that 3TS offsets were applied to the model for the predicted values. Uncertainties for measured values are represented by $SD_{pooled,SSM}$ 3.16
Figure 3.13. Measured and predicted densities for HLW-APPS glasses 3.17

Figure 3.14. Measured vs predicted ln(η_{1150}) where models predicted for a) Pa·s and b) P are shown. Uncertainties for measured values are represented by SD_{pooled} reported in Vienna et al. 2022. Uncertainties for the predicted values are For Information Only (FIO). 3.20

Figure 3.15. Measured vs. predicted ln(ε_{1150}). Uncertainties for measured values are represented by SD_{pooled} reported in Vienna et al. 2022. Uncertainties for the predicted values are FIO. 3.22

Figure 3.16. Normalized NL_B, NL_{Li}, and NL_{Na} release in natural logarithm scale of quenched vs. CCC DFHLW glasses. 3.25

Figure 3.17. Uncertainties for measured values are represented by SD_{pooled} reported in Vienna et al. 2022. Uncertainties for the predicted values are FIO..... 3.26

Figure 3.18. Logarithm of normalized TCLP results for boron vs element *i*. 3.28

Figure 3.19. Predicted vs. measured TCLP results for element *i* where predicted values are determined from a) Vienna et al. 2009 and b) Kim et al. 2004. ..... 3.29

Figure 3.20. Digital images of refractory coupons after corrosion testing with APPS glasses before and after HF acid cleaning. 3.30

Figure 3.21. Measured vs. predicted plot for K-3 neck corrosion. 3.33

Tables

Table 2.1. Summary of property limits used in initial glass formulation. 2.3
Table 2.2. Single component model validity constraints in mass fraction of oxide or halogen in glass. 2.4
Table 2.3. Summary of represented batches from each of 15 clusters. 2.7
Table 2.4. Glass compositions recommended for testing based on EWG2 formulation approach. 2.10
Table 2.5. Sample identification for the samples used in the analysis reported. 2.12
Table 2.6. Canister centerline cooling (CCC) profile for the DFHLW samples. 2.14
Table 2.7. Heat treatment temperatures and duration used for CF and T_L measurements. 2.15
Table 2.8. TCLP delisting criteria for hazardous constituents. 2.19
Table 3.1. Average of 10 data points from EPMA and 4 data points from qualitative LIBS for weight percent NiO in each sample compared with the target composition. All LIBS data is FIO. 3.2
Table 3.2. Average of 4 data points from qualitative LIBS for weight percent NiO in a re-batched version of HLW-APPS-07-2 compared with the target composition. All LIBS data is FIO. 3.2
Table 3.3. Qualitative LIBS-measured concentrations of Ni on the air- and crucible-contact surfaces of HLW-APPS-01 after the first melt. All LIBS data is FIO. 3.3
Table 3.4. Details on quenched glasses after the second and final melt and crystal phases identified from XRD patterns. 3.4
Table 3.5. Crystal fraction in wt% and identification of crystals by XRD in CCC glasses. 3.6
Table 3.6. Crystal fraction in wt%, identification of crystals, and T_L for isothermally heat-treated glasses. 3.8
Table 3.7. EDS weight % of detected elements for HLW-APPS-07-2 from 900 °C isothermal heat treatment. 3.11
Table 3.8. Measured SO_3 concentrations (wt%) of sulfur saturate glass melts from the DFHLW APPS matrix. 3.14
Table 3.9. Available glass property models with predicted SO_3 saturation concentrations. 3.15
Table 3.10. Measured densities in g/cm^3. ..... 3.16
Table 3.11. Measured ln η (Pa-s) values versus target temperature (in the sequence of measurement). 3.18
Table 3.12. Fitted of Arrhenius coefficients and calculated η for specific temperatures. 3.19
Table 3.13. Available glass property models with predicted viscosity. 3.19
Table 3.14. Measured electrical conductivity (S/m) values versus temperatures. 3.21
Table 3.15. Fitted coefficients of Arrhenius model for ε_{1150}. 3.21
Table 3.16. Available glass property models with predicted EC. 3.22
Table 3.17. Average normalized PCT loss (NLs) in g/m^2 for the DFHLW APPS quenched glasses. Values in bold highlight NLs that exceeded DWPF EA glass threshold. 3.23
Table 3.18. Average normalized PCT loss (NLs) in g/m^2 for the DFHLW APPS CCC glasses. Values in bold highlight NLs that exceeded DWPF EA glass threshold. 3.24

Table 3.19. Example glass property models with predicted PCT normalized loss. 3.25
Table 3.20. RCRA delisting criteria and UTS limit (grey field). All values are in mg/L. Se and Hg were not part of glass formulation, Se was used as a part of calculations for MS recovery. 3.27
Table 3.21. RCRA metals quenched glasses, values in mg/L. 3.27
Table 3.22. RCRA metals in CCC samples, values in mg/L. 3.28
Table 3.23. Initial refractory coupon data. 3.31
Table 3.24, Refractory coupon corrosion data. 3.32
Table 3.25. Summary of Property Model Comparisons 3.34

1.0 Introduction

The U.S. Department of Energy (DOE) Office of River Protection (ORP) is responsible for the safe storage, treatment, and immobilization of wastes stored in underground tanks at the Hanford Site. The Waste Treatment and Immobilization Plant (WTP) is the cornerstone of tank waste treatment and immobilization strategy at Hanford. This plant includes, as primary components, the Low-Activity Waste (LAW) Facility, the High-Level Waste (HLW) Facility, the Pretreatment (PT) Facility, the Laboratory (LAB), and the balance of facilities (BOF). The current strategy is to stage the startup of the LAW, HLW, and PT facilities (DOE 2013; Bernards et al. 2020). The startup of the LAW Facility along with the needed components of the LAB and the BOF are planned for 2024. To facilitate the startup of the LAW Facility prior to the PT Facility, a Tank Side Cesium Removal (TSCR) system was constructed to remove solids and cesium-137 (^{137}Cs) from the tank waste supernate, thereby removing much of the radioactivity of the supernatant liquid sufficiently to feed the LAW Facility (Westesen et al. 2022). The TSCR began operations on January 26, 2022.

An analysis of alternatives for startup and operations of the PT and HLW facilities was conducted to identify the most likely alternatives along with the upper-level implication of each (Parsons 2023). A total of 17 options were considered, including concurrent startup of the HLW and PT facilities and HLW Facility operations without the PT Facility. Based on the results of these options, ORP requested an 18th scenario (alternative 18 or Alt-18) in which the annual budget for Hanford was constrained (Bernards et al. 2021). This scenario includes a Waste Transfer Vault that couples the HLW Facility with tank farms using a waste feed transfer vessel and an effluent collection vessel. ORP empaneled a group of technical experts from ORP, Bechtel National Inc. (the WTP contractor), Washington River Protections Solutions (the tank farm operations contractor), and Pacific Northwest National Laboratory (PNNL) to develop a flowsheet that could efficiently operate the HLW Facility for a ~12-year period under a Direct Feed High-Level Waste (DFHLW) flowsheet while the HLW Pretreatment and Effluent Management Facility is brought on-line. The general operating strategy laid out in Alt-18 was to serve as the reference case for DFHLW flowsheet development. Through this effort, the team identified the need to formulate glass using the enhanced waste glass (EWG) method, which results in reasonable waste processing rates (Vienna et al. 2023).

To complete the final design of the HLW Facility, complete flowsheet assessments are required. These assessments include mass, energy, and heat balances through the unit operations of the plant. The Aspen Process Performance Simulation (APPS) tool is used to perform the flowsheet calculations (Gebhardt 2011). Thirty-one APPS runs were performed in support of the baseline HLW flowsheet in the Process Inputs Basis of Design (PIBOD) for HLW (Dunst 2020). The APPS software automatically generates a glass formulation based loosely on the WTP baseline glass formulation method (Vienna and Kim 2014). To enable the use of EWG formulations, the glass formulation method in APPS can be updated to include EWG formulation method or overridden with predetermined glass formulations. To support these options, glasses were formulated, fabricated, and tested using the EWG approach. The glass testing results will serve as quality-assured validation of the formulation method.

The objectives of the present task, *Direct Feed High-Level Waste APPS Model Glass Matrix (DFHLW APPS)*, were to fabricate and test a set of representative DFHLW compositions and compare the results to model predictions.

1.1 Quality Assurance

This work was performed in accordance with the PNNL Nuclear Quality Assurance Program (NQAP). The NQAP complies with DOE Order 414.1D, *Quality Assurance*, and 10 CFR 830, *Nuclear Safety Management*, Subpart A, *Quality Assurance Requirements*. The NQAP uses NQA-1-2012, *Quality Assurance Requirements for Nuclear Facility Application*, as its consensus standard and NQA-1-2012, Subpart 4.2.1, as the basis for its graded approach to quality.

The NQAP works in conjunction with PNNL's laboratory-level Quality Management Program, which is based on the requirements as defined in DOE Order 414.1D and 10 CFR 830 Subpart A.

The work of this report was performed to a technology readiness level of 6.

Corrosion testing of refractory task activities were controlled under the Task Technical and Quality Assurance Plan (TTQAP) for Hanford Waste Glass Development and Characterization.[1]

Requirements for performing reviews of technical reports and the extent of review are established in manual E7 2.60. SRNL documents the extent and type of review using the SRNL Technical Report Design Checklist contained in WSRC-IM-2002-00011, Rev. 2. Activities performed in this task are compliant to both American Society of Mechanical Engineers (ASME) NQA-1-2008 with NQA-1a-2009 addenda and NQA-1-2019

[1] Amoroso, J.W., *Task Technical and Quality Assurance Plan for Hanford Waste Glass Development and Characterization*. 2023, Savannah River National Laboratory: Aiken, SC.

2.0 Test Methods

This section describes how the test matrix of 15 glasses was generated and data were obtained. The descriptions include the methods for (1) glass matrix generation, (2) glass fabrication and chemical composition analysis, (3) secondary phase identification from canister centerline cooling (CCC) treatment, (4) isothermal crystal fraction (CF) and liquidus temperature (T_L), (5) sulfur solubility measurement, (6) density (ρ) determination, (7) viscosity (η) measurement, (8) electrical conductivity (EC, ε) measurement, (9) product consistency test (PCT) measurement, and (10) toxicity characteristic leaching procedure (TCLP) measurement. Refractory corrosion testing will be reported separately.

2.1 Matrix Design

This section describes how the glasses were formulated for representative DFHLW waste feed composition estimates using the current state-of-the-art glass property-composition models and constraint sets applicable to DFHLW.

2.1.1 Waste Composition Estimates

A preliminary set of four blended DFHLW waste feeds were generated by Britton (2023) from the insoluble solids of Hanford south-east quadrant tanks being retrieved using their supernate with a nominal specific gravity of 1.20. The difference between the four sets was the fraction of undissolved solids in each batch – 5, 10, 15, and 20[1] wt% solids sets were generated to span the range anticipated to be delivered during operations. Combined, these waste feeds include 154 unique waste compositions. Figure 2.1 shows the distributions of non-volatile waste oxide concentration. These waste feeds are considerably higher in Na_2O, Cl, and SO_3 concentrations compared to the waste feed estimated from washed and leached sludges previously studied for Hanford HLW vitrification.

[1] The waste batches were constrained to specific gravity limits for liquid = 1.2, slurry = 1.35, and nominal average solids = 2.9. Combined, these limited the maximum solids loading to roughly 18.5 wt% even when targeting 20 wt%.

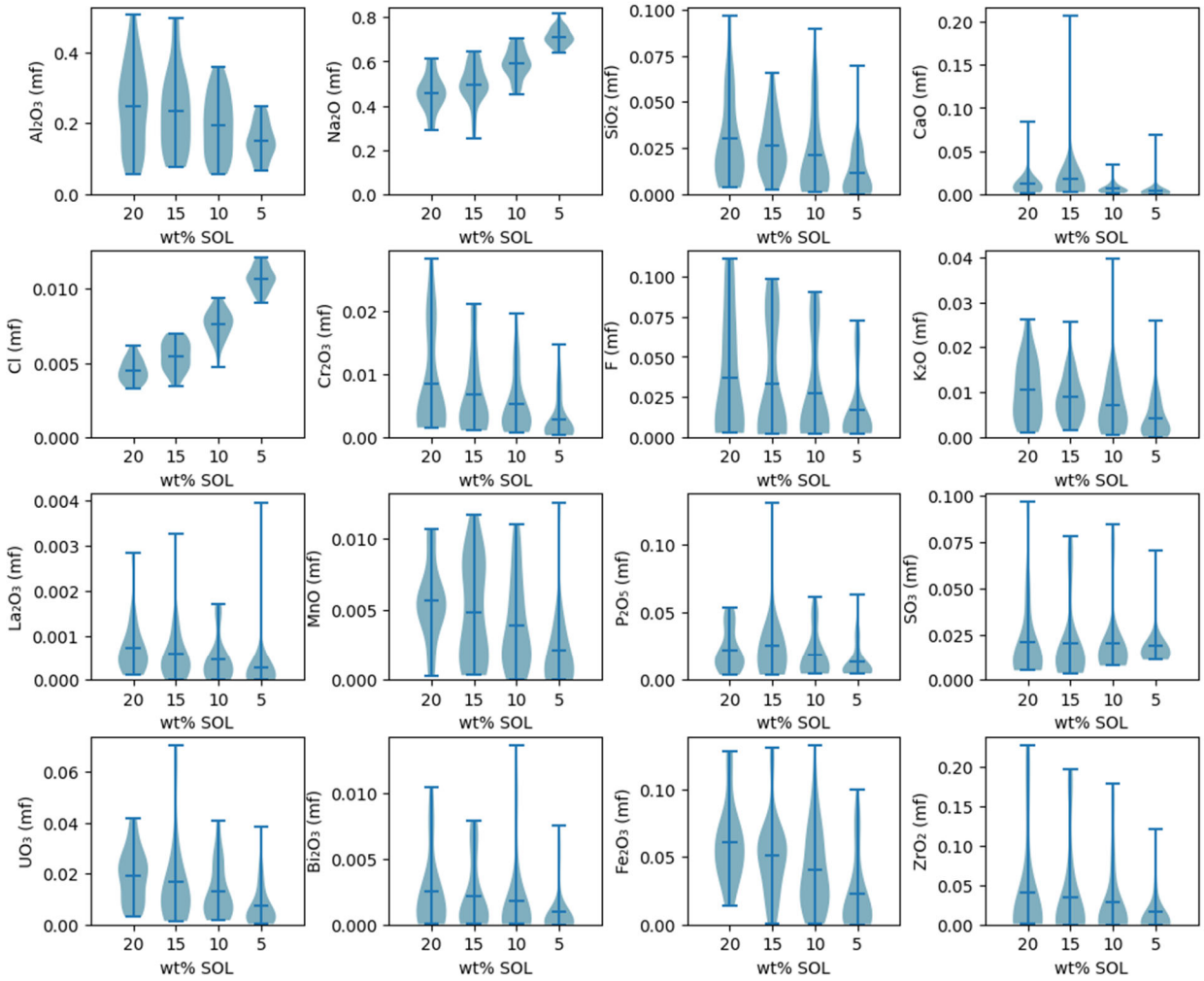

Figure 2.1. Distribution of non-volatile component concentrations in initial example of DFHLW blended feeds at four different target solids loadings. Mass fraction (mf) of calcined waste component basis.

2.1.2 Enhanced Waste Glass Formulation Approach

Glass formulations were optimized for each of the 154 waste batches in the blended feed vector using methods detailed by Vienna et al. (2022) using models and constraints in Vienna et al. (2016). Table 2.1 summarizes these EWG constraints. Most of the property constraints are satisfied using glass property-composition models that are valid only over the range of data used in their development. So, a set of model validity (MV) constraints were also applied (Table 2.2). The MV constraints of two components – F and V_2O_5 – were modified from those in Vienna et al. (2016) as noted in the table and discussed previously (Vienna et al. 2022).

The median waste loading (WL) decreases from ~45 wt% for the 20 wt% solids feed to ~35 wt% in the 5 wt% solids feeds. This decrease results from the higher content of sodium and sulfur in the supernate, which impacts the loading at which salt can be avoided and Na_2O MV limit is satisfied. Note that for most feed batches, multiple constraints are simultaneously limiting WL. The most significant constraints include probability of nepheline formation, SO_3 solubility, MV constraints (primarily Na_2O, B_2O_3, V_2O_5, CaO, and ZnO), viscosity, and combined CaO x P_2O_5 concentrations. If nepheline forms during CCC, the

durability response (e.g., PCT) will become unpredictable and potentially fail the constraints (Vienna et al. 2017). If SO_3 concentration exceeds the solubility limit, a molten salt will accumulate at the melt surface and increase the corrosion rate of glass contact materials (Vienna et al. 2014). If viscosity constraints are exceeded, the processing of glass in the WTP melters can be disrupted (Perez 2006). Excessive P_2O_5, particularly in the presence of higher CaO, may form phosphate phases that could disrupt the melting rate, settle in the melter, and decrease glass durability (Vienna 2008). MV constraints only reflect insufficient data to reliably predict properties.

The resulting 154 glass compositions are graphically represented in Figure 2.2.

Table 2.1. Summary of property limits used in initial glass formulation.

Constraint	Limit
Product consistency test (PCT) normalized element release (r_α)	$\ln[r_B\ (g/m^2)] \le 1.386$[(a)] $\ln[r_{Na}\ (g/m^2)] \le 1.386$[(a)] $\ln[r_{Li}\ (g/m^2)] \le 1.386$[(a)]
Probability of nepheline formation (p)	$p \le 0.3$ (probability)
Temperature at 2 vol% spinel ($T_{2\%}$)	$T_{2\%} \le 950$ °C
Liquidus temperature for zirconium-containing phases (T_L-Zr)	T_L-Zr ≤ 1050 °C if $g_{ZrO_2} > 0.04$
Viscosity at 1150 °C (η_{1150})	$1.386 \le \ln(\eta_{1150,}\ Pa{\cdot}s) \le 1.792$[(b)]
Combined P_2O_5 and CaO concentrations	$g_{P_2O_5} \times g_{CaO} \le 0.00065$ (mass fraction)^2
SO_3 concentration below solubility limit	$g_{SO_3} \le g_{SO_3}^{Limit}$
Cr_2O_3 concentration to avoid excessive Eskolaite formation	$g_{Cr_2O_3} \le 0.03$
Combined B_2O_3 and SiO_2 concentrations	$g_{SiO_2} + g_{B_2O_3} \ge 0.32$
Combined noble metal concentrations	$g_{PdO} + g_{Rh_2O_3} + g_{RuO_2} \le 0.0025$

(a) Corresponds to $r_\alpha \le 4$ g/m^2 (or 8 g/L in normalized loss units).
(b) Corresponds to $4 \le \eta_{1150} \le 6$ Pa·s.

Table 2.2. Single component model validity constraints in mass fraction of oxide or halogen in glass.

Component	Min	Max
Al_2O_3	0.019	0.300
B_2O_3	0.040	0.220
Bi_2O_3	0	0.070
CaO	0	0.100
CdO	0	0.015
Cr_2O_3	0	0.030
F[(a)]	0	0.045
Fe_2O_3	0	0.200
K_2O	0	0.060
Li_2O	0	0.060
MgO	0	0.060
MnO	0	0.080
Na_2O	0.041	0.240
NiO	0	0.030
P_2O_5	0	0.045
SiO_2	0.220	0.530
SrO	0	0.101
ThO_2	0	0.060
TiO_2	0	0.050
UO_3	0	0.063
V_2O_5[(b)]	0	0.04056
ZnO	0	0.040
ZrO_2	0	0.135

(a) F was increased from 2.5 to 4.5 wt%.
(b) Model validity limit from the HLW SO_3 solubility model in Vienna et al. 2016 for V_2O_5 ($\leq$ 4.056 wt%).

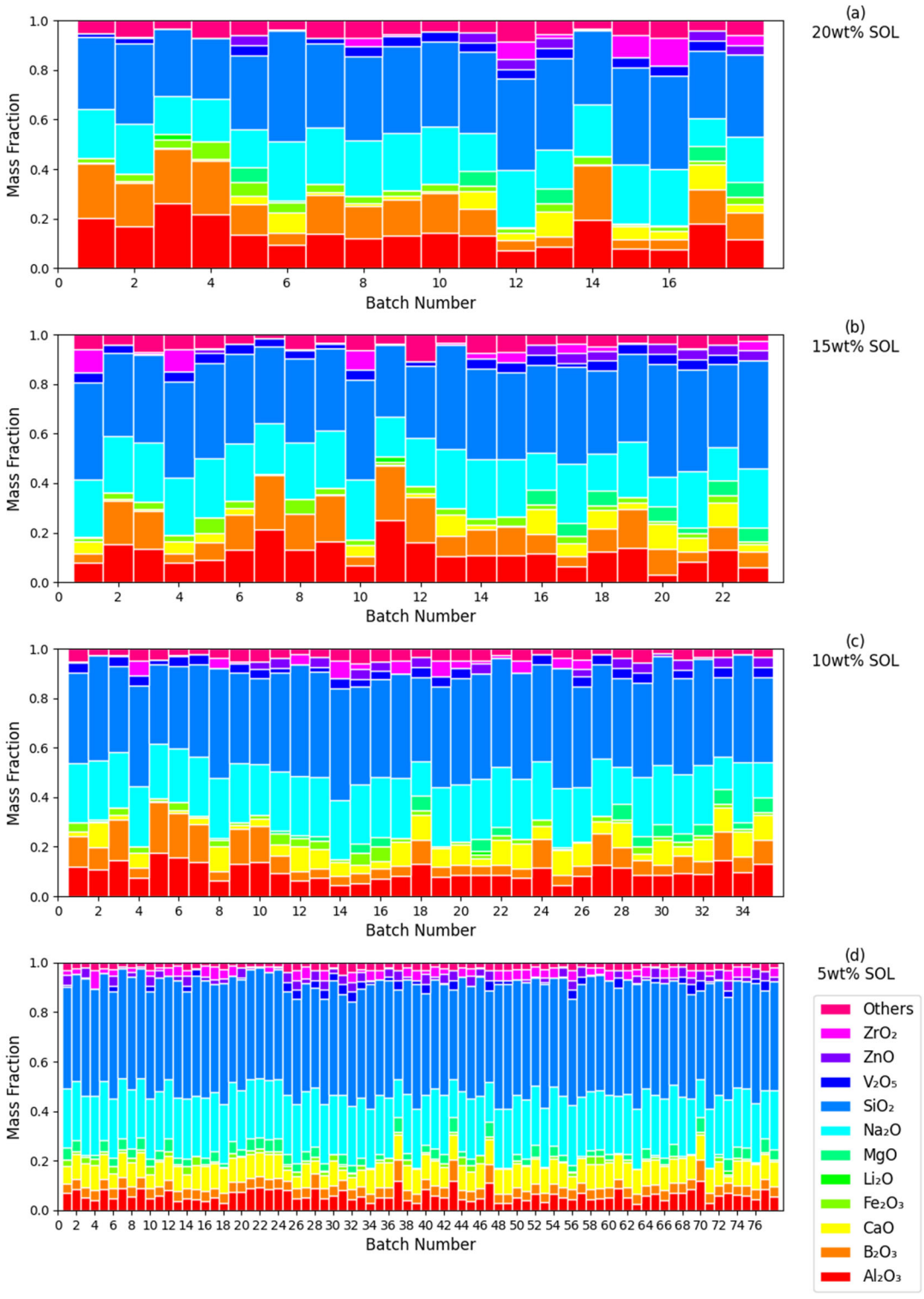

Figure 2.2. Graphical representation of glass compositions for 154 DFHLW feed batches.

2.1.3 Waste Composition Selection

Cluster analysis was performed to identify 15 representative glass compositions of the potential 154 to perform testing. K-means cluster analysis was based on the glass composition factors of most interest: NaK = Na_2O + 0.66 K_2O, SO_3, Li_2O, B_2O_3, and ZrO_2. Figure 2.3 shows the within cluster sum-of-squares distance versus number of clusters. This figure indicates that 15 clusters is well below the elbow, suggesting that 15 compositions can adequately represent the range of glass compositions in the dataset. A representative batch was selected for each of the 15 clusters as summarized in Table 2.3. There are five batches each from 5 wt% solids feeds, 20 wt% solids feeds, and combined 10-15 wt% solids feeds. The distribution of the 154 glass compositions is reported in Appendix A.

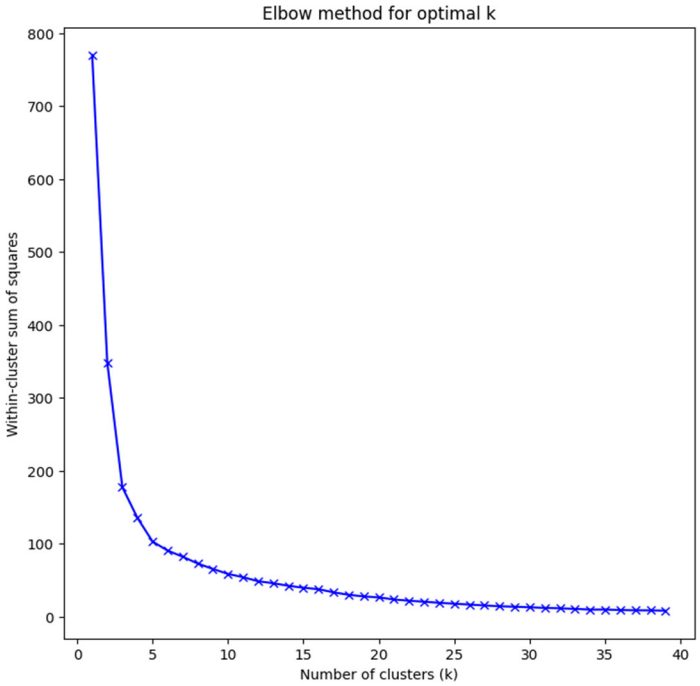

Figure 2.3. Within cluster sum of squares distance vs. number of clusters.

Table 2.3. Summary of represented batches from each of 15 clusters.

Batch #	Cluster #	wt% Sol	Constraints[(a)]
3	2	20	p, MV_{B2O3}, η
4	11	20	p, MV_{B2O3}
16	4	20	p, η, w_{SO3}, MV_{B2O3}, MV_{V2O5}
17	14	20	p, η, w_{SO3}, MV_{CaO}, MV_{MgO}, MV_{V2O5}, MV_{ZnO}
18	13	20	p, η, MV_{MgO}, MV_{ZnO}, CaxP
20	3	15	p, η, w_{SO3}
30	10	15	p, η, w_{SO3}
45	8	10	η, w_{SO3}, MV_{B2O3}, MV_{Na2O}, MV_{V2O5}
59	1	10	p, η, w_{SO3}, MV_{CaO}, MV_{MgO}, MV_{V2O5}, MV_{ZnO}
62	5	10	p, w_{SO3}, CaxP, MV_{B2O3}, MV_{Na2O}, MV_{ZnO}
101	12	5	η, w_{SO3}, CaxP, MV_{B2O3}, MV_{Na2O}, MV_{V2O5}, MV_{ZnO}
132	6	5	η, w_{SO3}, CaxP, MV_{B2O3}, MV_{Na2O}, MV_{ZnO}
134	0	5	η, w_{SO3}, MV_{B2O3}, MV_{Na2O}, MV_{CaO}
152	7	5	η, w_{SO3}, MV_{B2O3}, MV_{Na2O}, MV_{CaO}, MV_{ZnO}
153	9	5	p, η, w_{SO3}, MV_{B2O3}, MV_{CaO}, MV_{V2O5}, MV_{ZnO}

(a) p = probability of nepheline formation, MV_{α} = α component model validity, η = viscosity at 1150 °C, w_{SO3} = sulfur solubility, CaxP = CaO × P_2O_5

2.1.4 Modification to Formulation Approach

The 15 glass compositions representing the 15 clusters were analyzed in more detail. The loading of seven of the feeds was limited by single (or duel) waste component concentration constraints – Na_2O and CaO × P_2O_5. When one of these constraints is obtained, there is a non-unique solution to optimized glass composition. Both constraints are used due to a lack of data at higher concentrations to demonstrate acceptable properties. LAW models have recently been published with higher Na_2O MV (26.57 wt%) that predict the properties of concern for DFHLW glasses (Vienna et al. 2022b). More recent data than found in the EWG models has shown significantly higher P_2O_5 concentrations are possible (Lu et al. 2023). The EWG formulation method also selected glass-forming chemicals (GFCs) based on a WL optimization routine without regard to the cost and challenge of including some GFCs. More rational review of GFC usage would lead to minimizing the use of Li_2CO_3 and V_2O_5 for reasons of GFC cost and minimizing use of ZnO for GFC handling and minimizing $MgSiO_3$ for long-term corrosion resistance.

To remedy these concerns, a manual glass composition optimization was performed. In addition to the constraints and models described for the EWG process, the following sets of models were used:

- PCT response models: Vienna and Crum 2018, Kot et al. 2019, and Vienna et al. 2022b
- SO_3 solubility models: Vienna et al. 2022b, Vienna et al. 2013
- Viscosity models: Vienna et al. 2022b, Kot et al. 2019
- EC models (not included in Vienna et al. 2016): Vienna et al. 2009, Vienna et al. 2022b, Kot et al. 2019
- Nepheline: Lu et al. 2021
- Immiscibility: Peeler and Hrma 1994
- K-3 corrosion (not included in Vienna et al. 2016): Vienna et al. 2022b

With these additional models, the two most significant controlling variable constraints (Na_2O and $CaO \times P_2O_5$) were relaxed. Also, V_2O_5 was not used as a GFC unless the composition was SO_3 solubility limited. Li_2O, ZnO and MgO were only included as GFCs if they increased WL by ≥ 0.1 wt% absolute over the formulations without these additives. Combined, this formulation approach is referred to as second iteration of enhanced waste glass or EWG2.

Figure 2.4 compares the resulting WL values between the two formulation approaches – EWG and EWG2. EWG2 allowed for higher P_2O_5 (batch 18) and Na_2O (batches 45, 62, 101, 132, 134, and 152) concentrations due to expanded MV limits. The high-F batch (batch 16) had lower WL in EWG2 because EWG assumed the F limit was after volatility while EWG2 assumed a limit before volatile loss. EWG2 showed lower WL for high-SO_3 waste (batch 17) due to the use of multiple SO_3 solubility models that were found to be more limiting on WL. Figure 2.5 compares the differences in glass component concentrations for the glasses formulated using EWG and those formulated using EWG2. ZnO and MgO were not found in EWG2 formulations and did not make significant differences in WL. V_2O_5 is now only used in EWG2 for high-SO_3 wastes; Li_2O concentrations are higher than EWG in two batches (17 and 59), but Li_2O was not included in other batches (62, 101, and 134).

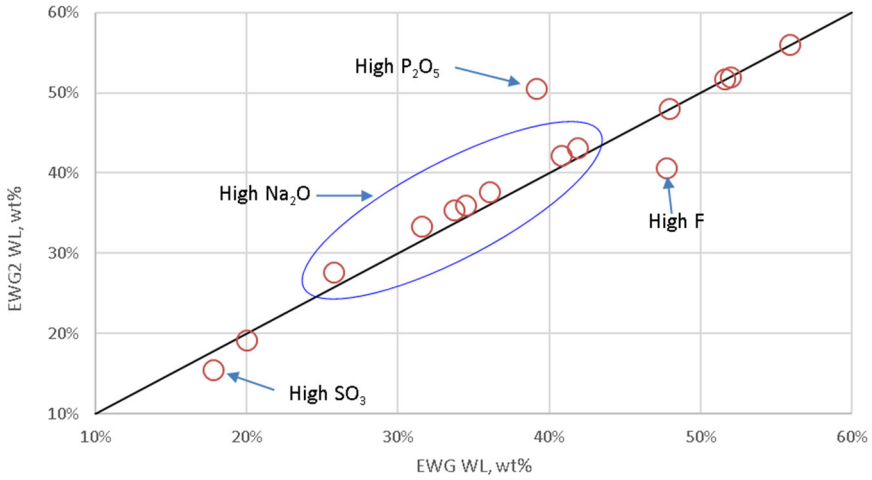

Figure 2.4. Waste loading comparison between EWG and EWG2 formulation approaches.

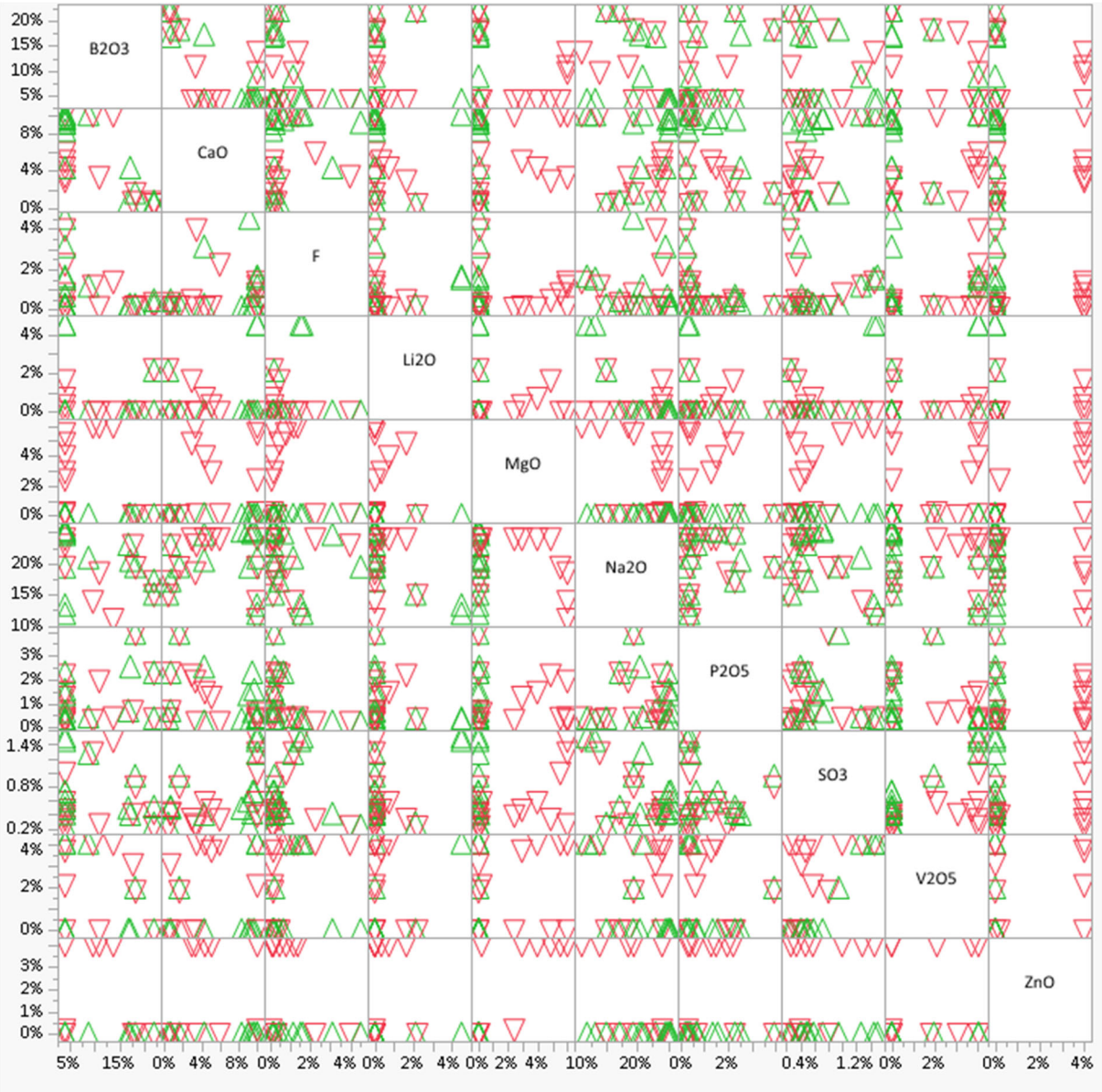

Figure 2.5. Comparison of component concentrations between EWG (▽) and EWG2 (△) formulation method for those glass components with significant differences.

2.1.5 Recommended Glass Compositions

Table 2.4 shows the glass compositions generated from the 15 waste cluster compositions. For simplicity these clusters are relabeled HLW-APPS-01 to -15 in order of batch number and are referred to as such in the remainder of this report. These 15 glass compositions were used for quality assured experimental validation of the EWG2 formulation method. The following process and quality product properties were measured: crystal formation during CCC and isothermal heat treatment (CF, T_L), sulfur solubility, density, viscosity, EC, and glass durability via PCT and TCLP. Refractory corrosion test results will be reported separately.

Table 2.4. Glass compositions recommended for testing based on EWG2 formulation approach.

Batch	3	4	16	17	18	20	30	45	59	62	101	132	134	152	153
Glass ID	HLW-APPS-01	HLW-APPS-02	HLW-APPS-03	HLW-APPS-04	HLW-APPS-05	HLW-APPS-06	HLW-APPS-07	HLW-APPS-08	HLW-APPS-09	HLW-APPS-10	HLW-APPS-11	HLW-APPS-12	HLW-APPS-13	HLW-APPS-14	HLW-APPS-15
Ag_2O	0.009	0.004	0.032	0.000	0.013	0.005	0.002	0.020	0.002	0.000	0.000	0.000	0.010	0.002	0.002
Al_2O_3	26.198	21.413	4.500	3.000	14.822	15.084	15.818	3.877	10.514	8.625	6.900	4.675	4.540	4.619	11.255
B_2O_3	22.000	22.000	4.000	4.000	17.169	16.813	18.199	4.000	4.000	4.000	4.000	4.000	4.000	4.000	8.750
BaO	0.006	0.007	0.003	0.001	0.003	0.005	0.000	0.011	0.005	0.000	0.000	0.000	0.001	0.004	0.001
Bi_2O_3	0.093	0.452	0.018	0.000	0.020	0.112	0.083	0.015	0.000	0.001	0.069	0.247	0.002	0.001	0.004
CaO	0.407	0.664	9.128	10.000	4.274	0.649	1.606	4.282	9.964	9.453	9.674	9.021	8.308	9.526	10.000
CdO	0.001	0.000	0.001	0.000	0.006	0.003	0.001	0.001	0.001	0.000	0.000	0.000	0.000	0.001	0.001
Cl	0.193	0.201	0.177	0.070	0.254	0.329	0.178	0.334	0.128	0.327	0.376	0.380	0.378	0.386	0.286
Cr_2O_3	0.131	0.089	0.082	0.037	1.429	0.909	0.101	0.042	0.030	0.242	0.023	0.037	0.119	0.215	0.409
F	0.210	0.451	4.500	1.628	0.237	0.154	0.226	3.101	1.520	0.673	0.165	0.244	0.123	0.217	1.159
Fe_2O_3	3.418	6.798	1.648	0.217	2.299	2.430	2.993	2.588	0.619	0.571	0.832	0.949	2.996	0.374	0.024
K_2O	0.201	0.066	0.724	0.099	1.327	0.459	0.571	0.465	0.062	0.075	0.020	0.028	0.151	0.345	0.210
Li_2O	2.121	0.000	0.001	4.500	0.005	0.009	0.002	0.000	4.500	0.000	0.000	0.000	0.001	0.002	0.000
MgO	0.014	0.013	0.063	0.000	0.070	0.016	0.010	0.069	0.004	0.000	0.000	0.000	0.002	0.006	0.014
MnO	0.345	0.281	0.232	0.005	0.122	0.115	0.071	0.220	0.044	0.123	0.010	0.094	0.444	0.028	0.004
Na_2O	15.042	17.192	19.368	11.928	20.433	22.962	19.432	24.554	13.271	24.843	25.081	25.242	25.153	25.398	20.849
Nd_2O_3	0.054	0.066	0.048	0.005	0.086	0.033	0.009	0.059	0.044	0.001	0.001	0.001	0.021	0.030	0.005
NiO	0.340	0.578	0.048	0.009	0.141	0.335	0.794	0.098	0.028	0.053	0.170	0.143	0.075	0.021	0.003
P_2O_5	0.368	2.281	0.188	0.368	2.520	0.683	3.923	0.231	0.298	2.284	1.558	1.346	0.326	0.649	0.428

Table 2.4 (cont.)

Batch	3	4	16	17	18	20	30	45	59	62	101	132	134	152	153
Glass ID	HLW-APPS-01	HLW-APPS-02	HLW-APPS-03	HLW-APPS-04	HLW-APPS-05	HLW-APPS-06	HLW-APPS-07	HLW-APPS-08	HLW-APPS-09	HLW-APPS-10	HLW-APPS-11	HLW-APPS-12	HLW-APPS-13	HLW-APPS-14	HLW-APPS-15
PbO	0.183	0.482	0.057	0.004	0.080	0.127	0.309	0.109	0.014	0.022	0.086	0.049	0.115	0.012	0.003
PdO	0.001	0.001	0.000	0.000	0.000	0.000	0.000	0.001	0.000	0.000	0.000	0.000	0.000	0.000	0.000
Rh_2O_3	0.000	0.000	0.000	0.000	0.000	0.000	0.000	0.000	0.000	0.000	0.000	0.000	0.000	0.000	0.000
RuO_2	0.007	0.012	0.000	0.000	0.000	0.000	0.000	0.008	0.002	0.000	0.000	0.000	0.000	0.001	0.000
SiO_2	27.226	24.566	44.875	58.457	32.833	37.541	28.907	48.777	49.351	46.121	49.374	52.624	52.658	53.363	41.104
SnO_2	0.000	0.000	0.000	0.000	0.000	0.000	0.000	0.000	0.000	0.000	0.000	0.000	0.000	0.000	0.000
SO_3	0.268	0.506	0.236	1.500	0.399	0.487	0.944	0.407	1.448	0.416	0.716	0.587	0.484	0.721	1.265
SrO	0.010	0.021	0.003	0.001	0.004	0.010	0.049	0.009	0.002	0.002	0.015	0.007	0.005	0.001	0.000
ThO_2	0.419	0.422	0.008	0.001	0.014	0.005	0.032	0.005	0.009	0.537	0.003	0.001	0.015	0.004	0.000
TiO_2	0.002	0.003	0.000	0.000	0.001	0.002	0.001	0.002	0.001	0.000	0.000	0.000	0.000	0.001	0.000
UO_3	0.457	1.180	0.807	0.051	1.005	0.558	3.664	0.565	0.039	0.491	0.917	0.234	0.056	0.034	0.152
V_2O_5	0.003	0.000	0.002	4.056	0.003	0.008	1.969	0.002	4.056	0.000	0.000	0.000	0.001	0.002	4.056
ZnO	0.007	0.007	0.001	0.000	0.007	0.013	0.004	0.005	0.001	0.000	0.000	0.000	0.001	0.002	0.000
ZrO_2	0.228	0.222	9.236	0.063	0.371	0.055	0.074	6.124	0.025	1.138	0.009	0.087	0.003	0.013	0.011
Others	0.038	0.022	0.013	0.000	0.053	0.091	0.027	0.020	0.017	0.001	0.001	0.001	0.011	0.022	0.003

2.2 Glass Fabrication

The glasses were batched using chemicals composed of single-metal oxides, single-metal carbonates, sodium salts, and boric acid in the appropriate masses to form the target composition for each glass (Table 2.4) and melted in platinum-10% rhodium crucibles (Pt/Rh). Laboratory crucible-scale fabrication of glasses is not intended to mimic the actual melter process or feed processability; rather, it is intended to fabricate a glass sample with a controlled composition for property testing.

After thoroughly mixing all the components in a plastic bag for at least 30 seconds and until uniform color developed, the powders were transferred to an agate milling chamber and milled for 4 minutes in a vibratory mill (Angstrom TE110). The powders were then transferred to a clean crucible for melting. Initial melting was performed at 1150 ± 10 ℃ for 1 hour ± 10 minutes.

After the first melt was air quenched on a stainless-steel pouring plate, the glass was observed under an optical microscope and the presence of undissolved particles and/or salts was reported. The glass was then ground to a fine powder for 5 minutes in a tungsten carbide vibratory mill (AngstromTE110) and a second melt was performed at 1150 °C ± 10 °C for 1 hour ± 10 minutes. The presence of any crystal after the final melt was recorded and the crystalline structure of the crystal was analyzed by X-ray diffraction (XRD) and scanning electron microscopy (SEM) as described in Section 2.3.

Re-batched glasses were given a replicate number starting with -1, e.g., HLW-APPS-4 was re-batched, and so the sample used for analysis is HLW-APPS-04-1. Table 2.5 gives the full list of sample names referring to those analyzed in the work described in this report.

To confirm that the “as-fabricated” glasses corresponded to the specified target compositions, a representative sample of each glass was chemically analyzed by electron probe microanalysis/wavelength dispersive spectroscopy (EPMA/WDS) as described in Section 2.4. These results are discussed in glass composition and secondary phase investigation in Section 3.1 and 3.1.1, respectively.

Table 2.5. Sample identification for the samples used in the analysis reported.

Composition Name	Sample Name Used
HLW-APPS-01	HLW-APPS-01
HLW-APPS-02	HLW-APPS-02
HLW-APPS-03	HLW-APPS-03
HLW-APPS-04	HLW-APPS-04-1
HLW-APPS-05	HLW-APPS-05
HLW-APPS-06	HLW-APPS-06
HLW-APPS-07	HLW-APPS-07-2
HLW-APPS-08	HLW-APPS-08
HLW-APPS-09	HLW-APPS-09
HLW-APPS-10	HLW-APPS-10
HLW-APPS-11	HLW-APPS-11
HLW-APPS-12	HLW-APPS-12
HLW-APPS-13	HLW-APPS-13-1
HLW-APPS-14	HLW-APPS-14
HLW-APPS-15	HLW-APPS-15

2.3 X-ray Diffraction and Scanning Electron Microscopy for Secondary Phase Investigation

Samples that had inhomogeneities by optical microscopy either after the final melt or after a heat treatment were prepared as powdered samples for XRD. Powdered glass samples were prepared using roughly 5 wt% CeO_2 as an internal standard phase with between 1 and 2 g of powdered glass. A glass piece representative of the whole sample (in the case of the CF, half sample was used) was milled alone for 1 minute and then homogenized with the CeO_2 for 30 seconds in a 10-cm^3 tungsten carbide disc mill. The homogenized samples were loaded into plastic holders and analyzed using a Bruker D8 Advance XRD (Bruker AXS Inc., Madison, Wisconsin) with Cu Kα emission. Samples were scanned at a 0.015° 2θ step size, 1.5-second dwell time, from 5° to 75° 2θ scan range. XRD spectra were analyzed with DIFFRAC.EVA (Bruker Corporation, Billerica, Massachusetts) for phase identification. Full-pattern Rietveld refinement using TOPAS 5 Software (Bruker AXS Inc., Madison, Wisconsin – for the CF and CCC samples) was performed to quantify the fraction of each crystal phase when present. Comparing the quantified fraction by Rietveld refinement to the quantity of the internal standard used allowed for quantification of the crystalline phases and amorphous phase in the sample.

For selected samples, SEM was performed using the JEOL JSM 5900 SEM (JEOL USA Inc., Peabody, Massachusetts) to examine surface morphology. Samples were placed in a sample holder and iridium-coated before being loaded into the instrument, and micrographs were obtained for regions of interest.

2.4 Electron Probe Microanalysis/Wavelength Dispersive Spectroscopy for Chemical Composition Analysis

To analyze the chemical composition of glass samples, a representative sample of each glass was chemically analyzed using EPMA/WDS with a JEOL JXA-8530F Hyperprobe (JEOL USA Inc., Peabody, MA). The samples were prepared as 2-mm-diameter cylinders using a drill press, mounted into an aluminum stage with an array of holes so multiple samples could be inserted. The samples were ground with 1500 grit paper and polished to a finish of 1 μm using 9-, 3-, and 1-μm diamond pads and polishing compound. Samples were then coated with iridium to dissipate charging.

The EPMA instrument uses a field-emission gun equipped with five wavelength dispersive spectrometers, each with a take-off angle of 40°. The microprobe data was collected at an accelerating voltage of 15 kV, beam current of 40 nA, and beam size of 100 μm.

Appropriate standards were used for each of the elements analyzed. Interferences were identified and corrected for by applying interference standards for each element. Wavescans were collected using arbitrarily chosen coupons to fit background functions for each glass composition. Oxygen and lithium were not directly analyzed. Instead, oxygen was calculated based on stoichiometry of the oxides analyzed. The presence of lithium was qualitatively confirmed with laser-induced breakdown spectroscopy (LIBS) and the “as-batched” values are reported in the results.

Each coupon was measured in 10 different locations in an approximate square grid with the intention of maximizing representation of the sample. The average of the 10 duplicates measured was used as the glass measured composition. Images were taken of the regions of the sample where data was collected from, and observations of the morphology were recorded.

2.5 Canister Centerline Cooling

A portion (~150 g) of each test glass was subjected to the simulated CCC temperature profile shown in Table 2.6 and Figure 2.6.

Table 2.6. Canister centerline cooling (CCC) profile for the DFHLW samples.

Segment	Start Temp (°C)	Stop Temp (°C)	Rate (°C/min)
1[(a)]	T_M[(a)]	T_M[(a)]	0.000[(a)]
2[(b)]	T_M	1050	free fall[(b)]
3	1050	980	-1.556
4	980	930	-0.806
5	930	875	-0.591
6	875	825	-0.388
7	825	775	-0.253
8	775	725	-0.278
9	725	400	-0.304

(a) Segment 1 is a 30-minute dwell at the glass melt temperature (T_M).
(b) Segment 2 free fall is at an estimated rate of -12.5 °C/minute.

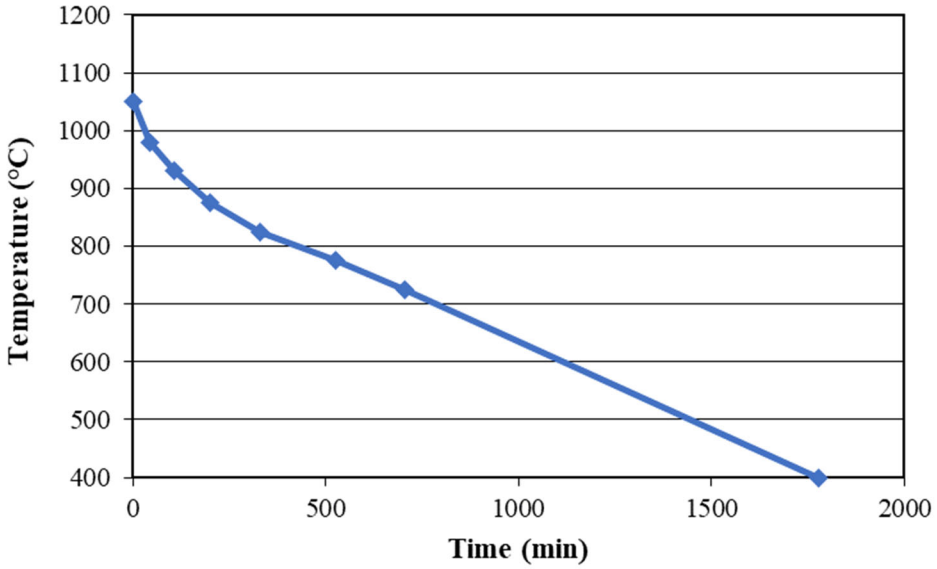

Figure 2.6. Plot of target temperature schedule during CCC treatment.

This profile is the temperature schedule of CCC treatment for Hanford HLW glasses planned for use at the WTP (Petkus 2003) and modified by PNNL to include a 30-min soak at the glass melt temperature (T_M) before the cooling began. Pieces of quenched glass, < 3 cm in diameter, were placed in a Pt-alloy crucible and covered with a Pt-alloy lid. The glass samples were placed in a furnace preheated to the T_M = 1150 °C. After 30 min at T_M, the furnace temperature was quickly dropped to 1050 °C and the cooling profile started. It progressed down to about 400 °C based on seven cooling segments shown in Table 2.6. The starting temperatures for the seven segments of cooling were 1050, 980, 930, 875, 825, 775, and 725 °C.

The amounts and types of crystalline phases that formed during CCC treatment were analyzed by XRD according to Section 12.4.4 of ASTM C1720, *Standard Test Method for Determining Liquidus Temperature of Immobilized Waste Glasses and Simulated Waste Glasses*. XRD was performed as described in Section 2.3. These results are discussed in Section 3.2.

2.6 Isothermal Crystal Fraction and Liquidus Temperature

Isothermal crystal fraction (CF) as a function of temperature was measured in Pt-alloy boats with tight-fitting lids to minimize volatility according to the ASTM C1720. Prior to measuring the CF, the furnace temperature accuracy was verified using ARG-1 glass (Smith 1993). Data measured and captured for the standard glass check was stored in a data package.

The heat treatment times and temperatures are reported in Table 2.7. The Pt boats were removed from the furnace and placed on a ceramic brick to cool. Due to the small size, water quenching was unnecessary to prevent crystal formation on cooling. The CF formed during heat treatment was analyzed using XRD according to Section 2.3.

Attempts were made to measure the T_L of the test-matrix glasses using the CF extrapolation method in ASTM C1720, where T_L is calculated by extrapolating CF as a function of temperature to zero crystals.

CF and T_L results are discussed in Section 3.3.

Table 2.7. Heat treatment temperatures and duration used for CF and T_L measurements.

Heat Treatment Temperatures and Duration	Glasses Tested
750 °C–72 h	01, 04-1, 06, 10, 11, 12, 13-1, and 14
850 °C–24 h	All glasses except 07-2
850 °C–48 h	06, 07-2, 12, 13-1, 14, and 15
900 °C–24 h	01, 05, 06, 07-2, 10, 11, 12, 13-1, 14, and 15
950 °C–24 h	05, 06, 07-2, 10, 11, and 14
1050 °C–24 h	07-2
1150 °C–24 h	07-2

2.7 SO_3 Solubility

SO_3 solubility (w_{SO3}) was determined using the three-time saturation melt method (3TS). Approximately 60 g of the quenched DFHLW APPS glasses was milled in a tungsten carbide (WC) chamber in the Angstrom milling instrument to generate fines (approximately 3 minutes). For each glass, 3.84 g of Na_2SO_4 (Fisher Chemical) was added to 50.00 g of the crushed quenched glass fraction and homogenized with the WC mill for 30 seconds. The Na_2SO_4 + glass mixtures were melted in Pt/Rh crucibles at 1150 °C for 1 hour. After 1 hour, each melt was quenched on a stainless-steel plate, resulting in a glass and a sulfate salt separated phase (see results section). Once cooled, each glass was crushed to fines in the WC mill and remelted for 1 hour at 1150 °C. This process continued until three melts were completed to generate the sulfur-saturated melt (SSM) glasses.

The SSM glass was crushed incrementally in the WC mill for ~1.2 seconds and sieved to obtain a 106- to 180-µm fraction using a Ro-Tap shaker (RX-29 model, W.C. Tyler) for 6 minutes for each session.

Approximately 5 to 10 sessions were required to crush and sieve the SSM glass fraction, resulting in > 15 g of the 106- to 180-µm fraction available for the washing steps.

From the > 15 g of the 106- to 180-µm glass fraction, 2.0 g of SSM glass and 20 g of deionized water were transferred into a centrifuge tube equipped with a 0.45-µm nylon filter. The centrifuge tube was closed and shaken by hand for ~2 minutes to ensure that the glass was completely exposed to the solution. After shaking, the centrifuge tubes were centrifuged at 3175 rpm for 5 minutes in a centrifuge instrument (Sorvall Legend Mach 1.6 model, Thermo Electron Corporation). The centrifuge filter with the washed glass powder was removed, and the rinse solution was decanted and stored for potential future use. The filter with glass powder was returned to the centrifuge tube and the washing procedure was repeated. After the second washing, the filter with glass powder was dried overnight in an 80 °C oven. The dried powder was separated from the centrifuge filter and prepared for EPMA analysis. A few milligrams of the dried washed SSM glass powders were mounted into an aluminum puck with epoxy (EpoxySet, Allied High Tech Products, Inc.) as shown in Figure 2.7. The mounted samples were analyzed by EPMA following the same procedure described in Section 2.13.

These results are discussed in Section 3.4.

Figure 2.7. Dried washed SSM glass powders mounted with epoxy in an aluminum puck for EPMA.

2.8 Density

Density of each glass was measured at room temperature using a MicroMeritics AccuPyc II 1340 gas pycnometer (MicroMeritics, Norcross, Georgia). Approximately 1 g of glass pieces was loaded into a sample holder and placed within the instrument. The density was determined by the difference in amount of helium gas needed to fill the vial with and without sample. The final density was the average of five measurements. The pycnometer was calibrated before and after measurements for that day using a National Institute of Standards and Technology traceable standard tungsten carbide ball.

These results are discussed in Section 3.5.

2.9 Viscosity

The viscosity of each glass was measured as a function of temperature using the viscosity dependance to the shear stress and shear rate (Eq. 2.1):

$$\eta = \frac{\tau}{\gamma} \quad 2.1$$

A rotating spindle digital viscometer capable of measuring viscosities from 1 to 100 Pa·s (Brookfield Digital Model LVTD) was staged above a high-temperature Deltech furnace (Deltech Model DT-31-RS, Denver, Colorado) equipped with a Pt/Rh spindle to fit through a hole in the top of the furnace. A 50-mL glass sample was measured by weight using the measured glass density, added into a Pt/Rh alloy crucible of 100 mL with approximate dimensions of 5 cm diameter × 6 cm height. The crucible was placed into the furnace set at 1150 °C and the glass was left to melt for about 20 minutes before the spindle was lowered into the molten glass in the center of the crucible with the lower end of the rod at 1 cm above the bottom of the crucible. The furnace was programmed to follow a set ramp schedule at the following temperatures: 1150, 1050, 950, 1150, 1200 °C, and back to 1150 °C. The soak time was 30 minutes at each temperature. The temperature profile followed allowed for the potential impacts of crystallization (at lower temperatures) and volatility (at high temperatures) to be assessed (via reproducibility) at the repeated T_M = 1150 °C. The viscometer was calibrated using the Defense Waste Processing Facility (DWPF) startup frit. At each target temperature, the maximum and minimum spindle torque values were recorded three times each at 3-minute. The average of the three measurements was used for data analysis. Results are discussed in Section 3.6.

2.10 Electrical Conductivity

The EC (σ in S/m) as a function of temperature was calculated from the resistance (R' in Ω) and cell constant (K in m-1) by Eq. 2.2:

$$\sigma = K/Rs \quad 2.2$$

where Rs is the solution resistance obtained for the KCl calibration solutions and K is the cell constant and is linked to the geometry of the system.

A Solartron 1470E CellTest System impedance analyzer (Solartron Analytical, Oak Ridge, Tennessee) connected to a two-blade Pt/Rh probe staged above a high-temperature Deltech furnace (Deltech Model DT-31-RS, Denver, Colorado) was used to measure the molten glass impedance.

About 50-mL of glass measured post-viscosity was added to a Pt/Rh alloy crucible and placed into the furnace at 1100 °C. The two-blade Pt/Rh probe was then lowered into the center of the molten glass through the hole in the top of the furnace at an approximate depth of 12.7 mm.

Data was recorded at 1200, 1100, 1000, and 900 °C after roughly 45-minute soaks at each temperature, allowing the program to collect impedance data at frequencies of 10,000, 1000, 100, and 63 Hz 5 minutes apart. EC was calculated using the 1000-Hz frequency, the closest values to predicted impedance in the melter. These results are discussed in Section 3.7.

2.11 Product Consistency Test

PCT responses were measured for quenched and CCC samples of each glass using Method A of ASTM C1285, *Standard Test Methods for Determining Chemical Durability of Nuclear, Hazardous, and Mixed Waste Glasses and Multiphase Glass Ceramics: The Product Consistency Test (PCT)*. Alongside each triplicate of the measured composition, the Approved Reference Material-1 (ARM-1, Mellinger and Daniel 1984) glass was also tested in triplicate. Two blanks were added in each round. Glass samples were ground, sieved to -100 +200 mesh, washed, and prepared according to ASTM C1285. The prepared glass was added to water in a 1.5 g to 15 mL ratio, resulting in a glass surface area-to-solution volume ratio of approximately 2000 m^{-1}. The desensitized Type 304L Parr stainless steel vessels with PTFE gaskets were used. The vessels were closed, sealed, and placed into an oven at 90 ±2 °C for 7 days ±3 hours.

After the 7-day PCT, the vessels were removed from the oven and allowed to cool to room temperature. The final mass of the vessel and the solution pH were recorded on a data sheet. Each test solution was then filtered through a 0.45-µm-size filter and acidified with concentrated, high-purity HNO_3 to 1 vol% in a 1:4 ratio to assure that the cations remained in solution.

Normalized concentrations were calculated based on target compositions using the average of the logarithms of the leachate concentrations. The resulting solutions were analyzed by inductive coupled plasma-optical emission spectroscopy (ICP-OES) for Si, Na, Li and B. Samples of multi-element, standard solutions were also analyzed as a check on the accuracy of the ICP-OES. Normalized concentrations (NC, g L^{-1}) were calculated with the following formula:

$$1\mathrm{NC}_i = \frac{C_i}{f_i} \qquad 2.3$$

where: NC_i = the normalized concentration of element i in solution (g L^{-1})
C_i = the concentration of element I in solution ($g_i \cdot L^{-1}$)
f_i = mass fraction of element I in the glass ($g_i \cdot gglass^{-1}$)

Subsequently, the normalized losses (NL, g m^{-2}):

$$\mathrm{NL}_i = \frac{NC_i}{S/V} \qquad 2.4$$

where: S = glass surface area (m^2)
V = volume of solution (m^3)

Assuming a spherical particle geometry and a density of 2.65 $g \cdot cm^{-3}$, this results in a glass surface area:solution volume ratio of approximately 2000 m^{-1}. The ratio was not adjusted to account for measured glass density.

The calculations of NC_i and NL_i were based on target and measured glass compositions. The target composition was used for data evaluation and analysis. These results are discussed in Section 3.8.

2.12 Toxicity Characteristic Leaching Procedure

The TCLP was based on EPA Method 1311 and applied on quenched and CCC glasses. No surface area control was exercised beyond the one specified in Method 1311. All particles used in this procedure were < 5 mm, without further pretreatments. The ratio of sample to extraction fluid mass was maintained at 1:20; sample: fluid mass ratio was kept at 15:300 g. The samples were tumbled end-over-end for 18 ± 2 hours (campaign). Ambient temperature was maintained at 23 ± 2 °C. The TCLP tests for each glass were performed in duplicate, alongside round-robin tested standard glass 76-68. Parallel with each set of tests initiated on a given day, two blank vessels with only the extracting fluid were added. At the end of each campaign, the samples were filtered in their entirety, and an aliquot was taken for pH measurement (according to the SW-846 Method 9040C).

Upon processing, each campaign contained one matrix spike (MS) composed of the glass sample, the extraction fluid, and the quality control (QC) solution, and one blank spike (BS) composed only of the extraction fluid and the QC solution. The QC solutions were added after filtration and prior to acidification. Samples, MS, and BS were analyzed by inductive coupled plasma-mass spectroscopy (ICP-MS) and ICP-OES for the Resource Conservation, and Recovery Act (RCRA) watched elements, Ag, As, Ba, Cd, Cr, Ni, Pb, Se, alongside V [according to Memorandum on Vanadium (Chow 1998)] and B for the reference on the vitreous matrix durability.

Measured concentrations of the abovementioned elements were compared to maximum allowed concentrations for TCLP according to the RCRA limits and delisting limits, as listed in Table 2.8.

Table 2.8. TCLP delisting criteria for hazardous constituents.

Element	Ag	As	Ba	Cd	Cr	Hg	Ni	Pb	Se	V
RCRA toxicity limit (mg/L)[1]	5	5	100	1	5	0.2	-	5	1	-
RCRA UTS limit (mg/L)[2]	0.14	5	21	0.11	0.6	0.025	11	0.75	5.7	-
Delisting limit (mg/L)[3]	3.07	3.08	100	0.48	5	0.2	22.6	5	1	16.9
Vanadium Memo limit (mg/L)[4]	-	-	-	-	-	-	-	-	-	2

[1] Toxicity Characteristic (EPA 2006)
[2] UTS = Universal Treatment Standards, (EPA 2024)
[3] Hanford Immobilized HLW Delisting Petition (Cook and Blumenkranz 2003)
[4] Treatment of Underlying Hazardous Constituents in Toxicity Characteristic Metal (D004-D011) Wastes (Chow 1998)

MS and BS recovery were calculated according to the Eq. 2.5:

$$Percent\ recovery = \frac{c_s - c}{S} \times 100, \quad 2.5$$

where c_s is spiked sample concentration, c is sample background concentration, and S is concentration equivalent of spike added to sample

These results are discussed in Section 3.9.

2.13 Corrosion Testing of Refractory

It is known that the predictive life of the refractory ceramic liner of nuclear waste glass melters is conservative, as demonstrated by performance of these materials such as in the DWPF (Jin et al. 2023). The motivation for this task is to (1) maximize the useful life of the WTP melters, which in turn will minimize procurement and disposal costs and melter outage times, and (2) identify maximum loadings in the waste glass of those species that corrode melter components. This task was initiated jointly with PNNL to develop a methodology and model to enable more accurate prediction of refractory service life under prototypic conditions from laboratory-scale material corrosion tests.

Refractory corrosion is generally reported as physical material loss, measured in units of distance (e.g., inch) or as physical material loss rate, measured in units of distance per time (e.g., inch/day). In post-operational melters, the refractory corrosion is measured directly, sometimes reported as corrosion depth. Crucible tests are used in the laboratory to accelerate the refractory corrosion to facilitate a meaningful measurement in a commensurate amount of time. Crucible tests are particularly useful in understanding refractory corrosion across a large glass composition space, where operational testing would be prohibitive. Some of the critical parameters known to influence refractory corrosion by molten glass in a crucible test are temperature, system redox, molten salt phases, glass chemistry, and test duration.

The majority of data collected for Monofrax K-3 (hereafter referred to as K-3) corrosion is from crucible tests, but a small amount comes directly from scaled and production melters. Crucible test data has been collected under varying conditions, whereas data collected from operational melters is relatively less and represents conditions specific to the melter campaign. The result is that the published data can be grouped and analyzed in multiple ways, not all of which are readily comparable.

The *Standard Test Method for Isothermal Corrosion Resistance of Refractories to Molten Glass* (ASTM C621) outlines the general guidelines used across industry. That method describes a sealed, static test in which the surface area of the refractory coupon and the volume of glass are fixed. A significant portion of the crucible data pertaining to nuclear waste glasses has been collected in a modified configuration; the most notable differences being the surface area of the refractory coupon to volume of the glass and use of a method for bubbling the melt. To our knowledge, the influence of those parameters on the refractory corrosion has not been quantified.

In this work, it was determined that static tests and bubbled tests would be performed. SRNL was tasked with setting up and performing static testing while PNNL was tasked with setting up and performing bubbled testing.[1] Initial activities were performed to establish laboratory methods that reproduce data comparable to existing data sets of K-3 refractory corrosion by LAW and HLW glass compositions. Later activities were focused on refining the test parameters to establish a standard test practice to be used between laboratories and collecting additional data to be used in the enhanced waste glass model development.

K-3 test coupons and pre-melted glass were prepared at PNNL and provided to SRNL for use in testing. An initial set of 15 glass compositions were provided to SRNL. These coupons were first measured for acceptable dimension and tolerances. Coupons that out of specification were brought into tolerance or

[1] The purpose of bubbling melts in this work was to induce a fluid flow between the refractory coupon and the molten glass prototypic of that observed in the WTP melters. This flow rate and bubbler geometry was developed with the Idaho National Laboratory (INL). In addition to the static and bubbled tests, a dynamic test in which the refractory coupon is moved thru the molten glass was conducted at University of Chemistry and Technology in Prague, Czech Republic. Those tests were intended to provide insight into the effects of erosion that contribute to the measured corrosion profile. These activities are reported elsewhere.

discarded. Coupon dimensions were maintained at approximately 10 mm (0.39 inch) square by approximately 64 mm (2.5 inch) long. Dimensions were controlled to within 0.05 mm (0.002 inch) along the entire length of the specimen. Prior to use, prepared coupons were sonicated in deionized water for 5-10 minutes to remove loose material and surface contamination and subsequently dried.

Orientation of coupons was maintained for initial and post-test coupon measurements using a distinguishing feature on the coupon or a registration mark made above the expected glass line. Each test coupon was measured at a minimum of three locations along the length of the coupon; one measurement at the anticipated melt line: one measurement below the expected melt line, approximately half-way between the expected melt line and the bottom of the coupon; and one measurement well above the expected melt line. Width was measured at each location using a caliper.

Pt/Au alloy crucibles were used in this testing, all of equal dimension and nominally 100 mL working volume with an opening diameter of approximately 57 mm and a height of 58 mm. Testing was conducted by placing the refractory coupon directly on the bottom of the crucible. The melt line was estimated using a known volume of glass and was located approximately 20 mm from the bottom of the coupon. The coupon protruded beyond the top of the crucible and was held in place with either a Pt/Au alloy or Al_2O_3 lid with a pre-made hold to stabilize the coupon. In this manner, while the system was covered, it was not sealed to the atmosphere. Figure 2.8 shows a schematic of the setup.

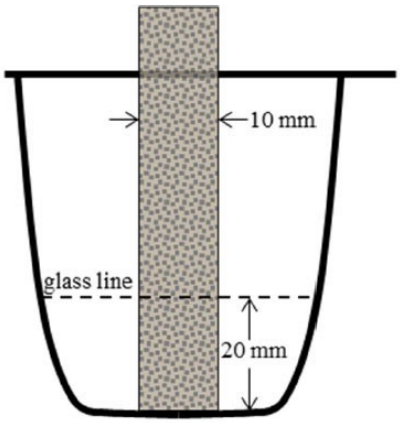

Figure 2.8. Schematic representation of the static crucible corrosion test configuration.

For each glass, a prepared refractory coupon was placed in the center of a Pt/Au alloy crucible. An appropriate amount of glass was added to the crucible, surrounding the coupon, to reach the targeted melt line. The estimated ratio of refractory surface area to glass volume was 0.27. A lid was fit to the crucible and coupon that was then loaded into a furnace at room temperature. The furnace was then heated nominally at 10 K/min to approximately 1208 °C.[1] The crucibles were held at temperature for 6 days. When the test duration time elapsed, the coupons were removed from the glass at temperature and allowed to cool.

After testing, the residual glass remaining in the coupons was removed using a hydrofluoric (HF) acid treatment. Coupons were submerged in HF acid and then rinsed in water for 15 minutes. The total time in HF acid for each coupon varied between 6-24 hours to remove the residual glass and expose the refractory for measurement.

[1] The temperature of 1208 °C was selected to facilitate comparison with existing data sets.

After removing the residual glass, the three positions on the coupon identified in Section 2.2 were established: the melt-line (g), the half-way line (h), and the top position above the melt-line (P1). The positions are shown schematically in Figure 2.9. All four faces at those locations were measured using a stereo optical microscope. The corrosion at a specific position was computed using the following equation:

$$P_c = \frac{[P-(p_1+p_2+p_3+p_4)/4]}{2}, \quad 2.6$$

where P_c = corrosion at position P, in mm, P = average width of coupon at position P before test, in mm, and $(p_1 + p_2 + p_3 + p_4)$ = width of the four faces of the cleaned coupon measured at position P after test, in mm.

To maintain a common nomenclature with the ASTM C621, neck-line (melt-line) corrosion is denoted with the letters G/g and half-way line corrosion is denoted with the letters H/h.

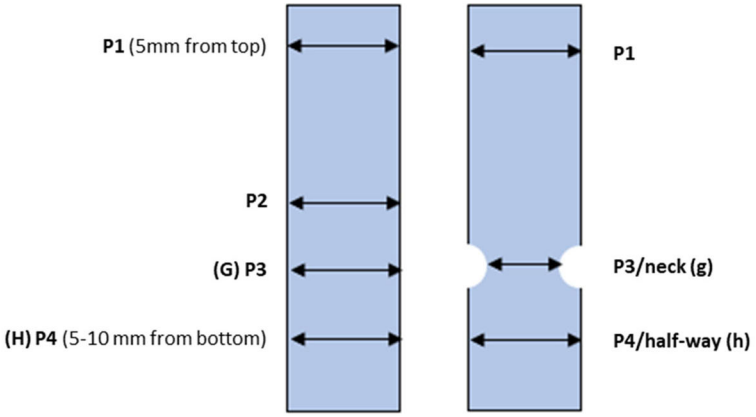

Figure 2.9. Schematic of refractory coupon position measurements before (left) and after (right) corrosion testing.

3.0 Results and Discussion

This section describes the results for the chemical composition, CCC, CF and T_L, sulfur solubility, density, viscosity, EC, PCT, and TCLP.

3.1 Glass Composition

Images of the quenched glasses after the second melt are given in Appendix B. The average of the duplicate measured components in weight percent in the quenched glasses are compared with the target compositions in Appendix C.

Overall, the measured sums of oxides for all glasses fell within the interval of 93.5 to 103.1 wt%, indicating acceptable recovery of the glass components. The main observations based on chemical analyses are summarized below.

The following was observed in the samples:

- Cl losses were from 17% to 30% across the samples.
- HLW-APPS-04-1, 09, 11, 12, and 15 retained > 90% of the target SO_3; the lowest retention was 62% in the HLW-APPS-07-2 sample.
- MgO relative differences were 10% or greater for HLW-APPS-03, 06, and 08.
- NiO relative differences were 10% or greater for HLW-APPS-01, 03, 05, 07, 09, 10, and 11.

Low values in the Cl, F, and SO_3 collected are attributed to the volatility of these species. The increase in MgO is due to impurities in the raw materials used to batch. Other discrepancies in the relative percentage difference between the target and measured values where the target is greater than or equal to 0.02 wt% found in B_2O_3, Bi_2O_3, Cr_2O_3, K_2O, MnO, Nd_2O_3, PbO, and ZrO_2 are attributed to experimental uncertainties. In the case of B_2O_3, the B is at the lower limit of detection of the instrument. For the others, the concentrations in the sample are small; therefore, there is greater variability due to the measurement uncertainty of small concentrations of EPMA.

The differences in Ni were explored further as they could not be attributed to experimental error since some of the samples were measured to high accuracy, including HLW-APPS-02, 04, 06, 08, 12, 13, and 14, as shown in Table 3.1. HLW-APPS-01, 03, 05, 07, 09, 10, and 11 have close to 100% loss of Ni. Any discrepancies in controllable batching, raw material source, and melting parameters were ruled out based on the detailed records kept.

Sample surfaces were analyzed using qualitative LIBS to investigate whether the error was in the analysis technique. While the technique in its current form is qualitative and all information from the technique is for information only (FIO), LIBS found the same large reductions in the Ni values in the same glasses as EPMA, specifically HLW-APPS-01, 05, 07, and 11 (Table 3.1). HLW-APPS-07 was re-batched and a similarly low value was again obtained by LIBS (Table 3.2).

Table 3.1. Average of 10 data points from EPMA and 4 data points from qualitative LIBS for weight percent NiO in each sample compared with the target composition. All LIBS data is FIO.

	EPMA			LIBS		
Sample	Target	Average Measured	RPD[(a)]	Target	Average Measured	RPD
HLW-APPS-01	0.34	0.00	-99%	0.34	0.03	-90%
HLW-APPS-02	0.58	0.55	-6%	0.58	0.74	28%
HLW-APPS-03	0.05	0.00	-99%	0.05	0.02	-57%
HLW-APPS-04-1	0.01	0.01	-70%	0.01	0.01	60%
HLW-APPS-05	0.14	0.01	-96%	0.14	0.02	-83%
HLW-APPS-06	0.34	0.35	4%	0.34	0.22	-36%
HLW-APPS-07-1	0.81	-	-	0.81	0.17	-79%
HLW-APPS-07-2	0.81	0.01	-99%	0.81	-	-
HLW-APPS-08	0.10	0.11	10%	0.10	0.10	-3%
HLW-APPS-09	0.03	0.00	-93%	0.03	0.01	-51%
HLW-APPS-10	0.05	0.00	-94%	0.05	0.09	74%
HLW-APPS-11	0.17	0.00	-100%	0.17	0.02	-86%
HLW-APPS-12	0.14	0.15	7%	0.14	0.12	-15%
HLW-APPS-13-1	0.08	0.00	98%	0.08	0.08	9%
HLW-APPS-14	0.02	0.02	9%	0.02	0.03	59%
HLW-APPS-15	0.00	0.01	106%	0.00	0.02	490%

[(a)]RPD = relative percentage difference

Table 3.2. Average of 4 data points from qualitative LIBS for weight percent NiO in a re-batched version of HLW-APPS-07-2 compared with the target composition. All LIBS data is FIO.

	LIBS		
Sample	Target	Average Measured	RPD
HLW-APPS-07-2	0.81	0.03	-96%

RPD = relative percentage difference

Further investigation involved checking a sample after the first melt. HLW-APPS-01 was re-batched as a powder and melted at 1150 ℃ for 1 hour only. The poured glass was measured by qualitative LIBS and the same result was found; however, on breaking the remaining glass from the crucible, it was observed that a metallic sheen was coating the surface in contact with the crucible wall but not the region in contact with air (Figure 3.1). The Ni concentrations as measured by qualitative LIBS in the two surfaces are reported in Table 3.3. An order of magnitude increase in the Ni concentration at the crucible-wall interface suggests that the Ni is lost during the melting to the crucible wall and is unrecoverable after the second melt.

Figure 3.1. Surface of sample of HLW-APPS-01-1st melt that quenched in contact with the air (left) and platinum crucible wall (right).

Table 3.3. Qualitative LIBS-measured concentrations of Ni on the air- and crucible-contact surfaces of HLW-APPS-01 after the first melt. All LIBS data is FIO.

Sample Region	Average Measured
HLW-APPS-01-1st melt poured sample	0.04
HLW-APPS-01-1st melt crucible wall contact	0.41

3.1.1 Secondary Phase Investigation in Quenched Glasses

Detailed recorded observations of the glasses after the second and final melt are reported in Table 3.4, with a summary of the crystalline phases identified by XRD. Eskolaite (Cr_2O_3) was found in HLW-APPS-05 and -06, which were both glasses highest in Cr_2O_3. Traces of crystalline peaks were found in the XRD pattern of HLW-APPS-01, Appendix D, but they were not defined enough for phase identification.

Table 3.4. Details on quenched glasses after the second and final melt and crystal phases identified from XRD patterns.

Glass Sample ID	Visual Observations/Optical Microscopy	Secondary Phase Identified by XRD[(a)]
HLW-APPS-01	Crystals	< DL[(b)]
HLW-APPS-02	On surfaces	Amorphous
HLW-APPS-03	None	Not measured
HLW-APPS-04-1	None	Amorphous
HLW-APPS-05	Crystals and phase separation on pouring	Eskolaite (3.55 wt%)
HLW-APPS-06	Crystals	Eskolaite (0.95 wt%)
HLW-APPS-07-2	Phase separation on pouring	Sodium sulfate (11.52 wt %)
HLW-APPS-08	None	Not measured
HLW-APPS-09	None	Not measured
HLW-APPS-10	Small on surfaces	Amorphous
HLW-APPS-11	Small on surfaces	Amorphous
HLW-APPS-12	On surfaces	Amorphous
HLW-APPS-13-1	Small on surfaces	Amorphous
HLW-APPS-14	None	Not measured
HLW-APPS-15	Crystals, S salts on crucible walls after first melt	Amorphous

(a) Some crystal concentrations are higher than possible based on glass composition; this is attributed to inhomogeneous distribution of crystals in the samples.
(b) DL = detection limit. Crystal content lower than XRD detection limit.

HLW-APPS-07-2 contained Na_2SO_4 crystals as determined by XRD, and the sample appeared visibly multiphase on pouring of the quenched glass. Therefore, the form of the apparent phase separation was further explored by SEM. Micrographs were taken at the top surface of the sample and on the bottom surface (the surface that quenched on the plate first). The image taken of the bottom surface of the sample which first came into contact with the quench plate on pouring, Figure 3.2 (left), showed homogeneous material, whereas the top surface of the sample that appeared opalescent and greener than the bottom showed regions of inhomogeneity, Figure 3.2 (right). At higher magnification shown in Figure 3.3, a dendrite crystalline phase is clear as are multiple other phases, including brighter contrast spots connected by darker contrast channels within a medium contrast matrix.

To achieve micrographs of this quality showing resolved sub-micron phases, the working distance used was 4 to 6 mm. This meant that there was not enough distance for accurate resolution of the X-rays detected from within the sample for electron dispersive spectroscopy to identify changes in the composition between the different phase separated regions. Further investigation would be required to identify the composition of the multiple phases present. However, the morphology is consistent with alkali-sulfate salts previously seen on the surfaces of glass samples, which is consistent with XRD results.

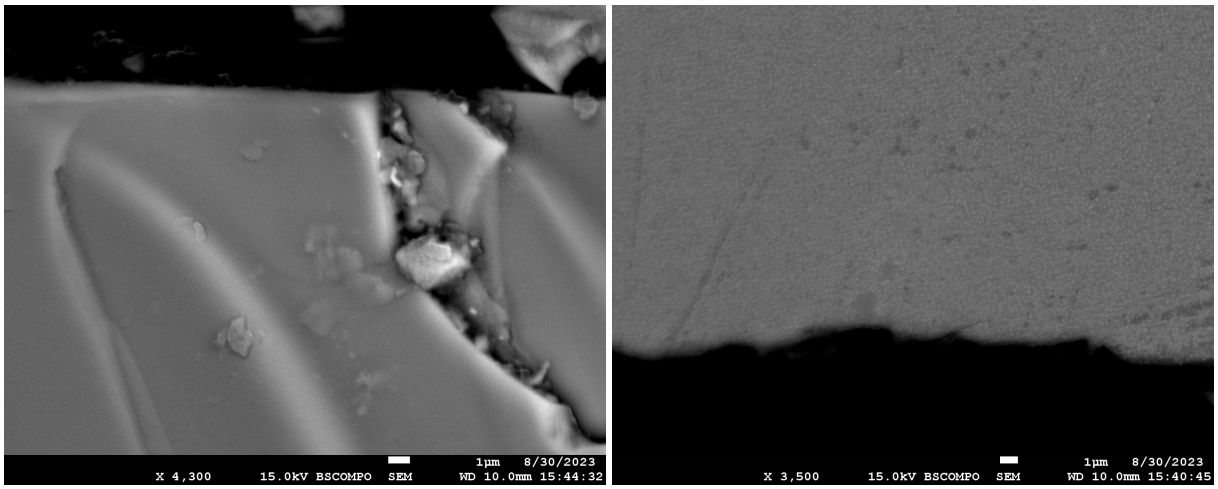

Figure 3.2. SEM micrograph of the bottom (quench plate contact) surface at 4.3 K× magnification (left) and top phase separated region at 3.5 K× magnification (right) of HLW-APPS-07-2 sample.

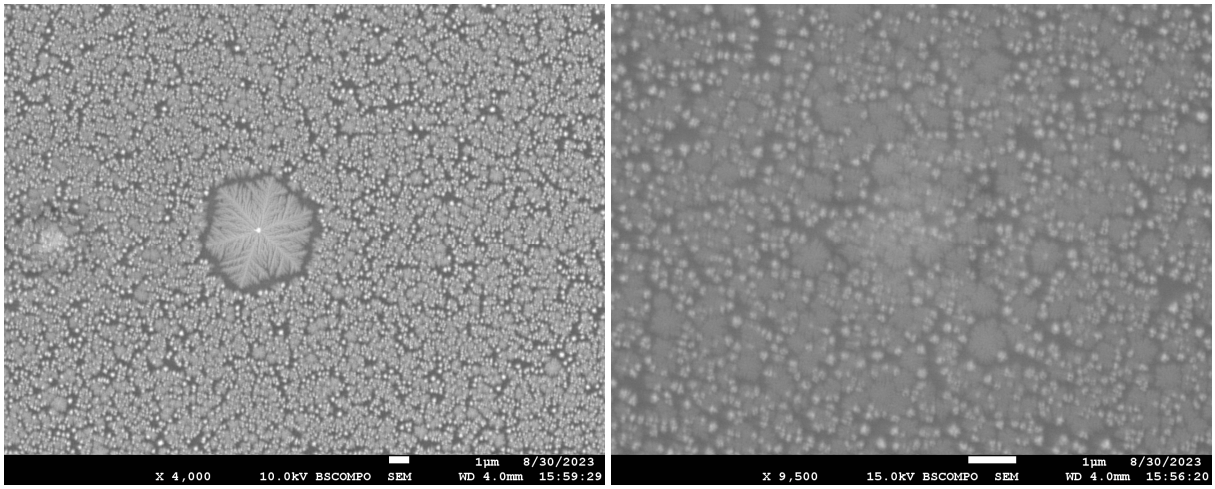

Figure 3.3. SEM micrograph of the phase separated region at 4K× magnification (left) and at 9.5 K× magnification (right) of HLW-APPS-07-2 sample.

3.2 Crystal Identification in Canister Centerline Cooling Glasses

The slow cooling of the molten glass in the canister core might impact glass durability by changing the residual glass composition (Kim et al. 1995; Kroll et al. 2019). Not all crystals affect durability in the same way, so identifying the crystal content after CCC is an important step toward understanding crystallization impacts on glass durability. Moreover, property-prediction models were formulated using quenched data; therefore, differences of glass durability responses after CCC via PCT and TCLP should be evaluated.

This section presents and discusses the CF results from CCC glasses obtained using the methods discussed in Section 2.5. The effects of CCC on PCT and TCLP are reported in Sections 3.8 and 3.9, respectively.

A total of 40% of the glasses were homogeneous after CCC (identified as amorphous in Table 3.5). Of the remaining glasses, three had CF ≤ 1 wt%, four had CF ≤ 4 wt% and the rest presented CF > 5 wt%. Two glasses (-05 and -06) formed > 20 wt% of nepheline. XRD analysis identified a range of different crystal phases. The XRD phases and wt% crystallinity results are summarized in Table 3.4.

Table 3.5. Crystal fraction in wt% and identification of crystals by XRD in CCC glasses.

Glass ID	Wt% Crystallinity	Crystal Phase Identification
HLW APPS-01	1	Magnetite (Fe_3O_4)
HLW APPS-02	1.4 1.1	Magnetite (Fe_3O_4) Fluorapatite ($Ca_5[PO_4]_3F$)
HLW APPS-03	0	Amorphous
HLW APPS-04-1	0	Amorphous
HLW APPS-05	22.1 3.4 0.6	Nepheline ($NaAlSiO_4$) Buchwaldite ($NaCaPO_4$) Eskolaite (Cr_2O_3)
HLW APPS-06	22.5 0.3	Nepheline ($NaAlSiO_4$) Eskolaite (Cr_2O_3)
HLW APPS-07-2	2.7 1.6 1.4	$Na_3Nd(PO_4)_2$ Vanadium Phosphate ($[VO]_2P_2O_7$) Srebrodolskite ($Ca_2Fe_2O_5$)
HLW APPS-08	0	Amorphous
HLW APPS-09	0	Amorphous
HLW APPS-10	0	Amorphous
HLW APPS-11	0.7	Combeite ($Na_2Ca_2Si_3O_9$)
HLW APPS-12	0.4	Combeite ($Na_2Ca_2Si_3O_9$)
HLW APPS-13-1	1.8	Combeite ($Na_2Ca_2Si_3O_9$)
HLW APPS-14	2.1	Combeite ($Na_2Ca_2Si_3O_9$)
HLW APPS-15	0	Amorphous

The most commonly detected crystal phase across all compositions was combeite ($Na_2Ca_2Si_3O_9$), followed by nepheline ($NaAlSiO_4$), magnetite (Fe_3O_4), and eskolaite (Cr_2O_3).

Combeite formed in HLW-APPS-11, 12, 13, and 14 – glasses with the highest amount of Na and among the highest for Ca. Nepheline was observed in glasses with high levels of Al and Na (-05 and -06).

Magnetite was found in glasses HLW-APPS-01 and -02, which had the highest Fe_2O_3 content. Eskolaite was found in glasses HLW-APPS-05 and -06, which had highest content of Cr_2O_3. Glasses HLW-APPS-02, -05, and -07-2 contained some form of phosphate phase even though the F content was not among the highest of the glass matrix (Table 2.4). Very large crystals were observed in the CCC sample of glass HLW-APPS-13-1, as shown in Figure 3.4. The crystals were found to be combeite, but the low CF (1.8 wt%) found from using a small sample size (1 g) seemed to be out of line with the visual appearance of the CCC glass. A second sample was analyzed by XRD using ~2 g of the material that was visually confirmed to contain a representative amount of the crystals and glass. This repeat resulted in 1.1 wt% combeite, which is in agreement with the first sample, thus confirming validity of the CF reported in Table 3.5.

Images of glasses after CCC and XRD scans when applicable are in Appendix E.

Figure 3.4. HLW-APPS-13-1 glass with large crystals after CCC.

3.3 Crystal Fraction and Liquidus Temperature

The long idling of the left-over glass in the melter at low temperatures might promote crystal formation, impacting both glass durability by sequestering GFCs, and/or glass processability by settling in the melter clogging the pour sprout (Vienna et al. 2001). Therefore, the study of crystalline phases, quantities, and T_L in isothermal heat-treatments is part of the regular investigation of HLW glasses.

This section presents and discusses the CF and T_L results obtained using the methods discussed in Section 2.6.

The majority of the glasses have a T_L below 900 °C, and only three have a T_L above 950 °C. Table 3.6 summarizes the temperatures run, CF (wt%), phases identified, and T_L values. Note that T_L is calculated based on the primary phase only.

Table 3.6. Crystal fraction in wt%, identification of crystals, and T_L for isothermally heat-treated glasses.

Glass ID	Temp (°C)	CF (wt%)	Crystal Phase Identification	T_L (°C)	C_{950}, vol%
HLW-APPS-01	750	1	Magnetite (Fe_3O_4)	< 950	-
	850/24 h	0.4	Magnetite (Fe_3O_4)		-
	900	0.2	Magnetite (Fe_3O_4)		-
HLW-APPS-02	850/24 h	0	None	< 850	-
HLW-APPS-03	850/24 h	0	None	< 850	-
HLW-APPS-04-1	850/24 h	0	None	< 850	-
HLW-APPS-05	850/24 h	3.4, 0.7	Buchwaldite ($NaCaPO_4$), Eskolaite (Cr_2O_3)	1186.8	-
	900	2.8, 0.6	Buchwaldite ($NaCaPO_4$), Eskolaite (Cr_2O_3)		-
	950	2.4, 0.5	Buchwaldite ($NaCaPO_4$), Eskolaite (Cr_2O_3)		2.01+0.27
HLW-APPS-06	750	0.3, 5.8, 0.4	Eskolaite (Cr_2O_3), Nepheline ($NaAlSiO_4$), Lazurite 1C [$Na_7Ca(Al_6Si_6O_{24})(SO_4)(S_3)$]	977.37 using 850 °C/24 h 975.58 using 850 °C/48 h	
	850/24 h	0.3, 0, 0.1	Eskolaite (Cr_2O_3), Nepheline ($NaAlSiO_4$), Lazurite 1C [$Na_7Ca(Al_6Si_6O_{24})(SO_4)(S_3)$]		
	850/48 h	0.2, 0.2, 0.1	Eskolaite (Cr_2O_3), Nepheline ($NaAlSiO_4$), Lazurite 1C [$Na_7Ca(Al_6Si_6O_{24})(SO_4)(S_3)$]		
	900	0.2	Eskolaite (Cr_2O_3)		
	950	0.1	Eskolaite (Cr_2O_3)		0.03
HLW-APPS-07-2	850/48 h	1.8, 1.2	$Na_3Nd(PO_4)_2$, Srebrodolskite ($Ca_2Fe_2O_5$)	Indeterminate - SEM confirms that crystal phases are reasonable, and srebrodolskite may be acting as a nucleating agent for the $Na_3Nd(PO_4)_2$	-
	900	1.7, 1.1	$Na_3Nd(PO_4)_2$, Srebrodolskite ($Ca_2Fe_2O_5$)		-
	950	1.9, 1	$Na_3Nd(PO_4)_2$, Srebrodolskite ($Ca_2Fe_2O_5$)		1.28+0.69
	1050	2.7, 1.7	$Na_3Nd(PO_4)_2$, Srebrodolskite ($Ca_2Fe_2O_5$)		-
	1150	2.7, 1.6	$Na_3Nd(PO_4)_2$, Srebrodolskite ($Ca_2Fe_2O_5$)		-
HLW-APPS-08	850/24 h	0	None	< 850	-
HLW-APPS-09	850/24 h	0	None	< 850	-
HLW-APPS-10	750	19.0	Combeite ($Na_2Ca_2Si_3O_9$)	908.5	-
	850/24 h	5.9	Combeite ($Na_2Ca_2Si_3O_9$)		-
	900	1.7	Combeite ($Na_2Ca_2Si_3O_9$)		-
	950	0	None		-
HLW-APPS-11	750	16.7	Combeite ($Na_2Ca_2Si_3O_9$)	1033.2	-
	850/24 h	10.8	Combeite ($Na_2Ca_2Si_3O_9$)		-
	900	7.5	Combeite ($Na_2Ca_2Si_3O_9$)		-
	950	0	None		-
HLW-APPS-12	750	13.5	Combeite ($Na_2Ca_2Si_3O_9$)	915.3 using 850 °C/24 h 915.7 using 850 °C/48 h	-
	850/24 h	7.1	Combeite ($Na_2Ca_2Si_3O_9$)		-
	850/48 h	7.6	Combeite ($Na_2Ca_2Si_3O_9$)		-
	900	0.5	Combeite ($Na_2Ca_2Si_3O_9$)		-
HLW-APPS-13-1	750	13.4	Combeite ($Na_2Ca_2Si_3O_9$)	919.7 using 850 °C/24 h 919.5 using 850 °C /48 h	-
	850/24 h	10.0	Combeite ($Na_2Ca_2Si_3O_9$)		-
	850/48 h	10.0	Combeite ($Na_2Ca_2Si_3O_9$)		-
	900	0.9	Combeite ($Na_2Ca_2Si_3O_9$)		-
HLW-APPS-14	750	15.0	Combeite ($Na_2Ca_2Si_3O_9$)	949.4 using 850 °C/24 h 949.3 using 850 °C/48 h	-
	850/24 h	11.0	Combeite ($Na_2Ca_2Si_3O_9$)		-
	850/48 h	10.9	Combeite ($Na_2Ca_2Si_3O_9$)		-
	900	2.4	Combeite ($Na_2Ca_2Si_3O_9$)		-
	950	0.2	Combeite ($Na_2Ca_2Si_3O_9$)		0.20
HLW-APPS-15	850/24 h	0.2	Nosean [$Na_8Al_6Si_6O_{24}(SO_4)$]	< 900	-
	850/48 h	0.4	Nosean [$Na_8Al_6Si_6O_{24}(SO_4)$]		-
	900	0	None		-

HLW-APPS-02, -03, -04-1, -08, and -09 were found to be amorphous by XRD at 850 °C, and therefore the T_L could be easily bound by < 850 °C. This is well below the melter pour-spout temperature of concern during idling (950 °C), so no additional analysis was run for these compositions.

Initially, the 850 °C isothermal heat treatments were held for 24 hours rather than the recommended 48 hours from the ASTM C1720. To verify that the length of the heat treatment did not affect the crystal content or T_L identification, several glasses were re-run for the recommended 48-hour hold. Specifically, HLW-APPS-06, -12, -13-1, and -14 were selected because they presented a slightly non-linear fit between temperatures and crystal content (Appendix F). As can be noted in Table 3.6, the CFs for these compositions are nearly identical between the 24- and 48-hour hold times at 850 °C. Furthermore, the T_L values for the two hold times are also nearly identical for each of the glasses verified. One notable variation was the formation of nepheline (0.2 wt%) in HLW-APPS-06 after the 48-hour hold, which was not observed after 24 hours. Overall, the differences were deemed to be within the experimental error; therefore, the rest of the glasses held for 24 hours at 850 °C were not remeasured. HLW-APPS-15 was also run with a 48-hour hold at 850 °C, as the 24-hour hold had only 0.2 wt% nosean. The crystal content did not change significantly (0.4% nosean). Since this sample was found to be amorphous by XRD at 900 °C, T_L is reported as < 900 °C.

HLW-APPS-07-2 appeared to be a problematic glass. XRD on this sample resulted in crystal content increasing with temperature. T_L is listed as “indeterminate” because it is impossible to predict its value when crystal content continues increasing with temperature. SEM and energy dispersive spectroscopy (EDS) were performed on the 850, 900, and 1150 °C to determine if crystals were forming upon cooling. Figure 3.5 shows a full-width micrograph montage for each of the 850, 900, and 1150 °C samples. It is apparent that the crystals are uniformly distributed across the width of the sample and not just in the bulk, suggesting that they are not forming on cooling. The amount of crystals was confirmed to be increasing with temperature. While the 1150 °C temperature appeared uniform in this low-magnification montage, increasing the magnification reveals a very large concentration of fine crystals within the sample (Figure 3.6). EDS of these samples indicates that the phases selected are reasonable.

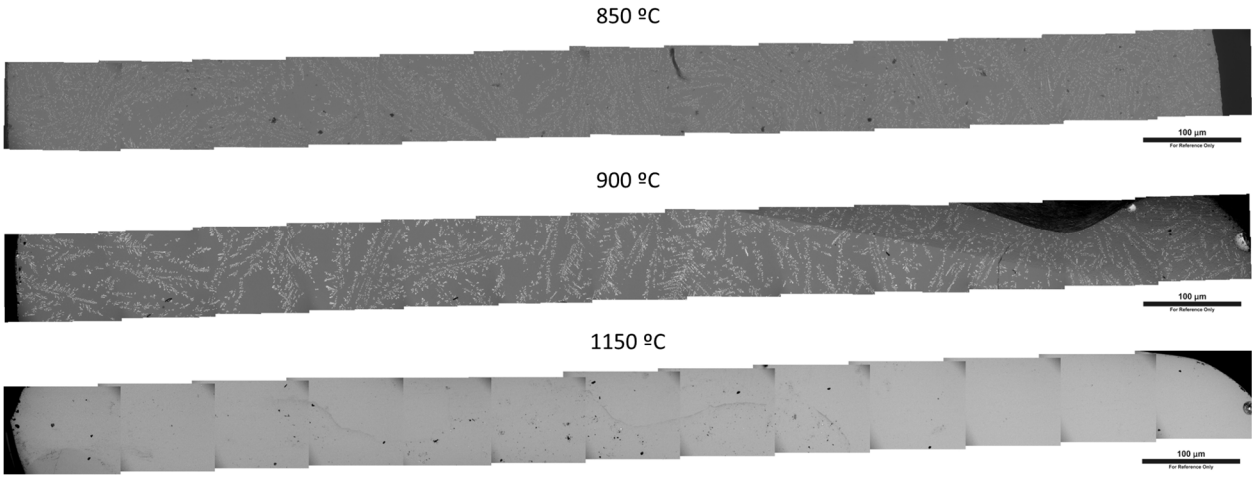

Figure 3.5. HLW-APPS-07-2 SEM of crystal distribution across the sample width.

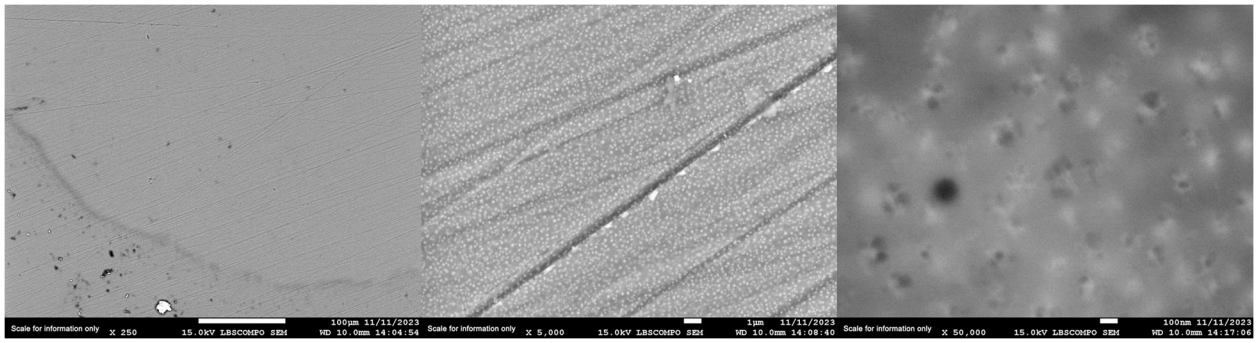

Figure 3.6. HLW-APPS-07-2 isothermally heat treated to 1150 °C SEM at 250×, 5K×, and 50K×.

Figure 3.7 shows the 900 °C isothermal heat treated HLW-APPS-07-2 sample at an intermediate magnification, and the same location with overlays indicating where spectra were collected to determine composition.

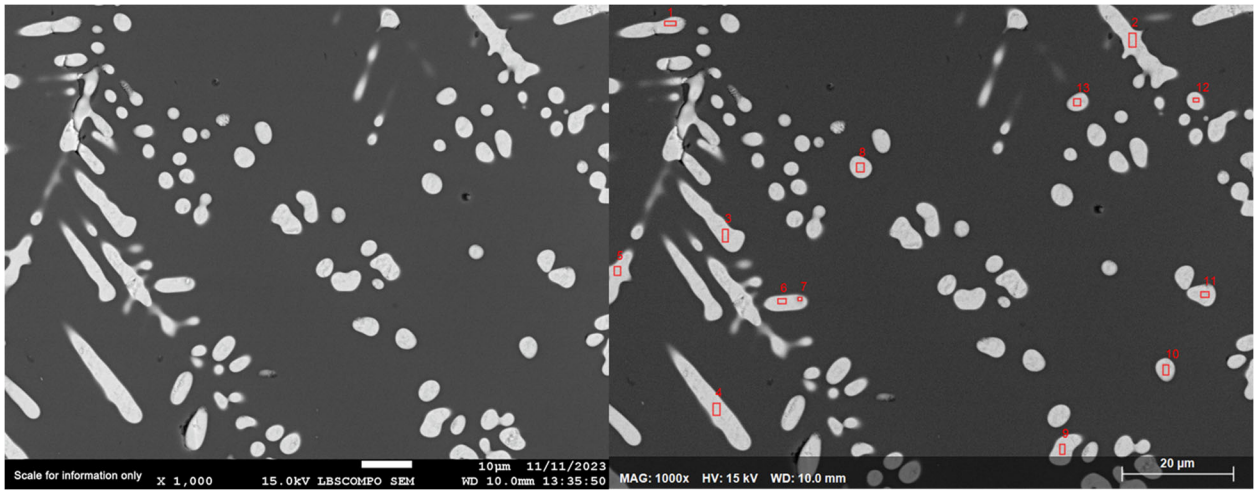

Figure 3.7. HLW-APPS-07-2 900 °C original image (left) and with EDS locations overlaid (right).

Table 3.7 summarizes the elements detected in each location in weight percentage. It is apparent that the large crystals contain Nd, P, Na, and O, indicating that the $Na_3Nd(PO_4)_2$ phase is reasonable. If EDS location 7 found in Figure 3.7 (right) and that region of the original image, Figure 3.7 (left) are overlaid, it can be observed that there appears to be a small bright region surrounded by the bulk of the crystal (EDS location 6). EDS location 6 in Table 3.7 is $Na_3Nd(PO_4)_2$ as expected; however, EDS location 7 is elevated in Fe and K. This likely indicates that $Ca_2Fe_2O_5$ is not correct and should be a potassium iron oxide with the same crystal structure; however, a suitable phase was not found in the XRD database during analysis.

Table 3.7. EDS weight % of detected elements for HLW-APPS-07-2 from 900 °C isothermal heat treatment.

Spectrum	O	Na	Al	S	P	S	K	Ca	V	Fe	Nd
1	33.43	15.96	3.44	4.97	12.62	0.61	0.18	12.85	0.77	0.79	14.38
2	33.42	15.86	3.25	4.91	12.34	0.52	0.27	12.80	0.67	0.82	15.16
3	33.06	15.40	3.56	5.36	13.28	0.52	0.16	13.16	0.59	0.88	14.05
4	32.91	15.46	3.23	4.70	12.45	0.51	0.24	12.40	0.77	0.86	16.48
5	32.89	16.82	3.16	4.68	12.38	0.48	0.19	12.40	0.69	0.80	15.51
6	32.58	16.68	3.16	4.67	12.40	0.50	0.14	12.50	0.69	0.75	15.94
7	33.93	14.55	3.92	4.88	11.95	0.45	1.69	10.70	0.80	2.81	14.32
8	32.97	15.58	3.67	5.22	12.82	0.49	0.17	13.41	0.59	0.91	14.17
9	32.62	15.30	3.32	4.98	12.84	0.65	0.18	12.41	0.81	0.74	16.16
10	33.57	17.19	3.68	5.39	11.13	0.49	0.20	12.28	0.96	0.91	14.20
11	32.63	14.70	3.72	5.38	13.01	0.58	0.19	13.10	0.74	1.00	14.95
12	32.66	15.81	3.37	4.86	12.16	0.52	0.25	12.62	0.81	0.96	15.97
13	33.42	16.19	3.65	5.34	12.21	0.46	0.19	12.82	0.70	0.86	14.16

Only two glasses were found to have T_L values over 1000 °C: HLW-APPS-05 and -07-2 (since it had crystals observed at 1050 and 1150 °C). Only four glasses (HLW-APPS-05, -06, -07-2, and -14) had measurable crystals at 950 °C – 2.1 vol%, 0.2, 1.9, and 0.8, respectively. The conservative WTP limit of 1 vol% (Vienna and Kim 2014) was proposed to be increased to a less conservative 2 vol% (Vienna et al. 2016). So, glasses HLW-APPS-05 and -07-2 are borderline.

Images of glasses after heat treatment and XRD scans when applicable are in Appendix E.

3.4 SO_3 Solubility

SO_3 solubility or SO_3 saturation concentration is controlled to avoid excessive corrosion of melter materials at the melt-line. Sulfur, expressed as SO_3, is a problematic component in nuclear waste glasses due to its limited solubility in borosilicate melts compared to the concentration of sulfur in Hanford tank wastes (Jin et al. 2019).

SO_3 solubilities are determined by measuring SO_3 concentrations in glasses that have been saturated with SO_3 by melting previously made glasses with excessive Na_2SO_4 multiple times. Jin et al. (2019) determined that crushing and mixing 50 g of quenched glass with 3.82 g of Na_2SO_4 (equivalent to 4 wt% of SO_3 in glass if fully dissolved and in the melt) and melting the mixture three times is sufficient to completely saturate SO_3 in the glass without excessive volatile losses. The third and final melt, known as the sulfur-saturated melt (SSM), is crushed, sieved, and washed to remove excess sulfate, and then its composition is analyzed.

The procedure used in this study varied slightly from the procedure historically used at PNNL for this test. Figure 3.9 summarizes the steps used in the historical and present procedures. In the steps leading to the fabrication of the third melt (i.e., the SSM), the present procedure requires that each melt be crushed directly to fines as opposed to incremental crushing and sieving sessions to produce fines. This change was implemented to save time and effort as the particle size is irrelevant between melts and both methods lead to the same number of fines. Other major differences in the procedures arise from the different analysis methods used to determine SO_3 saturation concentrations. Previously, washed solids and rinse solutions were analyzed by ICP-OES and the SO_3 saturation concentration was determined by mass

balance calculations using laboratory mass measurements and the measured ICP-OES concentrations. EPMA is currently used to measure SO_3 directly as the results are obtained quicker and at lower cost. Also, if any salts are dissolved in the glass, EPMA will identify those and only quantify the glass phase. Previously, the SSM glass was crushed and sieved to generate fines to maximize glass surface area exposed to water during the washing steps. EPMA requires particles that are large enough to be analyzed completely by the probe's beam. Thus, the SSM glass is crushed and sieved to a particle size range appropriate for EPMA analysis while still maximizing the surface area of the glass exposed to water during the washing steps.

A comparison of SSM glasses analyzed by EPMA and ICP-OES was performed on a previous set of glasses (Lu et al. 2024) to determine whether EPMA was a suitable substitution method for ICP-OES. The results are provided in Figure 3.8. The uncertainties are represented by an experimental SSM pooled standard deviation ($SD_{pooled,SSM}$ = 0.1548 wt %) determined from glasses analyzed with ICP-OES. This measure includes uncertainties in glass batching and melting, saturation of the melt, washing of the glass, and chemical analyses performed by different laboratories over a roughly 5-year period. The uncertainties in EPMA measurements are the standard deviation for the average measurements (SD_{EPMA}) for each glass. Note that the SD_{EPMA} does not include all the sources of uncertainty that are captured in the $SD_{pooled,SSM}$ and so does not represent the full experimental error. In all instances, the SO_3 concentrations measured by ICP-OES were slightly higher than those measured by EPMA. The increased ICP-OES concentrations were assumed to be caused by SO_3 in small sulfate salt crystals trapped within the washed glass particles. The glass particles are completely dissolved for ICP-OES analysis whereas EPMA analyzes only the surface of the glasses and trapped sulfate salts can be avoided. Regardless, since EPMA consistently provides lower concentrations of SO_3, the results are more conservative than those from ICP-OES.

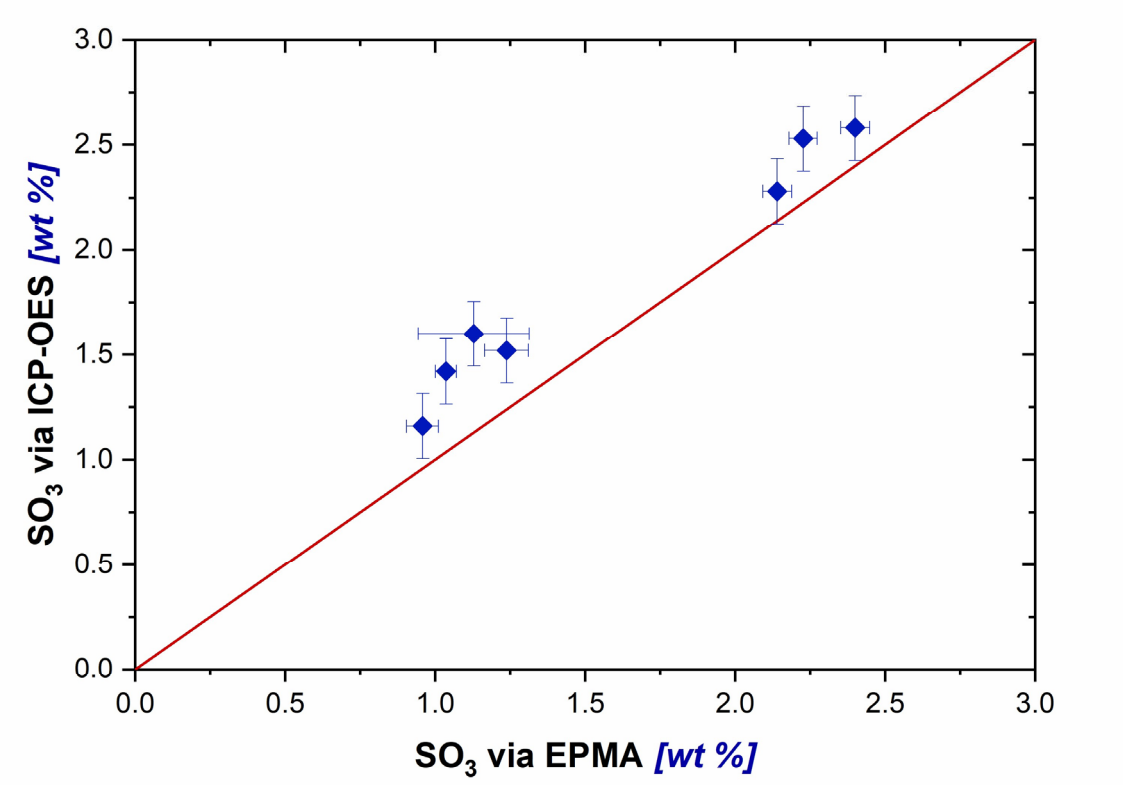

Figure 3.8. Comparison of SO_3 solubility concentrations determined via ICP-OES and EPMA for select glasses from the first machine learning matrix. Uncertainties are represented by $SD_{pooled,SSM}$ for the ICP-OES data and SD_{EPMA} for the EPMA data.

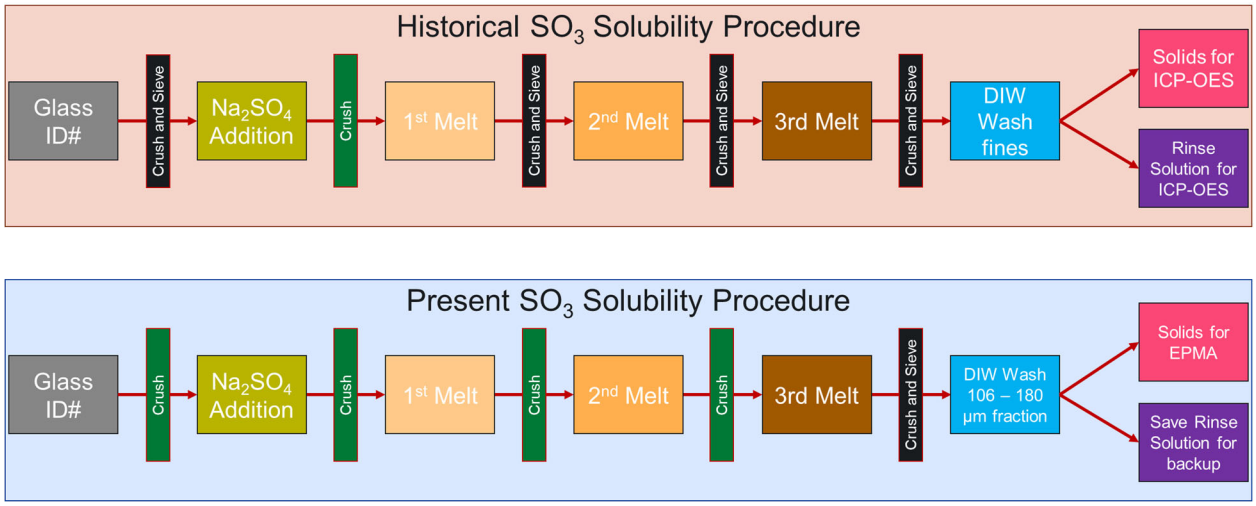

Figure 3.9. Summary of historical and present SO_3 solubility procedures.

3.4.1 SSM SO_3 Concentrations

For each HLW-APPS glass, an excess sulfate phase was observed in all three melts as seen for HLW-APPS-05 in Figure 3.10 as an example. An excess phase is expected as the amount of Na_2SO_4 added exceeds the conservative sulfur limit for the WTP used in the 2012 algorithm by more than 5× (4 wt% vs. 0.77 wt% SO_4) (Kim et al. 2012). However, while the excess phase may form for the first two melts, Jin et al. (2019) provided evidence that the glass is not completely saturated with SO_3 until the third melt.

Figure 3.10. Photos of the three melts (left to right: melts 1, 2, and 3, i.e., the SSM) for HLW-APPS-05.

The compositions of the washed SSM DFHLW APPS glasses were measured via EPMA, and the SO_3 concentrations are recorded in Table 3.8. The SO_3 concentrations range from 0.87 to 2.80 wt%.

Table 3.8. Measured SO_3 concentrations (wt%) of sulfur saturate glass melts from the DFHLW APPS matrix.

Glass ID	SO_3 Content (wt%)
HLW-APPS-01-SSM	0.87
HLW-APPS-02-SSM	0.93
HLW-APPS-03-SSM	1.19
HLW-APPS-04-SSM	2.80
HLW-APPS-05-SSM	1.25
HLW-APPS-06-SSM	0.93
HLW-APPS-07-SSM	1.31
HLW-APPS-08-SSM	1.40
HLW-APPS-09-SSM	1.96
HLW-APPS-10-SSM	1.90
HLW-APPS-11-SSM	2.17
HLW-APPS-12-SSM	2.51
HLW-APPS-13-SSM	2.16
HLW-APPS-14-SSM	2.48
HLW-APPS-15-SSM	2.00

The SO_3 concentration was higher in the SSM glass than the quench glass for every glass, as shown in Figure 3.11, indicating that all original glasses were formulated with SO_3 concentrations below their saturation limits despite the observation of undissolved salt in APPS-07-2. Thus, the algorithm used to generate the glass compositions does not require further limiting constraints based on SO_3 solubility; rather, the SO_3 solubility constraint could be loosened to allow more SO_3 into glass compositions in future matrices based on this data.

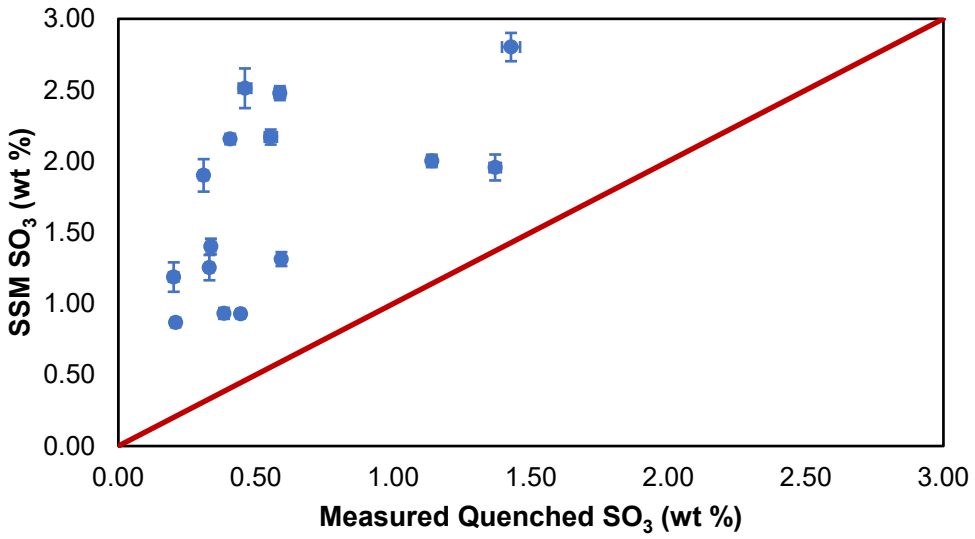

Figure 3.11. Measured SO_3 concentration in SSM and quenched glasses for the DFHLW APPS matrix. Uncertainties are represented by SD_{EPMA}.

3.4.2 Comparisons to Predicted SO_3 Saturation Concentrations

The SO_3 saturation concentrations determined experimentally for the DFHLW APPS matrix were compared to SO_3 saturation concentrations predicted from various existing models. Table 3.9 lists the available models with predicted SO_3 saturation concentration capabilities. All models were constructed using experimental data from multiple measurement methods (e.g., 3TS, bubbling, melter tolerance, batch saturation, and saturation re-melting) except the new model, which incorporates the 3TS HLW-APPS data with existing 3TS data, resulting in a model that used 3TS data exclusively (LAW 3TS only). Some of the models constructed with data from multiple measurement methods have offset values available to allow direct comparisons to experimental 3TS data and predicted values from models constructed with only 3TS data.

Table 3.9. Available glass property models with predicted SO_3 saturation concentrations.

Model Description	Offset Values for 3TS	Units for Predicted Values	References
LAW SO_3 model	0.540[(a)]	wt %	Vienna et al. 2014
Combined SO_3 model	0.216	wt %	Vienna et al. 2013
LAW SO_3 model	0.540[(a)]	wt %	Vienna et al. 2016
LAW SO_3 model, no offset	0.3938	wt %	Vienna et al. 2022b
HLW SO_3 model	NA	wt %	Vienna et al. 2016
Unspecified SO_3 model	NA	wt %	Muller et al. 2018
LAW 3TS only SO_3 model	NA	wt %	This work

(a) Offset values are cited from Skidmore et al. 2019.

Figure 3.12 provides a one-to-one comparison of the measured and predicted SO_3 solubilities using the models in Table 3.9 for the HLW-APPS glasses. Although all experimental SO_3 solubilities were determined by EPMA; $SD_{pooled,SSM}$ was used to represent uncertainty for measured SO_3 solubilities as it is more comprehensive than SD_{EPMA}. Models that included offset values for 3TS (indicated in Figure 3.12) resulted in a slight rise in the predicted values (shift to the right in Figure 3.12) compared to values determined without the offsets and from models constructed with multiple measurement methods. Even with offsets included, the models constructed with data from multiple methods don not perform well, whereas the LAW 3TS only model was consistent with the measured solubilities except between 1 and 1.75 wt%, where it overestimated solubilities. Overall, the LAW 3TS only model was more consistent with the experimental results, implying that future models should rely solely on 3TS data during construction.

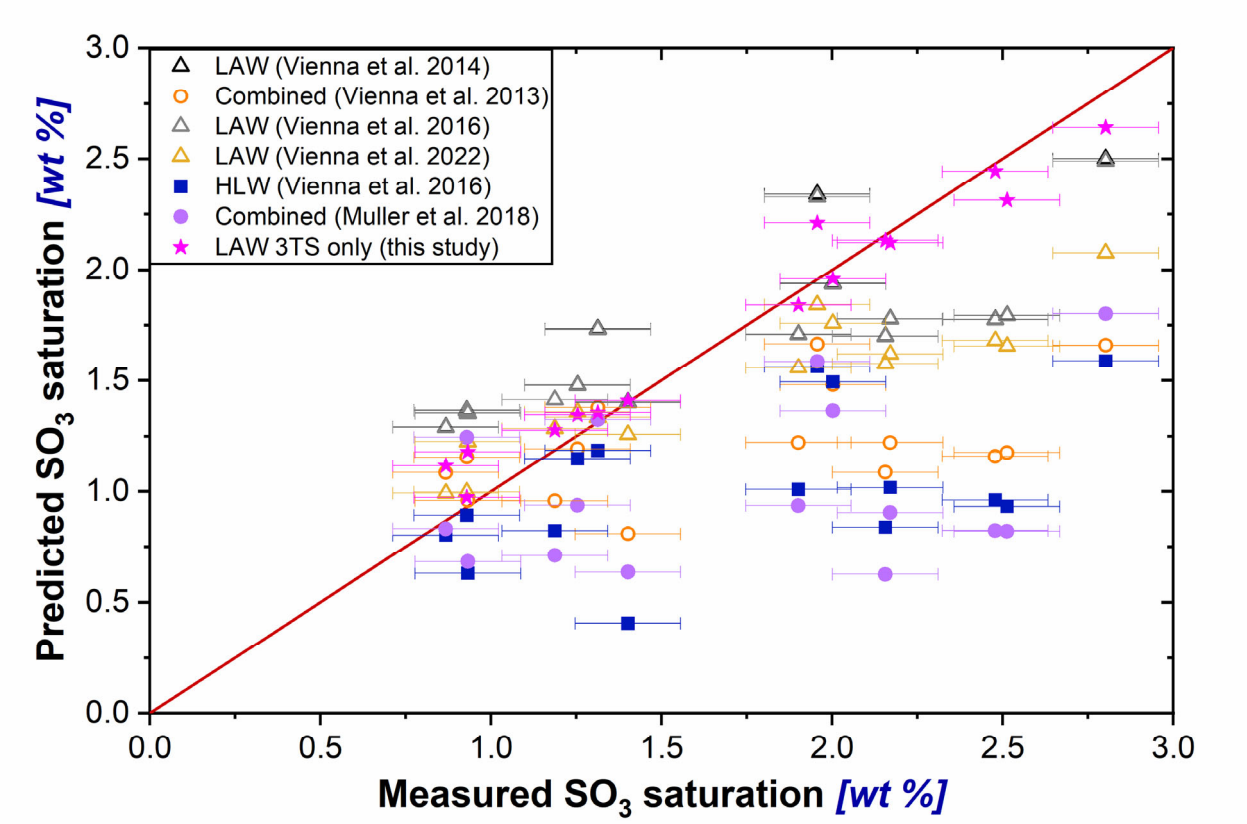

Figure 3.12. Measured SO_3 saturation and predicted SO_3 saturation values for HLW-APPS glasses. Open symbols indicate that 3TS offsets were applied to the model for the predicted values. Uncertainties for measured values are represented by $SD_{pooled,SSM}$.

3.5 Density

Density measurements were obtained using the methods discussed in Section 2.8. The median of these density values is 2.56 g/cm^3, with a minimum of 2.43 g/cm^3 and a maximum of 2.78 g/cm^3 (Table 3.10). The glasses have a density <3.7 g/cm^3, which meets WTP Contract Specification 2 (DOE 2000) for package dimension, weight, and void fraction limits.

Table 3.10. Measured densities in g/cm^3.

Glass ID	Measured Density (g/cm^3)	Glass ID	Measured Density (g/cm^3)
HLW-APPS-01	2.43	HLW-APPS-09	2.55
HLW-APPS-02	2.49	HLW-APPS-10	2.60
HLW-APPS-03	2.72	HLW-APPS-11	2.59
HLW-APPS-04-1	2.54	HLW-APPS-12	2.56
HLW-APPS-05	2.55	HLW-APPS-13-1	2.60
HLW-APPS-06	2.52	HLW-APPS-14	2.56
HLW-APPS-07-2	2.54	HLW-APPS-15	2.57
HLW-APPS-08	2.65		

The experimentally determined DFHLW APPS glass densities were compared to predicted values based on models from Vienna et al. (2002 and 2009). Figure 3.13 shows a comparison of predicted and measured models. Both models predict slightly higher density than the measured values with constant offsets of 0.05586 g/cm^3 (SD=0.02422 g/cm^3) for the Vienna et al. 2009 model and 0.03719 g/cm^3 (SD=0.01781 g/cm^3) for the Vienna et al. 2002 model. Therefore, it is recommended that the Vienna et al. 2002 model be used to predict the density of DFHLW glasses with a 0.03719 subtracted from the predicted value.

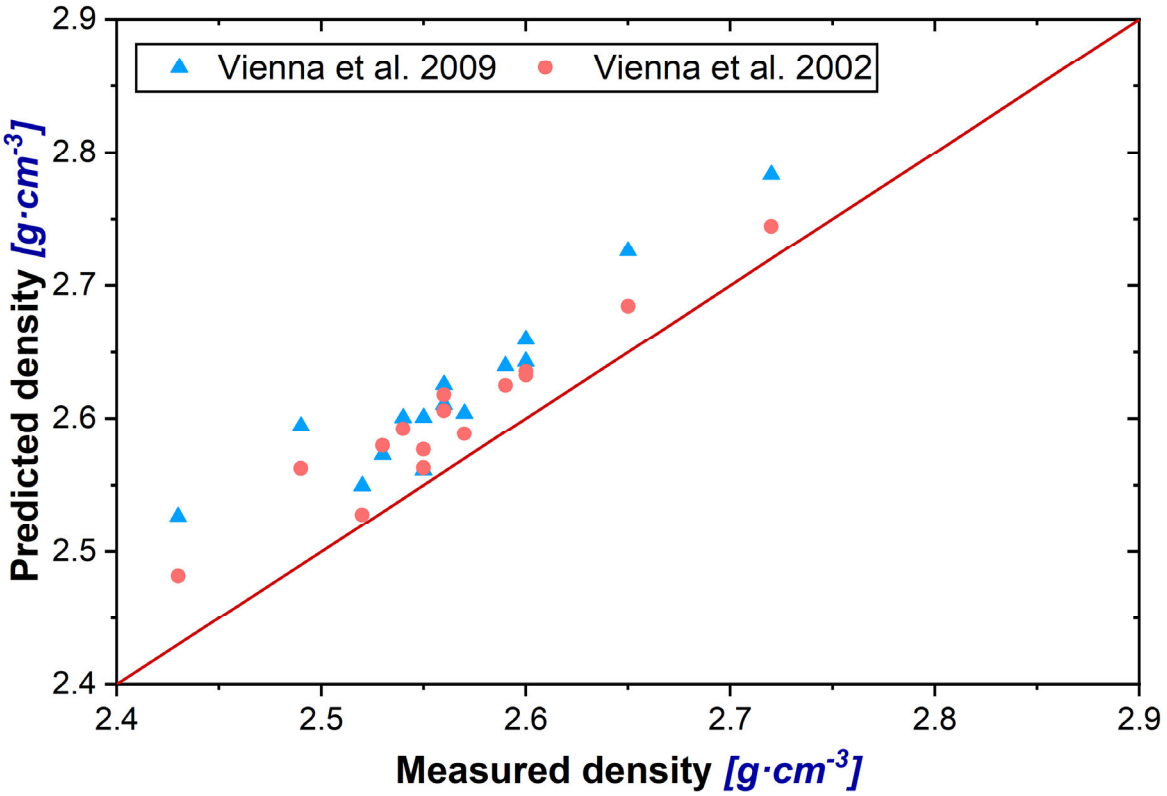

Figure 3.13. Measured and predicted densities for HLW-APPS glasses

3.6 Viscosity

This section presents the viscosity results obtained using the methods discussed in Section 2.9. The results are summarized in Table 3.11 and individually reported in Appendix G. Note the reported temperatures are different than target temperatures listed in Section 2.9 because of a difference between the furnace control thermocouple and the viscosity measurement thermocouple.

Table 3.11. Measured ln η (Pa-s) values versus target temperature (in the sequence of measurement).

Target *T*, °C	1170	1070	970	1170	1270	1170
Glass ID	ln η (Pa-s)	ln η (Pa-s)	ln η (Pa-s)	ln η (Pa-s)	ln η (Pa-s)	ln η (Pa-s)
HLW-APPS-01	1.808	2.743	3.790	1.871	1.165	1.873[(a)]
HLW-APPS-02	1.825[(a)]	2.848	4.055[(a)]	1.884	1.019[(a)]	1.795
HLW-APPS-03	1.592	2.716	4.127	1.636	0.809	1.711
HLW-APPS-04-1	1.660	2.492	3.493	1.674	0.996	1.686
HLW-APPS-05	1.259	2.085	3.123	1.338	0.480	1.134
HLW-APPS-06	1.459	2.205	3.208	1.421	0.746	1.408
HLW-APPS-07-2	1.180	1.965	2.998	1.202	0.545	1.169
HLW-APPS-08	1.677	2.578	3.716	1.625[(a)]	0.941	1.767
HLW-APPS-09	1.492	2.366	3.349	1.522	0.834	1.533
HLW-APPS-10	1.886	2.760	3.908	1.809[(a)]	1.050[(a)]	1.8274[(a)]
HLW-APPS-11	1.908	2.794	3.883	1.896	1.173	1.910
HLW-APPS-12	1.800	2.707	3.810	1.820	1.172	1.853
HLW-APPS-13-1	1.714	2.623	3.710	1.726	0.990	1.736
HLW-APPS-14	1.793	2.716	3.838	1.807	1.082	1.820
HLW-APPS-15	1.240	2.054	3.123	1.204	0.535	1.267

(a) Average of two measurements.

The Arrhenius model was used to fit the viscosity-temperature data for each waste glass. The model form is the Arrhenius equation:

$$\ln(\eta) = A + \frac{B}{T_K} \quad 3.1$$

where A and B are independent of temperature (T_K), which is in Kelvin (T(°C) + 273.15). For each glass, Table 3.12 provides the values for the A and B coefficients and summarizes the viscosity results at six target temperatures calculated using the Arrhenius equation [Eq. 3.1].

Table 3.12. Fitted of Arrhenius coefficients and calculated η for specific temperatures.

	Arrhenius Coefficients		Temperature (°C)					
	A	B	950	1050	1100	1150	1200	1250
Glass ID	(ln Pa-s)	(ln Pa-s*K)	ln η [Pa-s]					
HLW-APPS-01	10.3129	17601.76	4.078	2.990	2.506	2.055	1.636	1.243
HLW-APPS-02	12.0813	20127.71	4.374	3.131	2.577	2.062	1.582	1.133
HLW-APPS-03	13.5211	21942.95	4.419	3.063	2.459	1.898	1.374	0.885
HLW-APPS-04-1	10.0078	16882.75	3.795	2.752	2.287	1.855	1.452	1.076
HLW-APPS-05	10.9166	17537.01	3.421	2.337	1.855	1.406	0.988	0.597
HLW-APPS-06	9.8336	16254.00	3.455	2.451	2.003	1.588	1.200	0.838
HLW-APPS-07-2	10.1151	16330.66	3.236	2.227	1.778	1.360	0.970	0.607
HLW-APPS-08	11.0638	18427.86	4.002	2.863	2.356	1.885	1.445	1.035
HLW-APPS-09	10.0949	16806.12	3.645	2.607	2.144	1.714	1.313	0.939
HLW-APPS-10	11.0922	18691.77	4.189	3.034	2.520	2.042	1.596	1.180
HLW-APPS-11	10.5635	18037.97	4.184	3.069	2.573	2.111	1.681	1.279
HLW-APPS-12	10.4455	17763.68	4.077	2.980	2.491	2.036	1.613	1.217
HLW-APPS-13-1	10.9407	18284.08	4.008	2.878	2.375	1.907	1.471	1.063
HLW-APPS-14	11.0180	18524.98	4.127	2.983	2.473	1.999	1.557	1.144
HLW-APPS-15	10.6414	17163.04	3.390	2.330	1.858	1.418	1.009	0.627

The η_{1150} values interpolated from measured data are compared to predicted values. A list of example models for predicting viscosity is provided in Table 3.13.

Table 3.13. Available glass property models with predicted viscosity.

Model Description – Needs Description	Units for Predicted Values	References
η_{1150} for HLW	Pa·s	Vienna et al. 2009
η_T for HLW	Pa·s	Piepel et al. 2008
η_{1150} for HLW	Pa·s	Vienna et al. 2016
η_T for HLW (Global Model)	P	Kot et al. 2019
η_T for LAW	P	Heredia-Langner et al. 2022
η_{1150} for LAW	P	Vienna et al. 2022

Figure 3.14 displays two plots with a one-to-one comparison of measured and predicted viscosity expressed either in ln(η, Pa-s) or ln(η, P) using the models in Table 3.13.

All models present some scatter around the 45° line; more accentuated at higher viscosity values except for the Heredia-Langner et al. (2022) model. Most of the models underestimate the property (points below the 45° line in Figure 3.14, both plots). The models that appear to best predict the current matrix viscosity are the Hanford Tank Waste Operations Simulator (HTWOS) model (Vienna et al. 2009) with less scatter but still conservative and the Heredia-Langner et al. (2022) model with one overpredicted outlier at low viscosity.

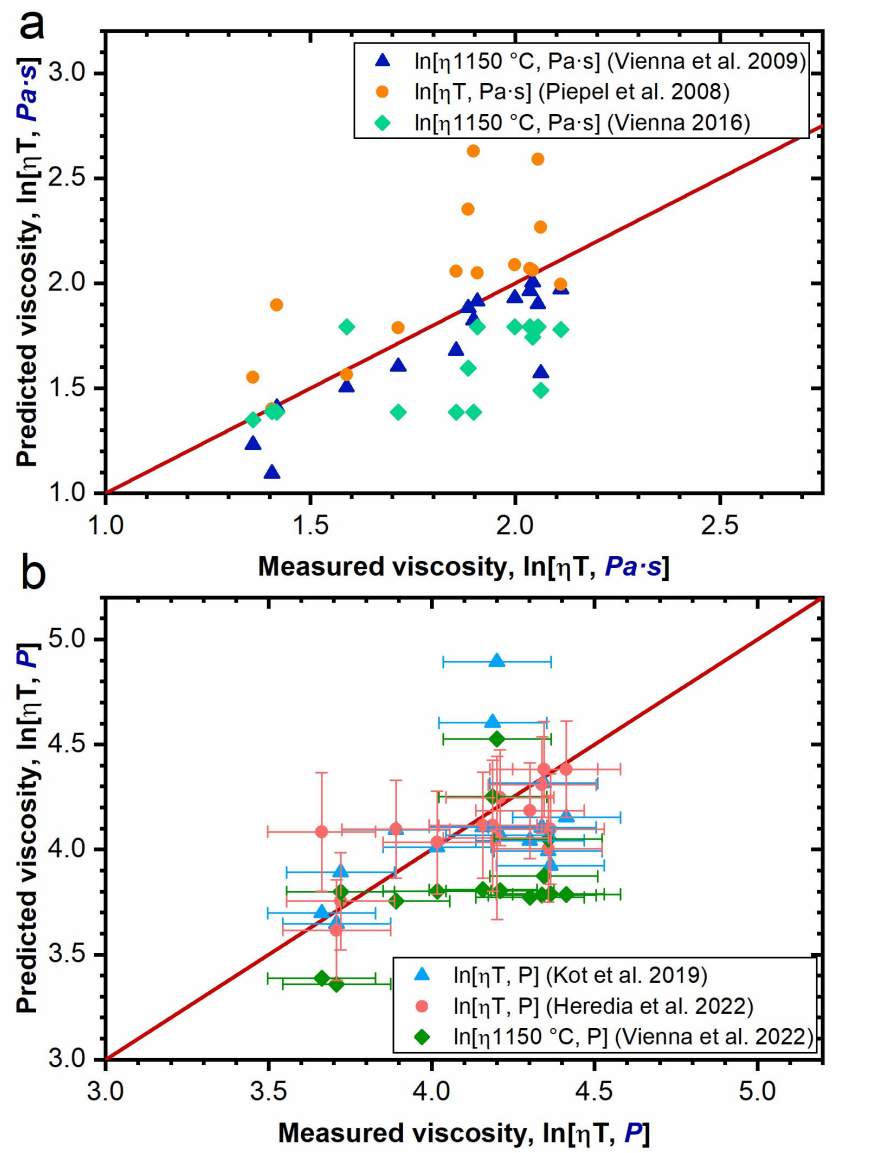

Figure 3.14. Measured vs predicted ln(η_{1150}) where models predicted for a) Pa·s and b) P are shown. Uncertainties for measured values are represented by SD_{pooled} reported in Vienna et al. 2022. Uncertainties for the predicted values are For Information Only (FIO).

3.7 Electrical Conductivity

This section presents the EC results obtained using the methods discussed in Section 2.9. The results are summarized in Table 3.14. Measured EC (S/m) values versus temperatures are individually reported in Appendix H.

Table 3.14. Measured electrical conductivity (S/m) values versus temperatures.

Target *T*, °C	950	950	1050	1050	1150	1150	1250	1250
Glass ID	Electrical Conductivity (S/m)							
HLW-APPS-01	-	9.2	14.54	14.54	20.34	20.39	26.2	26.03
HLW-APPS-02	15.34	15.31	23.66	23.64	37.42	37.42	-	45.99
HLW-APPS-03	12.81	12.78	-	20.58	29.09	29.03	-	36.52
HLW-APPS-04-1	14.42	14.17	23.38	23.40	32.89	32.85	40.89	40.94
HLW-APPS-05	13.01	12.97	-	20.88	-	28.94	36.00	36.00
HLW-APPS-06	25.26	25.24	-	35.00	-	43.45	-	50.72
HLW-APPS-07-2	18.84	18.78	-	27.07	-	35.23	41.91	43.72
HLW-APPS-08	25.02	24.93	35.35	35.32	44.25	-	-	51.28
HLW-APPS-09	20.91	20.50	-	34.00	-	52.50	-	60.78
HLW-APPS-10	58.63	58.31	-	77.66	82.74	-	83.98	85.52
HLW-APPS-11	24.50	24.43	35.27	35.23	46.06	46.08	55.54	55.79
HLW-APPS-12	23.98	23.86	34.77	34.75	44.76	44.80	54.19	54.53
HLW-APPS-13-1	24.24	24.02	35.80	35.74	-	45.50	-	54.01
HLW-APPS-14	21.62	21.52	31.50	31.38	40.08	40.02	47.07	47.18
HLW-APPS-15	10.63	10.58	-	16.13	-	21.40	-	25.15

The Arrhenius equation (Eq. 3.1) was used to fit ε-temperature data for each waste glass. Arrhenius coefficients and calculated ε_{1150} are reported in Table 3.15.

Glass HLW-APPS-10 did not fit the Arrhenius model due to the values measured at 950 °C. The non-Arrhenian behavior of this glass might be due to crystallization or phase separation moving from 1050 to 950 °C (Appendix H).

Table 3.15. Fitted coefficients of Arrhenius model for ε_{1150}.

	Arrhenius Coefficients		
Glass ID	A, ln[S/m]	B, ln[S/m]-K	ε1150 (S/m)
HLW-APPS-01	7.47097	-6372.93	19.94
HLW-APPS-02	8.63567	-7216.54	35.33
HLW-APPS-03	8.06696	-6723.78	28.29
HLW-APPS-04-1	8.06658	-6563.52	31.65
HLW-APPS-05	7.78	-6349	27.63
HLW-APPS-06	6.8578	-4420	42.61
HLW-APPS-07-2	7.13106	-5115.34	34.35
HLW-APPS-08	6.98437	-4574.4	43.38
HLW-APPS-09	8.8137	-7042	47.73
HLW-APPS-10	NR	NR	NR
HLW-APPS-11	7.40936	-5124	45.10
HLW-APPS-12	7.36394	-5092.47	44.06
HLW-APPS-13-1	7.38851	-5104.52	44.78
HLW-APPS-14	7.08014	-4861.64	39.02
HLW-APPS-15	6.91158	-5536.8	20.51

NR = not reported

Example EC models are listed in Table 3.16.

Table 3.16. Available glass property models with predicted EC.

Model Description – Needs Description	Units for Predicted Values	References
ε_{1150} for HLW	$S \cdot m^{-1}$	Vienna et al. 2009
ε_T for HLW	$S \cdot m^{-1}$	Piepel et al. 2008
ε_T for HLW (Global Model)	$S \cdot m^{-1}$	Kot et al. 2019
ε_{1150} for LAW	$S \cdot m^{-1}$	Vienna et al. 2022
ε_T for LAW (AR PQM)	$S \cdot m^{-1}$	Vienna et al. 2022

PQM = partial quadratic mixture.

The comparison between measured and predicted values using the model in Table 3.16 is reported in Figure 3.15.

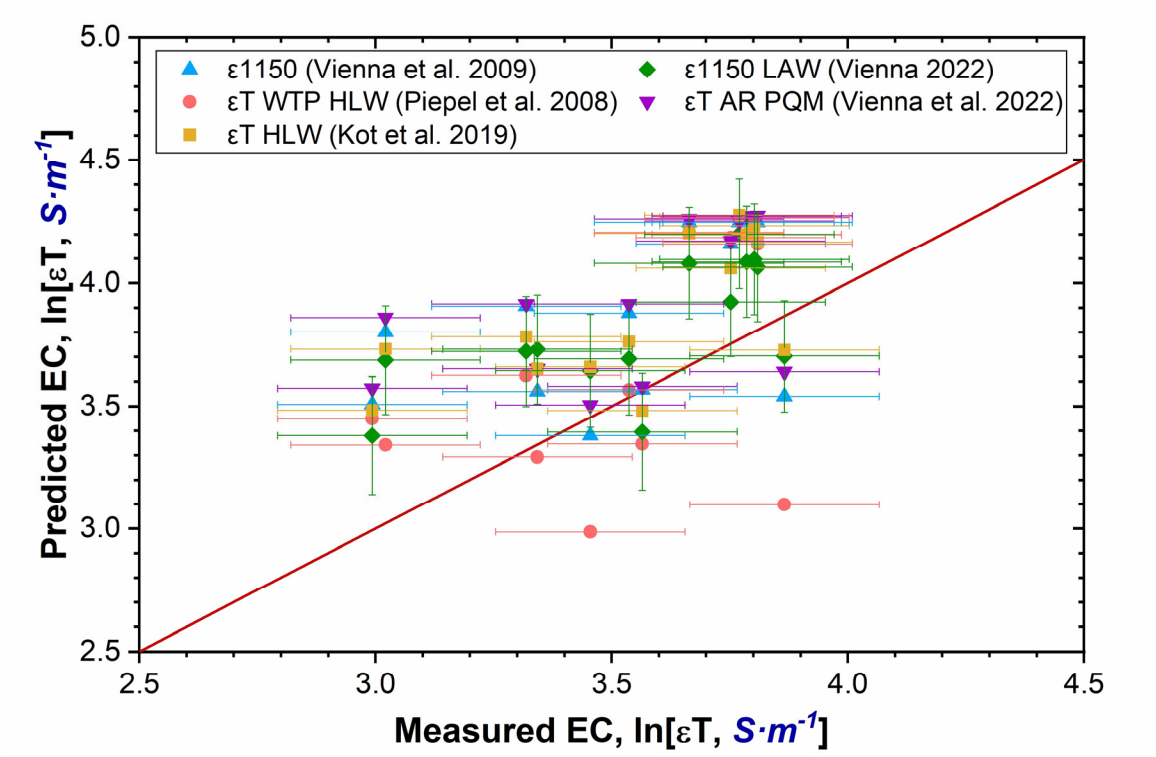

Figure 3.15. Measured vs. predicted ln(ε_{1150}). Uncertainties for measured values are represented by SD_{pooled} reported in Vienna et al. 2022. Uncertainties for the predicted values are FIO.

Overall, none of the models predicted correctly and, in general, predictions were higher than the measured value along the whole EC spectrum.

3.8 Product Consistency Test

This section presents the PCT results obtained using the methods discussed in Section 2.11.

The average normalized PCT losses (NLs) for B, Na, Si, and Li for quenched and CCC glass are reported in Table 3.17 and Table 3.18. The WTP contract (DOE 2000), specifies the waste acceptance product specifications will be met. The Waste Acceptance Product Specification (DOE 1996), the NL_B, NL_{Na}, and NL_{Li} values must be 2 standard deviations (SDs) below the associated values of the DWPF Environmental Assessment glass (Janzen et al. 1993).

Without considering the 2 SDs, the glasses APPS-06Q, -05CCC, and -06CCC failed to satisfy the constraints. Glasses APPS-05 and -06 did form nepheline during CCC, which explains the failure. Considering the 2 SDs, APPS-05Q is close to failing the NL_{Na} constraint.

Table 3.17. Average normalized PCT loss (NLs) in g/m^2 for the DFHLW APPS quenched glasses. Values in bold highlight NLs that exceeded DWPF EA glass threshold.

APPS No	B	Na	Si	Li
DWPF EA	8.35	6.675		4.785
APPS-01[(a)]	2.458	1.547	0.139	2.053
APPS-02[(a)]	4.532	2.797	0.105	
APPS-03[(a)]	0.410	0.595	0.135	
APPS-04-1	0.144	0.460	0.144	0.430
APPS-05[(a)]	2.753	5.567	0.104	
APPS-06	4.306	**8.987**	0.489	
APPS-07-2[(a)]	6.062	2.870	0.105	
APPS-08	5.475	4.444	1.423	
APPS-09[(a)]	0.117	0.272	0.089	0.239
APPS-10[(a)]	0.428	1.342	0.253	
APPS-11[(a)]	0.589	1.836	0.466	
APPS-12[(a)]	0.902	2.662	0.699	
APPS-13-1[(a)]	0.364	2.094	0.306	
APPS-14[(a)]	1.075	2.696	0.778	
APPS-15[(a)]	0.175	0.399	0.120	

(a) Value corrected for Na, B and/or Si concentration in the blanks.
EA = Environmental Assessment

Table 3.18. Average normalized PCT loss (NLs) in g/m^2 for the DFHLW APPS CCC glasses. Values in bold highlight NLs that exceeded DWPF EA glass threshold.

APPS No	B	Na	Si	Li
DWPF EA	8.35	6.675		4.785
APPS-01[(a)]	2.608	1.715	0.131	2.341
APPS-02[(a)]	6.097	3.814	0.092	
APPS-03[(a)]	0.378	0.588	0.153	
APPS-04-1	0.135	0.451	0.150	0.436
APPS-05[(a)]	**33.345**	**22.955**	0.319	
APPS-06	**37.613**	**24.949**	0.611	
APPS-07-2[(a)]	6.021	3.845	0.117	
APPS-08	4.679	3.849	1.436	
APPS-09[(a)]	0.101	0.272	0.097	0.251
APPS-10[(a)]	0.377	1.510	0.318	
APPS-11[(a)]	0.396	1.737	0.345	
APPS-12[(a)]	0.916	2.915	0.784	
APPS-13-1[(a)]	0.676	2.325	0.503	
APPS-14[(a)]	0.851	2.741	0.610	
APPS-15[(a)]	0.135	0.363	0.115	

(a) Value corrected for Na, B, and/or Si concentration in the blanks
EA = Environmental Assessment

To determine if the difference between quenched and CCC heat treated glasses was within experimental error, the following hypothesis was tested (Rieck 2018):

$$p_Q - p_C = 0 \tag{3.2}$$

where p_Q and p_C are the true but unknown values of quenched and the CCC $\ln NL_B$ or $\ln NL_{Na}$.

To test this hypothesis, we considered $\hat{p_C} - \hat{p_Q} \pm k \cdot SD(\hat{p_C} - \hat{p_Q})$ to see if:

$$0 \epsilon \left(\hat{p_c} - \hat{p_Q} - k \cdot SD\left(\hat{p_C} - \hat{p_Q}\right), \hat{p_c} - \hat{p_Q} + k \cdot SD\left(\hat{p_C} - \hat{p_Q}\right)\right) \tag{3.3}$$

where $\hat{p_Q}$ and $\hat{p_c}$ are the measured values of the quenched and the CCC $\ln NL_B$ or $\ln NL_{Na}$, k is a multiplying factor based on the assumed normal distribution of $\hat{p_C} - \hat{p_Q}$ and intended confidence level for the test (in the present study set at 95%), and $SD\left(\hat{p_C} - \hat{p_Q}\right)$ is the estimated standard deviation of $\hat{p_c} - \hat{p_Q}$. Assuming $SD(\hat{p_C}) = SD(\hat{p_Q}) = SD$, then:

$$\hat{p_c} - \hat{p_Q} \pm kSD\left(\hat{p_c} - \hat{p_Q}\right) = \hat{p_c} - \hat{p_Q} \pm k\sqrt{2}SD \tag{3.4}$$

That is, the measured property of CCC glass is considered the same as that of quenched glass within the experimental error if the following condition is satisfied:

$$\hat{p_Q} \epsilon \left(\hat{p_c} - k\sqrt{2}\ SD, \hat{p_c} + k\sqrt{2}\ SD\right) \tag{3.5}$$

Most of the DFHLW-APPS glasses satisfied the above condition for NL_B except for two, HLW-APPS-05, HLW-APPS-06, and the same glasses failed constraints for NL_{Na} (Figure 3.16). These glasses contained nepheline and therefore the increased releases recorded by PCT tests are in line with the character of the materials.

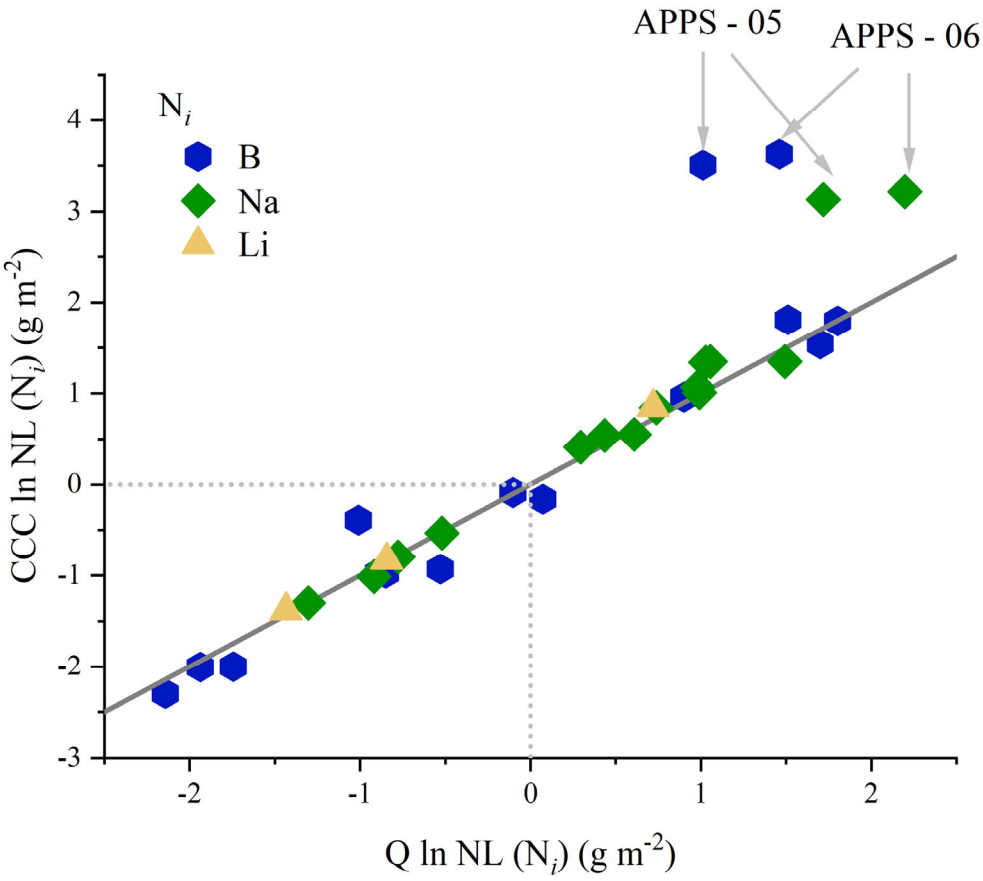

Figure 3.16. Normalized NL_B, NL_{Li}, and NL_{Na} release in natural logarithm scale of quenched vs. CCC DFHLW glasses.

Example glass property models with predicted normalized PCT loss are reported in Table 3.19.

Table 3.19. Example glass property models with predicted PCT normalized loss.

Model Description – Needs Description	Units for Predicted Values	References
NL_{Ave} (LAW + HLW)	$g \cdot m^{-2}$	Vienna and Crum 2018
NL_B (Updated Global Model)	g/L (converted to $g \cdot m^{-2}$ for comparison)	Kot et al. 2019
NL_B HLW	$g \cdot m^{-2}$	Vienna et al. 2016

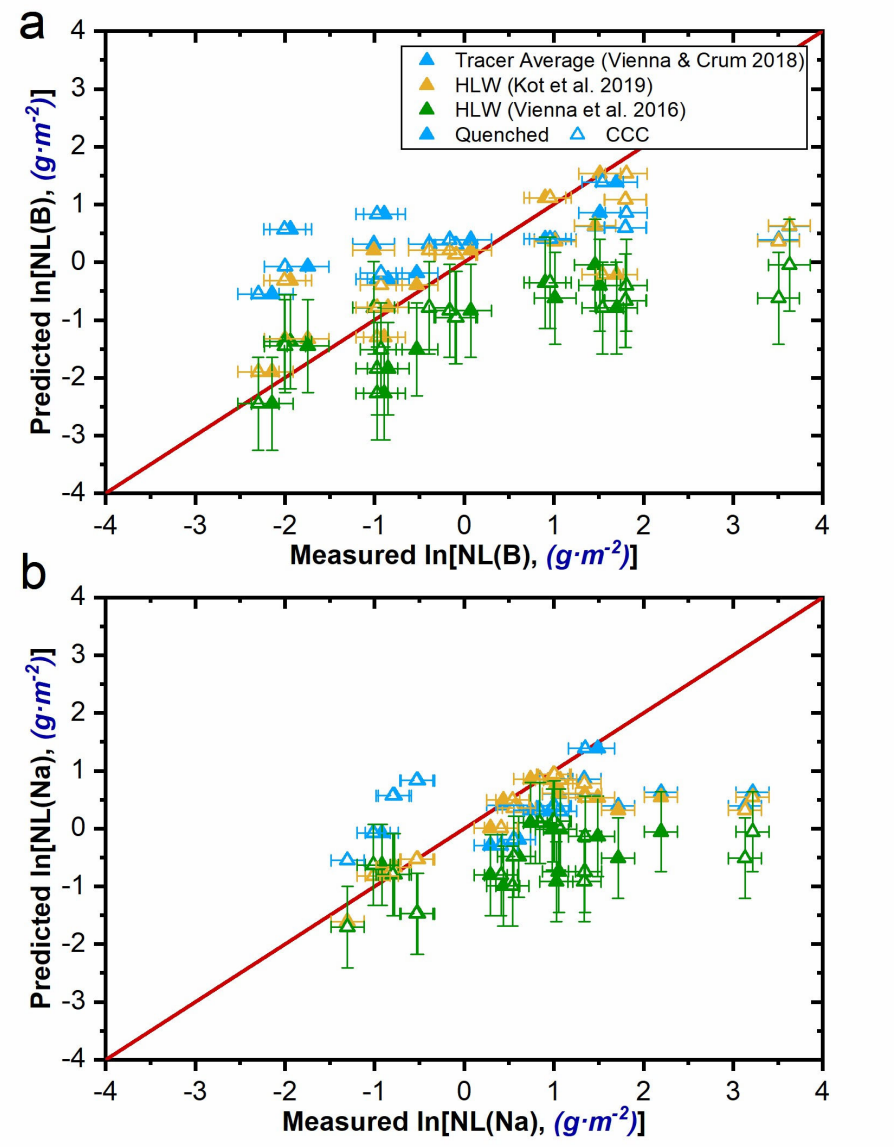

Figure 3.17. Uncertainties for measured values are represented by SD_{pooled} reported in Vienna et al. 2022. Uncertainties for the predicted values are FIO.

3.9 Toxicity Characteristic Leaching Procedure

This section presents the TCLP results obtained using the methods discussed in Section 2.12.

Out of 30 tested glasses, 29 were tested in extraction fluid number 1. One glass (HLW-APPS-10-Q) was tested in extraction fluid number 2 due to the results from the glass pre-testing, as described in the EPA Method 1311, Chapter 7.1.4.

Overall, eight campaigns of 18 ±2 hours were performed; during each campaign an MS, blank, and BS were tested. Each spiked element was present at 100-µg/L concentration. All of the MSs were retrieved within the demanded interval as specified in the EPA Method 1311, Chapter 8.4.

Ag, As, Ba, Cd, Cr, Ni, Pb, and V were measured by ICP-MS. The detection limit for each element must be an order of magnitude lower than those established for the UTS/RCRA toxicity testing, the analytical method met this criterion. Table 3.20 specifies TCLP toxicity, UTS limits, and analytical thresholds as reported by 331 Analytical Service Laboratories in mg/L. Note that Hg and Se were not part of glass formulation and B was measured only for the purpose of analyte release information.

Table 3.20. RCRA delisting criteria and UTS limit (grey field). All values are in mg/L. Se and Hg were not part of glass formulation, Se was used as a part of calculations for MS recovery.

	Ag	As	Ba	Cd	Cr	Hg	Ni	Pb	Se	V	B
RCRA Toxicity limit	5	5	100	1	5	0.2	NA	5	1	2	NA
UTS	0.14	5	21	0.11	0.6	0.025	11	0.75	5.7	NA	NA
ICP-OES	NA	NA	NA	NA	NA	NA	0.15	NA	NA	0.08	0.2
ICP-MS	3.00E-04	1.93E-03	4.30E-04	5.00E-04	5.10E-04	NA	7.48E-03	4.30E-04	2.84E-03	5.00E-04	NA

Table 3.21 and Table 3.22 show the TCLP results for quenched and CCC glasses. NA elements were not part of the glass composition; ND elements were not detected. Across all glass compositions, the cooling regimen quenched vs. CCC resulted in higher release of elements from CCC glasses. None of the ICP-MS measured TCLP releases exceeded the RCRA toxicity limit or D-listing limit (Table 2.8).

The CCC values for glasses 5, 6, 14, and 15 exceeded the UTS Cr limit. Glasses 5 and 6 contained a significant amount of nepheline, which is known to negatively affect glass durability when present in high concentration. Glasses 14 and 15 contained high concentrations of chromium from the formulation itself. No glass exceeded the delisting limits set forth in Cook and Blumenkranz (2003).

Table 3.21. RCRA metals quenched glasses, values in mg/L.

	Analyte in mg/L										
Glass ID	Ag	As	Ba	Cd	Cr	Hg[(a)]	Ni	Pb	Se[(a)]	V	B[(b)]
HLW-APPS-01	0.006	0.002	0.002	ND	0.041	NA	0.002	0.334	NA	0.001	8.170
HLW-APPS-02	0.001	0.002	0.001	ND	0.022	NA	0.157	0.333	NA	0.001	4.245
HLW-APPS-03	0.007	ND	0.001	ND	0.017	NA	0.003	0.115	NA	0.001	0.733
HLW-APPS-04-1	ND	ND	0.002	ND	0.012	NA	ND	0.002	NA	0.460	0.423
HLW-APPS-05	0.007	0.002	0.001	ND	0.177	NA	0.010	0.042	NA	0.002	5.130
HLW-APPS-06	0.007	ND	0.001	ND	0.130	NA	0.124	0.047	NA	0.003	3.135
HLW-APPS-07-2	0.001	ND	0.001	ND	0.029	NA	0.003	0.010	NA	0.479	4.090
HLW-APPS-08	0.003	0.003	0.001	ND	0.012	NA	0.019	0.023	NA	0.019	0.551
HLW-APPS-09	0.000	ND	0.002	ND	0.023	NA	0.018	0.038	NA	0.594	1.057
HLW-APPS-10	0.001	0.028	0.010	ND	1.54	NA	0.004	0.147	NA	0.002	NA
HLW-APPS-11	ND	0.004	0.005	ND	0.013	NA	0.005	0.119	NA	0.001	14.100
HLW-APPS-12	0.000	ND	0.008	ND	0.021	NA	0.923	0.050	NA	0.002	18.700
HLW-APPS-13-1	0.032	ND	0.005	ND	0.039	NA	0.054	0.166	NA	0.001	7.160
HLW-APPS-14	0.006	ND	0.009	ND	0.281	NA	0.074	0.015	NA	0.003	9.560
HLW-APPS-15	0.005	ND	0.004	ND	0.528	NA	0.014	0.002	NA	7.505	14.300

(a) Not part of the glass formulation.
(b) For information about the glass matrix dissolution only.

Table 3.22. RCRA metals in CCC samples, values in mg/L.

	Analyte in mg/L										
Glass ID	Ag	As	Ba	Cd	Cr	Hg[(a)]	Ni	Pb	Se[(a)]	V	B[(b)]
HLW-APPS-01	0.009	0.006	0.005	ND	0.012	NA	0.001	0.458	NA	0.011	24.1
HLW-APPS-02	0.004	0.003	0.004	ND	0.009	NA	0.004	0.587	NA	0.002	11.75
HLW-APPS-03	0.010	0.002	0.003	ND	0.020	NA	0.001	0.071	NA	0.005	1.845
HLW-APPS-04-1	ND	ND	0.003	ND	0.012	NA	0.001	0.010	NA	0.315	0.714
HLW-APPS-05	0.029	ND	0.004	ND	2.175	NA	0.037	0.002	NA	0.044	323
HLW-APPS-06	0.029	0.002	0.006	ND	3.575	NA	8.105	0.039	NA	0.096	283
HLW-APPS-07-2	0.001	ND	0.003	ND	0.014	NA	0.004	0.006	NA	1.220	14.80
HLW-APPS-08	0.004	ND	0.003	ND	0.022	NA	ND	0.028	NA	0.121	0.934
HLW-APPS-09	ND	ND	0.002	ND	0.012	NA	ND	0.002	NA	0.359	0.215
HLW-APPS-10	0.001	ND	0.005	ND	0.107	NA	0.004	0.017	NA	0.001	3.000
HLW-APPS-11	ND	0.003	0.008	ND	0.017	NA	0.004	0.107	NA	0.001	10.545
HLW-APPS-12	ND	ND	0.008	ND	0.036	NA	0.433	0.054	NA	0.001	7.065
HLW-APPS-13-1	0.019	ND	0.006	ND	0.187	NA	0.003	0.137	NA	0.001	5.060
HLW-APPS-14	0.005	ND	0.010	ND	0.650	NA	0.083	0.016	NA	0.318	7.980
HLW-APPS-15	0.001	ND	0.007	ND	1.080	NA	0.019	0.002	NA	11.95	21.65

(a) Not part of the glass formulation.
(b) For information about the glass matrix dissolution only.

Figure 3.18 shows the measured normalized TCLP results for boron vs element Ni, Pb, Cr, V and Ba on a logarithm scale. V release is reasonably close to congruent with B while all other elements have retarded release compared to B. This suggests that a boron-based model will be conservative.

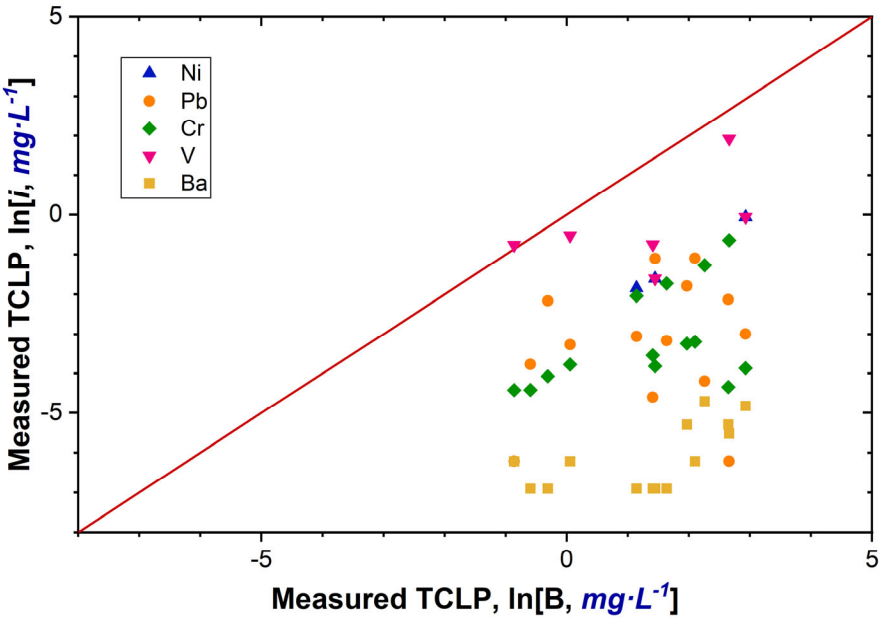

Figure 3.18. Logarithm of normalized TCLP results for boron vs element *i*.

The experimentally determined TCLP responses are compared to values predicted using models from Vienna et al. 2009 and Kim et al. 2004 in Figure 3.19. Although there is considerable scatter, both models appear to generally predict TCLP responses of the APPS glasses reasonably well. The Kim et al. 2004 has slightly lower scatter than the Vienna et al. 2009 model and is responses are more consistently conservative. Therefore, it is recommended that the Kim et al. 2004 model be used for predicting TCLP responses of DFHLW glasses until sufficient data is available to refit that model.

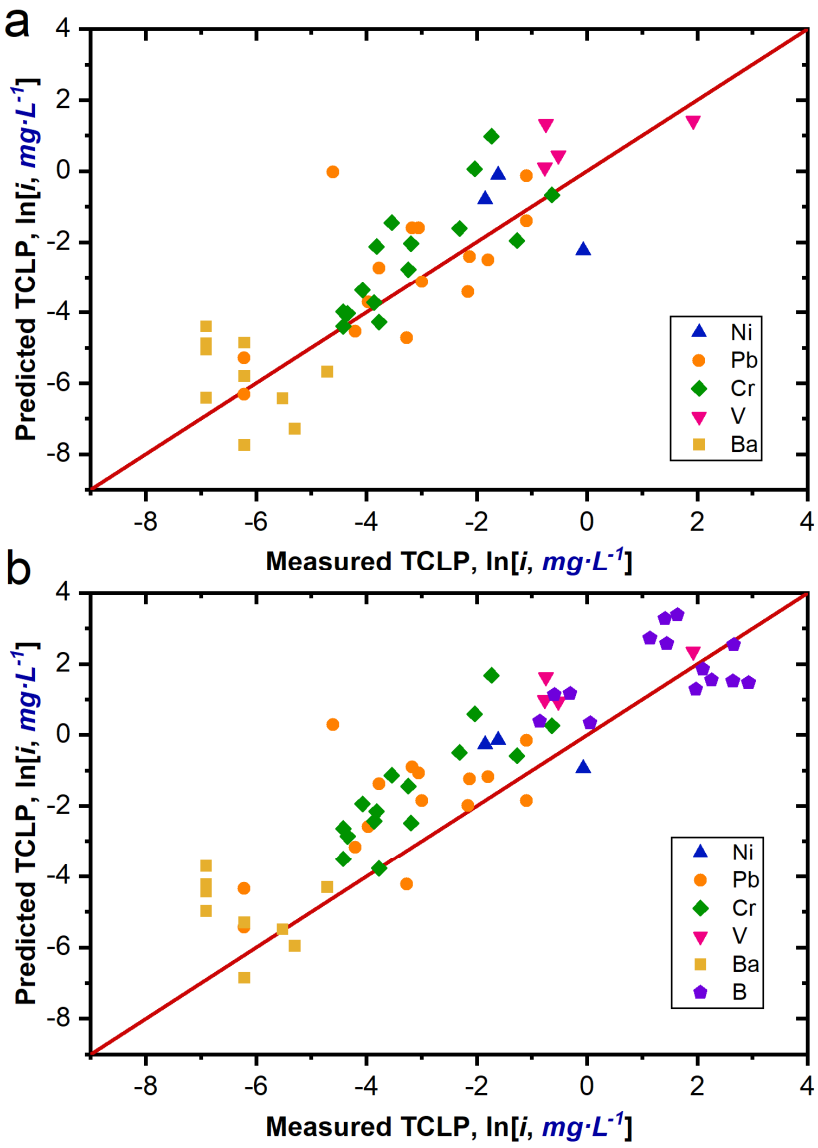

Figure 3.19. Predicted vs. measured TCLP results for element *i* where predicted values are determined from a) Vienna et al. 2009 and b) Kim et al. 2004.

3.10 Corrosion Testing of Refractory

Figure 3.20 provides images of the K-3 coupons after testing and cleaning in HF acid. In general, the melt line corrosion is readily visible, and all neck lines remained intact. The amount of exposed K-3 after HF acid cleaning was sufficient to measure the material loss at the melt-line and the half-way line.

Table 3.23 and Table 3.24 summarize the coupon dimensions and corrosion measurements (material loss), respectively, for three positions (including the melt-line and half-way positions) along the refractory coupons. After correcting for the offset between bubbled and static corrosion (0.510251 ln[in]) from Vienna et al. 2024, eight glasses failed to satisfy the 0.04 in neck corrosion limit: APPS-03, -08, -10, -11, -12, -13, -14, and -15.

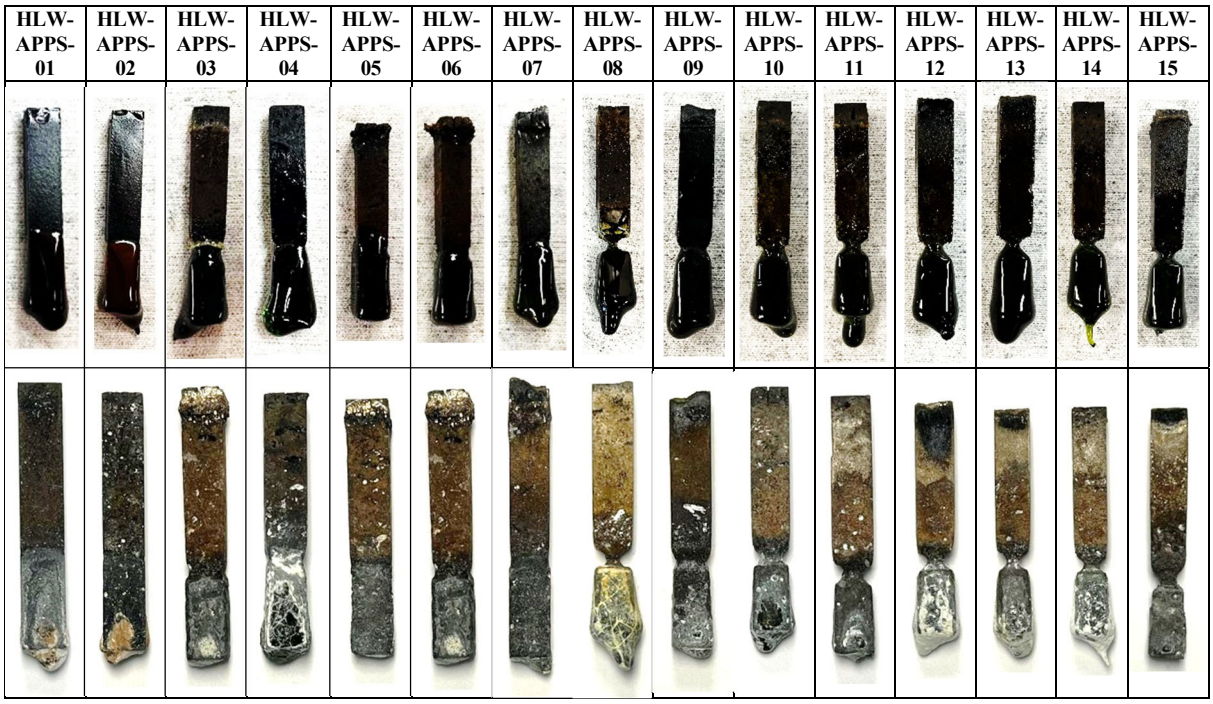

Figure 3.20. Digital images of refractory coupons after corrosion testing with APPS glasses before and after HF acid cleaning.

Table 3.23. Initial refractory coupon data.

Glass ID	Temperature (°C)	SA/V (in^{-1})	Corrosion	Length (L) from Bottom (mm)	Sides 1 and 3 (mm)	Sides 2 and 4 (mm)	Average (s) mm	Tolerance (mm/mm) = (sP1-sP4) / |(LP1-LP4)|
HLW- APPS-01	1208	0.27	P1 (top)	56.98	10.38	10.01	10.19	0.0022
			P3 (**G**, neck)	20.00	10.35	9.87	10.11	
			P4 (**H**, bottom)	10.00	10.35	9.83	10.09	
HLW- APPS-02	1208	0.27	P1 (top)	58.69	10.38	10.15	10.26	0.0006
			P3 (**G**, neck)	20.00	10.37	10.12	10.24	
			P4 (**H**, bottom)	10.00	10.37	10.10	10.23	
HLW- APPS-03	1208	0.27	P1 (top)	58.35	10.36	10.01	10.19	0.0012
			P3 (**G**, neck)	20.00	10.37	10.09	10.23	
			P4 (**H**, bottom)	10.00	10.39	10.10	10.24	
HLW- APPS-04	1208	0.27	P1 (top)	57.17	10.33	10.26	10.29	0.0009
			P3 (**G**, neck)	20.00	10.35	10.14	10.25	
			P4 (**H**, bottom)	10.00	10.37	10.13	10.25	
HLW- APPS-05	1208	0.27	P1 (top)	56.39	9.91	10.22	10.07	0.0032
			P3 (**G**, neck)	20.00	9.78	10.11	9.94	
			P4 (**H**, bottom)	10.00	9.75	10.09	9.92	
HLW- APPS-06	1208	0.27	P1 (top)	60.06	10.20	10.14	10.17	0.0004
			P3 (**G**, neck)	20.00	10.10	10.32	10.21	
			P4 (**H**, bottom)	10.00	10.05	10.34	10.19	
HLW- APPS-07	1208	0.27	P1 (top)	60.04	10.03	9.52	9.77	0.0014
			P3 (**G**, neck)	20.00	10.08	9.60	9.84	
			P4 (**H**, bottom)	10.00	10.09	9.60	9.84	
HLW- APPS-08	1208	0.27	P1 (top)	57.07	9.60	10.06	9.83	0.0003
			P3 (**G**, neck)	20.00	9.63	10.01	9.82	
			P4 (**H**, bottom)	10.00	9.63	10.00	9.82	
HLW- APPS-09	1208	0.27	P1 (top)	56.82	10.11	10.43	10.27	0.0020
			P3 (**G**, neck)	20.00	10.01	10.41	10.21	
			P4 (**H**, bottom)	10.00	9.98	10.38	10.18	
HLW- APPS-10	1208	0.27	P1 (top)	60.20	9.77	10.29	10.03	0.0019
			P3 (**G**, neck)	20.00	9.93	10.29	10.11	
			P4 (**H**, bottom)	10.00	9.92	10.33	10.13	
HLW- APPS-11	1208	0.27	P1 (top)	59.41	10.02	10.26	10.14	0.0055
			P3 (**G**, neck)	20.00	10.47	10.34	10.40	
			P4 (**H**, bottom)	10.00	10.48	10.33	10.41	
HLW- APPS-12	1208	0.27	P1 (top)	58.87	10.39	10.44	10.42	0.0001
			P3 (**G**, neck)	20.00	10.45	10.40	10.42	
			P4 (**H**, bottom)	10.00	10.46	10.37	10.41	
HLW- APPS-13	1208	0.27	P1 (top)	56.34	9.57	10.45	10.01	0.0001
			P3 (**G**, neck)	20.00	9.56	10.47	10.02	
			P4 (**H**, bottom)	10.00	9.56	10.47	10.01	
HLW- APPS-14	1208	0.27	P1 (top)	61.18	10.11	9.69	9.90	0.0024
			P3 (**G**, neck)	20.00	10.46	9.60	10.03	
			P4 (**H**, bottom)	10.00	10.48	9.57	10.02	
HLW- APPS-15	1208	0.27	P1 (top)	59.13	9.48	9.69	9.59	0.0026
			P3 (**G**, neck)	20.00	9.43	9.52	9.48	
			P4 (**H**, bottom)	10.00	9.44	9.48	9.46	

Table 3.24, Refractory coupon corrosion data.

Glass ID	Corrosion Position (P)	Side 1 (p1) (mm)	Side 2 (p2) (mm)	Side 3 (p3) (mm)	Side 4 (p4) (mm)	pavg. = (p1 + p2 + p3 + p4)/4 (mm)	Pc = (P-pavg)]/2 (mm)	Pc = (P-pavg)]/2 (in.)
HLW- APPS-01	P1 (top)	10.43	10.09	10.44	10.15	10.28	-0.04	-0.0017
	P3 (**G**, neck)	9.68	9.16	9.59	9.38	9.45	0.33	0.0129
	P4 (**H**, bottom)	10.18	9.51	10.09	9.58	9.84	0.13	0.0049
HLW- APPS-02	P1 (top)	10.41	10.15	10.43	10.19	10.30	-0.02	-0.0006
	P3 (**G**, neck)	9.24	9.24	9.62	9.37	9.37	0.44	0.0172
	P4 (**H**, bottom)	10.13	9.97	10.29	10.11	10.13	0.05	0.0021
HLW- APPS-03	P1 (top)	10.55	10.21	10.53	10.22	10.38	-0.10	-0.0038
	P3 (**G**, neck)	6.96	6.69	6.83	6.3	6.70	1.77	0.0695
	P4 (**H**, bottom)	10.07	10.17	10.09	10.17	10.13	0.06	0.0023
HLW- APPS-04	P1 (top)	10.38	10.33	10.37	10.31	10.35	-0.03	-0.0011
	P3 (**G**, neck)	7.25	8.15	8.36	7.99	7.94	1.15	0.0454
	P4 (**H**, bottom)	10.07	9.76	10.05	9.73	9.90	0.17	0.0068
HLW- APPS-05	P1 (top)	10.19	10.33	10.03	10.34	10.22	-0.08	-0.0031
	P3 (**G**, neck)	8.34	8.62	8.18	8.48	8.41	0.77	0.0302
	P4 (**H**, bottom)	9.21	9.73	9.35	9.77	9.52	0.20	0.0079
HLW- APPS-06	P1 (top)	10.19	10.32	10.3	10.39	10.30	-0.07	-0.0026
	P3 (**G**, neck)	7.92	8.52	8.07	8.24	8.19	1.01	0.0398
	P4 (**H**, bottom)	9.29	10.2	9.92	10.14	9.89	0.15	0.0060
HLW- APPS-07	P1 (top)	10.53	10.25	10.48	10.15	10.35	-0.29	-0.0114
	P3 (**G**, neck)	7.72	7.64	8.17	7.87	7.85	0.99	0.0391
	P4 (**H**, bottom)	9.84	9.3	9.79	9.22	9.54	0.15	0.0060
HLW- APPS-08	P1 (top)	9.72	10.25	9.78	10.23	10.00	-0.08	-0.0032
	P3 (**G**, neck)	2.57	2.98	2.61	2.8	2.74	3.54	0.1393
	P4 (**H**, bottom)	9.24	9.62	9.08	9.59	9.38	0.22	0.0085
HLW- APPS-09	P1 (top)	10.26	10.6	10.31	10.59	10.44	-0.09	-0.0033
	P3 (**G**, neck)	6.8	7.15	6.42	7.2	6.89	1.66	0.0653
	P4 (**H**, bottom)	8.89	9.44	8.76	9.44	9.13	0.52	0.0206
HLW- APPS-10	P1 (top)	9.85	10.35	9.82	10.33	10.09	-0.03	-0.0012
	P3 (**G**, neck)	4.67	5.05	4.56	4.25	4.63	2.74	0.1078
	P4 (**H**, bottom)	8.83	9.28	8.97	9.19	9.07	0.53	0.0208
HLW- APPS-11	P1 (top)	10.1	10.3	10.02	10.32	10.19	-0.02	-0.0010
	P3 (**G**, neck)	5	4.47	4.62	4.8	4.72	2.84	0.1118
	P4 (**H**, bottom)	9.24	9.12	9.07	9.03	9.12	0.65	0.0254
HLW- APPS-12	P1 (top)	10.58	10.67	10.61	10.65	10.63	-0.11	-0.0042
	P3 (**G**, neck)	4.14	4.3	4.46	4.22	4.28	3.07	0.1209
	P4 (**H**, bottom)	9.54	9.73	9.76	9.67	9.68	0.37	0.0145
HLW- APPS-13	P1 (top)	9.61	10.54	9.65	10.52	10.08	-0.03	-0.0014
	P3 (**G**, neck)	2.79	3.64	3.14	3.64	3.30	3.36	0.1321
	P4 (**H**, bottom)	8.4	9.37	8.48	9.22	8.87	0.57	0.0225
HLW- APPS-14	P1 (top)	10.12	9.71	10.13	9.73	9.92	-0.01	-0.0005
	P3 (**G**, neck)	3.98	3.72	4.42	4.02	4.04	3.00	0.1180
	P4 (**H**, bottom)	9.88	9.04	9.93	9.09	9.49	0.27	0.0106
HLW- APPS-15	P1 (top)	9.7	9.88	9.75	9.97	9.83	-0.12	-0.0047
	P3 (**G**, neck)	4.43	4	4	4.41	4.21	2.63	0.1036
	P4 (**H**, bottom)	8	7.8	8.38	7.92	8.03	0.72	0.0282

Figure 3.21 shows measured vs predicted plot for K-3 neck corrosion. All three models (Vienna et al. 2022, Muller et al. 2018, and Vienna et al. 2016) under-estimated the measured K-3 neck corrosion for values below ln[*k*, in] = -3.5. Therefore, updated models are needed to predict K-3 corrosion of DFHLW glasses.

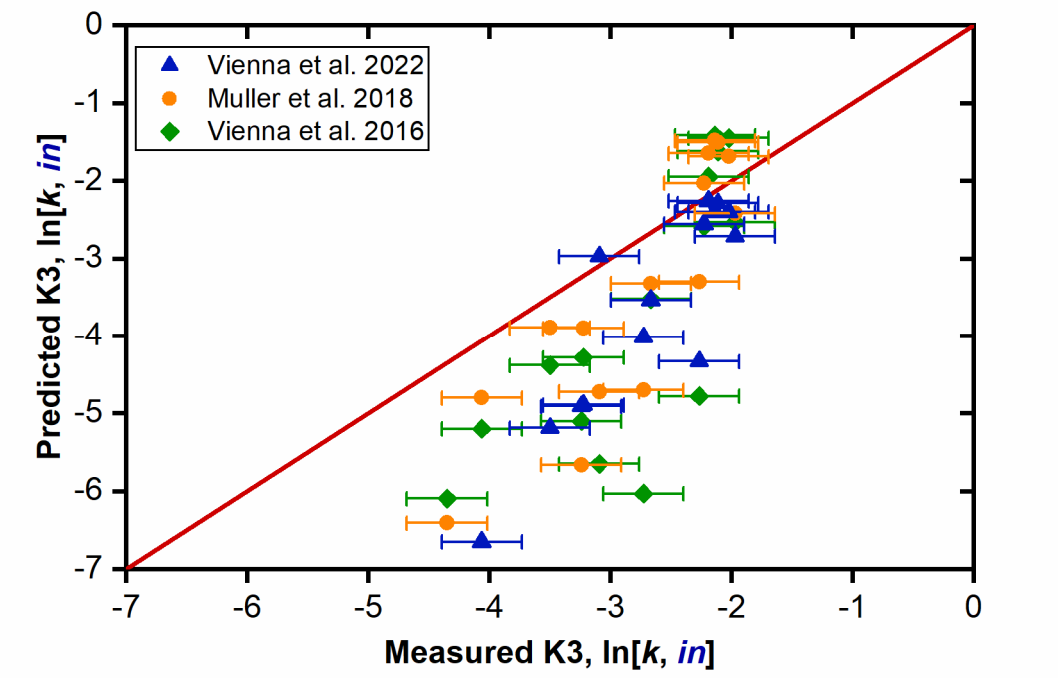

Figure 3.21. Measured vs. predicted plot for K-3 neck corrosion.

3.11 Future Modeling and Formulation Recommendations

The purpose of this effort was to experimentally validate the use of the EWG models for use in designing DFHLW glass compositions. Several models were found adequate for direct use in designing DFHLW glasses while others require additional refits or offsets. Table 3.25 summarizes the status and recommendation for use of models for each of the modelled properties.

Model updates, where needed, are underway and the results will be reported separately in an updated Enhanced Waste Glass formulation methods report.

Table 3.25. Summary of Property Model Comparisons

Property	Disposition
CCC crystallinity	Both Lu et al. 2021 and Vienna et al. 2016 nepheline precipitation models predicted that no nepheline would form in any of the glasses from this study. However, glasses APPS-05 and -06 both precipitated nepheline on CCC and the resulting samples failed PCT constraints. It is recommended that the more conservative predictions be used to control nepheline in DFHLW glasses.
Isothermal crystallinity	Zirconia containing phases T_L model and spinel $T_{2\%}$ models from Vienna et al. 2016 successfully limited unacceptably high concentrations of these crystals (either the conservative 1 vol% or the more optimal 2 vol%) at 950 °C. However, glass APPS-05 precipitated 1.9 vol% $NaCaPO_4$ and 0.2 vol% Cr_2O_3 at 950°C and glass APPS-07-2 precipitated 1.2 vol% $Na_3Nd(PO_4)_2$ and 0.6 vol% $Ca_2Fe_2O_5$ at 950°C. Additional constraints are needed to control the formation of these phases for which models don't currently exist.
Sulfur solubility	Previous models significantly underpredicted the measured values. A new model for sulfur solubility using only 3TS data was developed which adequately predicts measured values. This model will be reported elsewhere.
Density	Densities of APPS glasses are over predicted by models from Vienna et al. 2002 and 2009. The Vienna 2002 model with a -0.03719 g/cm^3 offset adequately predicts density of APPS glasses.
Viscosity	Viscosities of APPS glasses are not adequately predicted by models evaluated in this study. Updated models will be developed and applied to predict viscosities of DFHLW glasses.
Electrical conductivity	EC of APPS glasses are not adequately predicted by models evaluated in this study. Updated models will be developed and applied to predict EC of DFHLW glasses.
Product consistency test	PCT data are underpredicted by models evaluated in this study. Updated models will be developed and applied to predict PCT of DFHLW glasses.
Toxicity	TCLP values are slightly overpredicted by the Kim et al. 2004 model which will be used to predict TCLP responses of DFHLW glasses.
K-3 Neck corrosion	K-3 neck corrosion data are underpredicted by the models evaluated. Updated models are needed to predict K-3 neck corrosion of DFHLW glasses.

4.0 Conclusions

This report documents the results of the formulation, fabrication, and testing of a set of simulated DFHLW glasses. Of 15 glasses tested, 12 satisfied all target property constraints. Two glasses (APPS-05 and -06) formed nepheline on CCC heat-treatment and failed the PCT response limits. Eight glasses failed the K-3 neck corrosion constraint. Glasses APPS-05 and APPS-07-2 formed borderline high concentrations of crystals (primarily phosphate phases -- $NaCaPO_4$ and $Na_3Nd(PO_4)_2$) when heat treated at 950 °C. All other glasses were found to be satisfactory.

The measured property values were compared to predicted values from a set of current models. In many cases the current models were found to be inadequate for design of DFHLW glasses. These models are being adjusted to correct for mispredictions. Other models, e.g., density, TCLP, sulfur solubility, are adequate for formulation of DFHLW glasses.

5.0 Bibliography

10 CFR 830, *Nuclear Safety Management*. Code of Federal Regulations, as amended.

ASTM C1285, *Standard Test Methods for Determining Chemical Durability of Nuclear, Hazardous, and Mixed Waste Glasses and Multiphase Glass Ceramics: The Product Consistency Test (PCT).* ASTM International, West Conshohocken, PA.

ASTM C1720, *Standard Test Method for Determining Liquidus Temperature of Immobilized Waste Glasses and Simulated Waste Glasses*. ASTM International, West Conshohocken, PA.

ASTM C621, *Standard Test Method for Isothermal Corrosion Resistance of Refractories to Molten Glass*. 2018. ASTM International, West Conshohocken, PA Bernards JK, GA Hersi, KT Pak, AJ Schubick, LM Bergmann, AN Praga, and SN Tilanus. 2021. *High-Level Waste Analysis of Alternatives Model Results Report*. RPP-RPT-61957, Rev. 2, Washington River Protection Solutions, Richland, WA.

Bernards JK, GA Hersi, TM Hohl, RT Jasper, PD Mahoney, NK Pak, SD Reaksecker, AJ Schubick, EB West, LM Bergmann, et al. 2020. *River Protection Project System Plan*. ORP-11242, Rev. 9, U.S. Department of Energy, Office of River Protection, Richland, WA.

Britton MD. 2023. *Revised DFHLW Washing and Blending Study Campaign Inventory*.WRPS-2300881, Washington River Protection Solutions, Richland, WA.

Chow R. 1998. *Treatment of Underlying Hazardous Constituents in Toxicity Characteristic Metal (D004-D011) Wastes*, Memo to Record, dtd. 01/05/1998, U.S. Environmental Protection Agency, Washington, D.C.

Cook JR and DB Blumenkranz. 2003. *Data Quality Objectives Process in Support of LDR/Delisting at the WTP*. 24590-WTP-RPT-ENV-01-012, Rev. 1, River Protection Project, Hanford Tank Waste Treatment and Immobilization Plant, Richland, WA.

DOE. 1996. *Waste Acceptance Product Specifications for Vitrified High-Level Waste Forms (WAPS)*. DOE/EM-0093, U.S. Department of Energy, Office of Environmental Management, Washington, D.C.

DOE. 2000. *Design, Construction, and Commissioning of the Hanford Tank Waste Treatment and Immobilization Plant*. Contract DE-AC27-01RV14136, as amended, U.S. Department of Energy, Office of River Protection, Richland, WA.

DOE. 2013. *Hanford Tank Waste Retrieval, Treatment, and Disposition Framework*. U.S. Department of Energy, Washington, D.C.

DOE Order 414.1D, *Quality Assurance*. U.S. Department of Energy, Washington, D.C.

Dunst KP. 2020. *Process Inputs Basis of Design (PIBOD) for HLW*. 24590-HLW-DB-PET-19-001, Rev. 1, River Protection Project, Waste Treatment Plant, Richland, WA.

EPA 2006. Toxicity Characteristic. 40CFR261.24, Environmental Protection Agency, Washington, D.C.

EPA 2024. Universal Treatment Standards. 40CFR268.48, Environmental Protection Agency, Washington, D.C.

EPA Method 1311, "Toxicity Characteristic Leaching Procedure (TCLP)." In *Test Methods for Evaluating Solid Waste, Physical/Chemical Methods*, EPA Publication SW–846.

Gebhardt MJ. 2011. *APPS System Design Description*. 24590-WTP-SWD-PET-08-002, Rev. 5, River Protection Project, Waste Treatment Plant, Richland, WA.

Heredia-Langner A, V Gervasio, SK Cooley, CE Lonergan, DS Kim, AA Kruger, and JD Vienna. 2022. "Hanford low-activity waste glass composition-temperature-melt viscosity relationships." *International Journal of Applied Glass Science* 13(4):514-525.

Jantzen, C. M., N. E. Bibler, D. C. Beam, C. L. Crawford, and M. A. Pickett. 1993. *Characterization of the Defense Waste Processing Facility (DWPF) Environmental Assessment (EA) Glass Standard Reference Material (U)*. WSRC-TR-92-346, Rev. 1, Westinghouse Savannah River Company, Aiken, SC.

Jin T, D Kim, LP Darnell, BL Weese, NL Canfield, M Bliss, MJ Schweiger, JD Vienna, and AA Kruger. 2019. "A crucible salt saturation method for determining sulfur solubility in glass melt." *International Journal of Applied Glass Science* 10:92-102. https://doi.org/10.1111/ijag.12366

Jin, T., et al., Glass-contact refractory of the nuclear waste vitrification melters in the United States: a review of corrosion data and melter life. International Materials Reviews, 2023.Kim, DS and JD Vienna 2004. Glass composition-TCLP response model for waste glasses. In *Environmental Issues and Waste Management Technologies in the Ceramic & Nuclear Industries IX*: 297-305, American Ceramic Society.

Kim DS, D Peeler, and P Hrma. 1995. "Effect of Crystallization on the Chemical Durability of Simulated Nuclear Waste Glasses." In *Environmental Issues and Waste Management Technologies in the Ceramic and Nuclear Industries* 177-186.

Kim D, JD Vienna, and AA Kruger. 2012. *Preliminary ILAW Formulation Algorithm Description*. 24590-LAW-RPT-RT-04-0003. Rev. 1, River Protection Project, Waste Treatment Plant, Richland, WA.

Kot WK, K Gilbo, H Gan, and IL Pegg. 2019. *Enhancement of HLW Glass Property-Composition Models*. VSL-19R4480-1, Vitreous State Laboratory, The Catholic University of America, Washington, D.C.

Kroll JO, ZJ Nelson, CH Skidmore, DR Dixon, and JD Vienna. 2019. "Formulation of high-Al_2O_3 waste glasses from projected Hanford waste compositions." *Journal of Non-Crystalline Solids* 517:17-25.

Lu X, I Sargin, and JD Vienna. 2021. "Predicting nepheline precipitation in waste glasses using ternary submixture model and machine learning." *Journal of American Ceramic Society* 104:5636-5647.

Lu, X and JD Vienna 2023. *Selection of Example DFHLW Glasses for Validation Tests*, Memo to RL Hanson, dtd 7/26/2023. CCN-335241. River Protection Project, Waste Treatment Plant, Richland, WA.

Lu X, ZD Weller, V Gervasio, and JD Vienna. 2024. "Glass design using machine learning property models with prediction uncertainties: Nuclear waste glass formulation." *Journal of Non-Crystalline Solids*, Submitted.

Mellinger GB and JL Daniel. 1984. Approved Reference and Testing Materials for Use in Nuclear Waste Management Research and Development Programs. PNL-4955-2, Pacific Northwest Laboratory, Richland, WA. https://doi.org/10.2172/6224421

Muller IS, K Gilbo, M Chaudhuri, and IL Pegg. 2018. *K-3 Refractory Corrosion and Sulfate Solubility Model Enhancement*. VSL-18R4360-1, Rev. 0, Vitreous State Laboratory, The Catholic University of America, Washington, D.C.

NQA-1-2012, *Quality Assurance Requirements for Nuclear Facility Application*. American Society of Mechanical Engineers, New York, NY.

Parsons. 2023. *Waste Treatment and Immobilization Plant High Level Waste Treatment Analysis of Alternatives*. DE-NA0002895, Parsons Corporation, Boston, MA.

Peeler DK and P Hrma 1994. "Predicting liquid immiscibility in multicomponent nuclear waste glasses." *Ceramics Transactions* 45:219-229.

Perez JM. 2006. "Practical and Historical Bases for a Glass Viscosity Range for Joule-Heater Ceramic Melter Operation." Email to JD Vienna, Pacific Northwest National Laboratory, Dec. 22, 2006. CCN: 150054, River Protection Project, Waste Treatment Plant, Richland, WA.

Petkus LL. 2003. "Canister Centerline Cooling Data, Revision 1." To C.A. Musick, Oct. 29, 2003. CCN: 074851, River Protection Project, Waste Treatment Plant, Richland, WA.

Piepel GF, A Heredia-Langner, and SK Cooley. 2008. "Property–composition–temperature modeling of waste glass melt data subject to a randomization restriction." *Journal of the American Ceramic Society* 91(10):3222-3228.

Rieck BT. 2018. *ILAW Product Qualification Report – Waste Forming Testing*. 24590-LAWRPT-PENG-17-008-05, Rev 1, River Protection Project, Waste Treatment Plant. Richland, Washington

Skidmore CH, JD Vienna, T Jin, DS Kim, BA Stanfill, KM Fox, and AA Kruger. 2019. "Sulfur solubility in low activity waste glass and its correlation to melter tolerance." *International Journal of Applied Glass Science*, 10(4): 558-568.

Smith GL. 1993. *Characterization of Analytical Reference Glass-1 (ARG-1)*. PNL-8992, Pacific Northwest Laboratory, Richland, WA.

Vienna JD, P Hrma, A Jiricka, DE Smith, TH Lorier, IA Reamer, and RL Schultz. 2001. *Hanford Immobilized LAW Product Acceptance Testing: Tanks Focus Area Results*. PNNL-13744, Pacific Northwest National Laboratory, Richland, WA.

Vienna JD. 2008. "Phosphorous Limit in High-Level Waste Glass -- Supersedes CCN: 177731." CCN: 184901, River Protection Project, Waste Treatment Plant, Richland, WA.

Vienna JD, A Fluegel, DS Kim, and P Hrma. 2009. *Glass Property Data and Models for Estimating High-Level Waste Glass Volume*. PNNL-18501, Pacific Northwest National Laboratory, Richland, WA.

Vienna JD, DS Kim, DC Skorski, and J Matyas. 2013. *Glass Property Models and Constraints for Estimating the Glass to be Produced at Hanford by Implementing Current Advanced Glass Formulation Efforts*. PNNL-22631, Rev. 1, ORP-58289, Pacific Northwest National Laboratory, Richland, WA.

Vienna JD, DS Kim, IS Muller, GF Piepel, and AA Kruger. 2014. "Toward understanding the effect of low-activity waste glass composition on sulfur solubility." *Journal of the American Ceramic Society* 97(10):3135–3142.

Vienna JD and DS Kim. 2014. *Preliminary IHLW Formulation Algorithm Description*. 24590-HLW-RPT-RT-05-001, Rev. 1, River Protection Project, Waste Treatment Plant, Richland, WA.

Vienna JD, GF Piepel, DS Kim, JV Crum, CE Lonergan, BA Stanfill, BJ Riley, SK Cooley, and T Jin. 2016. *Update of Hanford Glass Property Models and Constraints for Use in Estimating the Glass Mass to be Produced at Hanford by Implementing Current Enhanced Glass Formulation Efforts*. PNNL-25835, Pacific Northwest National Laboratory, Richland, WA.

Vienna JD, JO Kroll, P Hrma, JB Lang, and JV Crum. 2017. "Submixture model to predict nepheline precipitation in waste glasses." *International Journal of Applied Glass Science* 8(2):143-157.

Vienna JD and JV Crum. 2018. "Non-linear effects of alumina concentration on Product Consistency Test response of waste glasses." *Journal of Nuclear Materials* 511:396-405.

Vienna JD, X Lu, P Ferkl, J Marcial, MS Fountain, and CL Bottenus. 2022. *Initial Evaluation of Direct-Feed High-Level Waste Glass Formulations and Processing Rates*. PNNL-32866, Rev. 1, Pacific Northwest National Laboratory, Richland, WA.

Vienna JD, A Heredia-Langner, SK Cooley, AE Holmes, DS Kim, and NA Lumetta. 2022b. *Glass Property-Composition Models for Support of Hanford WTP LAW Facility Operation*. PNNL-30932, Rev. 2, Pacific Northwest National Laboratory, Richland, WA.

Vienna JD, X Lu, P Ferkl, J Marcial, MS Fountain, M Trenidad, R Hanson, MD Britton, L Cree, and W Abdul. 2023. "High-Level Waste Glass Processing over Broad Range of Alternative Feed Compositions." In *Proceedings of the 2023 Waste Management Symposia*, Phoenix, AZ.

Vienna, JD, X Lu, P Ferkl, LL Gunnell, A Heredia-Langner, NA Lumetta, T Jin, and JT Reiser. 2024. *Glass Property-Composition Models Update for use in Direct Feed High-Level Waste Flowsheet Development*, PNNL-35884, Pacific Northwest National Laboratory, Richland, WA.

Westesen AM, EL Campbell, SK Fiskum, AM Carney, TT Trang-Le, and RA Peterson. 2022. "Impact of feed variability on cesium removal with multiple actual waste samples from the Hanford site." *Separation Science and Technology* 57(15). https://doi.org/10.1080/01496395.2022.2059378

Appendix A – Distribution of the 154 Glass Compositions

This appendix contains the distribution of the 154 glass compositions showing the 15 clusters do well represent the range of glass compositions.

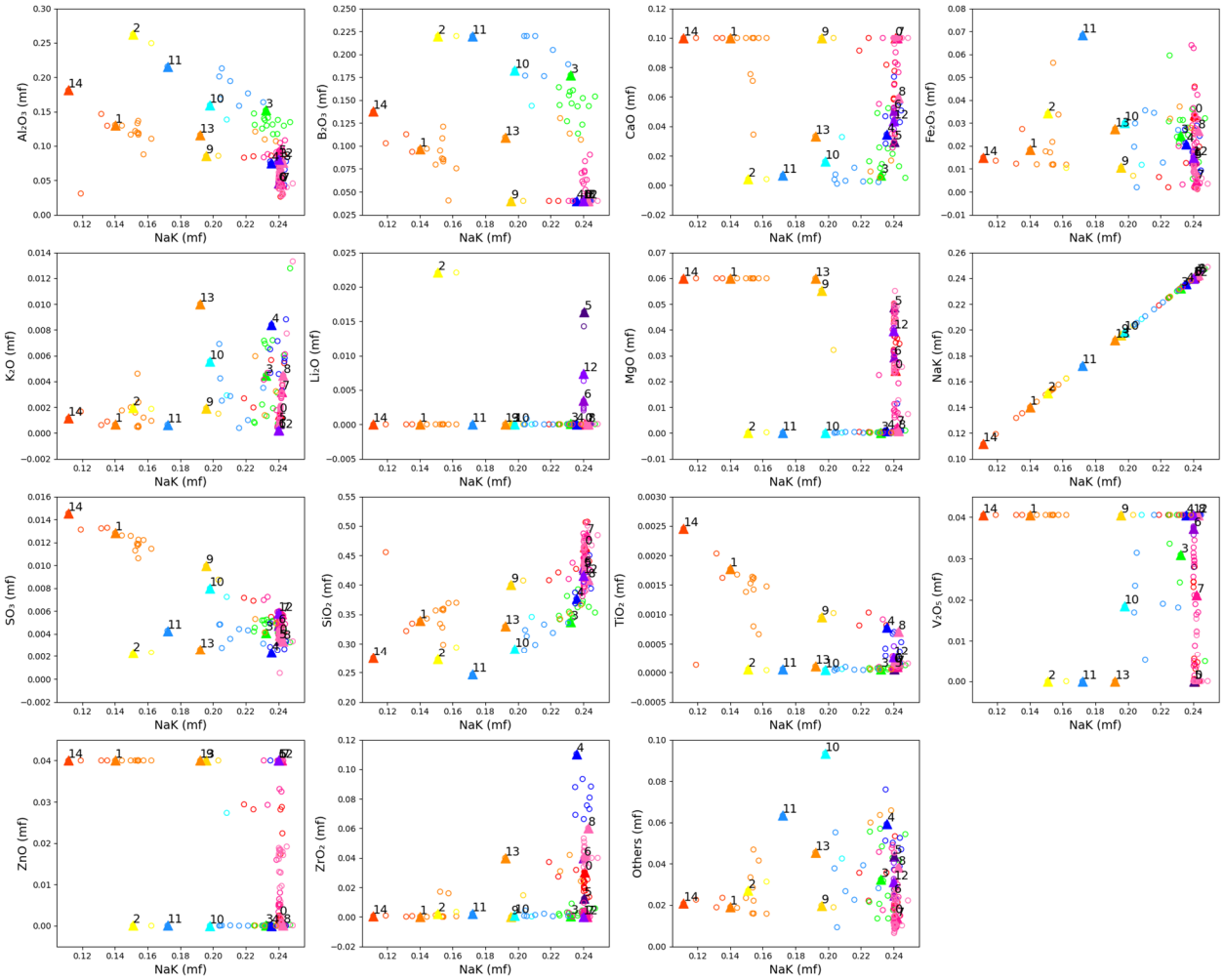

Figure A.1. Major component concentrations for 154 glass compositions versus NaK = Na_2O + 0.66 K_2O. Each color represents a cluster and the numbered triangles show the selected batch to represent each cluster.

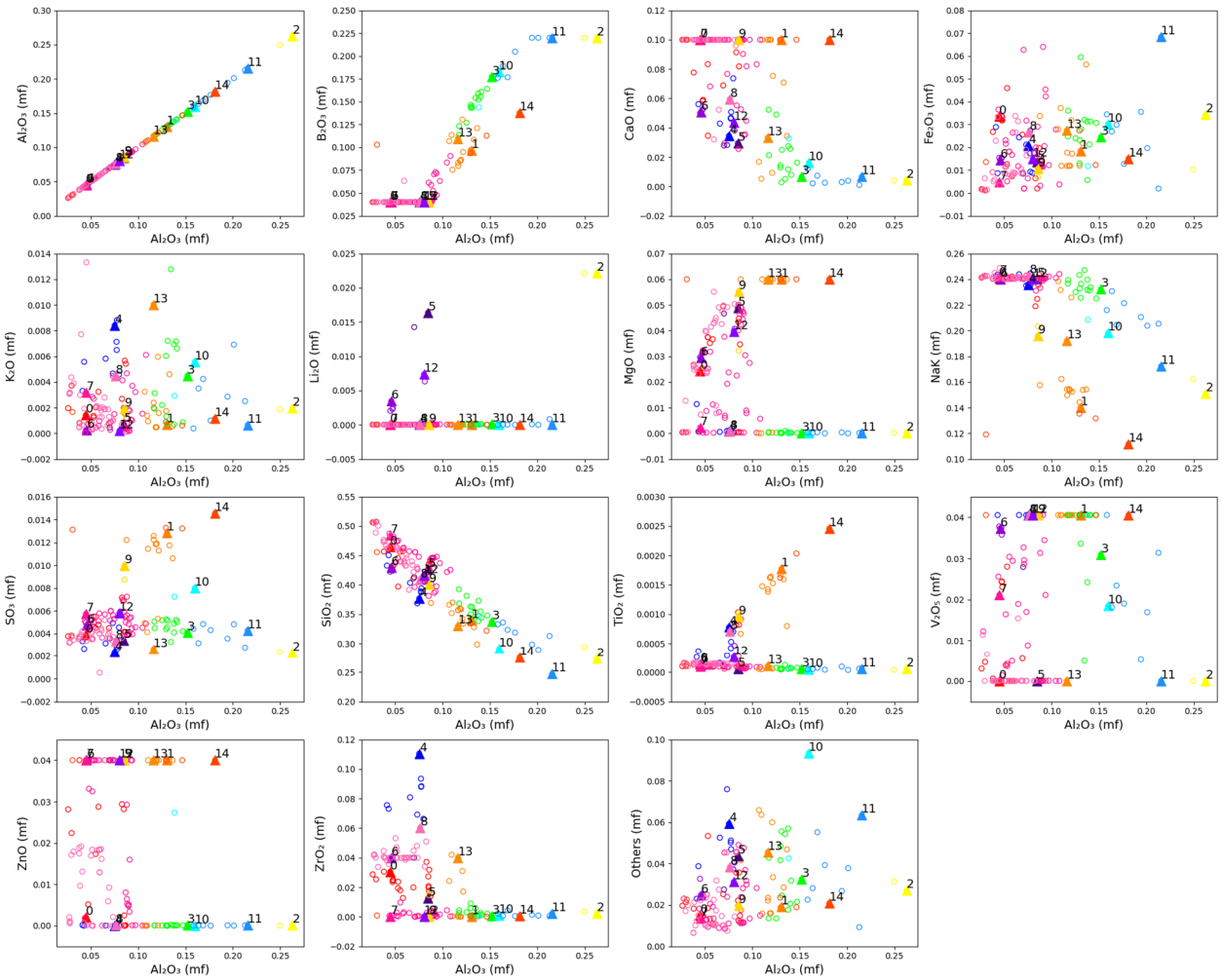

Figure A.2. Major component concentrations for 154 glass compositions versus Al_2O_3. Each color represents a cluster and the numbered triangles show the selected batch to represent each cluster.

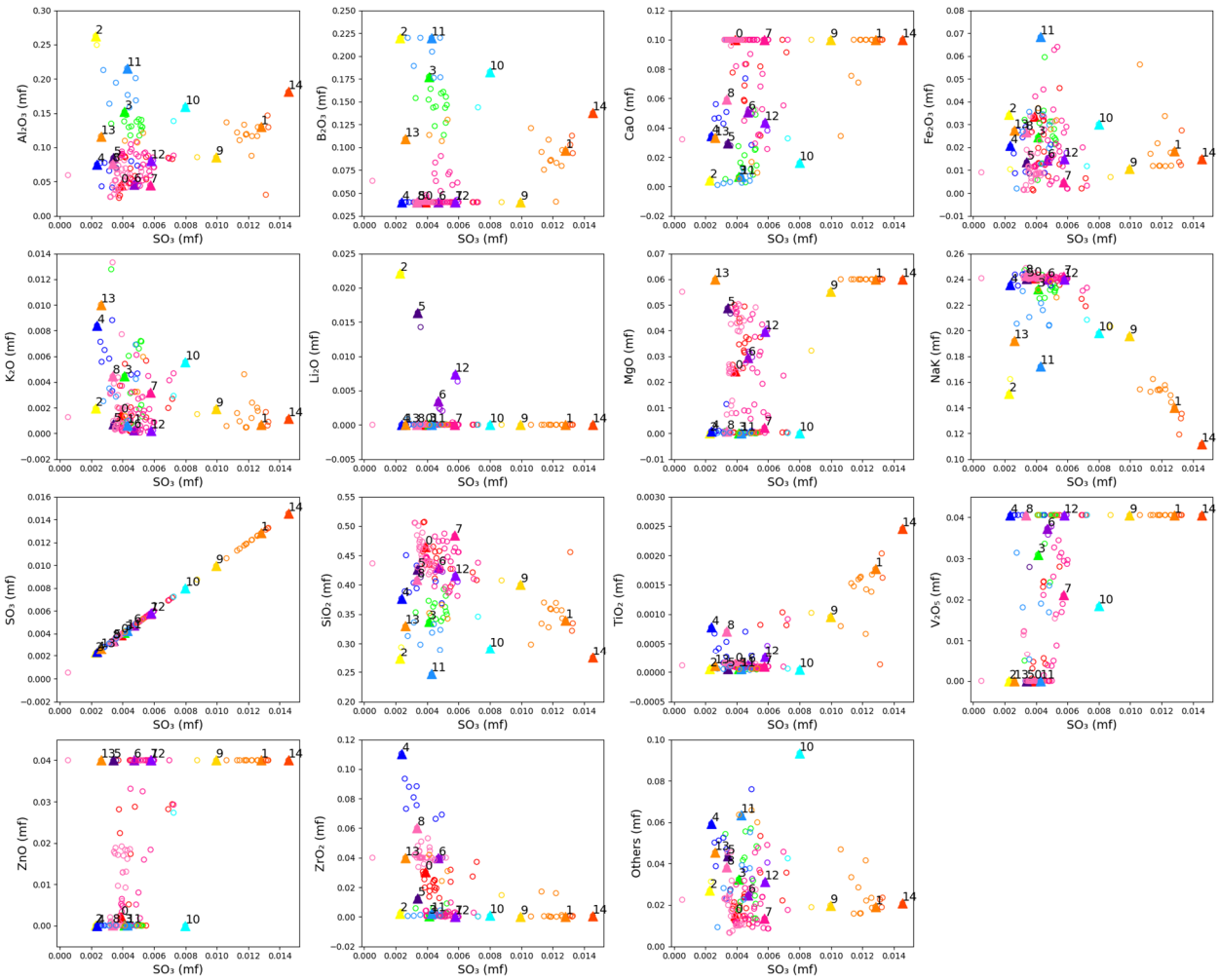

Figure A.3. Major component concentrations for 154 glass compositions versus SO_3. Each color represents a cluster and the numbered triangles show the selected batch to represent each cluster.

Appendix B – Morphology/Color of Each Quenched Glass

The photographs in this appendix show each glass after melting in a platinum/rhodium crucible at the melt temperatures and times specified in Section 2.2 of the main report.

Figure B.1. Photograph of glass HLW-APPS-01 morphology after the second melt.

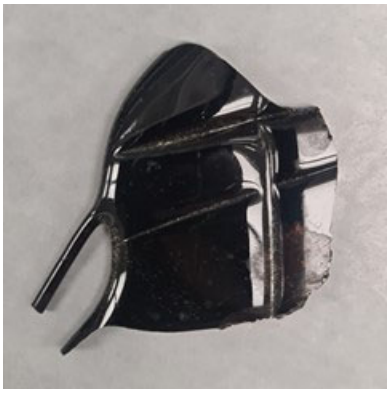

Figure B.2. Photograph of glass HLW-APPS-02 morphology after the second melt.

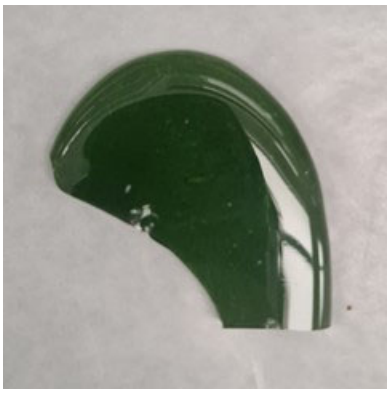

Figure B.3. Photograph of glass HLW-APPS-03 morphology after the second melt.

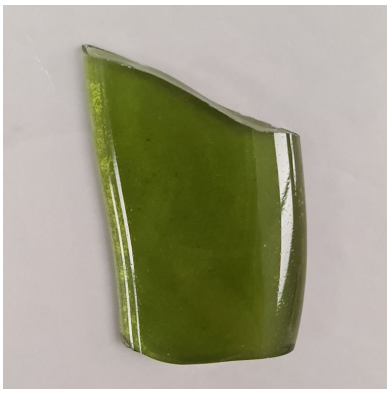

Figure B.4. Photograph of glass HLW-APPS-04-1 morphology after the second melt.

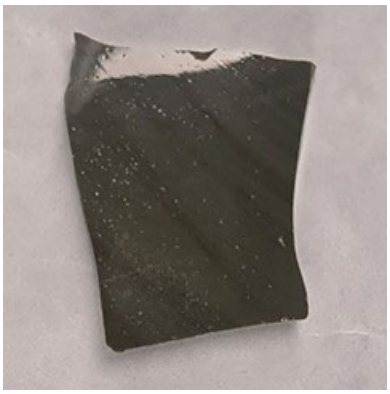

Figure B.5. Photograph of glass HLW-APPS-05 morphology after the second melt.

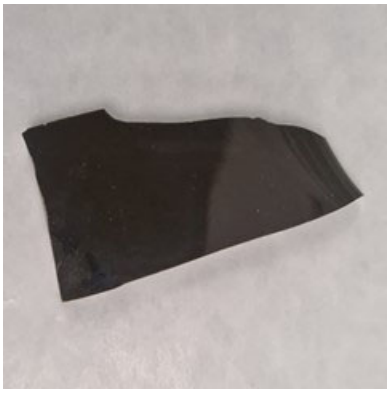

Figure B.6. Photograph of glass HLW-APPS-06 morphology after the second melt.

Figure B.7. Photograph of glass HLW-APPS-07-2 morphology after the second melt.

Figure B.8. Photograph of glass HLW-APPS-08 morphology after the second melt.

Figure B.9. Photograph of glass HLW-APPS-09 morphology after the second melt.

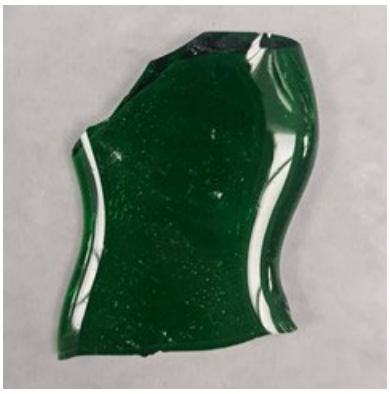

Figure B.10. Photograph of glass HLW-APPS-10 morphology after the second melt.

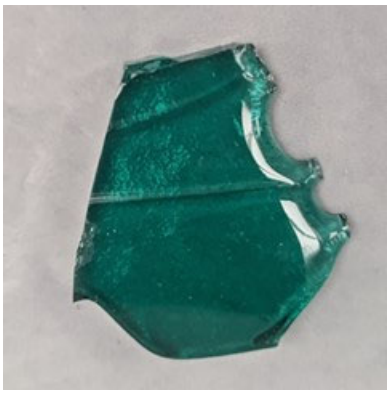

Figure B.11. Photograph of glass HLW-APPS-11 morphology after the second melt.

Figure B.12. Photograph of glass HLW-APPS-12 morphology after the second melt.

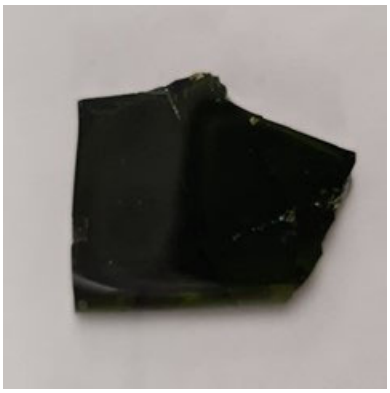

Figure B.13. Photograph of glass HLW-APPS-13-1 morphology after the second melt.

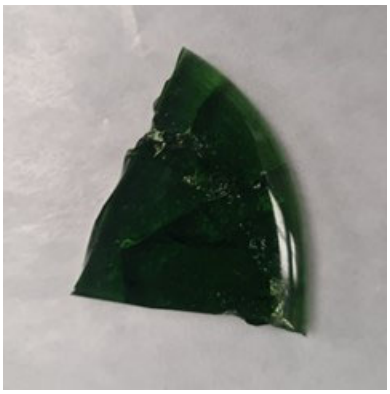

Figure B.14. Photograph of glass HLW-APPS-14 morphology after the second melt.

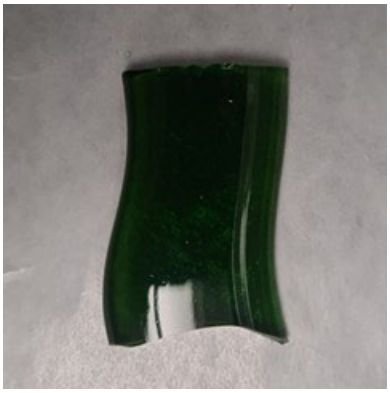

Figure B.15. Photograph of glass HLW-APPS-15 morphology after the second melt.

Appendix C – Comparison Measured and Target Chemical Compositions

The tables in this appendix compare the targeted glass compositions with the analyzed glass compositions and their percent differences.

Table C.1. Targeted vs. measured composition (mass fraction) for the HLW-APPS glasses.

	HLW-APPS-01	HLW-APPS-01-Q	HLW-APPS-01-Q	HLW-APPS-01-Q	HLW-APPS-02	HLW-APPS-02-Q	HLW-APPS-02-Q	HLW-APPS-02-Q
Oxide	Target (wt%)	Measured (wt%)	σ (wt%)	RPD* (%)	Target	Measured	σ (wt%)	RPD (%)
Ag_2O	0.009	0.005	0.006	-39%	0.004	0.004	0.005	5%
Al_2O_3	26.32	25.99	0.07	-1%	21.58	21.56	0.05	0%
B_2O_3	22.1	18.63	0.15	-16%	22.17	18.94	0.25	-15%
Bi_2O_3	0.09	0.08	0.01	-18%	0.46	0.40	0.02	-13%
CaO	0.41	0.41	0.01	-1%	0.67	0.66	0.01	-1%
Cl	0.19	0.15	0.00	-24%	0.20	0.16	0.00	-23%
Cr_2O_3	0.13	0.12	0.05	-9%	0.09	0.08	0.02	-15%
F	0.21	0.19	0.03	-11%	0.45	0.41	0.06	-9%
Fe_2O_3	3.43	3.35	0.04	-2%	6.85	6.61	0.12	-3%
K_2O	0.20	0.21	0.00	6%	0.07	0.08	0.00	20%
Li_2O	2.13	NM**	NM	NM	0.00	NM	NM	NM
MgO	0.01	0.02	0.01	60%	0.01	0.01	0.01	17%
MnO	0.35	0.35	0.01	0%	0.28	0.29	0.01	3%
Na_2O	15.11	15.16	0.05	0%	17.32	17.54	0.04	1%
Nd_2O_3	0.32	0.33	0.03	3%	0.77	0.74	0.05	-3%
NiO	0.34	0.003	0.004	-99%	0.58	0.55	0.08	-6%
P_2O_5	0.37	0.35	0.01	-4%	2.30	2.25	0.03	-2%
PbO	0.18	0.17	0.03	-8%	0.49	0.46	0.03	-6%
RuO_2	0.008	0.004	0.005	-44%	0.014	0.01	0.02	-47%
SiO_2	27.35	27.37	0.24	0%	24.76	24.84	0.11	0%
SO_3	0.27	0.21	0.02	-22%	0.51	0.44	0.01	-13%
V_2O_5	0.00	0.004	0.009	<100%	0.00	0.004	0.006	<100%
ZnO	0.01	0.017	0.009	137%	0.01	0.02	0.02	137%
ZrO_2	0.43	0.39	0.02	-8%	0.42	0.39	0.03	-7%
SUM	100	93.51			100	96.45		

* RPD - Relative Percentage Difference
** NM – not measured

Table C.1. Targeted vs. measured composition (mass fraction) for the HLW-APPS glasses (cont.).

	HLW-APPS-03	HLW-APPS-03-Q	HLW-APPS-03-Q	HLW-APPS-03-Q	HLW-APPS-04	HLW-APPS-04-1-Q	HLW-APPS-04-1-Q	HLW-APPS-04-1-Q
Oxide	Target (wt%)	Measured (wt%)	σ (wt%)	RPD* (%)	Target	Measured	σ (wt%)	RPD (%)
Ag_2O	0.032	0.027	0.006	-16%	0.000	0.001	0.001	> 100%
Al_2O_3	4.52	4.68	0.02	4%	3.00	3.07	0.02	2%
B_2O_3	4.01	4.34	0.23	8%	4.00	4.19	0.14	5%
Bi_2O_3	0.02	0.01	0.01	-52%	0.001	0.005	0.01	851%
CaO	9.16	9.07	0.02	-1%	10.00	9.89	0.03	-1%
Cl	0.18	0.15	0.01	-18%	0.07	0.06	0.00	-17%
Cr_2O_3	0.08	0.08	0.01	0%	0.04	0.03	0.01	-32%
F	4.52	5.25	0.11	16%	1.63	1.83	0.07	12%
Fe_2O_3	1.65	1.64	0.03	-1%	0.22	0.22	0.01	1%
K_2O	0.73	0.75	0.01	4%	0.10	0.13	0.00	34%
Li_2O	0	NM	NM	NM	4.50	NM	NM	NM
MgO	0.06	0.09	0.01	40%	0.000	0.01	0.01	>100%
MnO	0.23	0.24	0.01	4%	0.005	0.007	0.01	36%
Na_2O	19.44	19.89	0.04	2%	11.93	12.04	0.04	1%
Nd_2O_3	0.52	0.52	0.03	-2%	0.03	0.04	0.02	3%
NiO	0.05	0.000	0.001	-99%	0.009	0.003	0.004	-70%
P_2O_5	0.19	0.18	0.01	-4%	0.37	0.37	0.01	1%
PbO	0.06	0.03	0.03	-46%	0.004	0.004	0.01	9%
RuO_2	0	0.004	0.006	>100%	0.000	0.001	0.004	>100%
SiO_2	45.04	46.95	0.21	4%	58.47	61.46	0.88	5%
SO_3	0.24	0.20	0.02	-15%	1.50	1.43	0.03	-5%
V_2O_5	0	0.002	0.003	>9%	4.06	4.03	0.03	-1%
ZnO	0	0.013	0.018	>100%	0.000	0.008	0.007	>100%
ZrO_2	9.27	8.83	0.08	-5%	0.06	0.05	0.02	-22%
SUM	100	102.95			100.00	98.86		

* RPD - Relative Percentage Difference
** NM – not measured

Table C.1. Targeted vs. measured composition (mass fraction) for the HLW-APPS glasses (cont.).

	HLW-APPS-05	HLW-APPS-05-Q	HLW-APPS-05-Q	HLW-APPS-05-Q	HLW-APPS-06	HLW-APPS-06-Q	HLW-APPS-06-Q	HLW-APPS-06-Q
Oxide	Target (wt%)	Measured (wt%)	σ (wt%)	RPD* (%)	Target	Measured	σ (wt%)	RPD (%)
Ag_2O	0.013	0.004	0.003	-68%	0.005	0.002	0.002	-58%
Al_2O_3	14.89	14.90	0.06	0%	15.14	15.18	0.11	0%
B_2O_3	17.25	15.10	0.21	-12%	16.87	15.17	0.34	-10%
Bi_2O_3	0.02	0.01	0.01	-28%	0.11	0.11	0.01	-6%
CaO	4.29	4.22	0.02	-2%	0.65	0.65	0.00	0%
Cl	0.26	0.21	0.00	-18%	0.33	0.25	0.01	-24%
Cr_2O_3	1.44	1.49	0.40	4%	0.91	0.97	0.54	7%
F	0.24	0.26	0.04	8%	0.15	0.16	0.03	1%
Fe_2O_3	2.31	2.24	0.04	-3%	2.44	2.39	0.03	-2%
K_2O	1.33	1.34	0.01	0%	0.46	0.48	0.00	5%
Li_2O	0.00	NM	NM	NM	0.01	NM	NM	NM
MgO	0.07	0.08	0.01	9%	0.02	0.02	0.00	17%
MnO	0.12	0.12	0.01	1%	0.12	0.12	0.01	2%
Na_2O	20.53	20.56	0.07	0%	23.04	22.91	0.11	-1%
Nd_2O_3	0.68	0.67	0.03	-1%	0.36	0.35	0.03	-3%
NiO	0.14	0.005	0.004	-96%	0.34	0.35	0.01	4%
P_2O_5	2.53	2.52	0.03	-1%	0.69	0.68	0.02	-1%
PbO	0.08	0.06	0.04	-30%	0.13	0.12	0.03	-7%
RuO_2	0.000	0.000	0.001	> 100%	0.000	0.001	0.002	> 100%
SiO_2	32.99	32.65	0.31	-1%	37.67	38.20	0.19	1%
SO_3	0.40	0.33	0.01	-17%	0.49	0.38	0.01	-21%
V_2O_5	0.004	0.005	0.008	39%	0.008	0.007	0.014	-15%
ZnO	0.007	0.013	0.015	84%	0.013	0.014	0.014	8%
ZrO_2	0.38	0.36	0.02	-6%	0.06	0.05	0.02	-12%
SUM	100	97.14			100.00	98.57		

* RPD - Relative Percentage Difference
** NM – not measured

Table C.1. Targeted vs. measured composition (mass fraction) for the HLW-APPS glasses (cont.).

Oxide	HLW-APPS-07	HLW-APPS-07-2-Q	HLW-APPS-07-2-Q	HLW-APPS-07-2-Q	HLW-APPS-08	HLW-APPS-08-Q	HLW-APPS-08-Q	HLW-APPS-08-Q
	Target (wt%)	Measured (wt%)	σ (wt%)	RPD* (%)	Target	Measured	σ (wt%)	RPD (%)
Ag_2O	0.00	0.003	0.006	20%	0.02	0.013	0.007	-36%
Al_2O_3	16.08	15.95	0.06	-1%	3.89	4.04	0.03	4%
B_2O_3	18.50	18.56	0.29	0%	4.01	4.59	0.14	15%
Bi_2O_3	0.08	0.07	0.01	-13%	0.02	0.01	0.01	-21%
CaO	1.63	1.60	0.02	-2%	4.29	4.27	0.01	0%
Cl	0.18	0.13	0.00	-30%	0.33	0.26	0.01	-21%
Cr_2O_3	0.10	0.10	0.01	-4%	0.04	0.04	0.00	-7%
F	0.23	0.24	0.04	5%	3.11	3.30	0.08	6%
Fe_2O_3	3.04	2.96	0.05	-3%	2.59	2.59	0.02	0%
K_2O	0.58	0.57	0.01	-1%	0.47	0.50	0.00	8%
Li_2O	0.00	NM	NM	NM	0.00	NM	NM	NM
MgO	0.01	0.01	0.00	13%	0.07	0.08	0.01	19%
MnO	0.07	0.11	0.02	57%	0.22	0.23	0.02	2%
Na_2O	19.75	20.03	0.05	1%	24.62	24.91	0.03	1%
Nd_2O_3	2.20	2.11	0.05	-4%	0.39	0.40	0.02	1%
NiO	0.81	0.006	0.007	-99%	0.10	0.108	0.008	10%
P_2O_5	3.99	3.81	0.04	-4%	0.23	0.24	0.02	2%
PbO	0.31	0.30	0.04	-6%	0.11	0.09	0.03	-18%
RuO_2	0.00	0.001	0.002	> 100%	0.01	0.007	0.007	-20%
SiO_2	29.38	29.76	0.15	1%	48.91	50.95	0.28	4%
SO_3	0.96	0.59	0.02	-38%	0.41	0.34	0.02	-17%
V_2O_5	2.00	2.005	0.034	0%	0.00	0.000	0.000	-
ZnO	0.00	0.003	0.006	-19%	0.00	0.013	0.011	166%
ZrO_2	0.09	0.09	0.03	-4%	6.14	6.16	0.10	0%
SUM	100.00	99.00			100.00	103.14		

* RPD - Relative Percentage Difference
** NM – not measured

Table C.1. Targeted vs. measured composition (mass fraction) for the HLW-APPS glasses (cont.).

	HLW-APPS-09	HLW-APPS-09-Q	HLW-APPS-09-Q	HLW-APPS-09-Q	HLW-APPS-10	HLW-APPS-10-Q	HLW-APPS-10-Q	HLW-APPS-10-Q
Oxide	Target (wt%)	Measured (wt%)	σ (wt%)	RPD* (%)	Target	Measured	σ (wt%)	RPD (%)
Ag_2O	0.002	0.002	0.002	8%	0	0.002	0.003	>100%
Al_2O_3	10.52	10.57	0.04	1%	8.67	8.75	0.05	1%
B_2O_3	4.00	4.06	0.26	2%	4.02	4.22	0.16	5%
Bi_2O_3	0.001	0.01	0.01	>100%	0.001	0.00	0.01	>100%
CaO	9.97	9.79	0.02	-2%	9.50	9.39	0.05	-1%
Cl	0.13	0.10	0.00	-18%	0.33	0.27	0.00	-19%
Cr_2O_3	0.03	0.03	0.01	-3%	0.24	0.24	0.01	-2%
F	1.52	1.69	0.05	11%	0.68	0.80	0.04	18%
Fe_2O_3	0.62	0.61	0.02	-2%	0.57	0.57	0.02	-1%
K_2O	0.06	0.09	0.00	47%	0.08	0.10	0.00	33%
Li_2O	4.50			NM	0			NM
MgO	0.00	0.03	0.00	>100%	0	0.03	0.00	>100%
MnO	0.04	0.04	0.01	2%	0.12	0.13	0.01	5%
Na_2O	13.28	13.37	0.05	1%	24.97	24.98	0.12	0%
Nd_2O_3	0.07	0.07	0.01	0%	0.29	0.30	0.03	3%
NiO	0.028	0.002	0.003	-93%	0.054	0.00	0.00	-94%
P_2O_5	0.30	0.30	0.01	-1%	2.30	2.27	0.04	-1%
PbO	0.01	0.01	0.01	-41%	0.02	0.03	0.03	21%
RuO_2	0.002	0.001	0.001	-75%	0	0.00	0.00	>100%
SiO_2	49.37	50.89	0.26	3%	46.35	46.92	0.40	1%
SO_3	1.45	1.37	0.02	-5%	0.42	0.31	0.02	26%
V_2O_5	4.06	4.051	0.051	0%	0	0.01	0.01	>100%
ZnO	0.00	0.007	0.010	>100%	0	0.01	0.02	>100%
ZrO_2	0.03	0.02	0.02	-21%	1.40	1.37	0.05	-2%
SUM	100.00	97.12			100.0003	100.70		

* RPD - Relative Percentage Difference
** NM – not measured

Table C.1. Targeted vs. measured composition (mass fraction) for the HLW-APPS glasses (cont.).

	HLW-APPS-11	HLW-APPS-11-Q	HLW-APPS-11-Q	HLW-APPS-11-Q	HLW-APPS-12-Q	HLW-APPS-12-Q	HLW-APPS-12-Q	HLW-APPS-12-Q
Oxide	Target (wt%)	Measured (wt%)	σ (wt%)	RPD* (%)	Target	Measured	σ (wt%)	RPD (%)
Ag_2O	0.00	0.001	0.001	>100%	0.00	0.001	0.002	>100%
Al_2O_3	6.93	6.95	0.03	0%	4.68	4.77	0.03	2%
B_2O_3	4.02	4.27	0.25	6%	4.00	4.37	0.18	9%
Bi_2O_3	0.07	0.03	0.01	-52%	0.25	0.23	0.01	-7%
CaO	9.71	9.52	0.02	-2%	9.03	8.93	0.01	-1%
Cl	0.38	0.31	0.00	-19%	0.38	0.31	0.00	-19%
Cr_2O_3	0.02	0.02	0.01	4%	0.04	0.03	0.01	-12%
F	0.17	0.22	0.04	34%	0.24	0.27	0.04	12%
Fe_2O_3	0.84	0.82	0.03	-2%	0.95	0.95	0.02	0%
K_2O	0.02	0.05	0.00	>100%	0.03	0.06	0.00	>100%
Li_2O	0.00	NM	NM	NM	0.00	NM	NM	NM
MgO	0.00	0.03	0.00	>100%	0.00	0.03	0.01	>100%
MnO	0.01	0.02	0.01	47%	0.09	0.10	0.01	9%
Na_2O	25.18	24.95	0.07	-1%	25.27	25.26	0.06	0%
Nd_2O_3	0.54	0.52	0.04	-4%	0.14	0.14	0.02	2%
NiO	0.17	0.00	0.00	-100%	0.14	0.15	0.01	7%
P_2O_5	1.56	1.52	0.05	-3%	1.35	1.33	0.02	-2%
PbO	0.09	0.07	0.04	-21%	0.05	0.03	0.01	-41%
RuO_2	0.00	0.00	0.00	>100%	0.00	0.00	0.01	>100%
SiO_2	49.57	51.19	0.53	3%	52.68	53.44	0.57	1%
SO_3	0.72	0.55	0.02	-23%	0.59	0.46	0.02	-22%
V_2O_5	0.00	0.00	0.00	>100%	0.00	0.00	0.01	>100%
ZnO	0.00	0.01	0.01	>100%	0.00	0.01	0.01	>100%
ZrO_2	0.01	0.02	0.02	97%	0.09	0.07	0.03	-16%
SUM	100.00	101.06			100.00	100.96		

* RPD - Relative Percentage Difference
** NM – not measured

Table C.1. Targeted vs. measured composition (mass fraction) for the HLW-APPS glasses (cont.).

	HLW-APPS-13	HLW-APPS-13-1-Q	HLW-APPS-13-1-Q	HLW-APPS-13-1-Q	HLW-APPS-14	HLW-APPS-14-Q	HLW-APPS-14-Q	HLW-APPS-14-Q
Oxide	Target (wt%)	Measured (wt%)	σ (wt%)	RPD* (%)	Target (wt%)	Measured (wt%)	σ (wt%)	RPD* (%)
Ag_2O	0.010	0.006	0.007	-41%	0.002	0.001	0.001	-33%
Al_2O_3	4.54	4.60	0.03	1%	4.62	4.71	0.03	2%
B_2O_3	4.00	4.59	0.13	15%	4.00	4.22	0.19	5%
Bi_2O_3	0.002	0.004	0.006	80%	0.001	0.008	0.007	>100%
CaO	8.31	8.32	0.01	0%	9.53	9.50	0.03	0%
Cl	0.38	0.31	0.00	-18%	0.39	0.31	0.00	-19%
Cr_2O_3	0.12	0.12	0.01	-3%	0.22	0.21	0.01	-4%
F	0.12	0.12	0.05	1%	0.22	0.24	0.04	10%
Fe_2O_3	3.00	2.94	0.03	-2%	0.37	0.38	0.02	0%
K_2O	0.15	0.18	0.01	16%	0.34	0.37	0.01	8%
Li_2O	0.00	NM	NM	NM	0.00	NM	NM	NM
MgO	0.00	0.00	0.01	182%	0.006	0.007	0.006	14%
MnO	0.44	0.45	0.01	2%	0.03	0.03	0.01	6%
Na_2O	25.17	25.17	0.05	0%	25.41	25.38	0.06	0%
Nd_2O_3	0.05	0.04	0.02	-18%	0.05	0.05	0.02	1%
NiO	0.075	0.001	0.002	-98%	0.02	0.02	0.01	9%
P_2O_5	0.33	0.33	0.02	1%	0.65	0.65	0.02	0%
PbO	0.12	0.10	0.03	-10%	0.01	0.01	0.02	10%
RuO_2	0.000	0.001	0.003	>100%	0.001	0.003	0.006	85%
SiO_2	52.68	54.36	0.54	3%	53.39	55.72	0.19	4%
SO_3	0.48	0.41	0.02	-16%	0.72	0.59	0.02	-19%
V_2O_5	0.001	0.002	0.004	71%	0.00	0.01	0.01	>100%
ZnO	0.00	0.01	0.01	>100%	0.002	0.004	0.006	>100%
ZrO_2	0.02	0.02	0.02	>100%	0.01	0.02	0.02	51%
SUM	100	102.08			100	102.44		

* RPD - Relative Percentage Difference
** NM – not measured

Table C.1. Targeted vs. measured composition (mass fraction) for the HLW-APPS glasses (cont.).

	HLW-APPS-15	HLW-APPS-15-Q	HLW-APPS-15-Q	HLW-APPS-15-Q
Oxide	Target (wt%)	Measured (wt%)	σ (wt%)	RPD* (%)
Ag_2O	0.002	0.001	0.002	-49%
Al_2O_3	11.26	11.37	0.04	1%
B_2O_3	8.76	8.52	0.18	-3%
Bi_2O_3	0.00	0.01	0.01	>100%
CaO	10.01	9.96	0.02	0%
Cl	0.29	0.23	0.01	-18%
Cr_2O_3	0.41	0.37	0.01	-9%
F	1.16	1.23	0.05	6%
Fe_2O_3	0.02	0.04	0.01	61%
K_2O	0.21	0.23	0.00	11%
Li_2O	0.00	NM	NM	NM
MgO	0.014	0.020	0.005	44%
MnO	0.004	0.006	0.007	39%
Na_2O	20.86	20.86	0.06	0%
Nd_2O_3	0.10	0.08	0.02	-13%
NiO	0.003	0.006	0.006	>100%
P_2O_5	0.43	0.43	0.02	1%
PbO	0.003	0.02	0.025	>100%
RuO_2	0.000	0.003	0.005	>100%
SiO_2	41.13	43.07	0.19	5%
SO_3	1.27	1.14	0.02	-10%
V_2O_5	4.06	4.128	0.03	>100%
ZnO	0.00	0.007	0.010	>100%
ZrO_2	0.01	0.00	0.01	-58%
SUM	100.00	101.75		

* RPD - Relative Percentage Difference
** NM – not measured

Appendix D – XRD Patterns of Samples With Crystalline Phases Present

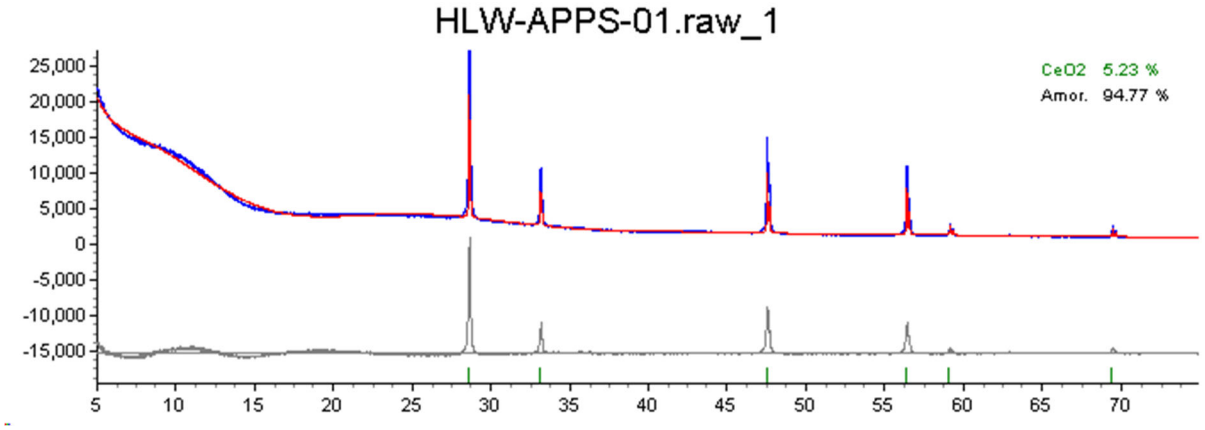

Figure D.1. X-ray diffraction pattern of HLW-APPS-05 sample showing minor traces of crystalline peaks in the sample.

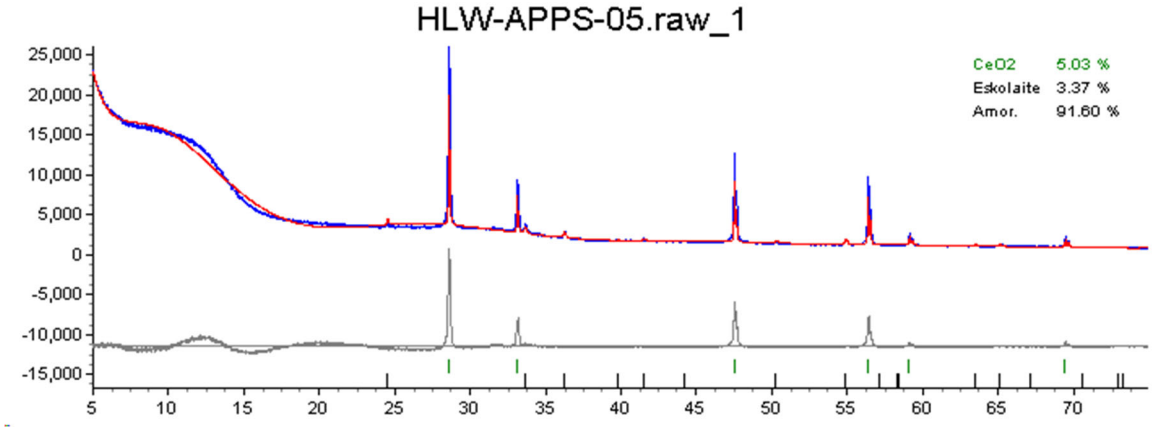

Figure D.2. X-ray diffraction pattern of HLW-APPS-05 sample showing crystalline Eskolaite.

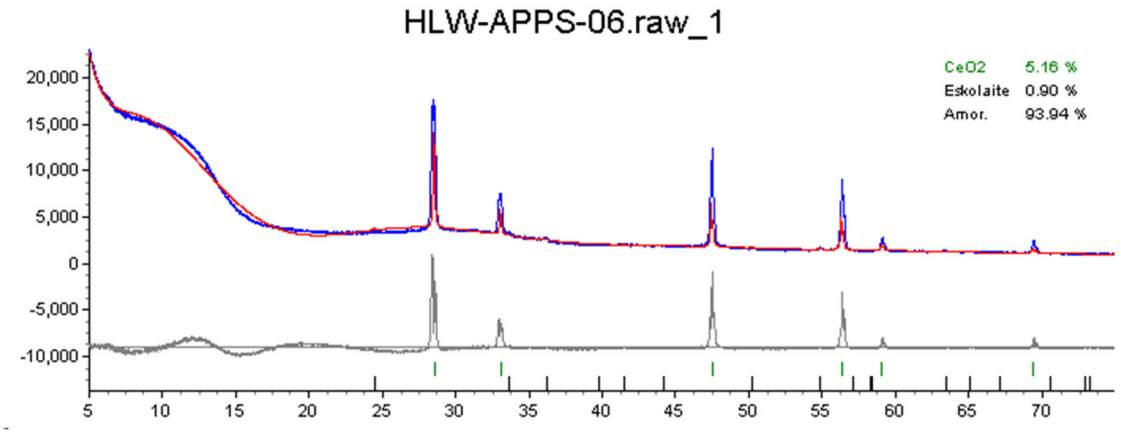

Figure D.3. X-ray diffraction pattern of HLW-APPS-06 sample showing crystalline Eskolaite.

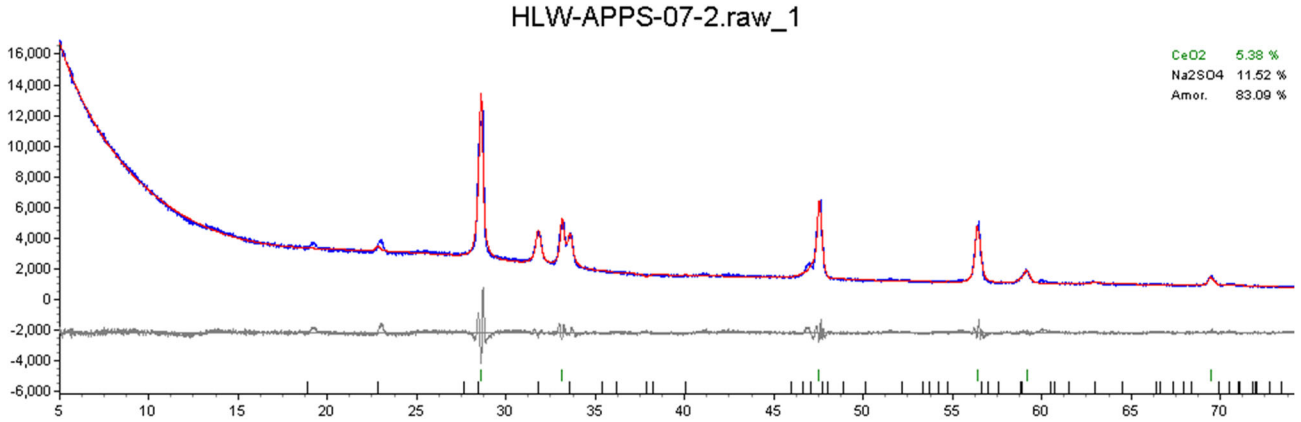

Figure D.4. X-ray diffraction pattern of HLW-APPS-07-2 sample showing crystalline Na_2SO_4.

Appendix E – Morphology/Color of Each Glass after Canister Centerline Cooling

The photographs in this appendix show each glass after canister centerline cooling (CCC) as described in Section 2.5. When applicable, X-ray diffraction (XRD) scans are reported.

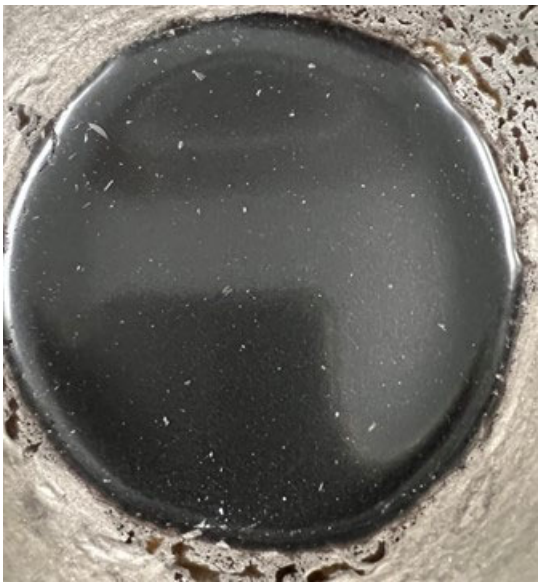

Figure E.1. Glass HLW-APPS-01 morphology after CCC. XRD scan on next page.

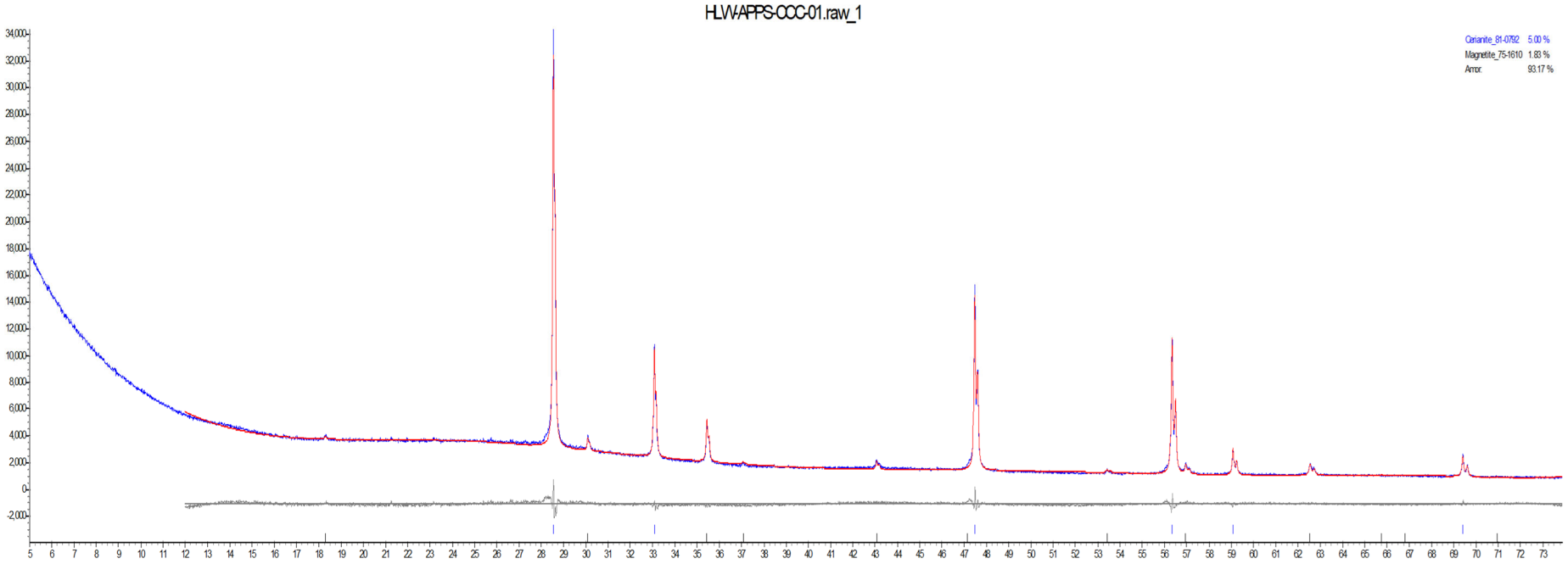

Figure E.2. XRD scan of glass HLW-APPS-01 after CCC.

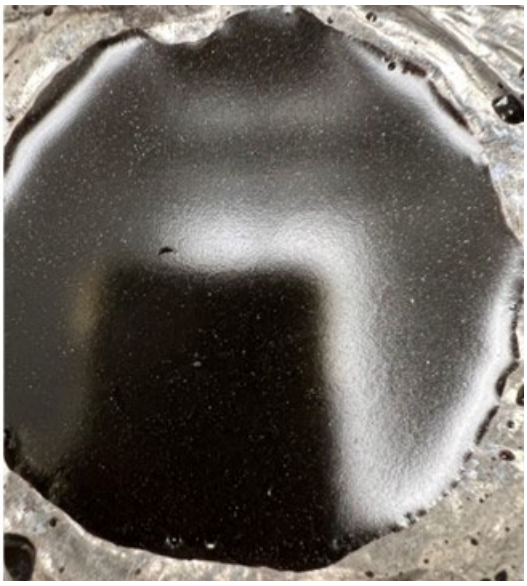

Figure E.3. Glass HLW-APPS-02 morphology after CCC. XRD scan on next page.

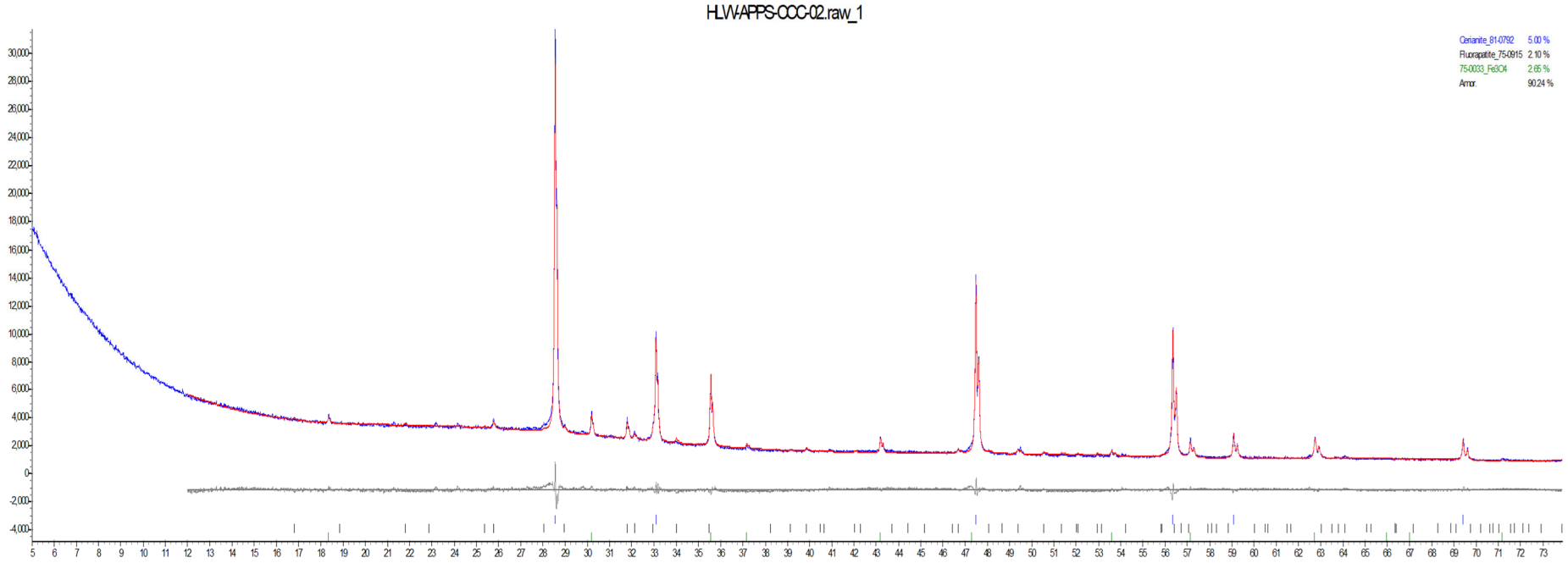

Figure E.4. XRD scan of glass HLW-APPS-02 after CCC.

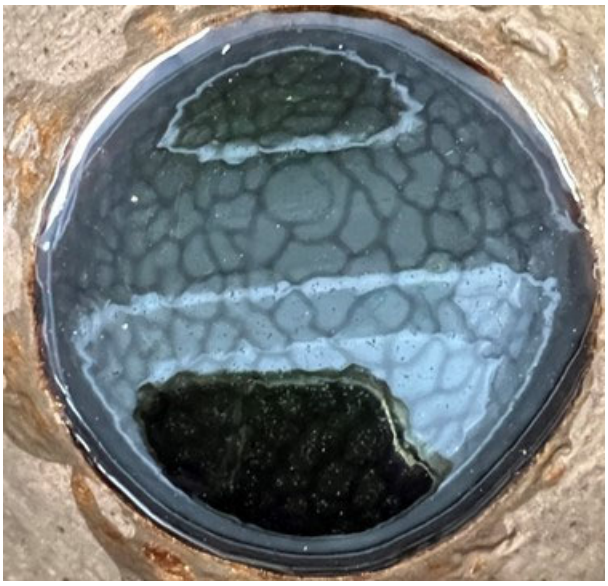

Figure E.5. Glass HLW-APPS-03 morphology after CCC. Amorphous by XRD analysis.

Figure E.6. Glass HLW-APPS-04-1 morphology after CCC. Amorphous by ARX analysis.

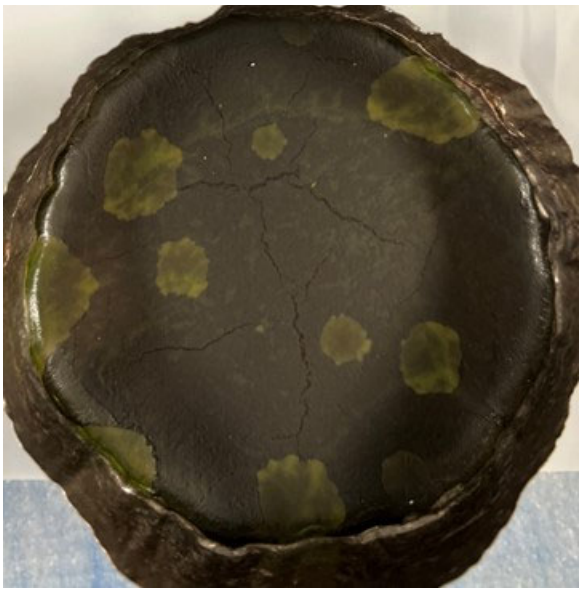

Figure E.7. Glass HLW-APPS-05 morphology after CCC. XRD scan on next page.

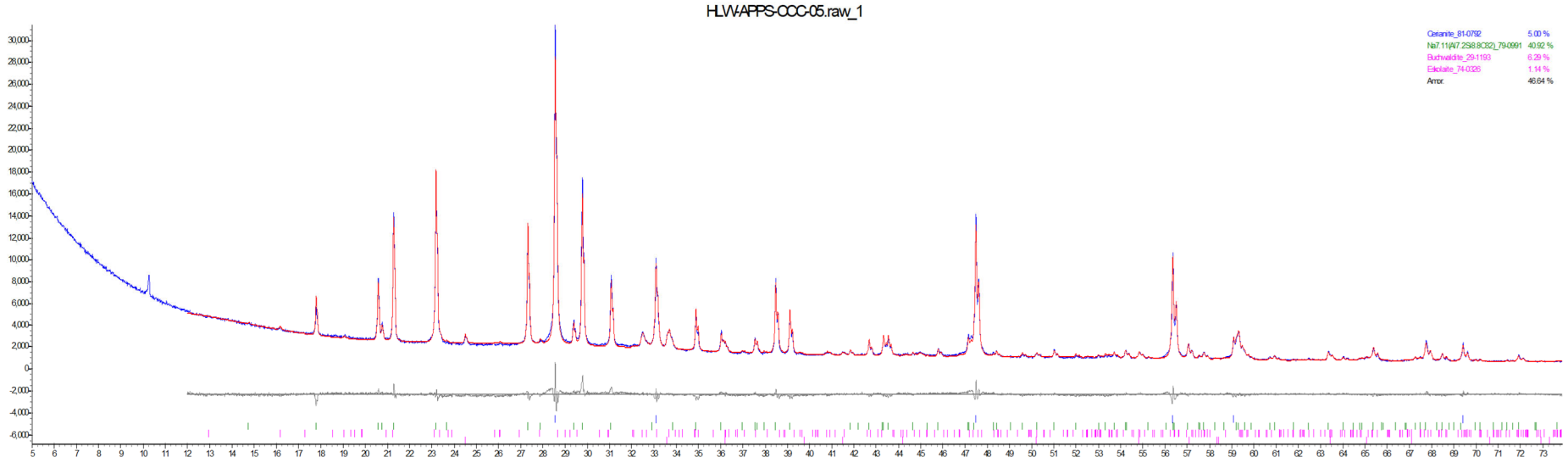

Figure E.8. XRD scan of glass HLW-APPS-05 after CCC.

Figure E.9. Glass HLW-APPS-06 morphology after CCC. XRD scan on next page.

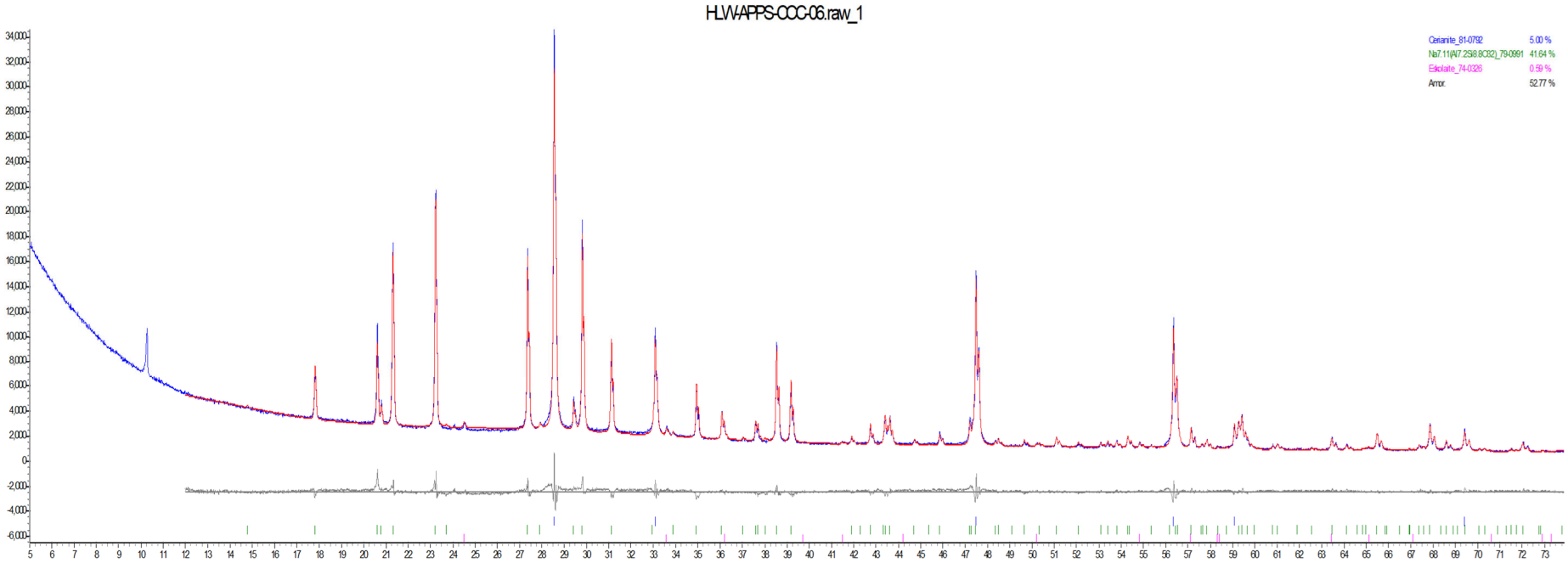

Figure E.10. XRD scan of glass HLW-APPS-06 after CCC.

Figure E.11. Glass HLW-APPS-07-2 morphology after CCC. XRD scan on next page.

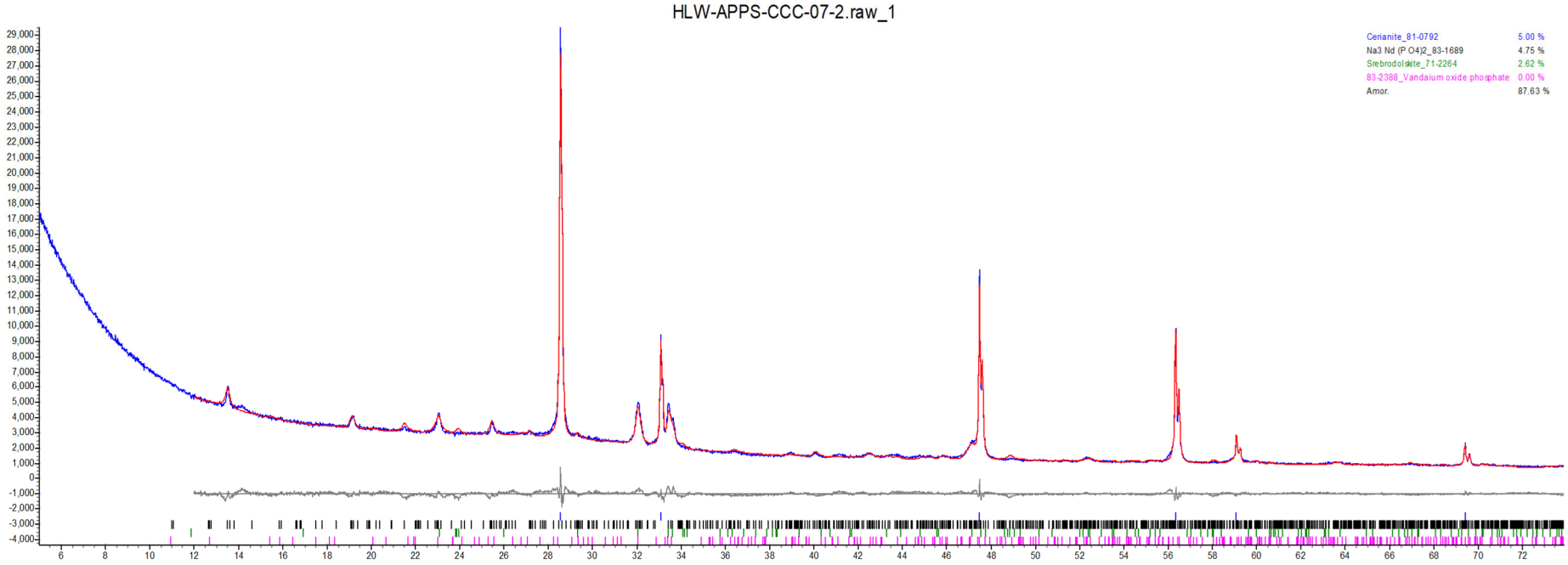

Figure E.12. XRD scan of glass HLW-APPS-07-2 after CCC.

Figure E.13. Glass HLW-APPS-08 morphology after CCC. Amorphous by XRD analysis.

Figure E.14. Glass HLW-APPS-09 morphology after CCC. Amorphous by XRD analysis.

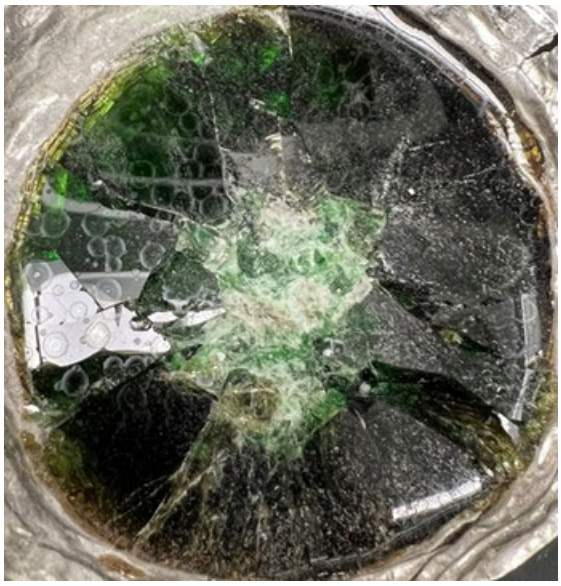

Figure E.15. Glass HLW-APPS-10 morphology after CCC. Amorphous by XRD analysis.

Figure E.16. Glass HLW-APPS-11 morphology after CCC. XRD scan on next page.

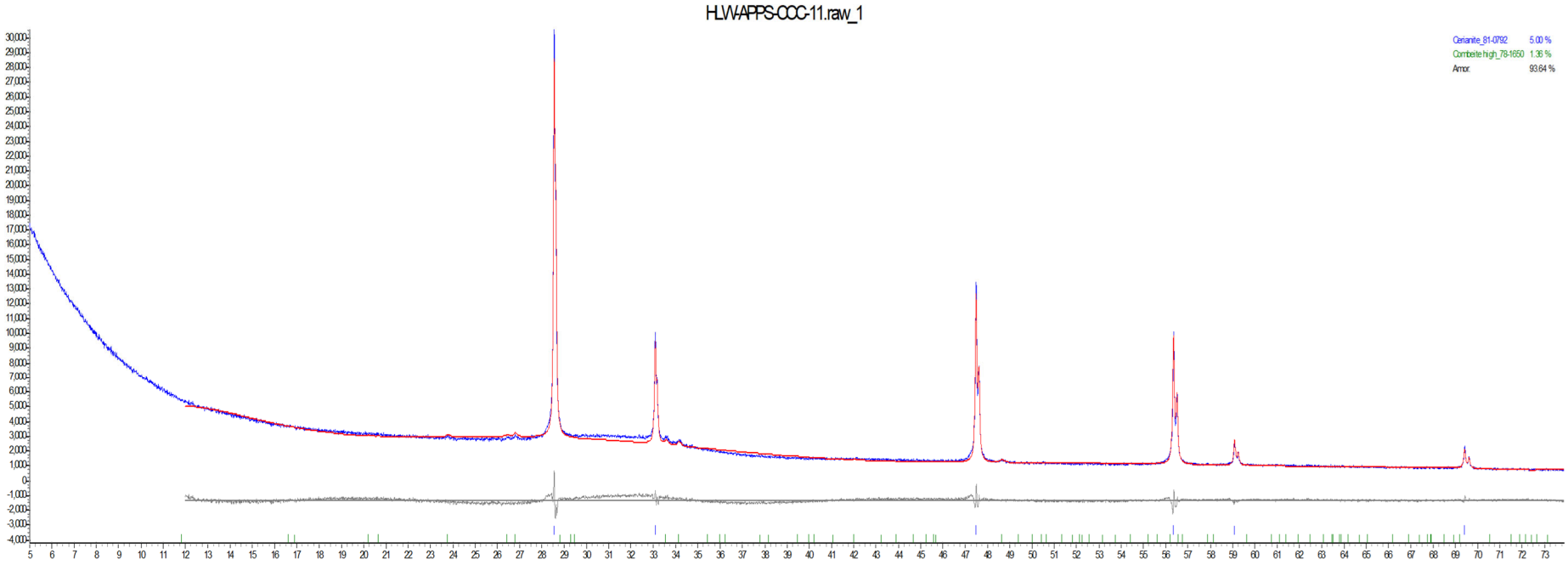

Figure E.17. XRD scan of glass HLW-APPS-11 after CCC.

Figure E.18. Glass HLW-APPS-12 morphology after CCC. XRD scan on next page.

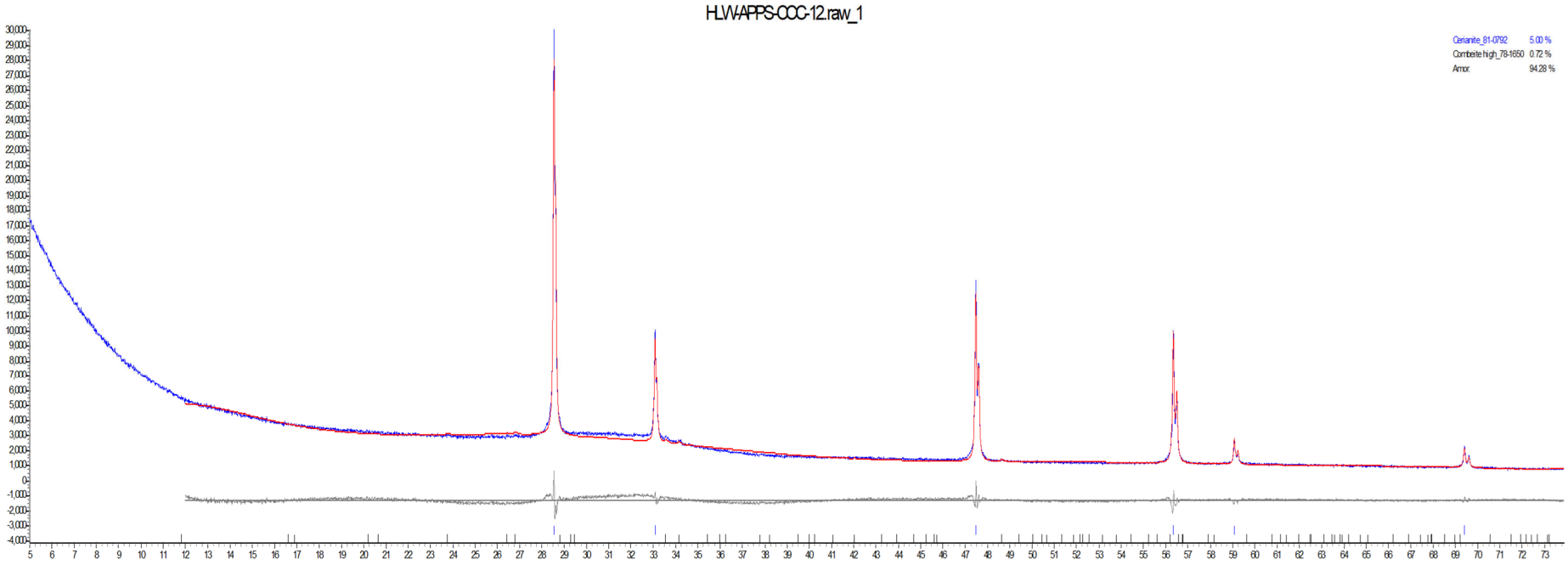

Figure E.19. XRD scan of glass HLW-APPS-12 after CCC.

Figure E.20. Glass HLW-APPS-13-1 morphology after CCC. XRD scan on next page.

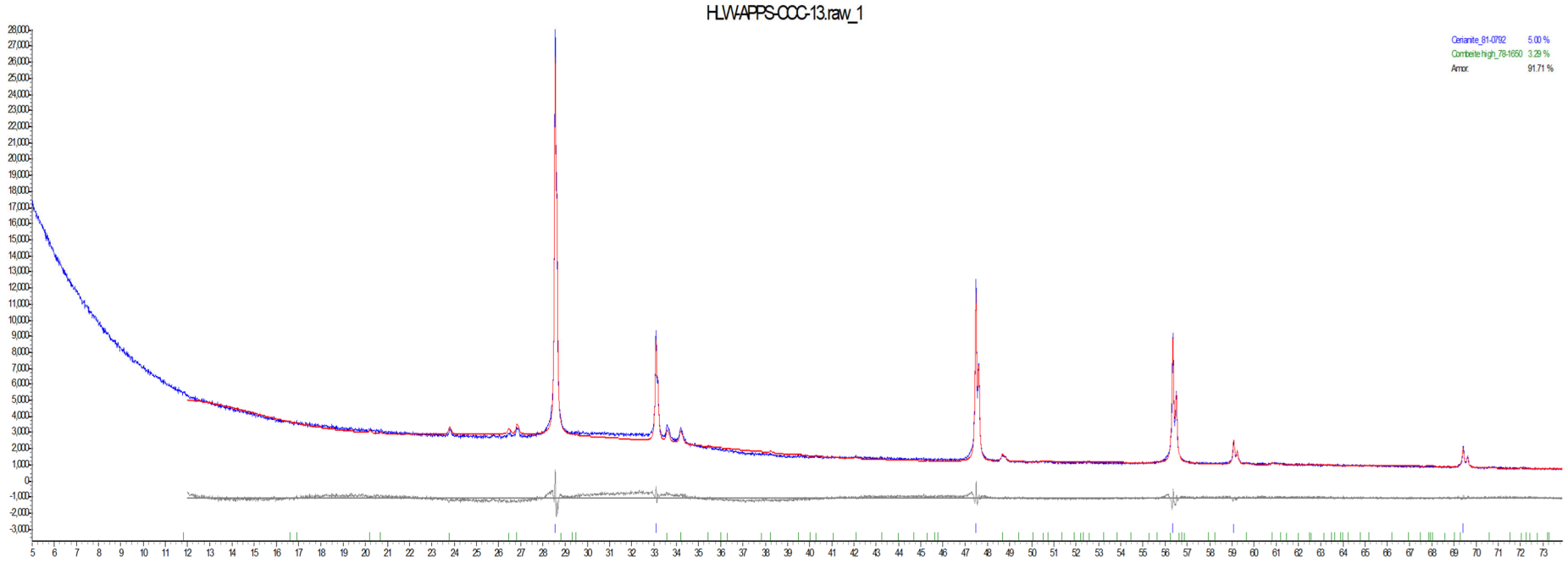

Figure E.21. XRD scan of glass HLW-APPS-13-1 after CCC using ~1 g of sample.

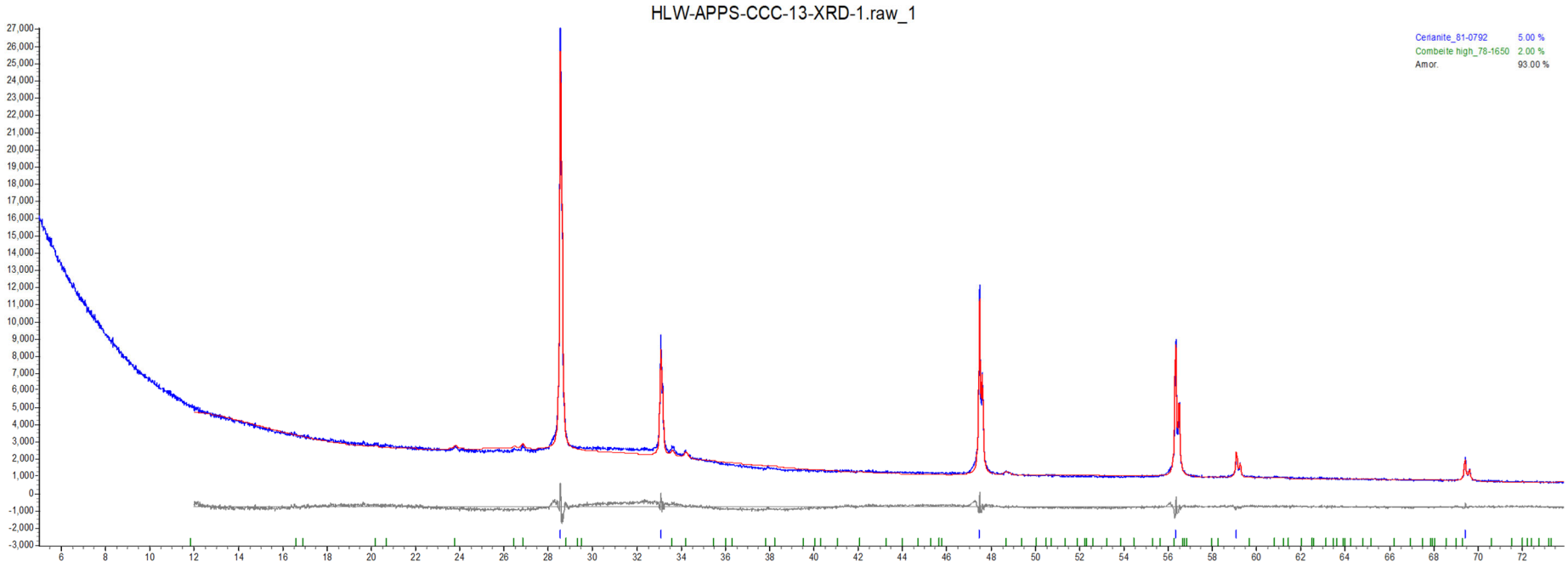

Figure E.22. XRD scan of glass HLW-APPS-13-1 after CCC using ~2 g of sample.

Figure E.23. Glass HLW-APPS-14 morphology after CCC. XRD scan on next page.

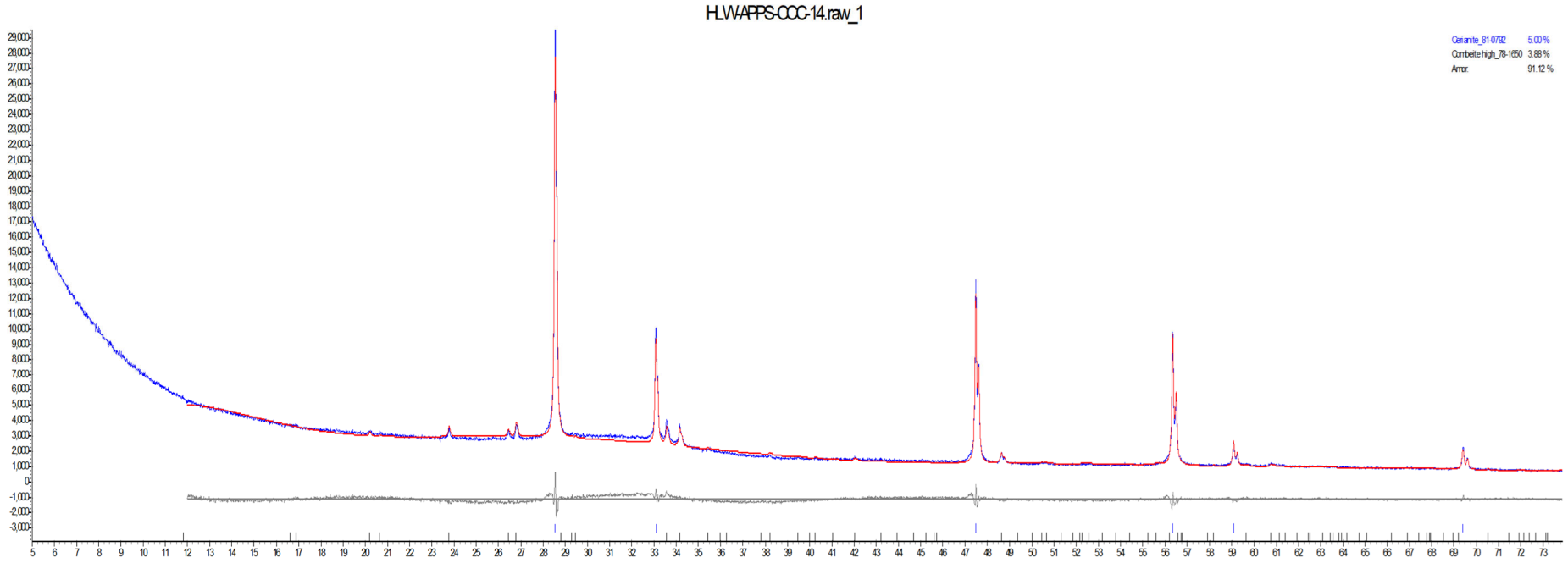

Figure E.24. XRD scan of glass HLW-APPS-14 after CCC.

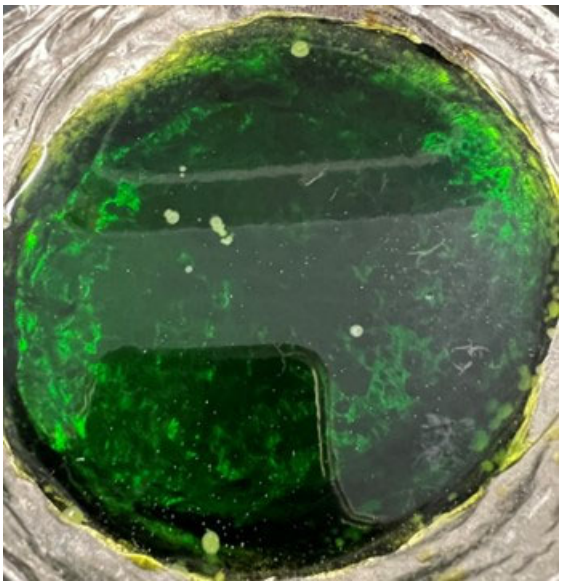

Figure E.25. Glass HLW-APPS-15 morphology after CCC. Amorphous by XRD analysis.

Appendix F – Crystal Fraction of Heat-Treated Glasses

This appendix contains photographs of the HWL-APPS glasses after they were heat-treated at 950 °C for 24 hours as described in Section 2.6. Note that the glasses HLW-APPS-09 and HLW-APPS-13-1 were not heat treated at 950 °C because found to be homogeneous at lower temperature, at 850 °C and 900 °C respectively. When T_L was estimated to be > 850 °C, the table with measured temperatures (°C), crystal content (wt%) and relative plot of the main crystalline phase is reported. XRD scan for 950 °C heat treated samples is reported when applicable. Percentage of crystal content in the reported XRD image are reported before adjustment made from using a spike chemical with < 100% purity.

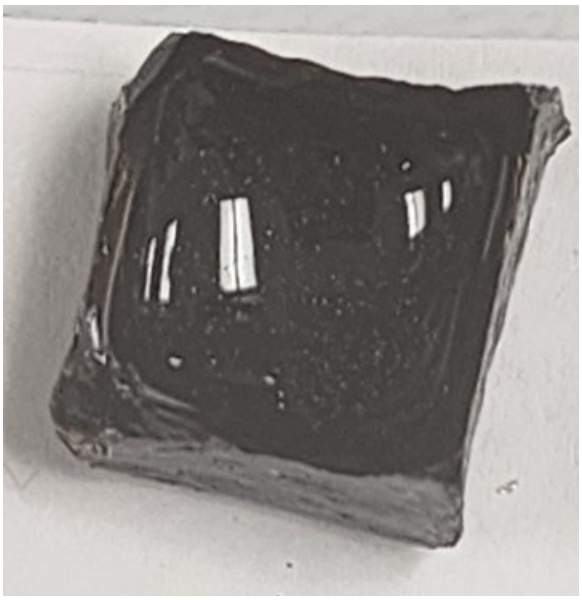

Figure F.1. Glass HLW-APPS-01 after isothermal heat treatment at 950 °C for 24 hrs. Amorphous by XRD analysis.

Table F.1. HWL-APPS-01 glass T_L calculated by extrapolating crystal fraction (CF) as a function of temperature to zero crystals for the main crystalline phase.

Magnetite (wt%)	Temperature (°C)
0.985	742.5
0.361	850.3
0.221	900.4

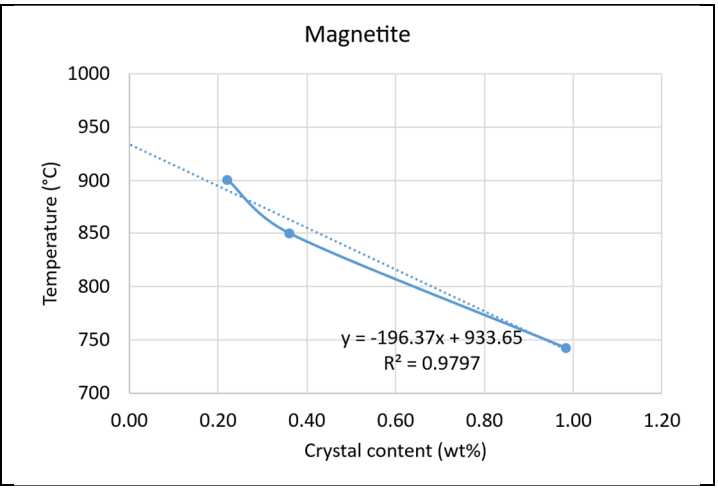

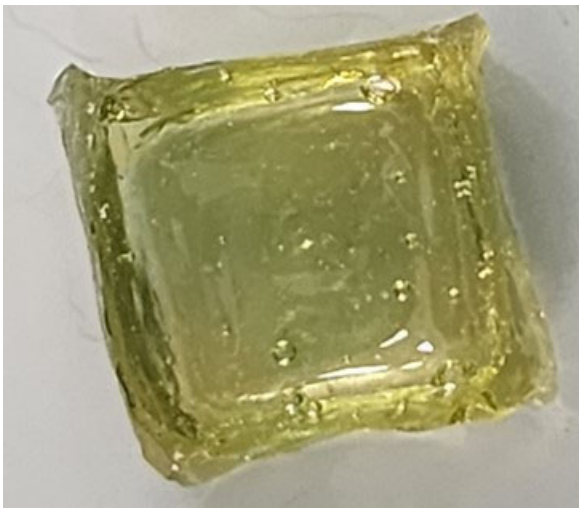

Figure F.2. Glass HLW-APPS-02 after isothermal heat treatment at 950 °C for 24 h. Amorphous by XRD analysis.

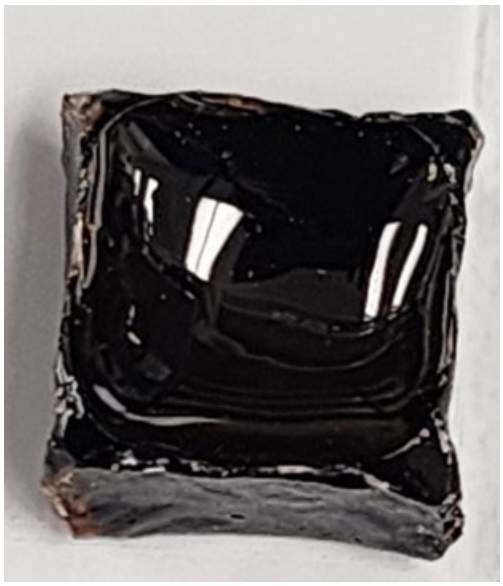

Figure F.3. Glass HLW-APPS-03 after isothermal heat treatment at 950 °C for 24 h. Homogeneous by XRD analysis.

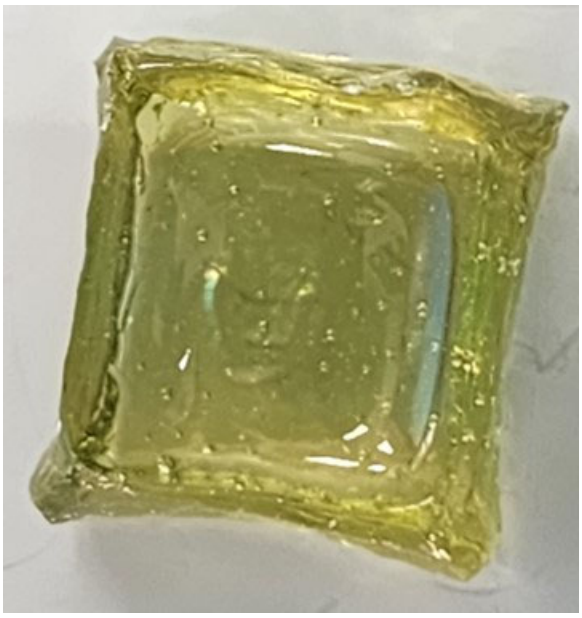

Figure F.4. Glass HLW-APPS-04-1 after isothermal heat treatment at 950 °C for 24 h. Amorphous by XRD analysis.

Figure F.5. Glass HLW-APPS-05 after isothermal heat treatment at 950 °C for 24 h. XRD scan in next figure.

Table F.2. HWL-APPS-05 glass T_L calculated by extrapolating CF as a function of temperature to zero crystals for the main crystalline phase.

Eskolaite (wt%)	**Temperature (°C)**
0.738	850.7
0.646	900.0
0.520	950.0

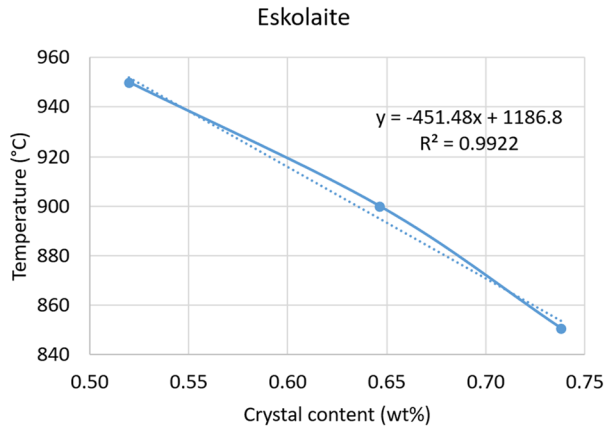

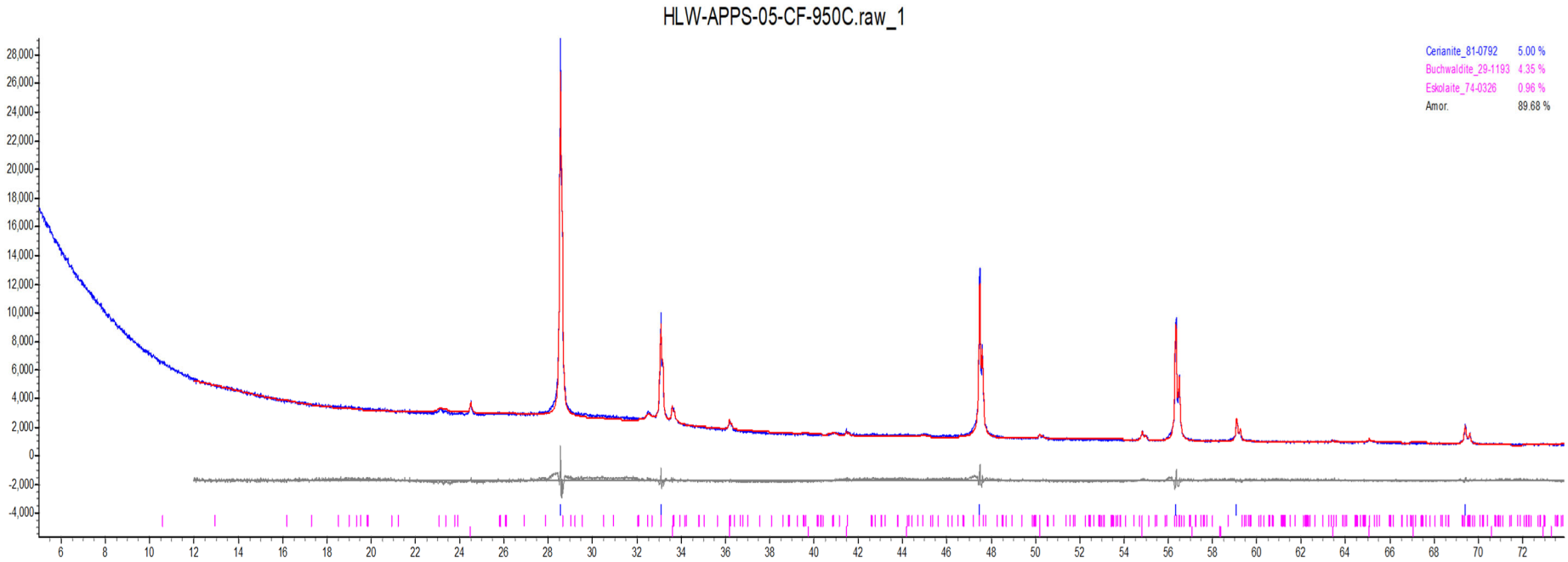

Figure F.6. Glass HLW-APPS-05 heat treated at 950 °C XRD scan.

Figure F.7. Glass HLW-APPS-06 after isothermal heat treatment at 950 °C for 24 h. XRD scan in next figure.

Table F.3. HLW-APPS-06 glass T_L calculated by extrapolating CF as a function of temperature to zero crystals for the main crystalline phase.

Eskolaite (wt%)	**Temperature (°C)**
0.055	950
0.209	900
0.203	848.3 (48 h hold)
0.271	850.7 (24 h hold)

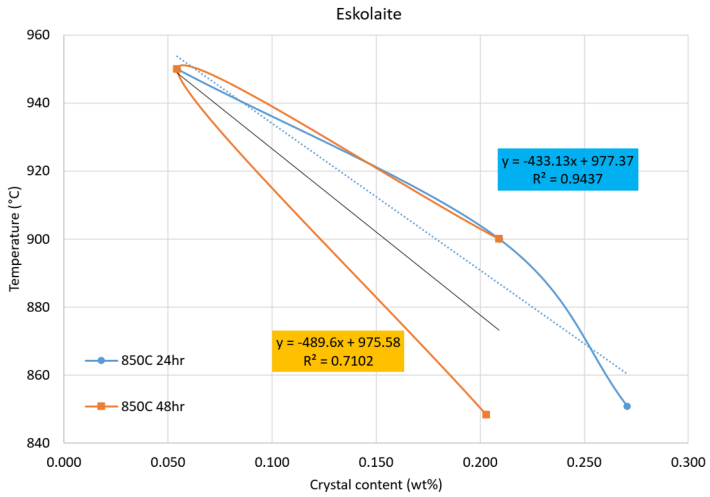

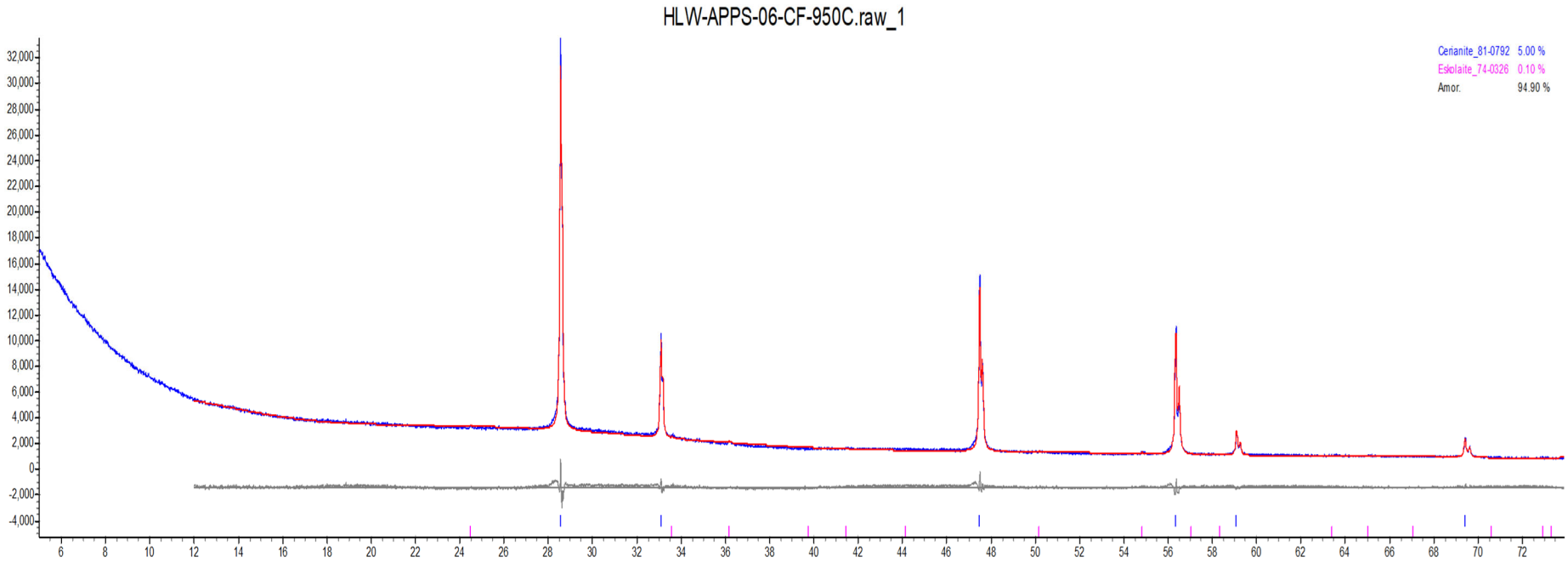

Figure F.8. Glass HLW-APPS-06 heat treated at 950 °C XRD scan.

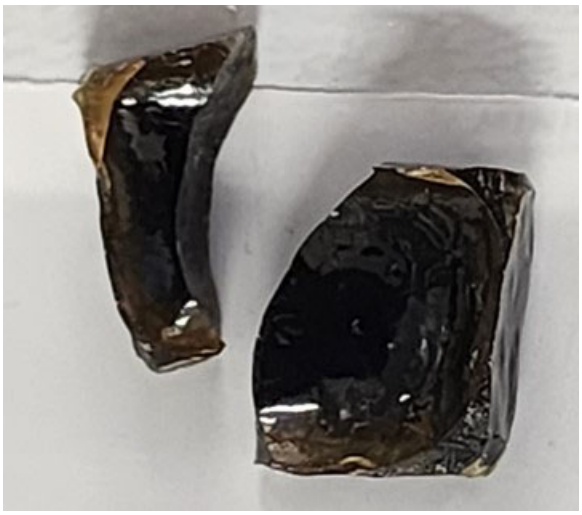

Figure F.9. Glass HLW-APPS-07-2 after isothermal heat treatment at 950 °C for 24 h. XRD scan in next figure.

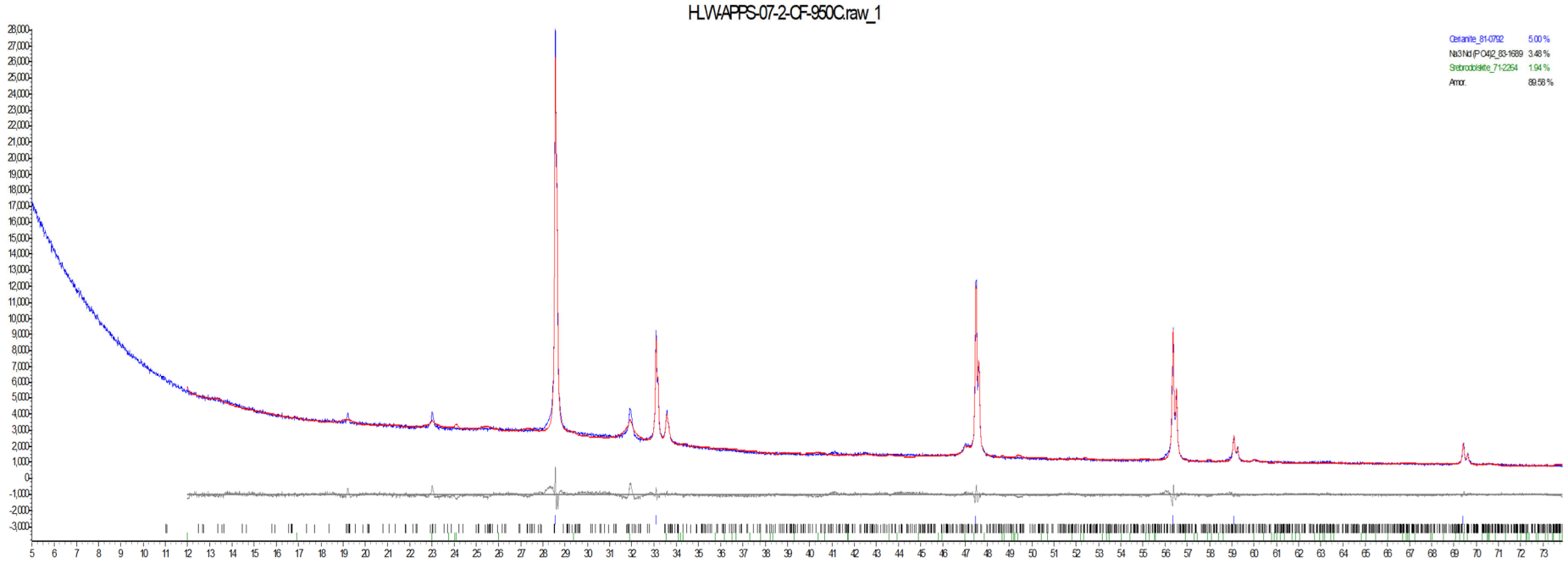

Figure F.10. Glass HLW-APPS-07-2 heat treated at 950 °C XRD scan.

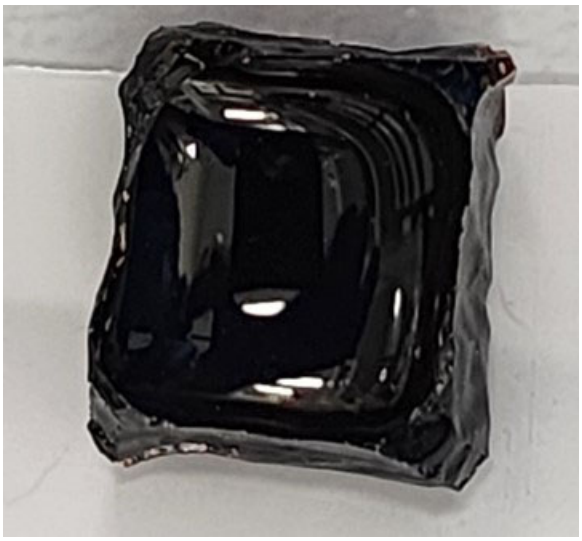

Figure F.11. Glass HLW-APPS-08 after isothermal heat treatment at 950 °C for 24 h. Amorphous by XRD analysis.

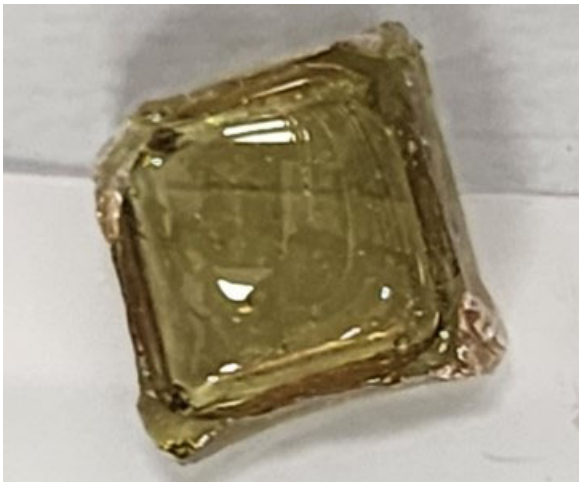

Figure F.12. Glass HLW-APPS-09 after isothermal heat treatment at 850 °C for 24 h. Amorphous by XRD analysis.

Figure F.13. Glass HLW-APPS-10 after isothermal heat treatment at 950 °C for 24 h. Amorphous by XRD analysis.

Table F.4. HLW-APPS-10 glass T_L calculated by extrapolating CF as a function of temperature to zero crystals for the main crystalline phase.

Combeite (wt%)	**Temperature (°C)**
18.973	750.7
5.862	850.4
1.663	901.0

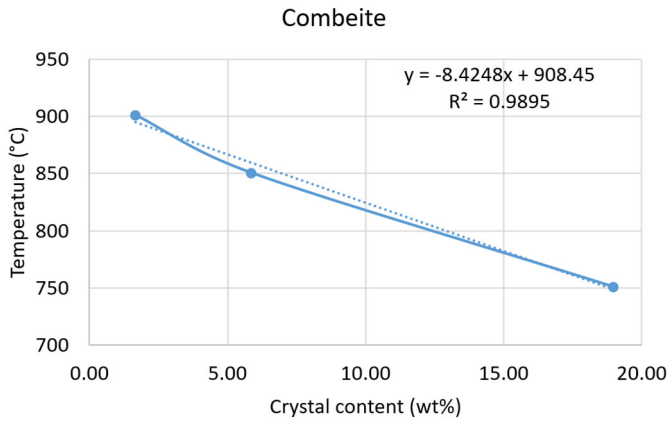

Figure F.14. Glass HLW-APPS-11 after isothermal heat treatment at 950 °C for 24 h. Amorphous by XRD analysis.

Table F.5. HLW-APPS-11 glass T_L calculated by extrapolating CF as a function of temperature to zero crystals for the main crystalline phase.

Combeite (wt%)	**Temperature (°C)**
16.670	742.5
10.839	849.0
7.467	901.2

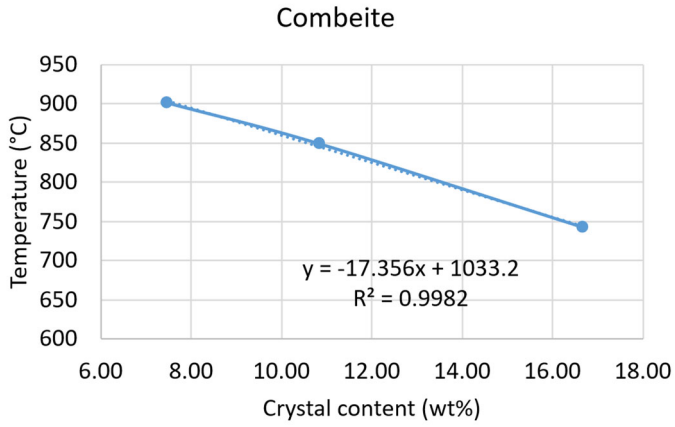

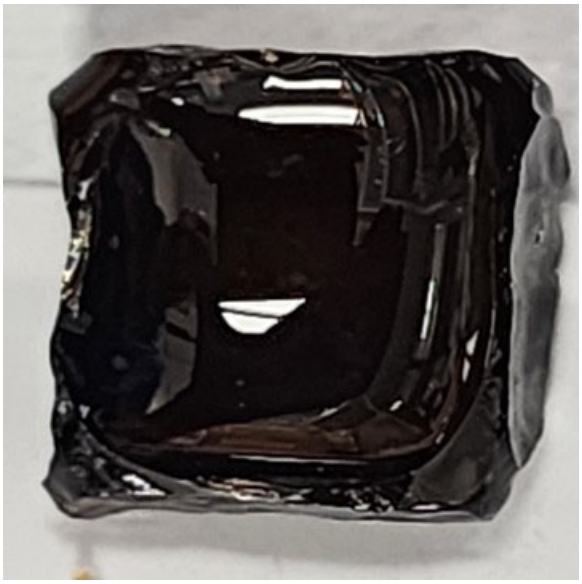

Figure F.15. Glass HLW-APPS-12 after isothermal heat treatment at 950 °C for 24 h. Amorphous by XRD analysis.

Table F.6. HLW-APPS-12 glass T_L calculated by extrapolating CF as a function of temperature to zero crystals for the main crystalline phase.

Combeite (wt%)	**Temperature (°C)**
13.468	750.7
7.630	848.3 (48 h hold)
7.1285	850.4 (24 h hold)
0.4992	901

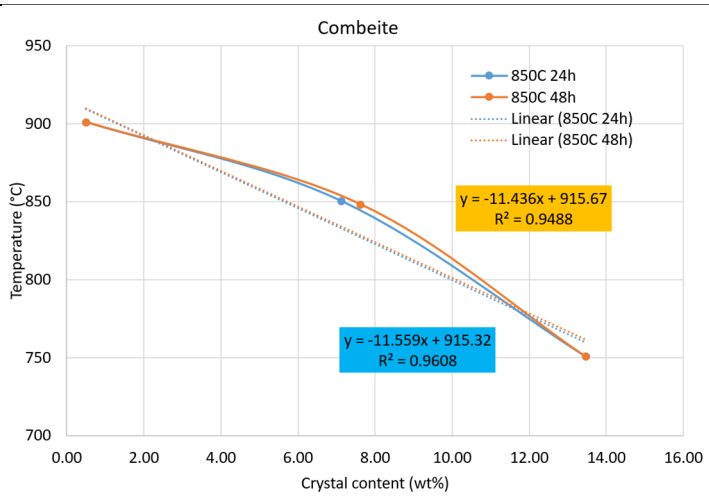

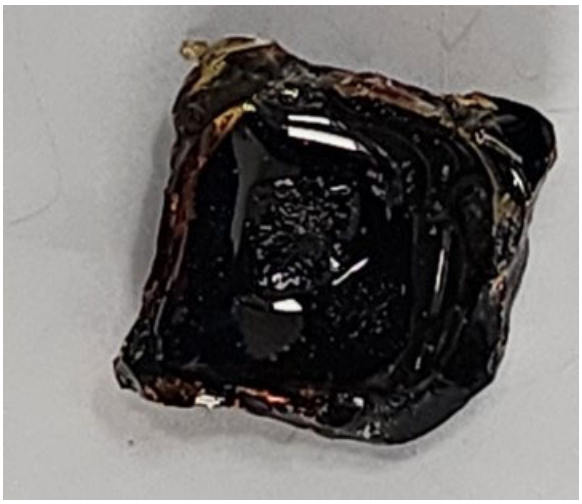

Figure F.16. Glass HLW-APPS-13-1 after isothermal heat treatment at 900 °C for 24 h. Amorphous by XRD analysis.

Table F.7. HLW-APPS-13-1 glass T_L calculated by extrapolating CF as a function of temperature to zero crystals for the main crystalline phase.

Combeite (wt%)	Temperature (°C)
13.411	750.7
9.968	848.3 (48 h hold)
9.996	848.3 (24 h hold)
0.877	900.4

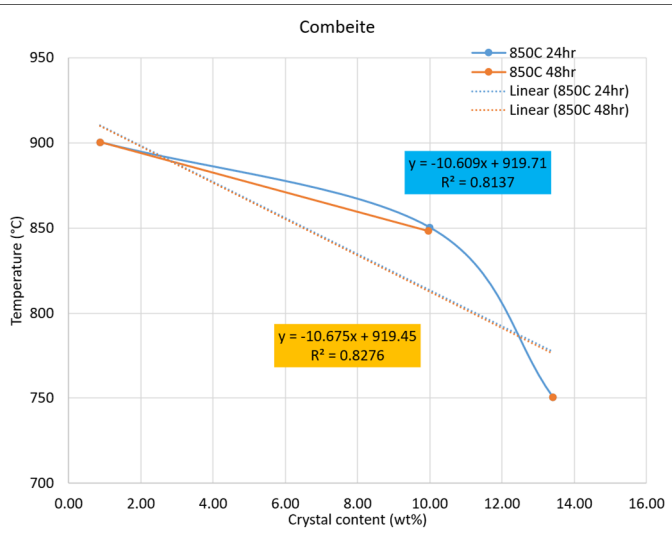

Figure F.17. Glass HLW-APPS-14 after isothermal heat treatment at 950 °C for 24 h. XRD scan on next page.

Table F.8. HLW-APPS-14 glass T_L calculated by extrapolating CF as a function of temperature to zero crystals for the main crystalline phase.

Combeite (wt%)	**Temperature (°C)**
15.025	742.5
10.947	848.3 - 48 h
11.012	848.3 - 24 h
2.403	900.0
0.210	954.2

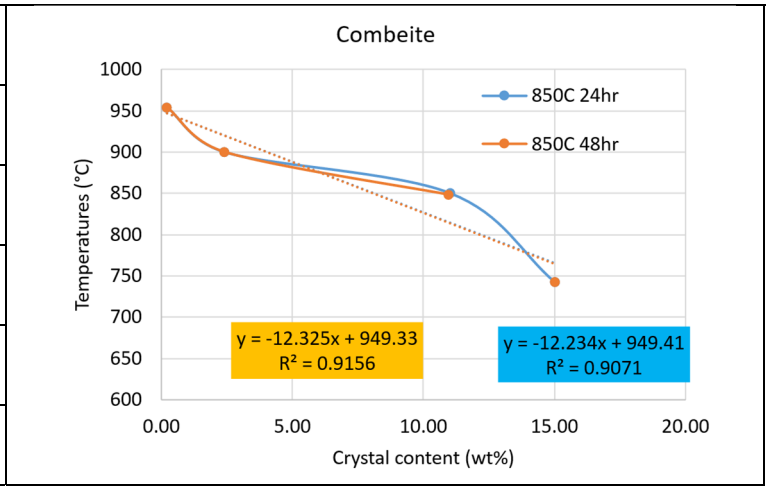

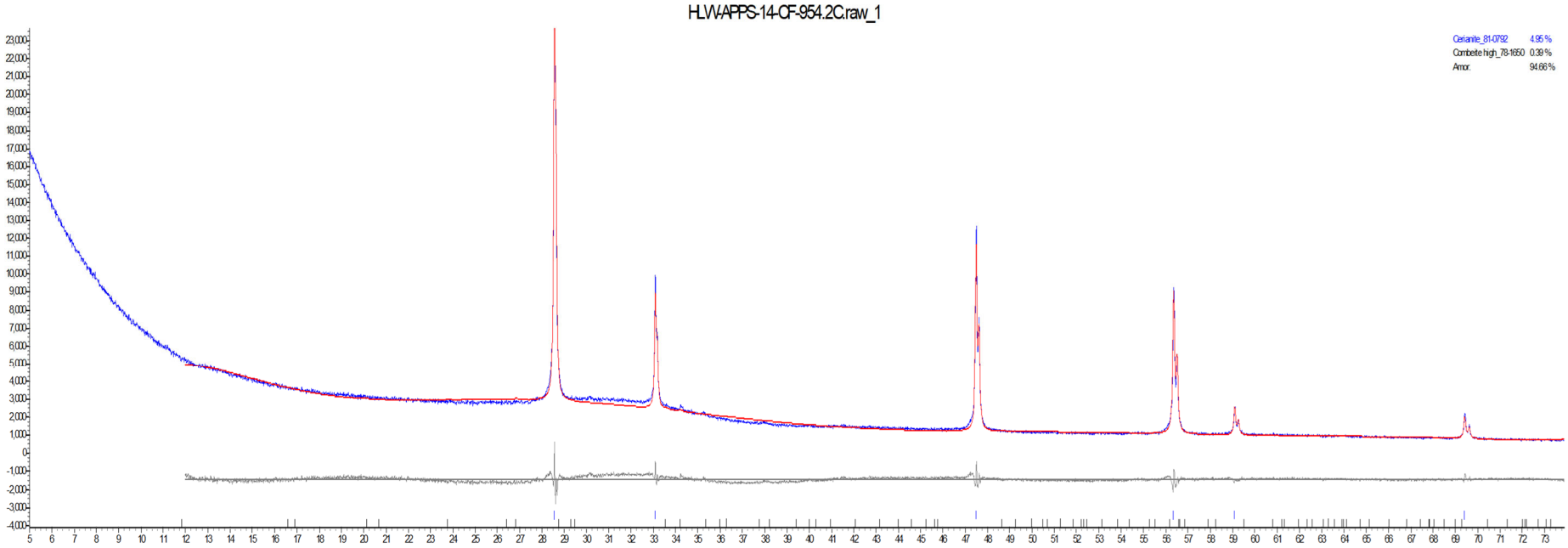

Figure F.18. Glass HLW-APPS-14 heat treated at 950 °C XRD scan.

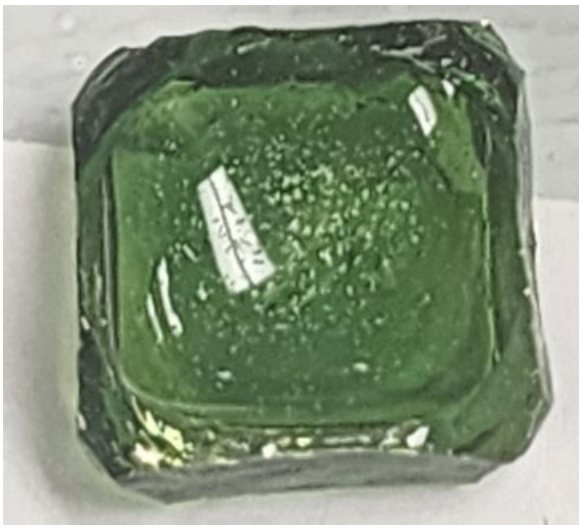

Figure F.19. Glass HLW-APPS-15 after isothermal heat treatment at 950 °C for 24 h. Amorphous by XRD analysis.

Appendix G – Viscosity Data

This appendix contains the temperatures at which viscosity was measured, and the measured viscosity data for each of the glasses in this matrix. The plots shown in this appendix are fitted to the Arrhenius equation:

$$\ln(\eta) = A + \frac{B}{T_K} \quad \text{G.1}$$

where A and B are independent of temperature and temperature (T_K) is in K (T(°C) + 273.15).

Table G.1. Temperatures (°C) at which the viscosities have been measured in order of measurement.

Glass ID	Temperature (°C)								
HLW-APPS-01	1171.47	1076.21	976.99	1166.51	1268.71	1172.46	1172.46		
HLW-APPS-02	1169.49	1169.49	1074.23	976.00	976.00	1169.49	1268.71	1268.71	1173.46
HLW-APPS-03	1170.48	1073.24	975.00	1169.49	1267.72	1172.46			
HLW-APPS-04-1	1166.51	1076.21	979.97	1169.49	1267.72	1173.46			
HLW-APPS-05	1167.50	1072.25	977.98	1168.49	1267.72	1171.47			
HLW-APPS-06	1169.49	1074.23	976.00	1164.53	1268.71	1171.47			
HLW-APPS-07-2	1169.49	1073.24	976.99	1168.49	1267.72	1171.47			
HLW-APPS-08	1169.49	1076.21	1076.21	976.99	1168.49	1268.71	1171.47		
HLW-APPS-09	1171.47	1075.22	978.97	1171.47	1270.70	1173.46			
HLW-APPS-10	1172.46	1075.22	976.00	1168.49	1168.49	1270.70	1270.70	1173.46	1173.46
HLW-APPS-11	1171.47	1077.21	976.99	1169.49	1268.71	1174.45			
HLW-APPS-12	1168.49	1074.23	977.98	1170.48	1268.71	1171.47			
HLW-APPS-13-1	1161.55	1073.24	977.98	1170.48	1266.73	1171.47			
HLW-APPS-14	1163.53	1073.24	977.98	1166.51	1267.72	1173.46			
HLW-APPS-15	1168.49	1075.22	976.99	1170.48	1268.71	1171.47			

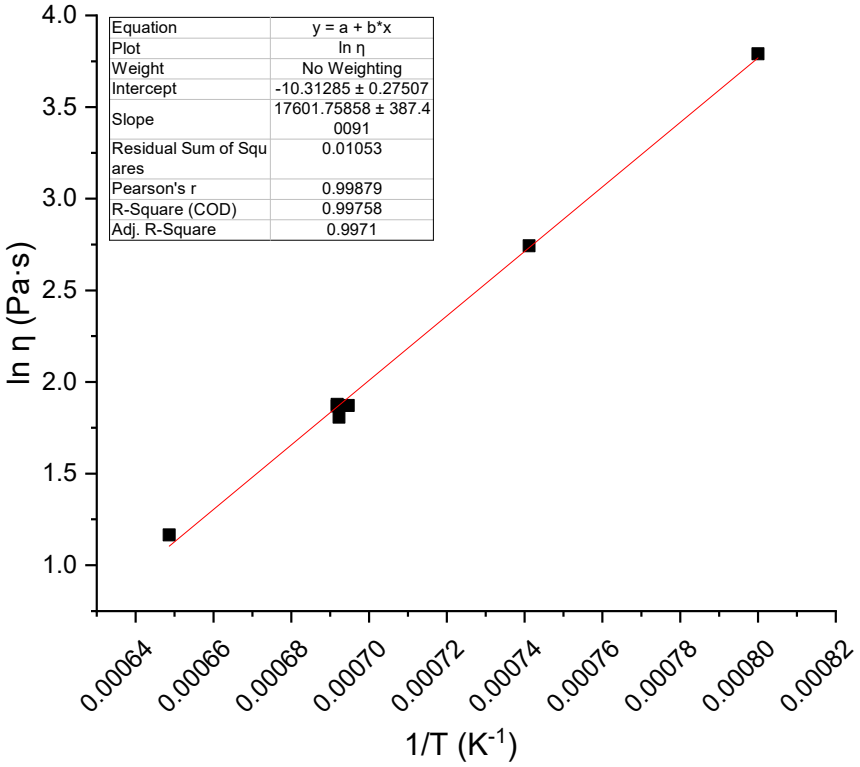

Figure G.1. Viscosity-temperature Data and Arrhenius equation fit for HLW-APPS-01.

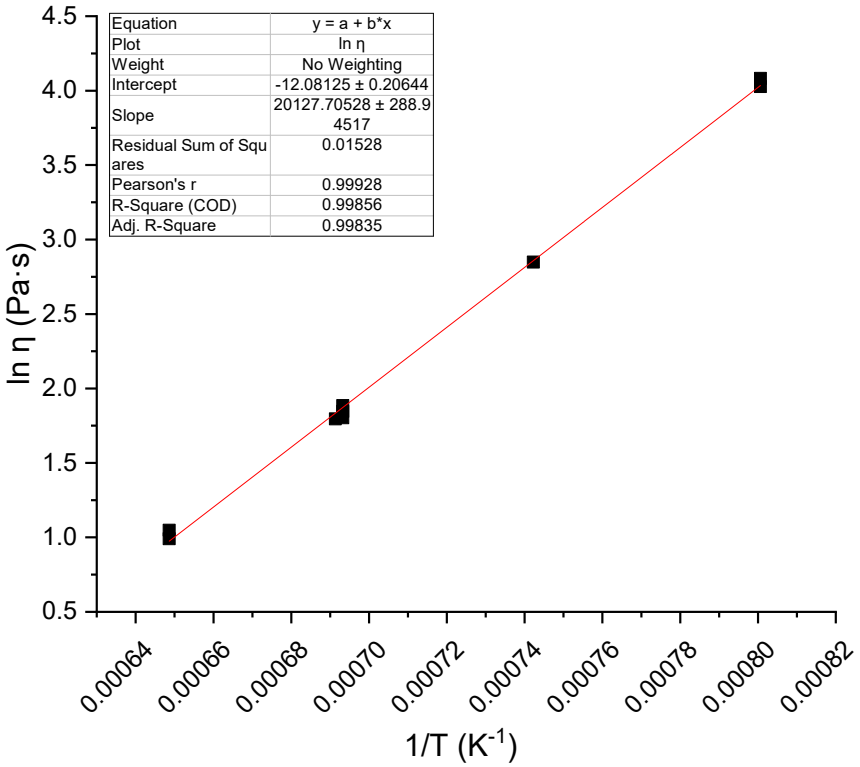

Figure G.2. Viscosity-temperature data and Arrhenius equation fit for HLW-APPS-02.

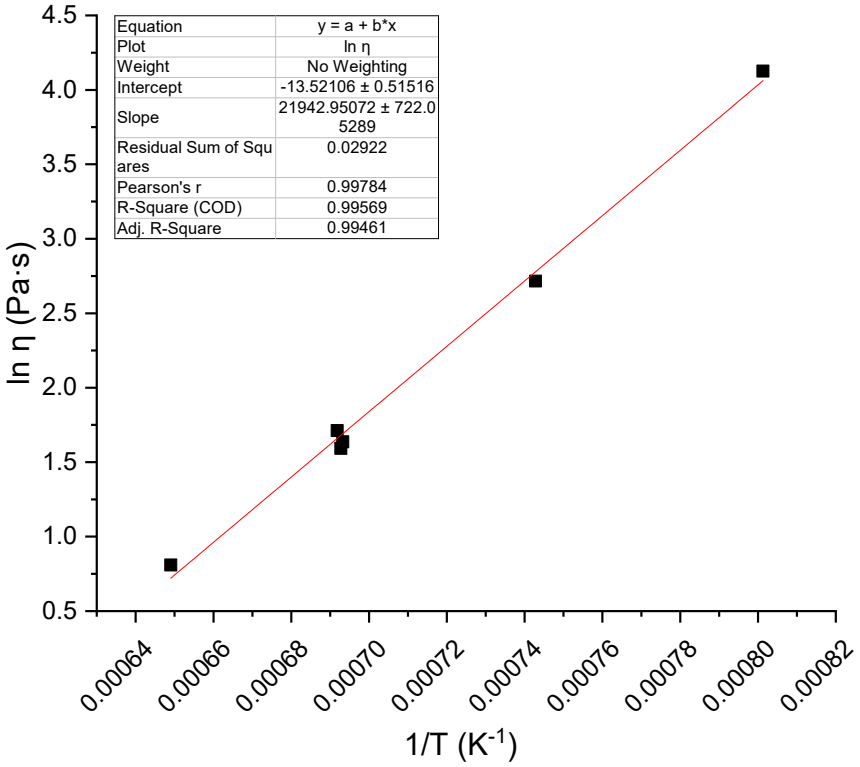

Figure G.3. Viscosity-temperature data and Arrhenius equation fit for HLW-APPS-03.

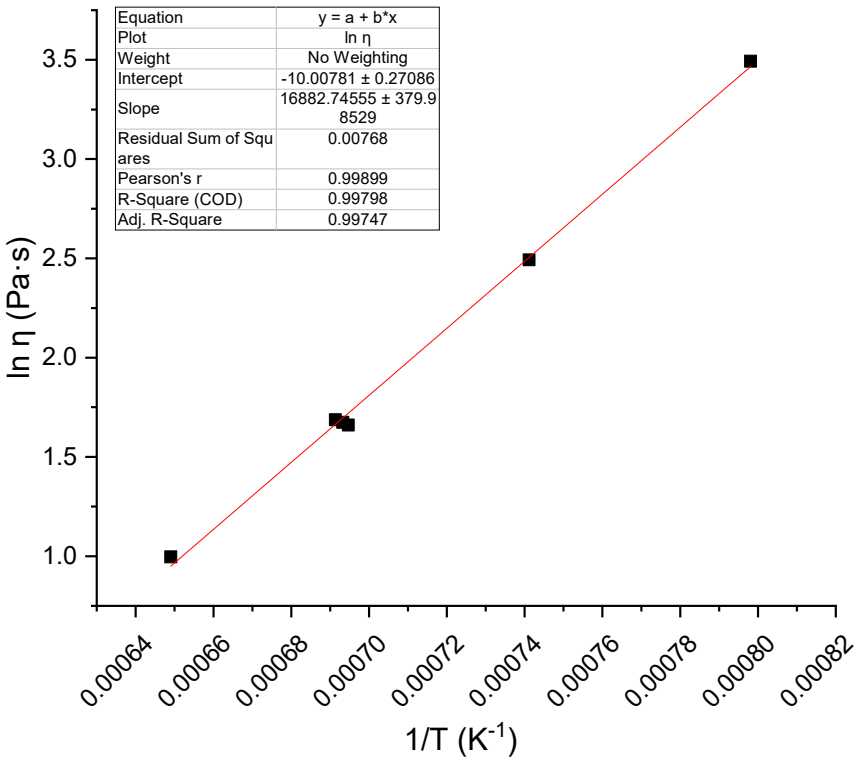

Figure G.4. Viscosity-temperature data and Arrhenius equation fit for HLW-APPS-04-1.

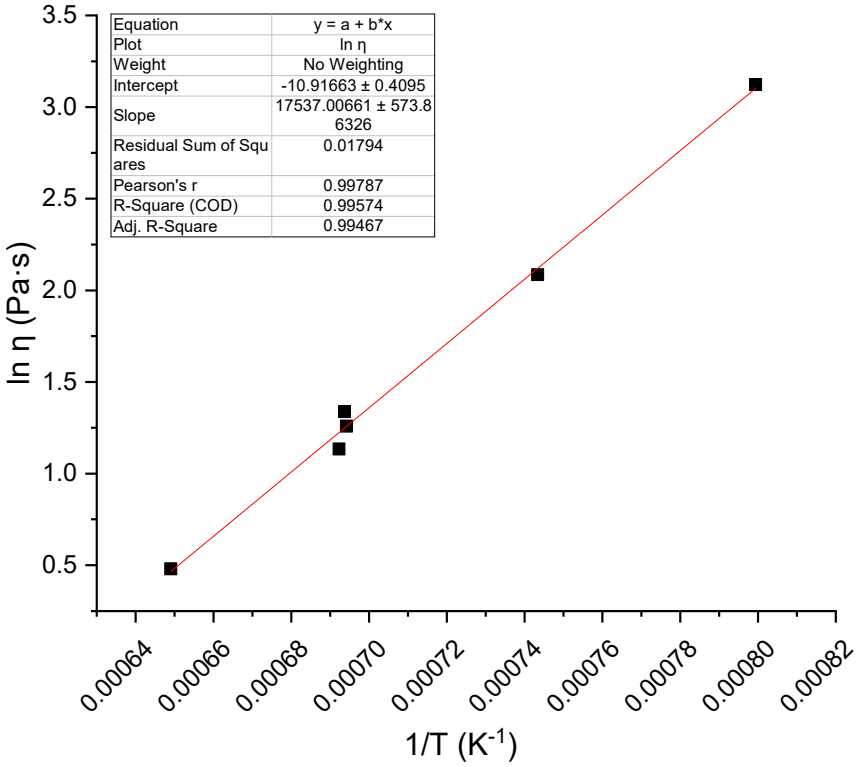

Figure G.5. Viscosity-temperature data and Arrhenius equation fit for HLW-APPS-05.

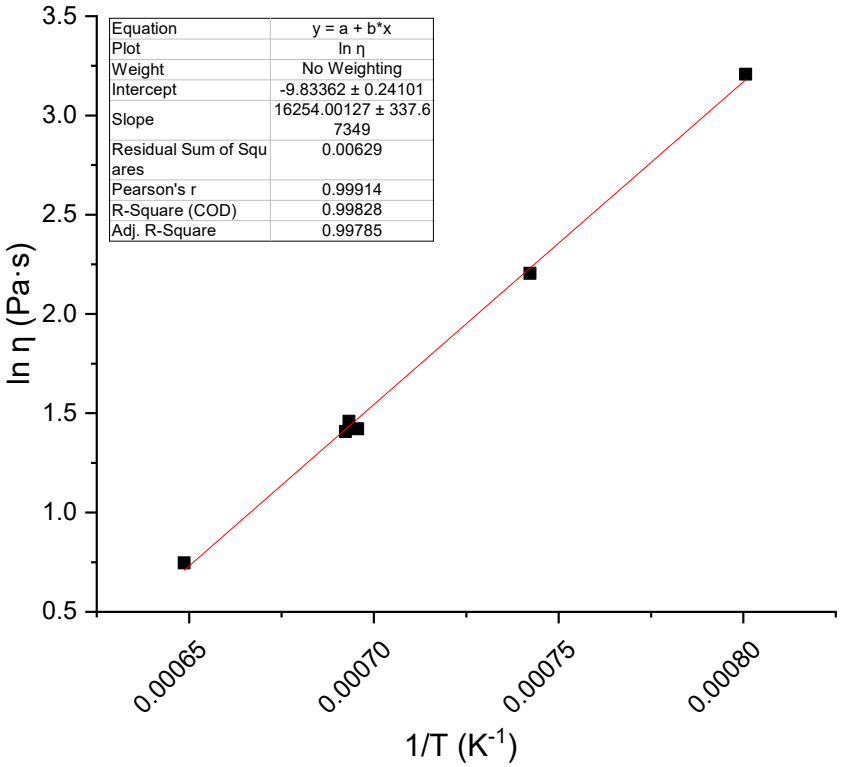

Figure G.6. Viscosity-temperature data and Arrhenius equation fit for HLW-APPS-06.

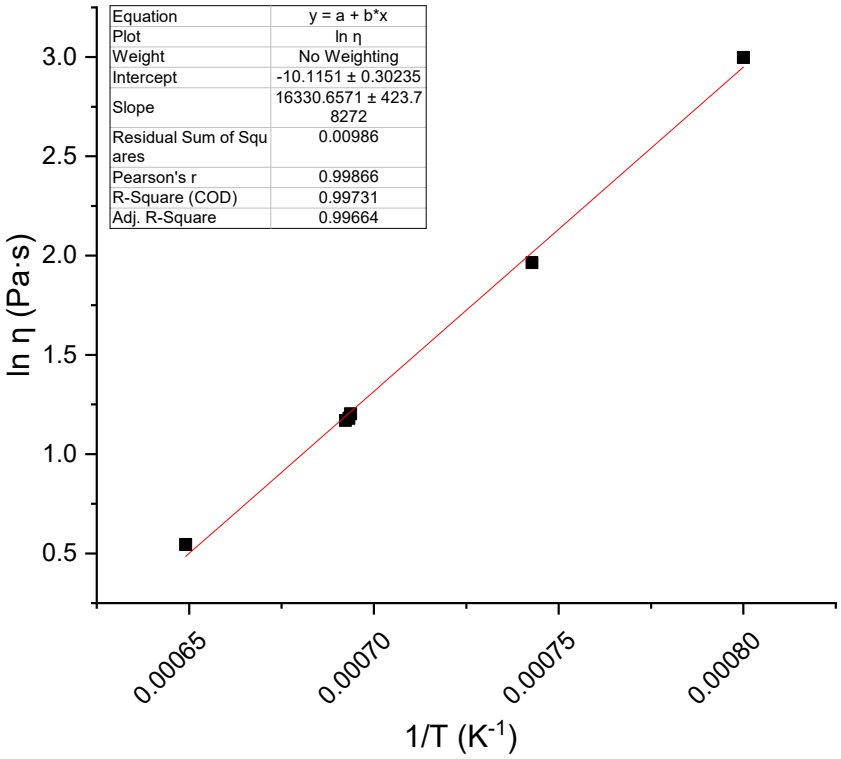

Figure G.7. Viscosity-temperature data and Arrhenius equation fit for HLW-APPS-07-2.

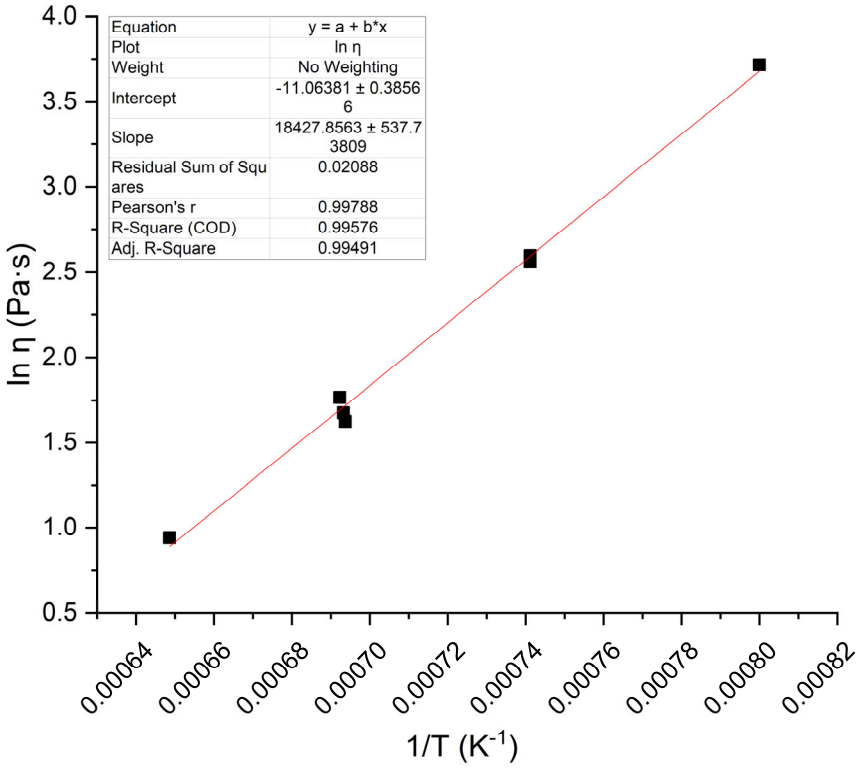

Figure G.8. Viscosity-temperature data and Arrhenius equation fit for HLW-APPS-08.

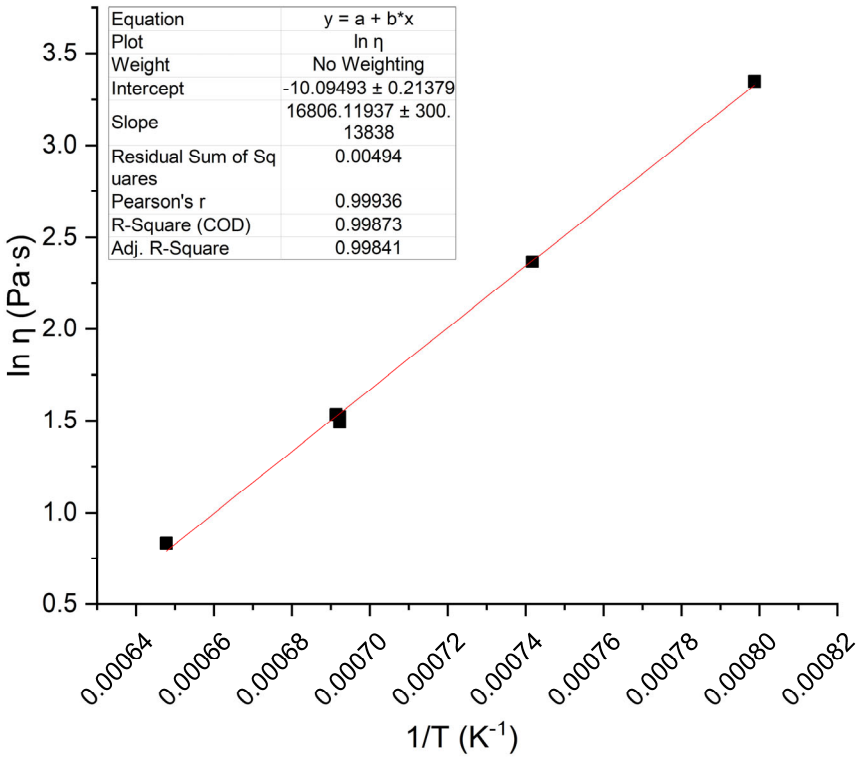

Figure G.9. Viscosity-temperature data and Arrhenius equation fit for HLW-APPS-09.

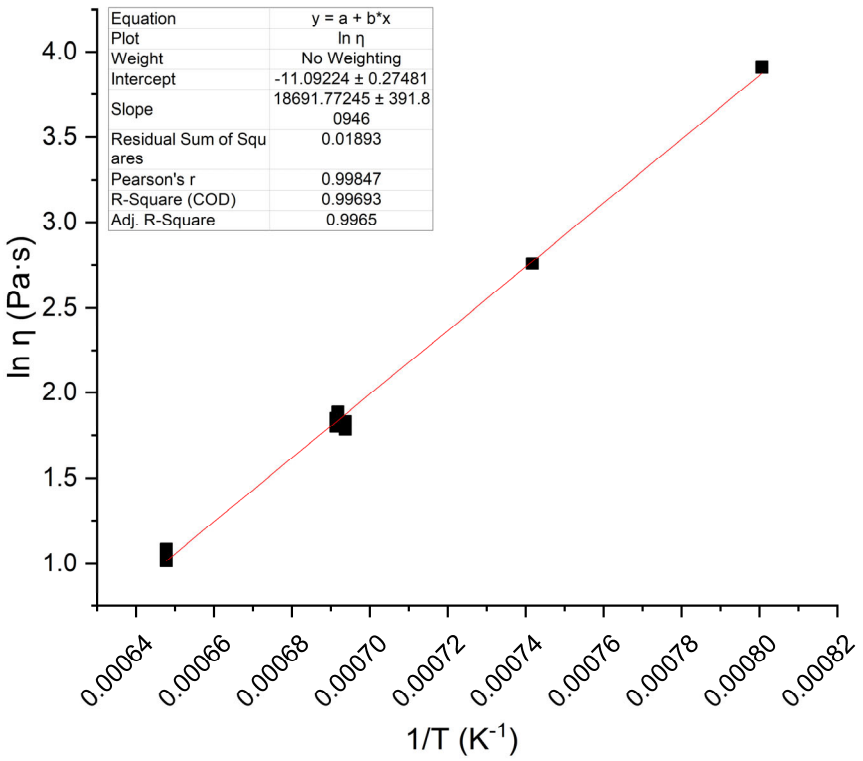

Figure G.10. Viscosity-temperature data and Arrhenius equation fit for HLW-APPS-10.

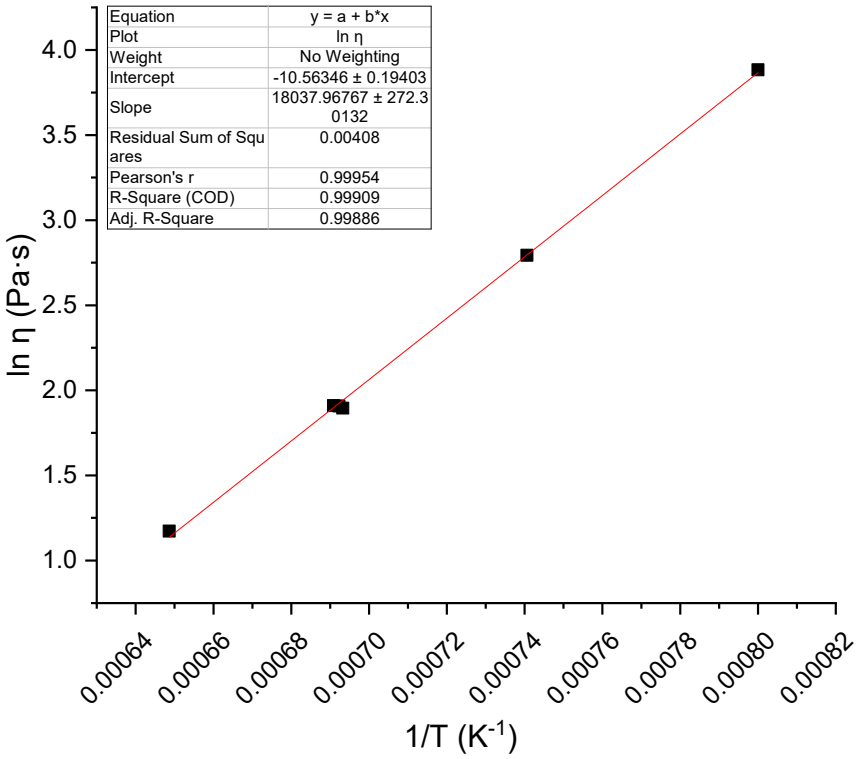

Figure G.11. Viscosity-temperature data and Arrhenius equation fit for HLW-APPS-11.

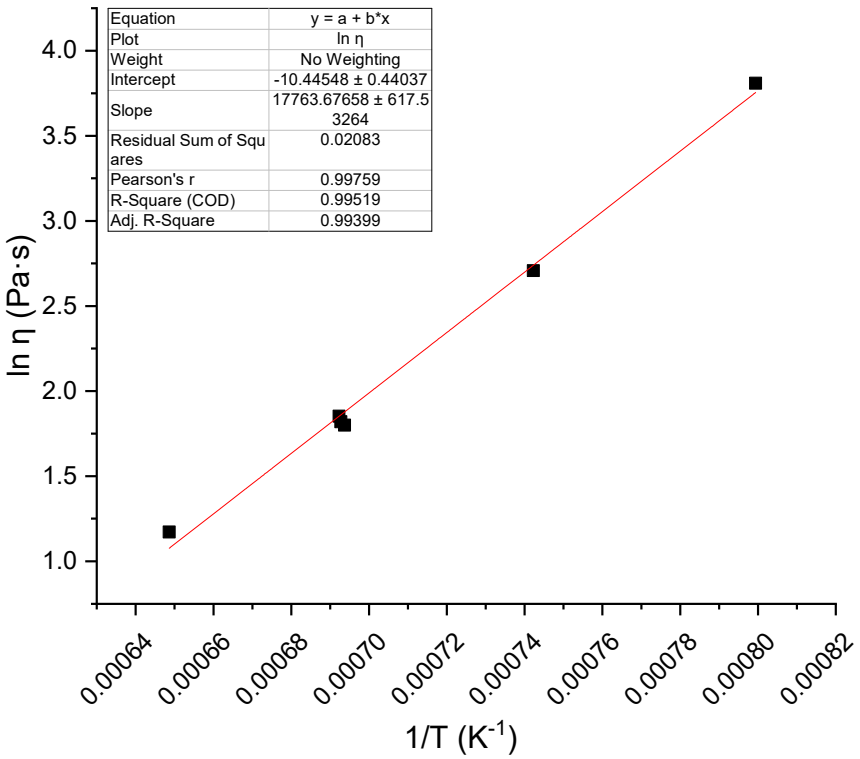

Figure G.12. Viscosity-temperature data and Arrhenius equation fit for HLW-APPS-12.

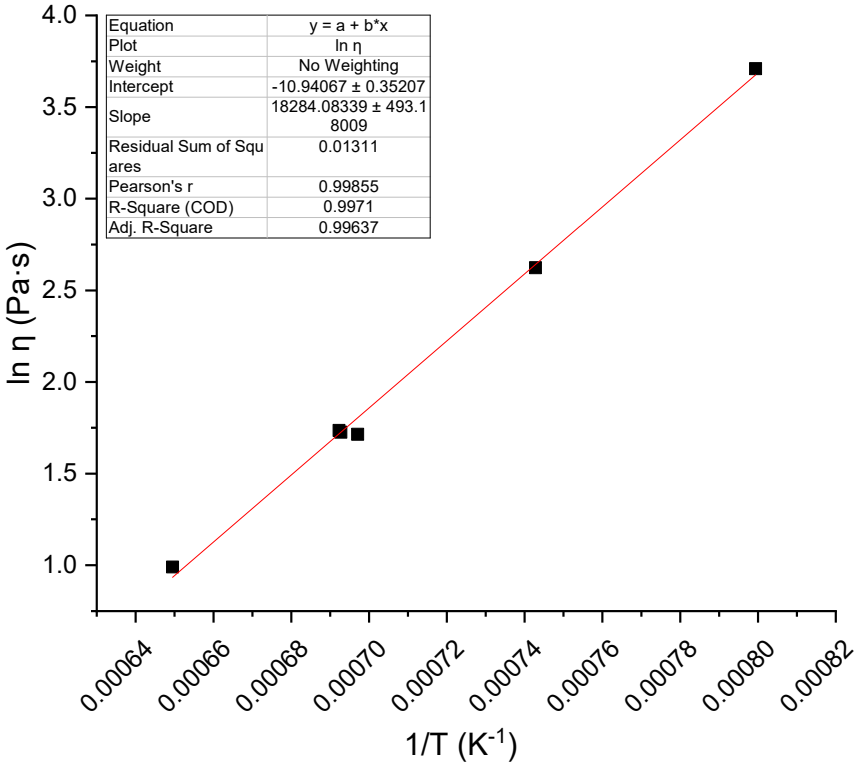

Figure G.13. Viscosity-temperature data and Arrhenius equation fit for HLW-APPS-13-1.

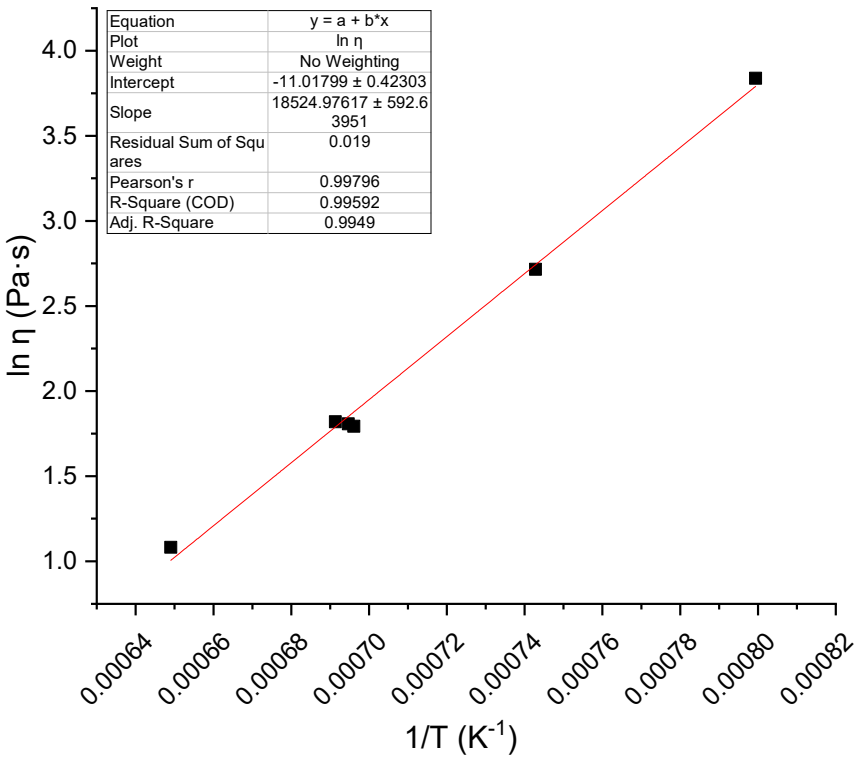

Figure G.14. Viscosity-temperature data and Arrhenius equation fit for HLW-APPS-14.

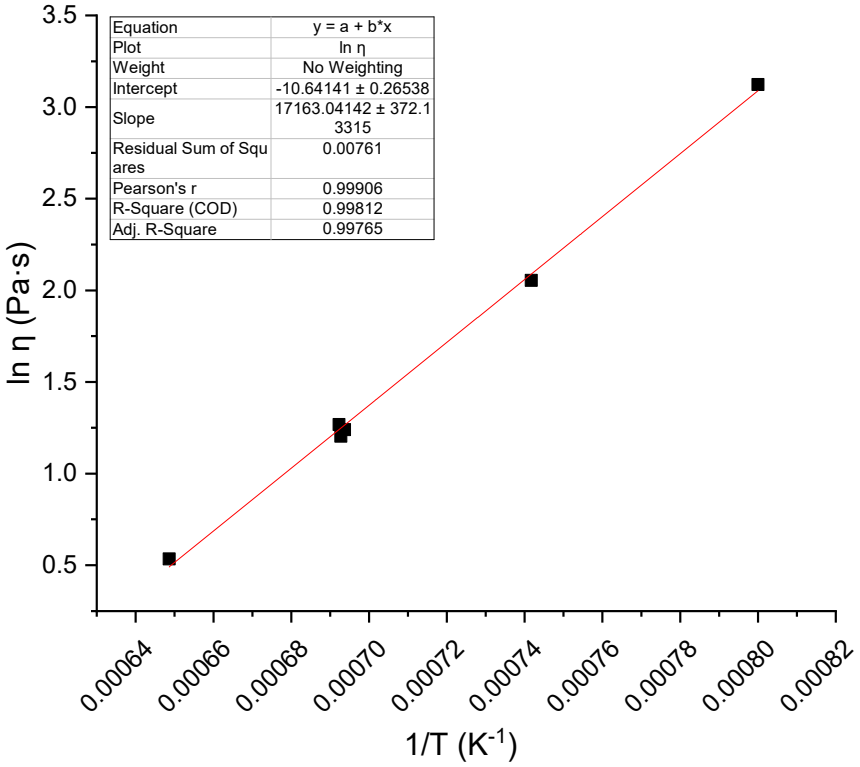

Figure G.15. Viscosity-temperature data and Arrhenius equation fit for HLW-APPS-15.

Appendix H – Electrical Conductivity Data

This appendix contains the measured electrical conductivity data for each of the glasses in this matrix following Section 2.10.

The plots shown in this appendix are fitted to the Arrhenius equation, which is shown below:

$$\ln(\varepsilon) = A + B/T_K \qquad \text{H.1}$$

where A and B are independent of temperature and temperature (T_K) is in K (T(°C) + 273.15).

The main intent of the figures and Arrhenius equation fits shown in this appendix is to assess trends in the data and provide observations about whether there may be sufficient curvature in the data to consider VFT fits in the subsequent work that will decide between fitting the data to the Arrhenius or VFT equations for the electrical conductivity-temperature data for each glass that is being made.

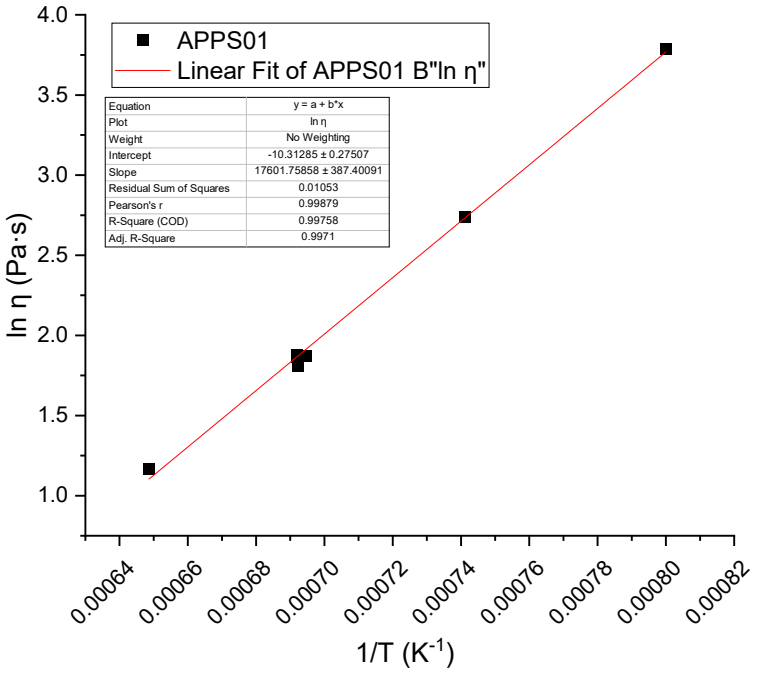

Figure H.1. Electrical conductivity-temperature data and Arrhenius equation fit for glass HLW-APPS-01.

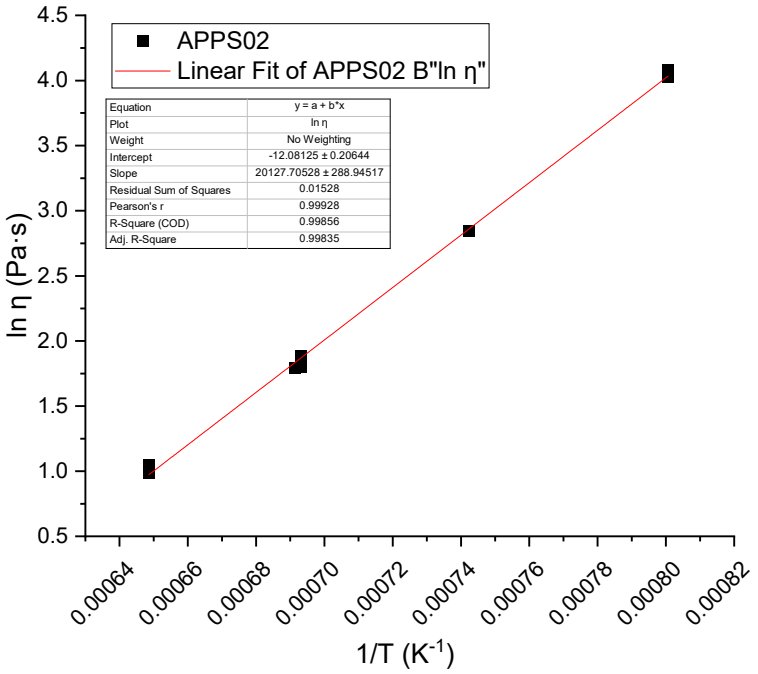

Figure H.2. Electrical conductivity-temperature data and Arrhenius equation fit for glass HLW-APPS-02.

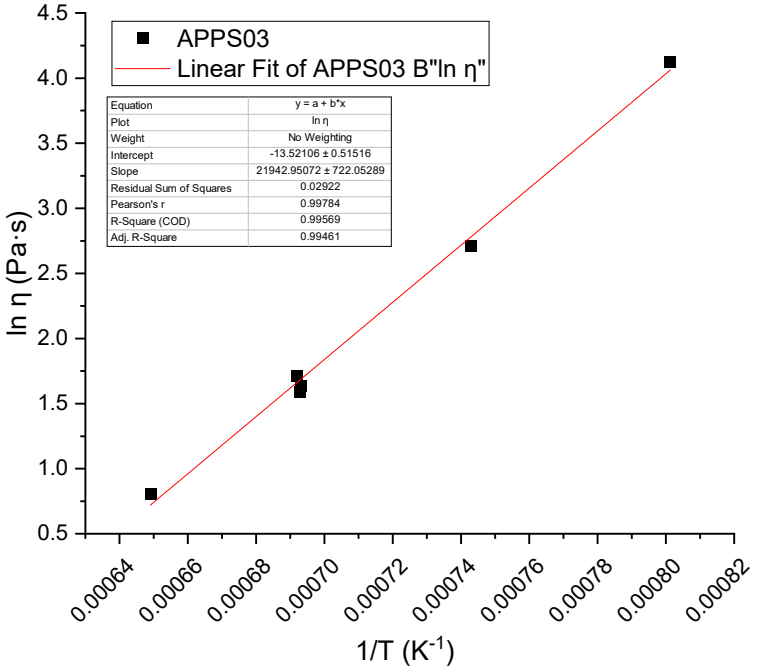

Figure H.3. Electrical conductivity-temperature data and Arrhenius equation fit for glass HLW-APPS-03.

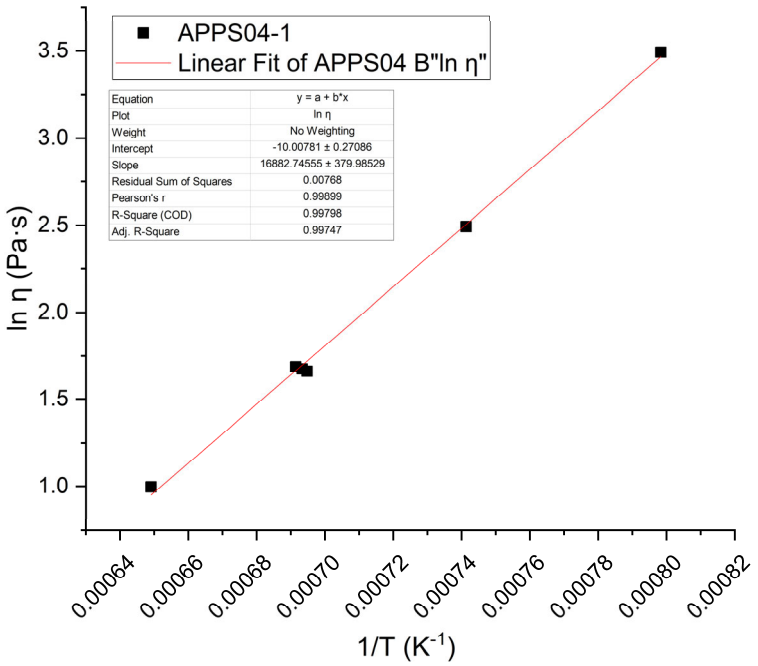

Figure H.4. Electrical conductivity-temperature data and Arrhenius equation fit for glass HLW-APPS-04-1.

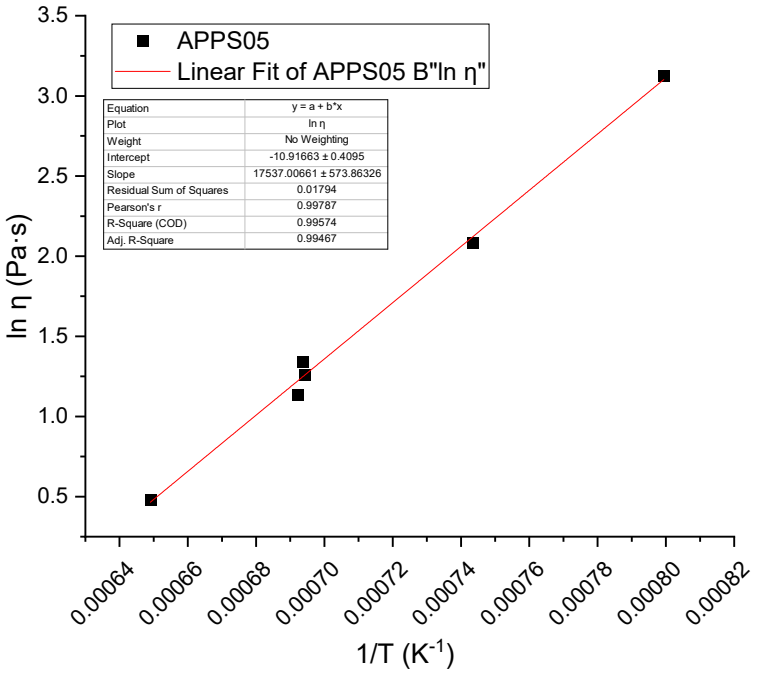

Figure H.5. Electrical conductivity-temperature data and Arrhenius equation fit for glass HLW-APPS-05.

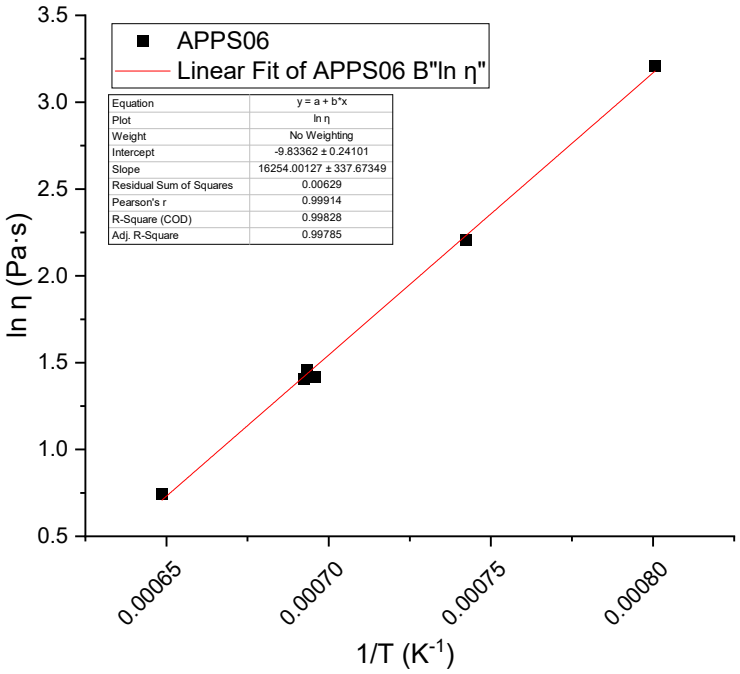

Figure H.6. Electrical conductivity-temperature data and Arrhenius equation fit for glass HLW-APPS-06.

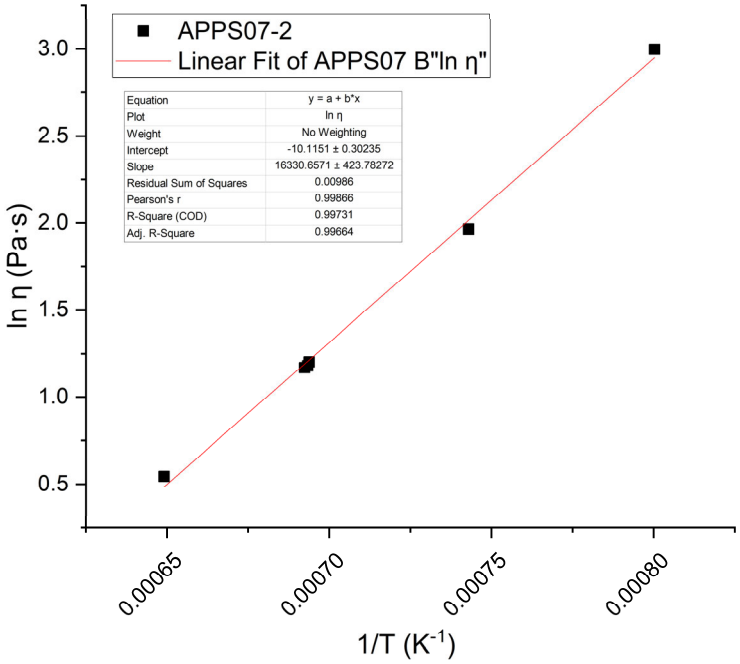

Figure H.7. Electrical conductivity-temperature data and Arrhenius equation fit for glass HLW-APPS-07-2.

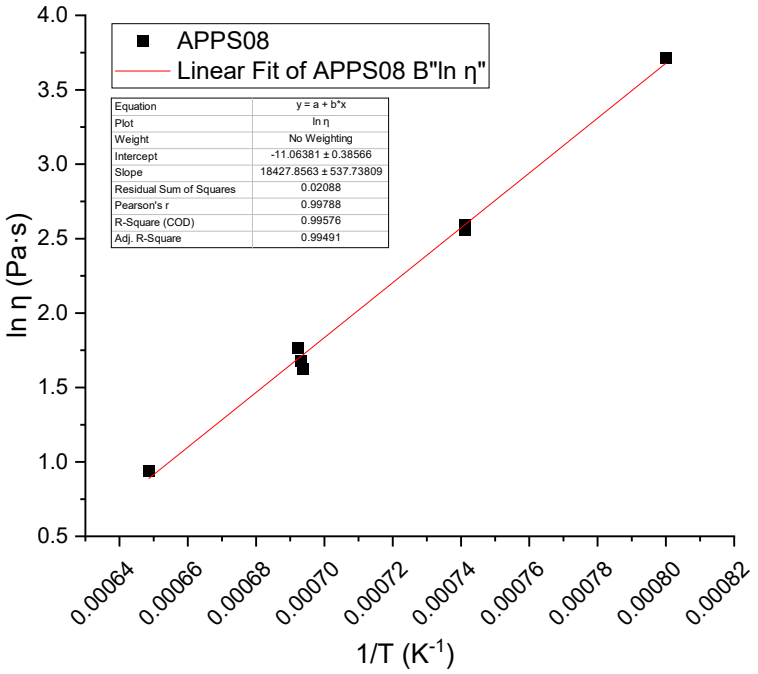

Figure H.8. Electrical conductivity-temperature data and Arrhenius equation fit for glass HLW-APPS-08.

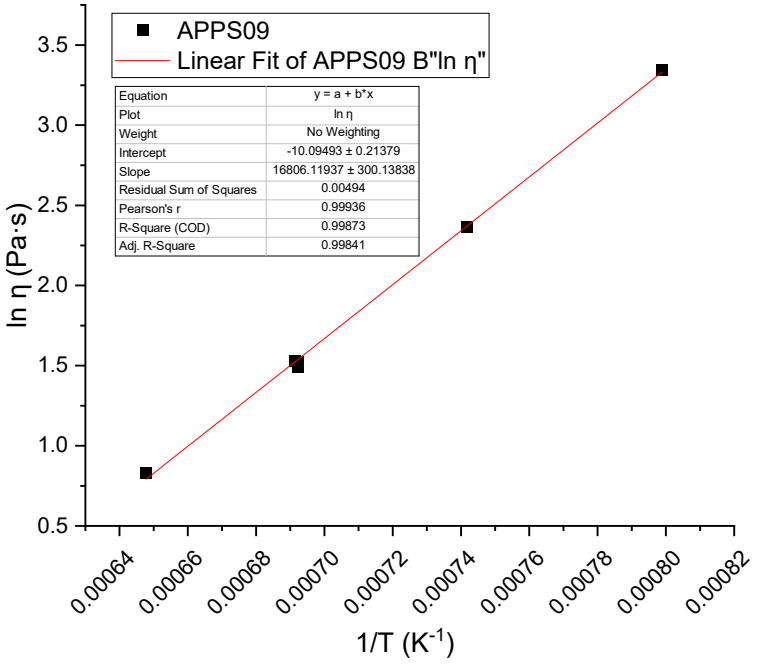

Figure H.9. Electrical conductivity-temperature data and Arrhenius equation fit for glass HLW-APPS-09.

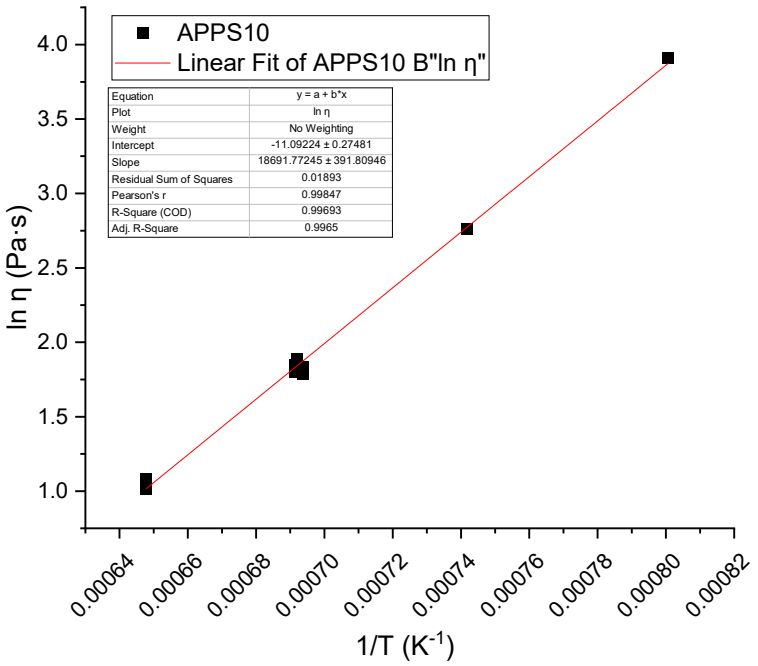

Figure H.10. Electrical conductivity-temperature data and Arrhenius equation fit for glass HLW-APPS-10.

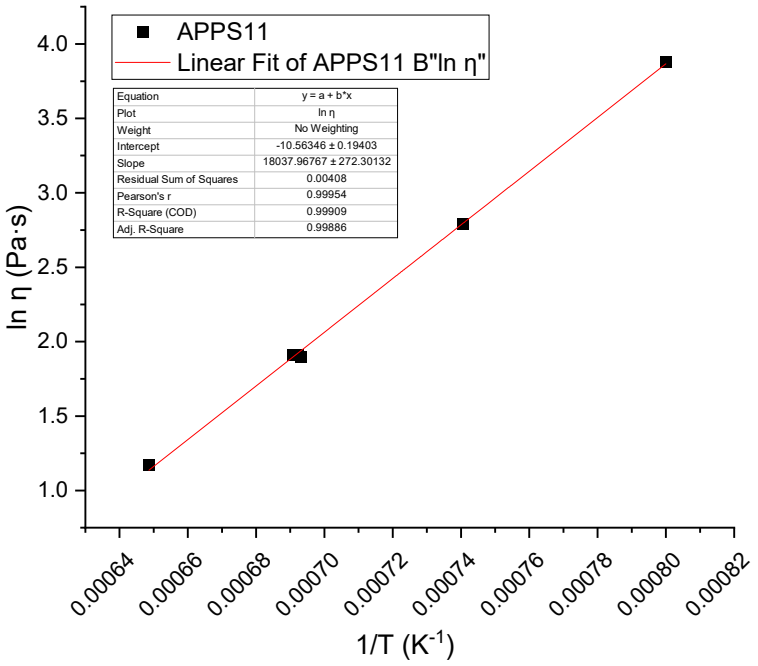

Figure H.11. Electrical conductivity-temperature data and Arrhenius equation fit for glass HLW-APPS-11.

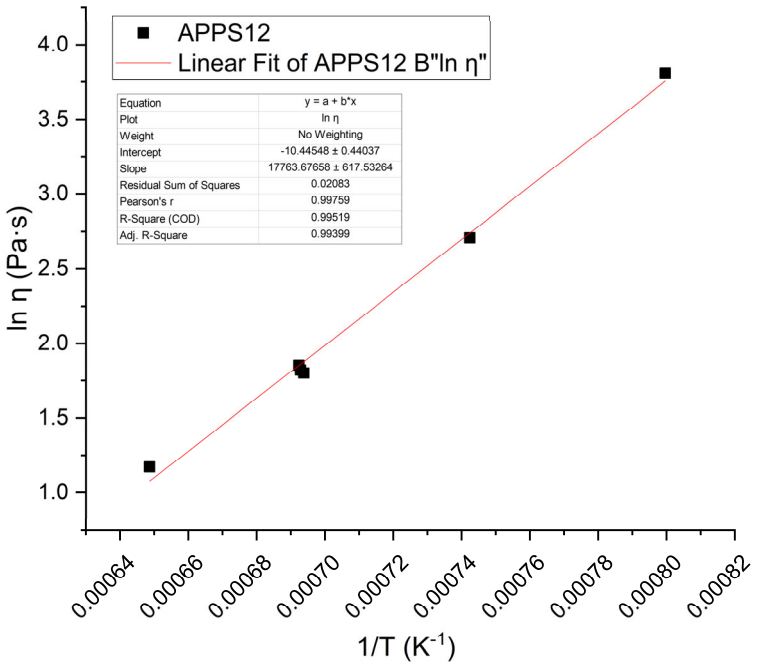

Figure H.12. Electrical conductivity-temperature data and Arrhenius equation fit for glass HLW-APPS-12.

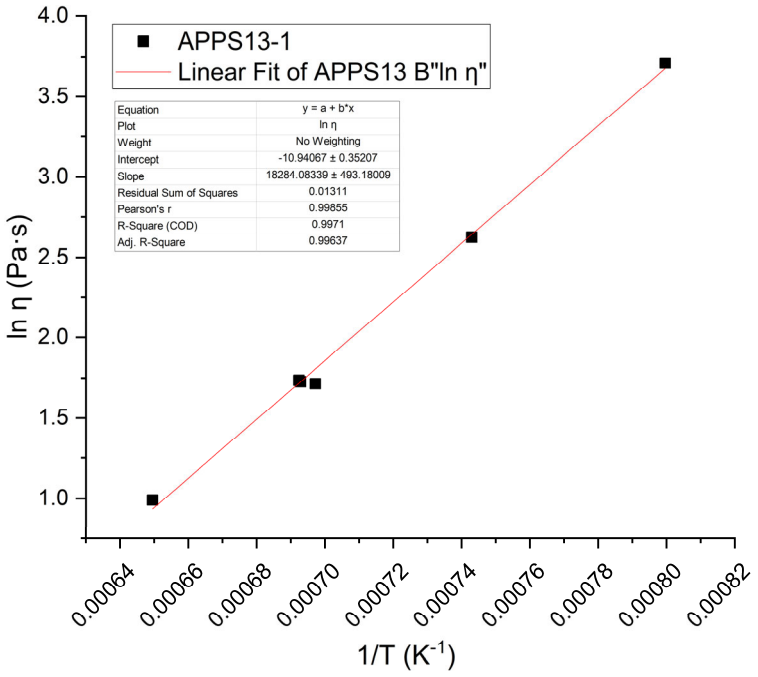

Figure H.13. Electrical conductivity-temperature data and Arrhenius equation fit for glass HLW-APPS-13-1.

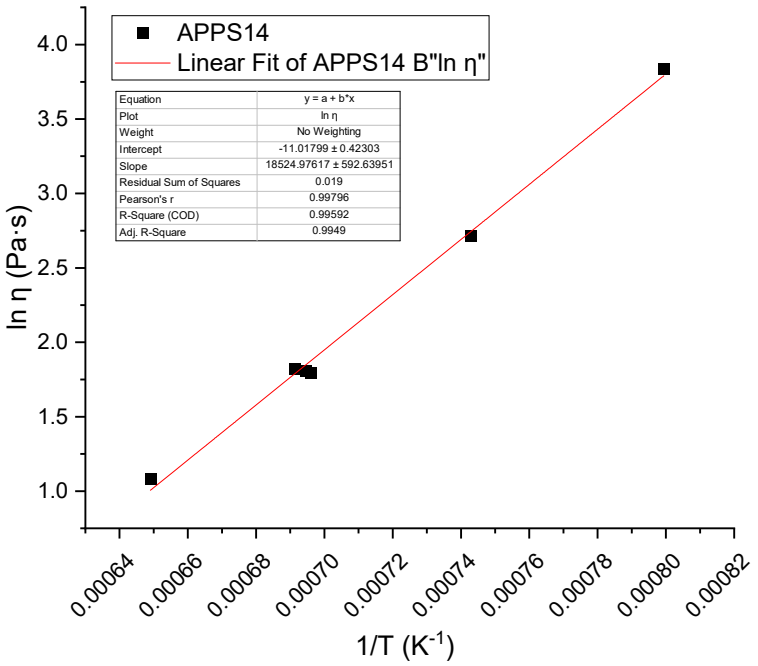

Figure H.14. Electrical conductivity-temperature data and Arrhenius equation fit for glass HLW-APPS-14.

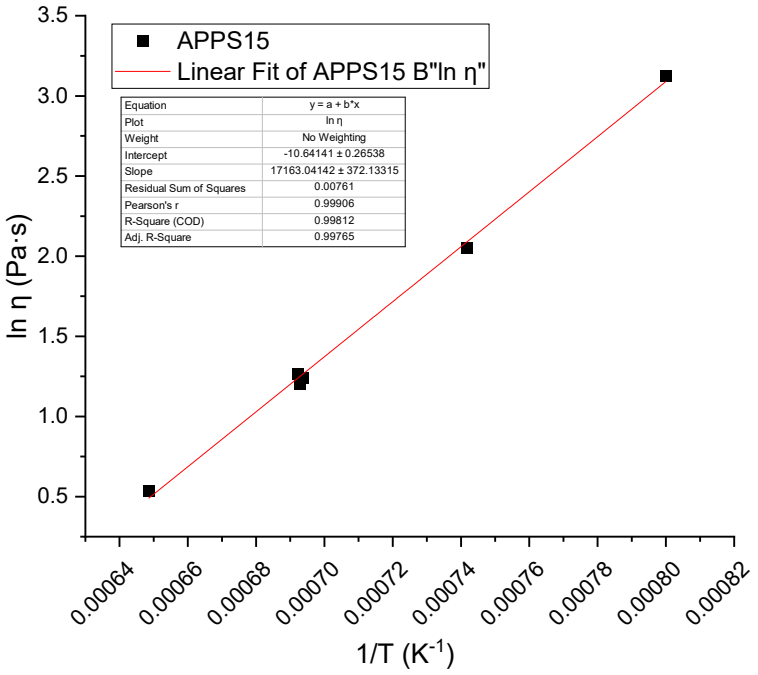

Figure H.15. Electrical conductivity-temperature data and Arrhenius equation fit for glass HLW-APPS-15.

Appendix I – Waste Compositions

Table I.1. Waste compositions in mass fraction.

Glass ID	1	2	3	4	5	6	7	8	9	10	11	12	13	14	15
Batch #	3	4	16	17	18	20	30	45	59	62	101	132	134	152	153
Ag2O	0.00017	0.00007	0.00079	0.00000	0.00025	0.00010	0.00005	0.00047	0.00008	0.00000	0.00000	0.00000	0.00028	0.00005	0.00008
Al2O3	0.50610	0.38248	0.05569	0.10680	0.29350	0.31425	0.30419	0.08025	0.07789	0.20444	0.18321	0.13201	0.12594	0.13852	0.09778
B2O3	0.00062	0.00001	0.00271	0.00000	0.00343	0.00145	0.00060	0.00241	0.00007	0.00000	0.00001	0.00000	0.00031	0.00067	0.00116
BaO	0.00012	0.00012	0.00008	0.00008	0.00006	0.00011	0.00001	0.00027	0.00024	0.00000	0.00000	0.00000	0.00002	0.00011	0.00002
Bi2O3	0.00179	0.00808	0.00045	0.00003	0.00040	0.00234	0.00159	0.00035	0.00002	0.00002	0.00183	0.00698	0.00007	0.00004	0.00015
CaO	0.00786	0.01185	0.00227	0.01310	0.08463	0.01352	0.03089	0.00300	0.00182	0.03436	0.00985	0.00748	0.00324	0.00151	0.00119
CdO	0.00002	0.00001	0.00002	0.00000	0.00012	0.00006	0.00001	0.00001	0.00006	0.00000	0.00000	0.00000	0.00001	0.00004	0.00004
Cl	0.00373	0.00359	0.00434	0.00453	0.00504	0.00685	0.00342	0.00774	0.00668	0.00775	0.00998	0.01074	0.01050	0.01158	0.01033
Cr2O3	0.00252	0.00159	0.00202	0.00240	0.02829	0.01894	0.00195	0.00097	0.00154	0.00574	0.00062	0.00103	0.00330	0.00646	0.01475
F	0.00406	0.00806	0.11068	0.10478	0.00470	0.00321	0.00434	0.07191	0.07933	0.01595	0.00437	0.00688	0.00341	0.00652	0.04184
Fe2O3	0.06603	0.12143	0.04053	0.01394	0.04553	0.05062	0.05756	0.06001	0.03227	0.01354	0.02209	0.02681	0.08310	0.01122	0.00086
K2O	0.00389	0.00118	0.01781	0.00637	0.02627	0.00957	0.01097	0.01078	0.00326	0.00177	0.00053	0.00079	0.00420	0.01033	0.00759
Li2O	0.00006	0.00000	0.00003	0.00000	0.00009	0.00018	0.00004	0.00001	0.00002	0.00000	0.00000	0.00000	0.00002	0.00006	0.00001
MgO	0.00027	0.00022	0.00154	0.00000	0.00138	0.00032	0.00020	0.00161	0.00023	0.00000	0.00000	0.00000	0.00005	0.00018	0.00050
MnO	0.00667	0.00503	0.00570	0.00031	0.00241	0.00239	0.00136	0.00510	0.00228	0.00292	0.00028	0.00266	0.01232	0.00083	0.00015
Na2O	0.29059	0.30709	0.47639	0.61537	0.40461	0.47837	0.37370	0.56945	0.69241	0.58889	0.66599	0.71268	0.69770	0.76174	0.75248
Nd2O3 +	0.00105	0.00117	0.00117	0.00030	0.00171	0.00068	0.00018	0.00136	0.00230	0.00003	0.00004	0.00002	0.00058	0.00091	0.00019
NiO	0.00656	0.01032	0.00117	0.00060	0.00279	0.00697	0.01526	0.00226	0.00145	0.00126	0.00452	0.00404	0.00208	0.00064	0.00010
P2O5	0.00711	0.04074	0.00463	0.02367	0.04991	0.01424	0.07544	0.00537	0.01554	0.05414	0.04137	0.03801	0.00904	0.01945	0.01546
PbO	0.00353	0.00861	0.00141	0.00025	0.00158	0.00265	0.00595	0.00252	0.00076	0.00051	0.00228	0.00139	0.00320	0.00036	0.00011
PdO	0.00001	0.00002	0.00000	0.00000	0.00000	0.00000	0.00000	0.00002	0.00000	0.00000	0.00000	0.00000	0.00000	0.00000	0.00000
Rh2O3	0.00000	0.00001	0.00000	0.00000	0.00000	0.00000	0.00000	0.00001	0.00001	0.00000	0.00000	0.00000	0.00000	0.00000	0.00000
RuO2	0.00014	0.00022	0.00000	0.00000	0.00000	0.00000	0.00000	0.00018	0.00012	0.00000	0.00000	0.00000	0.00000	0.00004	0.00000
SiO2	0.05944	0.04552	0.01703	0.00347	0.00651	0.04758	0.02006	0.00839	0.00114	0.00737	0.00892	0.02254	0.02468	0.00476	0.00352
SnO2	0.00000	0.00000	0.00000	0.00000	0.00000	0.00000	0.00000	0.00000	0.00000	0.00000	0.00000	0.00000	0.00000	0.00000	0.00000
SO3	0.00517	0.00904	0.00580	0.09653	0.00790	0.01014	0.01816	0.00943	0.07557	0.00986	0.01900	0.01656	0.01342	0.02161	0.04565
SrO	0.00019	0.00038	0.00008	0.00007	0.00008	0.00021	0.00094	0.00022	0.00009	0.00005	0.00039	0.00020	0.00015	0.00004	0.00001
ThO2	0.00810	0.00754	0.00021	0.00007	0.00028	0.00010	0.00062	0.00011	0.00048	0.01272	0.00008	0.00003	0.00041	0.00013	0.00001

Glass ID	1	2	3	4	5	6	7	8	9	10	11	12	13	14	15
Batch #	3	4	16	17	18	20	30	45	59	62	101	132	134	152	153
TiO2	0.00004	0.00005	0.00001	0.00000	0.00003	0.00003	0.00001	0.00005	0.00004	0.00000	0.00000	0.00000	0.00000	0.00002	0.00000
UO3	0.00884	0.02108	0.01986	0.00328	0.01991	0.01162	0.07047	0.01311	0.00205	0.01164	0.02434	0.00662	0.00155	0.00102	0.00550
V2O5	0.00007	0.00000	0.00004	0.00000	0.00007	0.00017	0.00002	0.00004	0.00001	0.00000	0.00000	0.00000	0.00002	0.00006	0.00002
ZnO	0.00013	0.00012	0.00003	0.00000	0.00014	0.00026	0.00007	0.00011	0.00003	0.00000	0.00000	0.00000	0.00002	0.00005	0.00001
ZrO2	0.00440	0.00396	0.22718	0.00402	0.00735	0.00114	0.00142	0.14202	0.00130	0.02699	0.00024	0.00247	0.00009	0.00038	0.00041
Others	0.00073	0.00039	0.00032	0.00001	0.00105	0.00189	0.00051	0.00046	0.00089	0.00003	0.00004	0.00003	0.00029	0.00067	0.00011

Table I.2. DFHLW blended waste stream composition (WRPS-2300881), as provided by Michael D. Britton on February 16, 2023.

	3	4	16	17	18	2	12	4	18	21	25	56	58	76	77	Units
	Batch 3	Batch 4	Batch 16	Batch 17	Batch 18	Batch 20	Batch 30	Batch 45	Batch 59	Batch 62	Batch 101	Batch 132	Batch 134	Batch 152	Batch 153	
	SOL20	SOL20	SOL20	SOL20	SOL20	SOL15	SOL15	SOL10	SOL10	SOL10	SOL5	SOL5	SOL5	SOL5	SOL5	
Waste Layer Name 1	AN-101_L02	AN-101_L02	AN-106_L04	AN-101_L08	AP-102_L02	AN-101_L01	AN-101_L03	AN-106_L01	AN-101_L06	AN-101_L06	AN-101_L03	AN-106_L03	AN-104_L01	AN-101_L08	AN-106_L04	
Waste Layer Name 2	AN-103_L01	AN-101_L03	AN-107_L01	AP-101_L01	AP-105_L01	AN-105_L01	AN-101_L04	AP-101_A5-L01	AN-104_L01	AP-101_A1-L01	AN-101_L04	AP-103_L01	AN-105_L01	AN-104_L01	AP-102_L02	
Waste Layer Name 3	AN-106_L01	AN-106_L02	AP-102_L01	AP-102_L02	AW-101_L01	AN-106_L01	AN-101_L05	AP-101_A4-L01	AN-107_L01	AP-102_L02	AN-103_L01	AW-104_L02	AP-102_L01	AN-105_L01	AW-101_L01	
Waste Layer Name 4	AP-101_A5-L01	AP-101_A5-L01	AW-103_L01	AP-104_L01	AW-103_L02	AP-101_A6-L01	AW-101_L01	AP-102_AX1-L01	AW-106_L01	AP-103_L01	AP-108_L01		AW-104_L02	AP-107_L01	AW-102_L01	
Waste Layer Name 5	AP-102_L01	AP-102_L01	AW-105_L02	AW-106_L01	AW-105_L02			AW-103_L01	AY-101_L01					AW-104_L02	AW-103_L02	
Waste Layer Name 6			AZ-101_L01	AZ-101_L01	AZ-102_L02				AZ-102_L02					AY-101_L01	AW-106_L01	
Waste Layer Name 7																
Waste Layer Name 8																
Waste Layer Name 9																
Waste Layer Name 10																
Waste Layer Name 11																
Waste Layer Name 12																
Waste Layer Name 13																
Waste Layer Name 14																
Waste Layer Name 15																
Waste Layer Fraction in Transfer 1	39%	35%	100%	100%	67%	99%	100%	3%	0%	16%	100%	19%	8%	100%	100%	
Waste Layer Fraction in Transfer 2	24%	100%	0%	100%	1%	83%	100%	48%	0%	25%	34%	13%	0%	18%	1%	
Waste Layer Fraction in Transfer 3	6%	41%	24%	33%	27%	19%	100%	42%	0%	59%	0%	1%	26%	0%	0%	
Waste Layer Fraction in Transfer 4	39%	60%	49%	2%	100%	56%	36%	0%	25%	97%	2%		1%	80%	2%	
Waste Layer Fraction in Transfer 5	15%	0%	37%	46%	0%			30%	29%					1%	100%	
Waste Layer Fraction in Transfer 6			8%	34%	17%				0%					7%	10%	
Waste Layer Fraction in Transfer 7																
Waste Layer Fraction in Transfer 8																
Waste Layer Fraction in Transfer 9																
Waste Layer Fraction in Transfer 10																
Waste Layer Fraction in Transfer 11																
Waste Layer Fraction in Transfer 12																
Waste Layer Fraction in Transfer 13																
Waste Layer Fraction in Transfer 14																
Waste Layer Fraction in Transfer 15																
Al(OH)4-	32,550	30,010	18,628	18,468	7,755	21,310	20,109	19,633	17,112	23,477	21,260	20,480	20,799	21,114	16,883	kg
CO3-2	43,903	34,280	43,328	37,594	6,316	42,920	21,676	39,202	49,473	35,707	33,540	39,212	49,229	44,073	33,912	kg
C2O4-2	1,336	735	1,541	2,569	694	2,360	1,314	982	3,345	2,297	858	3,434	1,323	3,079	3,065	kg
Cl-	1,928	1,853	3,174	2,966	938	3,436	1,601	3,871	3,171	3,225	3,331	3,729	3,677	4,007	3,873	kg
F-	2,103	2,461	6,021	5,957	523	1,611	1,413	5,291	6,127	2,980	1,134	1,578	1,043	1,619	5,052	kg
OH-	62,881	58,390	30,027	30,127	13,397	35,346	36,148	31,480	27,109	37,983	35,197	32,828	33,161	33,361	26,582	kg
Na+	105,888	100,419	159,543	159,518	43,111	155,242	109,144	172,064	174,941	158,480	160,351	174,152	177,197	182,154	183,013	kg
NO2-	41,617	46,888	65,196	67,307	22,892	68,165	48,011	75,958	68,722	69,531	71,074	76,321	76,017	79,339	80,955	kg
NO3-	75,178	80,894	122,773	116,659	39,209	122,586	112,295	145,353	124,980	120,106	146,362	149,656	138,354	145,655	151,667	kg
PO4-3	4,928	11,141	4,115	7,592	10,995	9,555	41,130	3,589	3,024	19,002	15,235	11,060	4,236	4,166	4,709	kg
SO4-2	3,212	5,598	5,084	21,114	1,766	6,101	10,229	5,658	21,347	4,923	7,609	6,903	5,640	8,975	18,281	kg
H2O	1,699,873	1,703,865	1,596,959	1,614,594	579,636	1,652,244	1,714,063	1,666,219	1,676,763	1,699,329	1,728,780	1,710,813	1,706,253	1,701,011	1,692,632	kg
Ag	6.9E-01	8.9E-03	1.1E+00	0.0E+00	4.9E-02	9.7E-02	5.3E-03	5.7E-02	6.8E-01	0.0E+00	2.9E-04	5.2E-03	1.1E+00	1.9E-01	1.1E-01	kg
Al+3																kg
AlOOH																kg
Aroclors (Total PCB) (as C)	2.3E-04	2.8E-06	1.2E-03	4.6E-04	1.9E-04	1.9E-03	1.3E-04	5.0E-04	4.1E-04	2.5E-04	7.5E-05	8.0E-05	4.1E-04	7.2E-04	4.6E-04	kg
As	2.2E-02	0.0E+00	4.6E-01	0.0E+00	4.7E-01	2.7E-01	1.4E-01	2.8E-01	5.7E-01	0.0E+00	1.2E-04	5.2E-02	5.3E-02	2.0E-01	8.7E-01	kg
B	2.1E-01	0.0E+00	1.1E+00	0.0E+00	6.8E-01	4.0E-01	1.2E-01	7.0E-01	1.1E+00	0.0E+00	8.9E-03	5.5E-02	9.1E-02	3.9E-01	1.4E+00	kg
Ba-cold	1.1E-02	0.0E+00	6.5E-02	7.9E-02	4.9E-02	1.3E-01	5.5E-03	2.7E-02	4.7E-02	0.0E+00	6.1E-05	2.6E-02	2.8E-02	4.2E-02	1.1E-01	kg
Be	3.1E-03	0.0E+00	7.6E-02	0.0E+00	4.1E-02	1.3E-02	7.1E-03	4.6E-02	4.7E-02	0.0E+00	1.7E-05	2.6E-03	2.9E-03	1.5E-02	8.6E-02	kg
Bi	1.0E+02	1.5E+02	7.0E+00	1.4E+00	2.2E+00	7.5E+01	8.4E+01	1.3E+00	1.5E+00	8.3E-01	7.5E+01	1.1E+01	5.3E+00	1.6E+00	1.6E+00	kg
Br	0.0E+00	0.0E+00	0.0E+00	0.0E+00	0.0E+00	0.0E+00	0.0E+00	0.0E+00	0.0E+00	0.0E+00	0.0E+00	0.0E+00	0.0E+00	0.0E+00	0.0E+00	kg
Ca	3.0E+00	1.0E+01	1.8E+00	1.9E+00	2.1E-01	8.0E+00	1.3E+00	1.2E+02	2.1E+00	1.9E+00	5.5E-01	4.2E+01	9.9E-01	2.7E+00	1.7E+00	kg
Cd-cold	5.3E-02	6.1E-02	3.3E-02	0.0E+00	4.1E-02	1.3E-02	6.8E-03	6.8E-02	1.6E-01	0.0E+00	1.2E-03	0.0E+00	5.6E-04	4.1E-02	8.6E-02	kg
Ce	2.2E-02	0.0E+00	6.4E-01	0.0E+00	2.3E-01	2.7E-01	6.8E-03	3.9E-01	7.2E-01	0.0E+00	1.2E-04	5.2E-02	6.4E-02	2.5E-01	5.4E-01	kg
Cl-bound	2.3E-05	2.9E-07	1.2E-04	4.7E-05	1.9E-05	1.9E-04	1.3E-05	5.1E-05	4.2E-05	2.5E-05	7.7E-06	8.2E-06	4.2E-05	7.4E-05	4.7E-05	kg

	3	4	16	17	18	2	12	4	18	21	25	56	58	76	77	Units
	Batch 3	Batch 4	Batch 16	Batch 17	Batch 18	Batch 20	Batch 30	Batch 45	Batch 59	Batch 62	Batch 101	Batch 132	Batch 134	Batch 152	Batch 153	
	SOL20	SOL20	SOL20	SOL20	SOL20	SOL15	SOL15	SOL10	SOL10	SOL10	SOL5	SOL5	SOL5	SOL5	SOL5	
CN	0.0E+00	0.0E+00	0.0E+00	0.0E+00	0.0E+00	0.0E+00	0.0E+00	0.0E+00	1.0E+00	0.0E+00	0.0E+00	0.0E+00	0.0E+00	2.5E-01	0.0E+00	kg
CO3-bound	5.1E+01	2.2E+02	2.0E+02	1.6E+01	5.6E+01	1.9E+02	3.7E+01	1.0E+02	1.5E+01	6.1E+00	1.1E+01	1.7E+02	4.1E+00	2.8E+00	2.9E+01	kg
Co-cold	4.8E-03	0.0E+00	3.4E-02	0.0E+00	6.2E-02	5.3E-02	1.1E-02	2.1E-02	5.6E-02	0.0E+00	2.0E-03	1.0E-02	1.2E-02	2.6E-02	1.3E-01	kg
CrO4	2.1E+02	2.6E+02	3.8E+02	2.0E+02	2.6E+02	3.1E+02	1.6E+02	9.9E+01	2.6E+02	1.4E+02	6.0E+01	1.5E+02	1.8E+02	2.8E+02	5.5E+02	kg
CrOOH																kg
Cs-cold	1.5E+00	7.8E-01	2.7E+00	3.7E+00	1.4E+00	1.4E+00	3.8E+00	7.7E-01	1.3E+00	7.4E-01	9.9E-01	1.7E-01	1.6E+00	1.1E+00	7.9E-01	kg
Cu	1.1E-02	0.0E+00	5.2E-02	0.0E+00	5.3E-02	2.9E-02	7.1E-03	3.1E-02	1.7E-01	0.0E+00	1.4E-03	5.2E-03	7.8E-03	5.3E-02	1.1E-01	kg
Eu-cold	0.0E+00	0.0E+00	0.0E+00	0.0E+00	0.0E+00	0.0E+00	0.0E+00	0.0E+00	1.1E-01	0.0E+00	0.0E+00	0.0E+00	0.0E+00	2.6E-02	0.0E+00	kg
Fe	1.3E+02	5.8E+02	2.3E+02	4.2E+00	2.5E+00	3.9E+01	2.2E+01	1.8E+01	1.9E+00	6.4E-01	9.2E+00	1.4E+02	2.2E+02	1.7E+00	5.5E+00	kg
H-bound	7.2E+01	4.5E+01	1.4E+02	2.0E+01	5.0E+00	2.2E+01	9.1E+01	3.0E+01	8.5E+00	5.3E+01	3.0E+01	2.9E+00	6.5E+01	6.0E+00	3.0E+00	kg
H2O-bound	0.0E+00	0.0E+00	0.0E+00	0.0E+00	0.0E+00	0.0E+00	0.0E+00	0.0E+00	0.0E+00	0.0E+00	0.0E+00	0.0E+00	0.0E+00	0.0E+00	0.0E+00	kg
Hg	1.3E+01	1.1E+01	1.9E+01	3.4E-02	1.1E-02	3.9E+00	6.4E-01	1.4E+00	1.5E+00	3.0E-01	2.6E-01	4.8E+00	2.2E+01	4.0E-01	6.7E-02	kg
K	9.5E+02	2.5E+02	1.0E+04	1.6E+03	1.8E+03	6.7E+02	1.4E+03	4.3E+03	8.4E+02	4.0E+02	6.7E+01	1.5E+02	7.2E+02	7.8E+02	2.0E+03	kg
La	3.8E-02	6.3E-01	9.8E-01	7.6E-02	4.7E-01	1.2E-01	5.5E-02	3.9E-01	1.4E+00	1.4E-02	2.1E-02	5.4E-02	4.7E-02	3.9E-01	1.0E-01	kg
Li	6.6E-02	0.0E+00	3.1E-02	0.0E+00	4.8E-02	3.2E-02	1.7E-02	1.9E-02	1.2E-01	0.0E+00	1.1E-03	5.2E-03	1.2E-02	4.8E-02	8.7E-02	kg
Mg	1.6E-01	0.0E+00	2.8E-01	0.0E+00	2.3E-01	2.7E-01	5.2E-03	1.7E-01	1.6E-01	0.0E+00	8.8E-04	5.2E-02	5.3E-02	9.4E-02	5.4E-01	kg
Mn	8.5E+01	5.1E+00	1.3E+02	3.1E-01	1.2E-01	4.0E+00	8.7E-02	2.4E-01	1.7E-01	5.7E-01	1.6E-02	2.2E+00	1.5E+02	2.0E-01	1.3E-01	kg
Mo	3.1E-01	0.0E+00	1.8E+00	0.0E+00	1.4E+00	5.3E-01	1.7E-01	1.1E+00	2.5E+00	0.0E+00	1.6E-02	7.5E-02	1.2E-01	7.8E-01	3.2E+00	kg
Na-bound	9.9E+02	5.0E+02	1.1E+03	2.1E+02	3.6E+01	6.7E+01	1.8E+02	2.7E+02	4.1E+01	8.9E+01	7.0E+01	5.9E+01	7.5E+02	2.6E+01	5.3E+01	kg
Nb-cold	0.0E+00	0.0E+00	0.0E+00	0.0E+00	0.0E+00	0.0E+00	0.0E+00	0.0E+00	0.0E+00	0.0E+00	0.0E+00	0.0E+00	0.0E+00	0.0E+00	0.0E+00	kg
Nd	1.6E-01	0.0E+00	2.6E-01	0.0E+00	1.1E-01	2.7E-01	2.1E-02	1.6E-01	4.3E-01	0.0E+00	8.8E-04	5.2E-02	8.5E-02	2.3E-01	2.2E-01	kg
NH3	0.0E+00	0.0E+00	4.3E-03	0.0E+00	0.0E+00	0.0E+00	0.0E+00	0.0E+00	1.1E+00	0.0E+00	0.0E+00	0.0E+00	0.0E+00	2.6E-01	0.0E+00	kg
Ni-cold	1.2E+02	1.1E+02	1.2E+02	1.2E+00	3.3E+00	5.5E+01	2.0E+02	1.5E+01	1.4E+01	1.4E+01	5.1E+01	8.9E+00	7.8E+01	4.8E+00	7.5E+00	kg
NO3-bound	0.0E+00	0.0E+00	0.0E+00	0.0E+00	0.0E+00	0.0E+00	0.0E+00	0.0E+00	0.0E+00	0.0E+00	0.0E+00	0.0E+00	0.0E+00	0.0E+00	0.0E+00	kg
O-bound	3.0E+03	1.8E+03	5.3E+03	8.0E+02	2.0E+02	7.9E+02	3.0E+03	1.1E+03	3.0E+02	1.7E+03	1.0E+03	1.7E+02	2.6E+03	2.1E+02	1.4E+02	kg
OH-bound	4.0E+02	8.8E+02	3.1E+03	1.2E+01	1.4E+01	1.3E+02	2.5E+02	1.1E+03	3.4E+01	1.9E+01	9.0E+01	1.9E+02	4.9E+02	1.2E+01	1.8E+01	kg
Pb	2.2E+02	1.5E+02	2.0E+02	1.8E+00	7.0E-01	7.2E+01	3.5E+02	3.3E+01	4.1E+01	2.0E+01	1.2E+02	7.3E+00	2.2E+02	1.3E+01	8.4E-01	kg
Pd	0.0E+00	0.0E+00	0.0E+00	0.0E+00	0.0E+00	0.0E+00	0.0E+00	0.0E+00	0.0E+00	0.0E+00	0.0E+00	0.0E+00	0.0E+00	0.0E+00	0.0E+00	kg
Pr	0.0E+00	0.0E+00	0.0E+00	0.0E+00	0.0E+00	0.0E+00	0.0E+00	0.0E+00	1.9E-02	0.0E+00	0.0E+00	0.0E+00	0.0E+00	4.6E-03	0.0E+00	kg
Rb	0.0E+00	0.0E+00	0.0E+00	0.0E+00	0.0E+00	0.0E+00	0.0E+00	0.0E+00	2.8E-01	0.0E+00	0.0E+00	0.0E+00	0.0E+00	6.9E-02	0.0E+00	kg
Rh	0.0E+00	0.0E+00	0.0E+00	0.0E+00	0.0E+00	0.0E+00	0.0E+00	0.0E+00	9.3E-02	0.0E+00	0.0E+00	0.0E+00	0.0E+00	2.3E-02	0.0E+00	kg
Ru-cold	0.0E+00	0.0E+00	0.0E+00	0.0E+00	0.0E+00	0.0E+00	0.0E+00	0.0E+00	4.8E-01	0.0E+00	0.0E+00	0.0E+00	0.0E+00	1.2E-01	0.0E+00	kg
Sb-cold	9.5E-02	0.0E+00	5.6E-01	0.0E+00	2.9E-01	1.6E-01	8.7E-02	3.4E-01	2.5E-03	0.0E+00	5.3E-04	3.1E-02	5.1E-02	7.3E-02	5.4E-01	kg
Se-cold	1.6E-01	0.0E+00	9.3E-01	0.0E+00	4.6E-01	2.7E-01	5.4E-02	5.7E-01	4.3E-02	0.0E+00	8.8E-04	5.2E-02	5.3E-02	6.4E-02	1.0E+00	kg
Si	1.2E+03	6.1E+02	1.4E+03	2.6E+02	4.4E+01	8.2E+01	2.2E+02	3.2E+02	5.0E+01	1.1E+02	8.5E+01	7.3E+01	9.2E+02	3.2E+01	6.5E+01	kg
Sm-cold	0.0E+00	0.0E+00	0.0E+00	0.0E+00	0.0E+00	0.0E+00	0.0E+00	0.0E+00	4.1E-01	0.0E+00	0.0E+00	0.0E+00	0.0E+00	1.0E-01	0.0E+00	kg
Sn-cold	0.0E+00	0.0E+00	0.0E+00	0.0E+00	0.0E+00	0.0E+00	0.0E+00	0.0E+00	0.0E+00	0.0E+00	0.0E+00	0.0E+00	0.0E+00	0.0E+00	0.0E+00	kg
Sr-cold	7.1E+00	6.3E+00	2.1E-01	3.0E-01	1.1E-01	3.2E-01	7.7E+00	2.5E-01	2.8E-01	5.1E-01	7.5E+00	4.3E-01	1.0E-01	2.7E-01	3.7E-01	kg
Ta	0.0E+00	0.0E+00	1.6E-04	0.0E+00	0.0E+00	0.0E+00	0.0E+00	0.0E+00	1.6E-04	0.0E+00	0.0E+00	0.0E+00	0.0E+00	0.0E+00	0.0E+00	kg
Te	0.0E+00	0.0E+00	0.0E+00	0.0E+00	0.0E+00	0.0E+00	0.0E+00	0.0E+00	7.2E-02	0.0E+00	0.0E+00	0.0E+00	0.0E+00	1.8E-02	0.0E+00	kg
Th-cold	1.3E-03	2.8E-03	3.6E-08	9.1E-05	9.6E-09	1.1E-03	3.4E-05	2.5E-08	7.5E-05	3.3E-03	8.5E-06	4.9E-06	1.3E-06	1.7E-05	1.9E-05	kg
Ti	1.6E-02	0.0E+00	5.1E-02	0.0E+00	2.9E-02	2.7E-02	1.4E-02	3.1E-02	1.2E-01	0.0E+00	8.8E-05	5.2E-03	5.3E-03	3.5E-02	4.3E-02	kg
Tl	0.0E+00	0.0E+00	4.6E-01	0.0E+00	9.7E-01	5.3E-01	1.1E-01	2.8E-01	8.5E-03	0.0E+00	0.0E+00	0.0E+00	1.6E-03	3.7E-03	2.2E+00	kg
TOC-Other	3.5E+02	2.7E+02	1.1E+03	1.3E+02	4.1E+01	2.3E+02	9.9E+02	2.1E+02	7.7E+01	5.8E+02	3.3E+02	4.0E+00	3.8E+02	5.7E+01	8.4E+00	kg
V	8.0E-02	0.0E+00	3.1E-02	0.0E+00	4.5E-02	1.3E-01	5.2E-04	1.9E-02	8.6E-02	0.0E+00	4.4E-04	2.6E-02	3.1E-02	5.8E-02	1.1E-01	kg
W	0.0E+00	0.0E+00	0.0E+00	0.0E+00	0.0E+00	0.0E+00	0.0E+00	0.0E+00	1.3E+01	0.0E+00	0.0E+00	0.0E+00	0.0E+00	3.2E+00	0.0E+00	kg
Y-cold	0.0E+00	0.0E+00	6.2E-02	0.0E+00	3.6E-02	0.0E+00	0.0E+00	3.8E-02	1.6E-01	0.0E+00	0.0E+00	5.2E-03	5.2E-03	4.5E-02	8.6E-02	kg
Zn	3.3E-02	0.0E+00	1.3E-01	0.0E+00	5.8E-02	1.7E-01	1.6E-02	7.8E-02	1.3E+00	0.0E+00	1.8E-04	5.2E-03	1.3E-02	3.4E-01	1.1E-01	kg
Zr-cold	9.6E-01	1.4E-01	3.4E+03	5.5E+00	7.1E+00	5.4E-01	4.9E-01	1.5E+03	1.2E+01	1.8E+00	2.5E-04	3.5E+00	2.0E+00	2.5E+00	3.7E+00	kg
H-3	2.9E-07	2.4E-07	8.1E-07	5.9E-08	1.1E-07	2.7E-07	8.5E-07	5.9E-08	2.1E-08	1.9E-07	3.5E-07	8.2E-08	1.8E-08	2.8E-08	2.9E-08	kg
C-14	1.8E-04	2.1E-04	2.0E-04	3.1E-04	1.3E-04	1.7E-04	6.0E-04	4.0E-05	1.8E-04	2.1E-04	1.6E-04	3.6E-05	3.4E-05	1.5E-04	1.2E-04	kg
Co-60	5.2E-08	4.1E-08	4.3E-07	3.0E-07	2.1E-08	2.4E-08	2.2E-08	1.2E-07	2.1E-08	2.4E-08	8.8E-09	1.1E-08	4.4E-08	1.3E-08	4.8E-08	kg
Ni-59	7.1E-03	1.7E-03	1.0E-02	1.4E-03	3.6E-03	1.8E-03	3.1E-03	4.5E-04	3.1E-03	6.2E-04	9.5E-04	9.1E-04	1.0E-02	1.7E-03	8.8E-03	kg
Ni-63	7.5E-04	1.8E-04	1.0E-03	6.2E-05	3.9E-04	1.8E-04	3.3E-04	1.5E-05	2.1E-04	6.2E-05	1.0E-04	8.2E-05	1.1E-03	1.4E-04	9.6E-04	kg
Se-79	4.6E-03	7.2E-03	6.3E-03	1.9E-02	9.8E-03	7.3E-03	2.9E-02	1.1E-03	1.3E-02	5.5E-02	6.9E-03	5.3E-03	3.7E-03	1.0E-02	1.8E-02	kg
Sr-90	7.2E-03	7.1E-03	7.6E-03	6.5E-03	1.7E-03	7.2E-03	7.6E-03	7.4E-03	7.4E-03	7.3E-03	7.6E-03	7.5E-03	7.6E-03	7.5E-03	7.5E-03	kg
Y-90	1.8E-06	1.8E-06	1.9E-06	1.6E-06	4.4E-07	1.8E-06	1.9E-06	1.9E-06	1.9E-06	1.9E-06	1.9E-06	1.9E-06	1.9E-06	1.9E-06	1.9E-06	kg
Zr-93	2.0E-01	3.2E-02	4.2E-01	1.1E+00	2.7E-01	3.1E-01	1.8E-01	8.2E-02	1.2E+00	3.5E-01	4.8E-02	5.2E-02	1.8E-01	7.0E-01	6.1E-01	kg
Nb-93m	2.1E-06	2.7E-07	5.0E-06	1.2E-05	3.8E-06	3.7E-06	1.8E-06	2.8E-06	2.4E-05	2.2E-06	5.0E-07	4.8E-07	2.2E-06	1.0E-05	7.4E-06	kg
Tc-99	5.6E-01	7.5E-01	2.1E+00	3.4E+00	1.4E+00	2.0E+00	1.7E+00	9.5E-01	1.7E+00	9.7E-01	4.0E-01	6.5E-01	6.2E-01	1.4E+00	1.5E+00	kg
Ru-106	3.4E-19	2.3E-20	1.1E-16	5.1E-16	3.8E-19	7.5E-17	9.8E-22	5.8E-18	3.2E-16	6.9E-17	6.8E-19	9.5E-18	1.5E-19	2.9E-16	1.7E-17	kg
Cd-113m	7.4E-07	1.0E-07	2.5E-06	2.6E-06	1.0E-06	2.0E-06	9.6E-07	8.1E-07	1.8E-06	9.2E-07	4.0E-07	1.5E-07	1.1E-06	1.8E-06	2.4E-06	kg

	3	4	16	17	18	2	12	4	18	21	25	56	58	76	77	Units
	Batch 3	Batch 4	Batch 16	Batch 17	Batch 18	Batch 20	Batch 30	Batch 45	Batch 59	Batch 62	Batch 101	Batch 132	Batch 134	Batch 152	Batch 153	
	SOL20	SOL20	SOL20	SOL20	SOL20	SOL15	SOL15	SOL10	SOL10	SOL10	SOL5	SOL5	SOL5	SOL5	SOL5	
Sn-126	2.1E-02	4.8E-04	3.7E-02	8.5E-03	9.9E-03	9.4E-03	1.8E-03	4.6E-03	1.1E-02	3.2E-03	8.7E-05	9.9E-04	3.4E-02	1.3E-02	2.1E-02	kg
Sb-125	8.4E-10	1.8E-09	4.4E-08	1.1E-07	2.8E-08	1.6E-09	2.7E-10	1.6E-08	1.1E-08	9.4E-10	1.1E-10	1.3E-10	1.3E-09	5.1E-09	3.4E-09	kg
I-129	3.6E-01	1.1E+00	3.2E-01	4.4E-01	1.1E-01	2.3E-01	3.1E-01	1.2E-01	2.0E-01	3.1E-01	1.5E-01	7.2E-02	1.1E-01	1.2E-01	1.9E-01	kg
Cs-134	1.1E-11	1.7E-12	1.3E-07	5.2E-07	6.6E-10	4.5E-11	9.8E-12	1.2E-10	1.6E-10	3.0E-11	1.4E-12	4.7E-12	7.1E-12	1.2E-10	1.3E-11	kg
Cs-137	3.2E-01	1.7E-01	6.1E-01	9.2E-01	3.0E-01	3.1E-01	8.2E-01	1.7E-01	2.8E-01	1.6E-01	2.1E-01	3.8E-02	3.4E-01	2.3E-01	1.7E-01	kg
Ba-137m	4.8E-08	2.6E-08	9.3E-08	1.4E-07	4.5E-08	4.7E-08	1.3E-07	2.5E-08	4.2E-08	2.4E-08	3.3E-08	5.7E-09	5.2E-08	3.5E-08	2.6E-08	kg
Sm-151	5.0E-04	2.8E-06	3.5E-04	5.1E-03	2.1E-03	4.5E-03	5.7E-03	3.7E-05	1.6E-03	1.3E-03	2.4E-03	2.0E-04	4.9E-04	3.6E-03	4.9E-03	kg
Eu-152	3.3E-08	2.7E-08	1.2E-07	8.3E-08	2.2E-07	8.3E-08	7.2E-09	2.2E-07	4.9E-07	2.9E-08	3.1E-09	1.2E-08	5.0E-08	1.9E-07	2.5E-08	kg
Eu-154	5.8E-07	2.7E-07	1.2E-06	8.0E-07	6.1E-06	4.2E-07	5.8E-08	1.3E-06	8.0E-06	2.4E-07	1.6E-08	2.6E-07	9.2E-07	2.3E-06	4.9E-07	kg
Eu-155	1.6E-08	6.3E-09	6.9E-08	5.3E-08	7.7E-07	2.8E-08	4.4E-09	1.7E-07	2.7E-07	1.4E-08	1.6E-09	6.5E-09	2.4E-08	9.3E-08	1.5E-08	kg
Ra-226	1.5E-09	4.6E-11	5.5E-09	5.3E-09	1.6E-09	4.1E-09	2.2E-09	2.1E-09	3.9E-09	1.7E-09	9.1E-10	6.3E-10	2.1E-09	3.4E-09	3.2E-09	kg
Ra-228	4.5E-09	3.8E-10	7.2E-09	1.6E-10	4.0E-10	1.9E-10	1.8E-12	2.1E-10	5.5E-09	3.3E-10	7.9E-12	1.4E-11	7.7E-09	1.5E-09	8.4E-11	kg
Ac-227	2.6E-09	5.1E-11	3.0E-09	4.9E-09	1.0E-08	4.8E-09	2.2E-09	5.8E-10	1.8E-09	2.8E-09	4.0E-10	4.3E-10	2.6E-09	1.0E-08	2.3E-08	kg
Th-229	1.3E-06	1.4E-06	1.9E-06	6.6E-06	5.8E-09	2.9E-06	2.5E-07	2.9E-07	1.7E-06	4.6E-07	1.1E-07	1.6E-08	3.4E-07	5.8E-07	2.7E-08	kg
Th-232	3.8E+00	6.6E+00	6.0E-01	2.0E-01	1.5E+00	8.3E-01	2.1E-01	1.3E-01	7.4E+00	4.7E+00	2.8E-02	1.7E-01	5.8E-01	2.0E+00	6.6E-02	kg
Pa-231	2.3E-05	7.8E-06	1.0E-05	4.3E-05	3.0E-05	3.2E-05	1.0E-05	1.4E-06	2.2E-05	3.6E-05	9.2E-07	2.8E-06	8.5E-06	3.6E-05	7.6E-05	kg
U-232	2.0E-08	1.3E-07	8.1E-09	7.9E-09	1.7E-08	5.2E-09	7.3E-09	2.4E-09	5.1E-09	1.8E-08	3.0E-09	1.8E-09	1.7E-09	2.3E-09	4.5E-08	kg
U-233	4.0E-03	2.4E-02	9.2E-04	1.2E-03	3.1E-03	4.8E-04	4.0E-03	3.0E-05	3.9E-03	4.6E-03	1.6E-03	3.1E-04	5.1E-04	1.1E-03	8.4E-03	kg
U-234	3.5E-03	1.5E-02	2.0E-02	1.4E-03	5.1E-03	1.4E-02	1.6E-03	9.2E-03	1.3E-03	4.0E-04	4.5E-04	1.2E-02	3.1E-04	2.5E-04	2.4E-03	kg
U-235	4.4E-01	1.9E+00	2.3E+00	1.6E-01	5.9E-01	1.7E+00	3.3E-01	1.1E+00	1.5E-01	5.7E-02	9.7E-02	1.5E+00	3.7E-02	2.8E-02	2.7E-01	kg
U-236	6.7E-03	3.5E-02	1.9E-01	1.0E-02	3.6E-02	2.4E-02	4.2E-03	6.4E-02	9.5E-03	1.3E-03	1.1E-03	2.6E-02	1.3E-03	1.7E-03	7.3E-03	kg
U-238	6.7E+01	2.8E+02	2.6E+02	2.1E+01	7.3E+01	2.6E+02	4.9E+01	1.4E+02	2.0E+01	8.0E+00	1.5E+01	2.3E+02	5.4E+00	3.7E+00	3.9E+01	kg
Np-237	1.6E-02	2.1E-03	2.1E-02	4.3E-02	2.1E-01	2.9E-02	7.5E-03	5.9E-03	6.6E-02	6.7E-03	1.6E-03	6.7E-03	1.3E-02	1.9E-02	2.0E-02	kg
Pu-238	1.7E-05	6.8E-06	1.0E-04	6.3E-05	3.2E-07	4.6E-06	1.9E-07	1.7E-05	5.3E-06	1.5E-07	4.1E-08	3.0E-06	2.9E-05	1.4E-06	4.7E-07	kg
Pu-239	1.5E-01	9.1E-02	4.8E-01	1.7E-01	1.6E-03	3.4E-02	2.2E-03	6.0E-02	8.3E-03	5.2E-04	7.4E-04	2.7E-02	2.6E-01	2.1E-03	2.7E-03	kg
Pu-240	9.3E-03	3.8E-03	3.3E-02	1.3E-02	1.1E-04	1.8E-03	1.5E-04	4.5E-03	5.4E-04	3.1E-05	4.8E-05	1.4E-03	1.6E-02	1.4E-04	1.7E-04	kg
Pu-241	3.4E-05	1.7E-05	3.3E-04	1.8E-04	1.1E-06	7.1E-06	3.8E-07	6.5E-05	6.2E-06	1.9E-07	1.9E-08	7.3E-06	5.9E-05	1.6E-06	1.2E-06	kg
Pu-242	5.9E-05	1.7E-05	2.4E-04	9.9E-05	6.6E-07	2.2E-05	1.0E-05	4.0E-05	2.4E-05	3.2E-05	4.4E-06	1.2E-05	9.8E-05	1.0E-05	2.3E-06	kg
Am-241	5.5E-03	4.1E-03	2.8E-02	4.3E-02	6.1E-02	6.4E-04	2.1E-04	1.9E-03	3.8E-02	3.6E-04	5.5E-05	6.9E-04	9.1E-03	9.1E-03	3.3E-04	kg
Am-243	5.1E-05	1.6E-05	1.5E-04	2.9E-04	3.7E-04	2.4E-05	5.8E-07	5.9E-06	1.3E-03	1.6E-06	9.5E-08	3.9E-06	8.1E-05	3.2E-04	3.6E-06	kg
Cm-242	3.2E-08	1.8E-08	7.0E-08	8.3E-08	5.2E-09	1.9E-08	4.5E-10	1.1E-08	2.3E-10	2.4E-09	9.5E-11	8.3E-09	5.5E-08	1.0E-10	4.2E-10	kg
Cm-243	4.7E-07	6.7E-08	8.0E-07	2.8E-07	2.2E-08	4.8E-08	2.8E-09	2.2E-08	1.0E-09	6.2E-09	5.9E-10	2.3E-08	8.2E-07	5.1E-10	7.3E-10	kg
Cm-244	4.6E-06	7.1E-07	7.8E-06	2.9E-06	2.2E-07	4.6E-07	2.7E-08	2.1E-07	9.8E-09	6.0E-08	6.2E-09	2.2E-07	7.9E-06	4.9E-09	7.3E-09	kg
Al(OH)3	3.4E+05	2.4E+05	4.3E+04	8.8E+04	7.1E+04	2.0E+05	1.8E+05	2.6E+04	4.1E+04	1.1E+05	7.0E+04	4.6E+04	5.0E+04	5.4E+04	3.6E+04	kg
Na2C2O4	3.5E+03	0.0E+00	1.3E+03	3.0E+04	1.2E+04	1.2E+04	9.5E+03	6.2E+01	1.7E+04	9.0E+03	3.0E+00	2.5E+03	1.5E+03	7.5E+03	1.1E+04	kg
NaCl	0.0E+00	0.0E+00	0.0E+00	0.0E+00	0.0E+00	0.0E+00	0.0E+00	0.0E+00	0.0E+00	0.0E+00	0.0E+00	0.0E+00	0.0E+00	0.0E+00	0.0E+00	kg
Na2CO3(H2O)10	0.0E+00	0.0E+00	0.0E+00	0.0E+00	0.0E+00	0.0E+00	0.0E+00	0.0E+00	0.0E+00	0.0E+00	0.0E+00	0.0E+00	0.0E+00	0.0E+00	0.0E+00	kg
Na2CO3(H2O)7	0.0E+00	0.0E+00	0.0E+00	0.0E+00	0.0E+00	0.0E+00	0.0E+00	0.0E+00	0.0E+00	0.0E+00	0.0E+00	0.0E+00	0.0E+00	0.0E+00	0.0E+00	kg
Na2CO3H2O	0.0E+00	0.0E+00	0.0E+00	0.0E+00	0.0E+00	0.0E+00	0.0E+00	0.0E+00	0.0E+00	0.0E+00	0.0E+00	0.0E+00	0.0E+00	0.0E+00	0.0E+00	kg
Na2HPO4(H2O)2	0.0E+00	0.0E+00	0.0E+00	0.0E+00	0.0E+00	0.0E+00	0.0E+00	0.0E+00	0.0E+00	0.0E+00	0.0E+00	0.0E+00	0.0E+00	0.0E+00	0.0E+00	kg
Na2HPO4(H2O)7	0.0E+00	0.0E+00	0.0E+00	0.0E+00	0.0E+00	0.0E+00	0.0E+00	0.0E+00	0.0E+00	0.0E+00	0.0E+00	0.0E+00	0.0E+00	0.0E+00	0.0E+00	kg
Na2HPO4(H2O)12	0.0E+00	0.0E+00	0.0E+00	0.0E+00	0.0E+00	0.0E+00	0.0E+00	0.0E+00	0.0E+00	0.0E+00	0.0E+00	0.0E+00	0.0E+00	0.0E+00	0.0E+00	kg
Na2SO4	0.0E+00	0.0E+00	0.0E+00	0.0E+00	0.0E+00	0.0E+00	0.0E+00	0.0E+00	0.0E+00	0.0E+00	0.0E+00	0.0E+00	0.0E+00	0.0E+00	0.0E+00	kg
Na2SO4(H2O)10	0.0E+00	0.0E+00	0.0E+00	0.0E+00	0.0E+00	0.0E+00	0.0E+00	0.0E+00	0.0E+00	0.0E+00	0.0E+00	0.0E+00	0.0E+00	0.0E+00	0.0E+00	kg
Na3FSO4	0.0E+00	0.0E+00	0.0E+00	1.0E+05	0.0E+00	0.0E+00	0.0E+00	0.0E+00	4.2E+04	0.0E+00	0.0E+00	0.0E+00	0.0E+00	0.0E+00	4.3E+03	kg
Na3(NO3)(SO4)H2O	0.0E+00	0.0E+00	0.0E+00	0.0E+00	0.0E+00	0.0E+00	0.0E+00	0.0E+00	0.0E+00	0.0E+00	0.0E+00	0.0E+00	0.0E+00	0.0E+00	0.0E+00	kg
Na3PO4(NaOH)0.25(H2O)12	0.0E+00	0.0E+00	0.0E+00	0.0E+00	0.0E+00	0.0E+00	0.0E+00	0.0E+00	0.0E+00	0.0E+00	0.0E+00	0.0E+00	0.0E+00	0.0E+00	0.0E+00	kg
Na3PO4(H2O)6	0.0E+00	0.0E+00	0.0E+00	0.0E+00	0.0E+00	0.0E+00	0.0E+00	0.0E+00	0.0E+00	0.0E+00	0.0E+00	0.0E+00	0.0E+00	0.0E+00	0.0E+00	kg
Na3PO4(H2O)8	0.0E+00	0.0E+00	0.0E+00	0.0E+00	0.0E+00	0.0E+00	0.0E+00	0.0E+00	0.0E+00	0.0E+00	0.0E+00	0.0E+00	0.0E+00	0.0E+00	0.0E+00	kg
Na7F(PO4)2(H2O)19	0.0E+00	6.4E+04	1.5E+03	4.9E+04	5.4E+03	0.0E+00	2.3E+04	0.0E+00	2.6E+04	4.2E+04	1.2E+04	2.5E+04	0.0E+00	1.8E+04	1.1E+04	kg
NaAlCO3(OH)2	0.0E+00	0.0E+00	0.0E+00	0.0E+00	0.0E+00	0.0E+00	0.0E+00	0.0E+00	0.0E+00	0.0E+00	0.0E+00	0.0E+00	0.0E+00	0.0E+00	0.0E+00	kg
NaF	0.0E+00	0.0E+00	1.7E+05	1.1E+05	4.6E+02	0.0E+00	0.0E+00	6.8E+04	5.9E+04	5.6E+03	0.0E+00	3.4E+02	3.4E+02	3.4E+02	2.2E+04	kg
NaHCO3	0.0E+00	0.0E+00	0.0E+00	0.0E+00	0.0E+00	0.0E+00	0.0E+00	0.0E+00	0.0E+00	0.0E+00	0.0E+00	0.0E+00	0.0E+00	0.0E+00	0.0E+00	kg
NaNO2	0.0E+00	0.0E+00	0.0E+00	0.0E+00	0.0E+00	0.0E+00	0.0E+00	0.0E+00	0.0E+00	0.0E+00	0.0E+00	0.0E+00	0.0E+00	0.0E+00	0.0E+00	kg
NaNO3	0.0E+00	0.0E+00	0.0E+00	0.0E+00	0.0E+00	0.0E+00	0.0E+00	0.0E+00	0.0E+00	0.0E+00	0.0E+00	0.0E+00	0.0E+00	0.0E+00	0.0E+00	kg
Na3(CO3)(HCO3)(H2O)2	0.0E+00	0.0E+00	0.0E+00	0.0E+00	0.0E+00	0.0E+00	0.0E+00	0.0E+00	0.0E+00	0.0E+00	0.0E+00	0.0E+00	0.0E+00	0.0E+00	0.0E+00	kg
Na5(CO3)(HCO3)3	0.0E+00	0.0E+00	0.0E+00	0.0E+00	0.0E+00	0.0E+00	0.0E+00	0.0E+00	0.0E+00	0.0E+00	0.0E+00	0.0E+00	0.0E+00	0.0E+00	0.0E+00	kg
Na6(CO3)(SO4)2	0.0E+00	0.0E+00	0.0E+00	0.0E+00	0.0E+00	0.0E+00	0.0E+00	0.0E+00	0.0E+00	0.0E+00	0.0E+00	0.0E+00	0.0E+00	0.0E+00	0.0E+00	kg
Ag	8.1E+01	3.3E+01	5.4E+02	1.7E-01	4.4E+01	4.8E+01	2.1E+01	2.2E+02	3.6E+01	3.0E-01	5.8E-02	3.4E-02	9.1E+01	1.7E+01	2.8E+01	kg
Al+3	1.1E+04	1.3E+04	1.4E+03	1.2E+03	2.1E+03	9.5E+03	6.8E+03	3.1E+03	5.3E+02	1.6E+03	2.0E+03	2.2E+03	1.5E+02	6.6E+02	2.2E+03	kg
AlOOH	2.2E+03	4.1E+03	1.3E+02	0.0E+00	0.0E+00	6.8E+02	0.0E+00	7.8E+03	0.0E+00	7.5E+02	0.0E+00	6.4E+02	0.0E+00	0.0E+00	1.3E+02	kg

	3	4	16	17	18	2	12	4	18	21	25	56	58	76	77	Units
	Batch 3	Batch 4	Batch 16	Batch 17	Batch 18	Batch 20	Batch 30	Batch 45	Batch 59	Batch 62	Batch 101	Batch 132	Batch 134	Batch 152	Batch 153	
	SOL20	SOL20	SOL20	SOL20	SOL20	SOL15	SOL15	SOL10	SOL10	SOL10	SOL5	SOL5	SOL5	SOL5	SOL5	
Aroclors (Total PCB) (as C)	1.8E+00	1.5E+00	1.6E+00	1.6E-01	9.7E-01	2.1E+00	1.0E+01	8.4E-01	2.5E-02	3.5E-01	4.4E-01	5.0E+00	3.5E-01	2.3E-01	5.7E-02	kg
As	4.0E+01	1.9E+00	1.0E+01	0.0E+00	2.5E+01	9.8E+01	3.0E+01	7.7E+00	4.4E+00	0.0E+00	2.1E-01	2.3E-01	9.7E+00	2.1E+01	2.6E+00	kg
B	1.0E+02	1.5E+00	6.1E+02	0.0E+00	2.0E+02	2.3E+02	8.8E+01	3.7E+02	9.7E+00	0.0E+00	1.1E+00	1.3E-01	3.3E+01	7.2E+01	1.3E+02	kg
Ba-cold	5.6E+01	5.7E+01	5.5E+01	4.5E+01	1.0E+01	4.9E+01	4.0E+00	1.2E+02	1.0E+02	0.0E+00	1.1E-01	1.2E-01	4.9E+00	3.5E+01	6.9E+00	kg
Be	2.0E+00	1.2E-01	4.4E+01	0.0E+00	7.2E+00	4.9E+00	8.8E-01	1.8E+01	6.6E-01	0.0E+00	1.1E-02	1.2E-02	4.9E-01	1.2E+00	6.5E+00	kg
Bi	7.3E+02	3.6E+03	2.9E+02	1.6E+01	6.5E+01	9.8E+02	5.9E+02	1.5E+02	9.1E+00	8.5E+00	4.7E+02	2.2E+03	1.6E+01	9.6E+00	4.9E+01	kg
Br	5.3E-01	8.3E-01	0.0E+00	0.0E+00	0.0E+00	0.0E+00	0.0E+00	6.6E-01	0.0E+00	0.0E+00	0.0E+00	0.0E+00	0.0E+00	0.0E+00	0.0E+00	kg
CO3-bound	1.0E+02	1.3E+02	3.3E+02	2.4E+01	3.2E+01	8.8E+01	2.7E+02	1.8E+02	4.5E+01	1.1E+01	7.5E+01	4.0E+01	8.0E+01	1.6E+01	1.6E+01	kg
Ca	2.9E+03	4.4E+03	1.2E+03	6.1E+03	1.1E+04	4.8E+03	1.0E+04	9.5E+02	6.2E+02	1.0E+04	2.3E+03	1.8E+03	8.1E+02	3.7E+02	3.2E+02	kg
Cd-cold	9.0E+00	3.6E+00	1.4E+01	0.0E+00	1.9E+01	2.8E+01	6.0E+00	5.2E+00	2.6E+01	0.0E+00	1.3E-01	0.0E+00	2.4E+00	1.1E+01	1.4E+01	kg
Ce	9.7E+01	9.1E+01	4.9E+00	0.0E+00	1.5E+01	9.8E+01	1.9E+01	7.4E+01	8.6E+01	0.0E+00	2.1E-01	2.3E-01	9.7E+00	4.1E+01	8.0E-01	kg
Cl-bound	1.8E-01	1.5E-01	1.6E-01	1.6E-02	9.9E-02	2.1E-01	1.1E+00	8.6E-02	2.5E-03	3.6E-02	4.5E-02	5.1E-01	3.6E-02	2.3E-02	5.9E-03	kg
CN	1.1E-01	1.7E-01	0.0E+00	0.0E+00	0.0E+00	0.0E+00	0.0E+00	1.4E-01	1.1E+00	0.0E+00	0.0E+00	0.0E+00	0.0E+00	2.7E-01	0.0E+00	kg
Co-cold	3.5E+01	3.3E+00	2.4E+00	0.0E+00	3.6E+00	2.0E+01	4.4E+00	3.4E+00	5.5E+00	0.0E+00	3.8E-01	4.7E-02	1.9E+00	5.4E+00	3.0E-01	kg
CrO4																kg
CrOOH	1.3E+03	7.3E+02	1.4E+03	1.6E+03	5.7E+03	1.0E+04	9.1E+02	4.7E+02	6.2E+02	2.6E+03	1.9E+02	3.0E+02	1.2E+03	2.3E+03	5.8E+03	kg
Cs-cold	1.1E+00	7.8E-01	1.0E+00	1.5E+00	9.5E-01	6.1E+00	2.0E+00	3.9E-01	9.7E-01	9.0E-01	4.2E-01	1.0E+00	1.2E+00	2.6E+00	4.9E-01	kg
Cu	4.7E+01	6.8E+01	9.8E+00	0.0E+00	7.4E+00	1.7E+01	8.8E+00	5.6E+01	3.7E+01	0.0E+00	1.1E-01	2.3E-02	1.9E+00	1.3E+01	8.4E-01	kg
Eu-cold	1.6E+00	2.5E+00	0.0E+00	0.0E+00	0.0E+00	0.0E+00	0.0E+00	2.0E+00	4.9E+00	0.0E+00	0.0E+00	0.0E+00	0.0E+00	1.2E+00	0.0E+00	kg
Fe	2.4E+04	4.3E+04	2.0E+04	6.4E+03	5.9E+03	1.8E+04	1.9E+04	2.1E+04	1.1E+04	3.9E+03	5.1E+03	6.4E+03	2.0E+04	2.7E+03	2.2E+02	kg
H-bound	1.6E+02	9.9E+01	2.0E+02	7.5E+02	2.9E+02	7.8E+02	4.2E+02	6.4E+01	4.1E+02	3.2E+02	4.7E+01	1.2E+02	1.1E+02	2.8E+02	2.6E+02	kg
H2O-bound	4.6E+02	8.6E+00	2.6E+03	0.0E+00	8.5E+02	1.1E+03	4.0E+02	1.6E+03	1.0E+02	0.0E+00	6.2E+00	6.9E-01	1.5E+02	3.5E+02	5.6E+02	kg
Hg	3.9E+01	5.1E+01	1.4E+01	7.5E-01	9.8E-01	1.1E+02	2.2E+01	4.1E+01	7.6E+00	6.9E+00	7.0E+00	2.5E+00	1.6E+01	2.2E+00	1.7E-01	kg
K	7.1E+02	2.6E+02	5.4E+02	1.8E+03	2.3E+03	3.3E+03	2.9E+03	1.9E+02	4.4E+02	2.1E+02	7.8E+01	7.5E+01	5.0E+02	2.2E+03	3.4E+02	kg
La	1.6E+02	1.7E+02	5.7E+02	1.7E+02	2.3E+02	9.2E+01	4.3E+01	2.5E+02	6.0E+02	1.2E+01	1.0E+01	5.7E+00	1.5E+02	1.5E+02	4.3E+01	kg
Li	1.4E+01	3.2E-01	1.1E+01	0.0E+00	7.8E+00	4.2E+01	9.5E+00	2.3E+00	5.3E+00	0.0E+00	4.7E-01	2.3E-02	3.9E+00	9.5E+00	8.5E-01	kg
Mg	8.3E+01	7.0E+01	6.8E+02	0.0E+00	1.5E+02	9.8E+01	5.7E+01	4.9E+02	6.7E+01	0.0E+00	2.1E-01	2.3E-01	9.7E+00	3.7E+01	1.1E+02	kg
Mn	2.6E+03	2.0E+03	3.1E+03	1.6E+02	3.5E+02	9.3E+02	5.0E+02	2.0E+03	8.4E+02	9.4E+02	7.2E+01	7.1E+02	3.2E+03	2.2E+02	4.2E+01	kg
Mo	2.7E+01	2.9E+00	5.4E+00	0.0E+00	2.2E+01	1.3E+02	2.8E+01	5.0E+00	4.9E+00	0.0E+00	1.1E+00	2.0E-01	1.2E+01	2.7E+01	1.3E+00	kg
Na-bound	3.6E+03	2.3E+03	6.3E+03	1.7E+04	7.0E+03	1.9E+04	1.2E+04	1.7E+03	9.6E+03	7.7E+03	1.7E+03	2.8E+03	2.7E+03	6.6E+03	6.3E+03	kg
Nb-cold	4.5E-01	7.0E-01	0.0E+00	0.0E+00	0.0E+00	0.0E+00	0.0E+00	5.6E-01	0.0E+00	0.0E+00	0.0E+00	0.0E+00	0.0E+00	0.0E+00	0.0E+00	kg
Nd	1.6E+02	1.8E+02	1.4E+02	0.0E+00	2.2E+01	9.8E+01	9.3E+00	1.9E+02	1.6E+02	0.0E+00	2.1E-01	2.3E-01	9.7E+00	5.9E+01	1.4E+01	kg
NH3	1.2E+02	2.0E+02	1.1E-01	0.0E+00	0.0E+00	0.0E+00	0.0E+00	1.6E+02	2.5E+00	0.0E+00	0.0E+00	0.0E+00	0.0E+00	5.8E-01	0.0E+00	kg
Ni-cold	2.5E+03	4.1E+03	5.5E+02	3.1E+02	4.1E+02	2.7E+03	5.4E+03	8.7E+02	5.3E+02	4.0E+02	1.1E+03	1.1E+03	5.0E+02	1.7E+02	2.1E+01	kg
NO3-bound	1.1E+03	4.1E+02	8.6E+02	2.9E+03	3.6E+03	5.2E+03	4.5E+03	3.0E+02	7.1E+02	3.3E+02	1.2E+02	1.2E+02	8.0E+02	3.5E+03	5.4E+02	kg
O-bound	2.3E+04	1.9E+04	6.0E+04	2.6E+04	1.2E+04	4.0E+04	2.5E+04	2.4E+04	1.4E+04	1.7E+04	4.7E+03	8.9E+03	9.3E+03	1.0E+04	9.8E+03	kg
OH-bound	2.6E+04	4.7E+04	2.2E+04	1.1E+04	1.6E+04	2.3E+04	2.9E+04	2.2E+04	1.1E+04	1.3E+04	7.5E+03	8.5E+03	1.9E+04	3.1E+03	7.1E+02	kg
Pb	1.5E+03	4.0E+03	7.5E+02	1.5E+02	2.7E+02	1.2E+03	2.2E+03	1.1E+03	2.9E+02	1.8E+02	5.8E+02	4.4E+02	8.2E+02	1.0E+02	3.7E+01	kg
Pd	6.0E+00	9.3E+00	0.0E+00	0.0E+00	0.0E+00	0.0E+00	0.0E+00	7.4E+00	0.0E+00	0.0E+00	0.0E+00	0.0E+00	0.0E+00	0.0E+00	0.0E+00	kg
Pr	3.0E+01	4.7E+01	0.0E+00	0.0E+00	0.0E+00	0.0E+00	0.0E+00	3.8E+01	5.6E+01	0.0E+00	0.0E+00	0.0E+00	0.0E+00	1.4E+01	0.0E+00	kg
Rb	0.0E+00	0.0E+00	0.0E+00	0.0E+00	0.0E+00	0.0E+00	0.0E+00	0.0E+00	2.0E-01	0.0E+00	0.0E+00	0.0E+00	0.0E+00	5.1E-02	0.0E+00	kg
Rh	2.0E+00	3.1E+00	0.0E+00	0.0E+00	0.0E+00	0.0E+00	0.0E+00	2.5E+00	2.8E+00	0.0E+00	0.0E+00	0.0E+00	0.0E+00	6.9E-01	0.0E+00	kg
Ru-cold	5.4E+01	8.5E+01	0.0E+00	0.0E+00	0.0E+00	0.0E+00	0.0E+00	6.8E+01	4.2E+01	0.0E+00	0.0E+00	0.0E+00	0.0E+00	1.0E+01	0.0E+00	kg
Sb-cold	2.4E+01	2.1E+00	4.9E+00	0.0E+00	1.4E+01	5.9E+01	1.8E+01	2.3E+00	7.1E-01	0.0E+00	1.3E-01	1.4E-01	5.8E+00	1.2E+01	4.4E-01	kg
Se-cold	4.1E+01	3.5E+00	1.2E+01	0.0E+00	1.9E+01	9.8E+01	2.3E+01	4.8E+00	5.6E-01	0.0E+00	2.1E-01	2.3E-01	9.7E+00	2.0E+01	1.0E+00	kg
Si	1.3E+04	1.0E+04	4.4E+03	8.0E+02	5.2E+02	1.1E+04	4.2E+03	1.6E+03	2.0E+02	1.3E+03	1.3E+03	3.6E+03	3.1E+03	7.4E+02	5.5E+02	kg
Sm-cold	2.7E+01	4.2E+01	0.0E+00	0.0E+00	0.0E+00	0.0E+00	0.0E+00	3.3E+01	4.4E+01	0.0E+00	0.0E+00	0.0E+00	0.0E+00	1.1E+01	0.0E+00	kg
Sn-cold	1.5E+00	2.3E+00	0.0E+00	0.0E+00	0.0E+00	0.0E+00	0.0E+00	1.8E+00	0.0E+00	0.0E+00	0.0E+00	0.0E+00	0.0E+00	0.0E+00	0.0E+00	kg
Sr-cold	7.0E+01	1.5E+02	4.3E+01	2.9E+01	9.5E+00	8.3E+01	3.6E+02	8.6E+01	3.5E+01	1.7E+01	1.0E+02	5.8E+01	4.1E+01	1.1E+01	1.7E+00	kg
Ta	1.4E+00	2.2E+00	7.1E-04	0.0E+00	0.0E+00	0.0E+00	0.0E+00	1.7E+00	7.1E-04	0.0E+00	0.0E+00	0.0E+00	0.0E+00	0.0E+00	0.0E+00	kg
Te	1.1E+01	1.7E+01	0.0E+00	0.0E+00	0.0E+00	0.0E+00	0.0E+00	1.4E+01	2.5E+01	0.0E+00	0.0E+00	0.0E+00	0.0E+00	6.2E+00	0.0E+00	kg
Th-cold	1.9E+00	1.3E+00	8.5E-01	1.8E-01	1.4E+00	6.6E-03	9.0E-02	4.5E-02	7.6E+00	3.2E+00	4.0E-03	7.8E-04	8.8E-01	1.9E+00	2.5E-02	kg
Ti	1.3E+01	1.5E+01	4.8E+00	0.0E+00	3.3E+00	9.8E+00	3.1E+00	1.4E+01	1.2E+01	0.0E+00	2.1E-02	2.3E-02	9.7E-01	5.0E+00	9.3E-01	kg
Tl	1.1E+00	1.7E+00	2.2E+00	0.0E+00	3.5E+01	2.0E+02	4.6E+01	2.0E+00	2.2E-01	0.0E+00	0.0E+00	0.0E+00	5.9E-01	6.4E-01	7.8E-01	kg
TOC-Other	1.6E+03	7.6E+02	2.4E+03	8.9E+03	3.4E+03	9.3E+03	5.0E+03	4.3E+02	4.9E+03	3.8E+03	5.6E+02	1.4E+03	1.4E+03	3.4E+03	3.1E+03	kg
V	1.9E+01	1.2E-01	1.8E+01	0.0E+00	7.1E+00	4.9E+01	4.4E+00	1.0E+01	3.3E+00	0.0E+00	1.1E-01	1.2E-01	4.9E+00	1.1E+01	3.7E+00	kg
W	1.2E+00	1.9E+00	0.0E+00	0.0E+00	0.0E+00	0.0E+00	0.0E+00	1.5E+00	2.2E+02	0.0E+00	0.0E+00	0.0E+00	0.0E+00	5.5E+01	0.0E+00	kg
Y-cold	1.4E+01	2.2E+01	1.6E+01	0.0E+00	3.2E+00	0.0E+00	0.0E+00	2.6E+01	2.4E+01	0.0E+00	0.0E+00	2.3E-02	2.3E-02	6.0E+00	3.1E+00	kg
Zn	5.6E+01	5.2E+01	1.6E+01	0.0E+00	2.1E+01	1.1E+02	2.6E+01	4.5E+01	1.0E+01	0.0E+00	1.3E-01	2.3E-02	5.2E+00	1.3E+01	1.9E+00	kg
Zr-cold	1.7E+03	1.5E+03	1.2E+05	1.9E+03	1.0E+03	4.1E+02	4.9E+02	5.1E+04	4.2E+02	8.3E+03	6.0E+01	6.3E+02	2.0E+01	8.4E+01	1.1E+02	kg
H-3	0.0E+00	0.0E+00	0.0E+00	0.0E+00	0.0E+00	0.0E+00	0.0E+00	0.0E+00	0.0E+00	0.0E+00	0.0E+00	0.0E+00	0.0E+00	0.0E+00	0.0E+00	kg
C-14	4.1E-06	7.6E-06	6.9E-06	1.6E-05	6.4E-06	3.7E-06	1.8E-05	2.3E-05	3.0E-05	9.0E-05	4.2E-06	1.3E-05	3.0E-07	1.1E-05	1.5E-06	kg

	3	4	16	17	18	2	12	4	18	21	25	56	58	76	77	Units
	Batch 3	Batch 4	Batch 16	Batch 17	Batch 18	Batch 20	Batch 30	Batch 45	Batch 59	Batch 62	Batch 101	Batch 132	Batch 134	Batch 152	Batch 153	
	SOL20	SOL20	SOL20	SOL20	SOL20	SOL15	SOL15	SOL10	SOL10	SOL10	SOL5	SOL5	SOL5	SOL5	SOL5	
Co-60	1.9E-06	3.1E-06	1.9E-06	5.1E-06	2.7E-06	1.4E-06	2.6E-07	2.6E-06	3.2E-06	7.5E-07	2.9E-08	6.1E-07	3.8E-07	9.3E-07	1.2E-07	kg
Ni-59	1.4E-01	9.1E-02	8.4E-02	1.5E-01	5.8E-02	1.7E-01	1.4E-01	6.2E-02	1.2E-01	5.8E-02	2.4E-02	4.0E-02	7.5E-02	6.9E-02	2.9E-02	kg
Ni-63	2.0E-02	1.9E-02	9.1E-03	1.6E-02	6.4E-03	1.9E-02	1.5E-02	1.4E-02	1.1E-02	6.3E-03	2.5E-03	3.7E-03	8.0E-03	7.0E-03	3.2E-03	kg
Se-79	4.5E-03	3.3E-04	1.9E-03	5.8E-03	3.6E-03	1.8E-02	3.5E-03	5.4E-05	1.5E-03	1.3E-03	1.4E-04	8.6E-04	1.1E-03	2.8E-03	1.7E-03	kg
Sr-90	5.2E+00	6.6E+00	5.4E+00	6.6E+00	2.3E+00	6.7E+00	1.8E+00	6.9E+00	2.7E+00	3.3E-01	3.9E-01	1.0E+00	4.2E+00	7.3E-01	5.1E-02	kg
Y-90	1.3E-03	1.7E-03	1.4E-03	1.7E-03	5.9E-04	1.7E-03	4.6E-04	1.7E-03	6.8E-04	8.4E-05	9.8E-05	2.6E-04	1.1E-03	1.8E-04	1.3E-05	kg
Zr-93	3.9E+00	9.1E-01	1.7E+00	7.5E+00	4.5E+00	1.3E+01	3.5E+00	8.9E-01	2.5E+01	1.3E+00	7.9E-02	7.8E-01	1.4E+00	9.8E+00	3.0E+00	kg
Nb-93m	4.0E-05	9.6E-06	1.6E-05	7.3E-05	4.4E-05	1.2E-04	3.6E-05	5.1E-06	2.4E-04	3.5E-05	7.7E-07	8.1E-06	1.4E-05	9.4E-05	2.9E-05	kg
Tc-99	4.0E+00	3.4E-01	4.4E-01	2.1E+00	1.7E+00	4.8E+00	3.0E+00	2.5E-01	7.4E-01	1.9E+00	3.0E-01	1.3E-01	1.2E-01	7.8E-01	4.0E-01	kg
Ru-106	2.5E-17	9.9E-19	8.6E-15	3.3E-14	1.6E-15	7.7E-17	2.5E-17	1.7E-16	6.4E-17	7.0E-18	1.5E-19	1.1E-18	7.4E-18	2.5E-17	7.2E-18	kg
Cd-113m	1.2E-05	2.4E-06	4.9E-05	2.0E-04	4.7E-05	3.1E-05	1.1E-05	1.8E-06	1.3E-05	2.0E-05	7.8E-07	1.4E-06	3.9E-06	1.6E-05	1.4E-05	kg
Sn-126	5.0E-01	4.7E-01	2.2E-01	1.3E-01	8.1E-02	2.0E-01	6.7E-02	3.8E-01	5.6E-01	6.9E-02	1.7E-03	2.0E-02	2.5E-01	2.0E-01	5.1E-02	kg
Sb-125	7.8E-09	3.3E-08	2.3E-07	6.5E-07	3.0E-07	2.8E-08	2.9E-09	4.2E-08	7.7E-08	1.0E-08	1.4E-10	2.0E-10	5.3E-09	1.9E-08	1.5E-08	kg
I-129	2.6E-01	3.8E-01	1.6E-01	3.6E-01	5.9E-02	4.3E-01	4.1E-01	2.4E-02	3.7E-02	3.2E-01	1.7E-01	1.3E-02	7.1E-02	1.6E-01	3.9E-02	kg
Cs-134	3.0E-12	2.1E-12	1.3E-10	3.9E-10	5.6E-10	5.1E-11	4.3E-12	1.2E-11	3.5E-11	1.1E-11	7.6E-13	1.6E-12	9.8E-12	3.0E-11	1.4E-12	kg
Cs-137	2.3E-01	1.7E-01	2.2E-01	3.2E-01	2.1E-01	1.3E+00	4.4E-01	8.5E-02	2.1E-01	1.9E-01	9.1E-02	2.3E-01	2.7E-01	5.6E-01	1.1E-01	kg
Ba-137m	3.5E-08	2.6E-08	3.3E-08	4.9E-08	3.1E-08	2.0E-07	6.6E-08	1.3E-08	3.2E-08	3.0E-08	1.4E-08	3.4E-08	4.1E-08	8.5E-08	1.6E-08	kg
Sm-151	1.1E+00	2.6E+00	8.7E-01	1.7E+00	1.2E+00	4.6E+00	2.1E-01	1.6E+00	2.6E+00	3.8E-01	6.7E-03	2.1E-01	5.9E-01	7.7E-01	1.0E-01	kg
Eu-152	3.7E-05	4.5E-05	3.1E-05	4.8E-05	1.9E-05	5.4E-05	1.4E-06	6.3E-05	3.3E-05	5.3E-06	5.4E-08	2.0E-06	2.1E-05	8.9E-06	4.7E-07	kg
Eu-154	8.7E-04	9.4E-04	8.8E-04	1.3E-03	5.2E-04	1.1E-03	6.5E-05	8.4E-04	6.3E-04	1.0E-04	1.0E-05	1.1E-04	6.1E-04	1.7E-04	9.2E-06	kg
Eu-155	3.4E-05	3.9E-05	5.1E-05	1.3E-04	6.6E-05	4.2E-05	2.9E-06	5.3E-05	1.9E-05	4.2E-06	4.9E-07	4.6E-06	2.2E-05	4.9E-06	3.1E-07	kg
Ra-226	1.8E-08	6.2E-09	1.3E-08	5.9E-08	2.0E-08	4.7E-08	3.6E-08	1.4E-09	1.5E-08	3.7E-08	3.0E-09	5.7E-08	5.1E-09	1.9E-08	1.3E-08	kg
Ra-228	1.5E-06	1.4E-06	3.9E-08	1.1E-08	1.4E-08	9.8E-09	1.0E-07	1.1E-08	7.0E-08	1.9E-06	8.4E-09	3.0E-09	3.9E-08	1.3E-08	3.4E-10	kg
Ac-227	3.1E-06	2.6E-06	3.8E-08	3.2E-07	1.9E-07	5.5E-07	1.8E-07	2.4E-09	1.8E-07	1.9E-06	3.1E-09	1.2E-08	5.1E-08	2.1E-07	1.5E-07	kg
Th-229	8.6E-04	7.9E-04	8.4E-09	3.6E-07	6.4E-07	1.2E-07	6.7E-06	4.8E-10	2.9E-06	3.4E-04	6.9E-06	1.1E-08	1.1E-08	4.2E-08	3.4E-08	kg
Th-232	3.7E+03	3.4E+03	1.1E+02	2.7E+01	3.4E+01	2.4E+01	2.5E+02	3.4E+01	1.8E+02	4.6E+03	2.1E+01	7.3E+00	1.2E+02	3.5E+01	9.8E-01	kg
Pa-231	1.1E-03	6.8E-04	7.6E-05	6.2E-04	3.9E-04	9.9E-04	3.2E-04	5.4E-06	3.3E-04	5.8E-04	2.8E-06	2.3E-05	9.0E-05	4.1E-04	3.1E-04	kg
U-232	2.0E-05	1.9E-05	1.2E-07	7.3E-07	1.8E-06	1.4E-07	1.8E-06	1.6E-08	3.3E-07	1.6E-05	8.4E-07	1.1E-08	2.2E-08	1.7E-07	1.7E-06	kg
U-233	3.9E+00	3.7E+00	5.9E-02	1.0E-01	3.3E-01	2.6E-02	3.6E-01	6.3E-04	1.3E-01	4.6E+00	1.6E-01	2.1E-03	5.2E-02	4.5E-02	3.2E-01	kg
U-234	2.5E-01	5.2E-01	9.1E-01	1.2E-01	2.0E-01	2.5E-01	1.5E+00	3.7E-01	5.4E-02	3.7E-01	3.6E-01	9.0E-02	2.6E-02	1.9E-02	1.0E-01	kg
U-235	2.5E+01	5.8E+01	1.0E+02	1.4E+01	2.3E+01	3.1E+01	1.8E+02	4.2E+01	6.1E+00	2.8E+01	4.4E+01	1.1E+01	3.0E+00	2.2E+00	1.2E+01	kg
U-236	4.7E-01	9.9E-01	8.3E+00	9.8E-01	1.1E+00	4.4E-01	2.5E+00	2.8E+00	3.6E-01	1.2E+00	7.0E-01	1.3E-01	1.1E-01	1.0E-01	3.5E-01	kg
U-238	3.7E+03	8.7E+03	1.2E+04	1.8E+03	3.0E+03	4.6E+03	2.7E+04	5.3E+03	7.8E+02	4.0E+03	6.7E+03	1.7E+03	4.4E+02	2.9E+02	1.7E+03	kg
Np-237	2.2E+00	1.9E+00	2.7E+00	6.4E+00	4.3E+00	1.3E+00	9.2E-01	1.5E+00	1.1E+00	1.2E+00	1.6E-01	1.4E-01	1.3E+00	5.3E-01	3.2E-01	kg
Pu-238	2.4E-03	2.8E-03	3.0E-03	2.5E-03	1.5E-03	1.8E-03	7.2E-04	2.0E-03	2.3E-03	2.8E-03	1.4E-04	2.5E-04	6.1E-04	5.4E-04	7.2E-05	kg
Pu-239	2.6E+01	3.2E+01	1.3E+01	7.0E+00	3.7E+00	1.5E+01	7.9E+00	1.2E+01	3.9E+00	6.9E+00	2.3E+00	2.7E+00	6.0E+00	8.6E-01	3.7E-01	kg
Pu-240	1.7E+00	1.9E+00	9.4E-01	5.3E-01	2.7E-01	9.1E-01	3.8E-01	8.4E-01	3.2E-01	4.8E-01	1.1E-01	1.6E-01	3.7E-01	7.1E-02	2.6E-02	kg
Pu-241	6.3E-03	6.9E-03	1.0E-02	7.1E-03	3.0E-03	3.6E-03	1.1E-03	4.8E-03	5.4E-03	3.5E-03	2.1E-04	5.2E-04	1.4E-03	1.2E-03	2.3E-04	kg
Pu-242	5.8E-03	6.5E-03	5.6E-03	3.8E-03	1.6E-03	3.4E-03	8.8E-04	3.9E-03	6.2E-03	2.5E-03	1.8E-04	5.0E-04	1.3E-03	1.5E-03	1.5E-04	kg
Am-241	4.3E-01	7.8E-01	9.2E-01	2.2E+00	1.2E+00	2.8E-01	1.3E-01	4.9E-01	7.3E-01	1.9E-01	2.7E-02	8.5E-02	3.3E-01	1.8E-01	8.0E-03	kg
Am-243	2.9E-03	4.4E-03	6.3E-03	1.5E-02	7.2E-03	8.7E-03	4.3E-04	4.4E-03	2.5E-02	9.6E-04	4.7E-05	6.3E-04	2.9E-03	6.2E-03	8.4E-05	kg
Cm-242	5.2E-07	7.1E-07	4.7E-07	8.2E-07	1.0E-06	3.6E-07	2.6E-08	6.6E-07	3.3E-06	5.9E-08	4.9E-09	7.9E-08	3.0E-07	8.1E-07	3.8E-09	kg
Cm-243	2.8E-06	7.6E-07	4.7E-06	2.8E-06	4.3E-06	9.4E-07	1.8E-07	7.6E-07	1.4E-05	1.9E-07	3.2E-08	1.4E-07	4.5E-06	3.4E-06	5.9E-09	kg
Cm-244	2.7E-05	7.3E-06	4.6E-05	2.8E-05	4.2E-05	9.0E-06	1.7E-06	7.1E-06	1.3E-04	1.9E-06	3.3E-07	1.2E-06	4.3E-05	3.3E-05	5.7E-08	kg
Slurry Mass	2,556,632	2,555,846	2,556,948	2,561,760	895,556	2,498,706	2,499,146	2,421,046	2,420,606	2,422,485	2,344,219	2,349,044	2,341,000	2,348,100	2,340,784	kg
Slurry Density	1,351	1,350	1,351	1,353	1,351	1,320	1,320	1,279	1,279	1,280	1,239	1,241	1,237	1,241	1,237	kg/kL
Slurry Volume	1,893	1,893	1,893	1,893	663	1,893	1,893	1,893	1,893	1,893	1,893	1,893	1,893	1,893	1,893	kL
Liquid Mass	2,083,385	2,082,708	2,083,681	2,087,782	729,795	2,123,900	2,124,229	2,178,685	2,177,876	2,180,229	2,226,778	2,231,589	2,223,754	2,230,005	2,223,585	kg
Liquid Density	1,201	1,200	1,201	1,204	1,201	1,201	1,202	1,202	1,202	1,203	1,201	1,204	1,200	1,203	1,200	kg/kL
Liquid Volume	1,735	1,735	1,735	1,735	608	1,768	1,768	1,812	1,812	1,812	1,854	1,854	1,854	1,853	1,854	kL
Solids Mass	473,247	473,138	473,267	473,978	165,761	374,806	374,917	242,361	242,730	242,256	117,440	117,455	117,245	118,095	117,199	kg
Solids Volume	158	158	158	158	55	125	125	81	81	81	39	39	39	39	39	kL
Solids Concentration	19%	19%	19%	19%	19%	15%	15%	10%	10%	10%	5%	5%	5%	5%	5%	wt%
Waste Oxide Mass	515,629	512,803	655,654	603,875	184,789	498,378	469,214	462,539	447,967	412,413	333,678	346,669	349,891	345,452	363,376	kg
Feed Batches	154.3	154.3	154.3	154.3	54.0	147.3	147.3	139.1	139.1	139.1	132.2	132.3	132.2	132.2	132.2	Feed Batches
Bulk Density	1.35	1.35	1.35	1.35	1.35	1.32	1.32	1.28	1.28	1.28	1.24	1.24	1.24	1.24	1.24	mg/L slurry
Liquid Density	1.20	1.20	1.20	1.20	1.20	1.20	1.20	1.20	1.20	1.20	1.20	1.20	1.20	1.20	1.20	mg/L liquid
Na+ Molar Concentration	2.7	2.5	4.0	4.0	3.1	3.8	2.7	4.1	4.2	3.8	3.8	4.1	4.2	4.3	4.3	mol/L liquid

	3	4	16	17	18	2	12	4	18	21	25	56	58	76	77	Units
	Batch 3	Batch 4	Batch 16	Batch 17	Batch 18	Batch 20	Batch 30	Batch 45	Batch 59	Batch 62	Batch 101	Batch 132	Batch 134	Batch 152	Batch 153	
	SOL20	SOL20	SOL20	SOL20	SOL20	SOL15	SOL15	SOL10	SOL10	SOL10	SOL5	SOL5	SOL5	SOL5	SOL5	
NO3- Molar Concentration	0.70	0.75	1.14	1.08	1.04	1.12	1.02	1.29	1.11	1.07	1.27	1.30	1.20	1.27	1.32	mol/L liquid
NO2- + NO3- Molar Concentration	1.22	1.34	1.96	1.93	1.86	1.96	1.61	2.20	1.94	1.90	2.11	2.20	2.10	2.20	2.27	mol/L liquid
NH3/NH4+ Molar Concentration	0.0E+00	0.0E+00	1.5E-07	0.0E+00	0.0E+00	0.0E+00	0.0E+00	0.0E+00	3.5E-05	0.0E+00	0.0E+00	0.0E+00	0.0E+00	8.4E-06	0.0E+00	mol/L liquid
Cl-/OH- Molar Ratio	0.01	0.02	0.05	0.05	0.03	0.05	0.02	0.06	0.06	0.04	0.05	0.05	0.05	0.06	0.07	mol/mol
Cl-/Na+ Molar Ratio	1.18E-02	1.20E-02	1.29E-02	1.21E-02	1.41E-02	1.44E-02	9.51E-03	1.46E-02	1.18E-02	1.32E-02	1.35E-02	1.39E-02	1.35E-02	1.43E-02	1.37E-02	mol/mol
F-/Na+ Molar Ratio	2.40E-02	2.97E-02	4.57E-02	4.52E-02	1.47E-02	1.26E-02	1.57E-02	3.72E-02	4.24E-02	2.28E-02	8.56E-03	1.10E-02	7.12E-03	1.08E-02	3.34E-02	mol/mol
SO4-2/Na+ Molar Ratio	7.26E-03	1.33E-02	7.63E-03	3.17E-02	9.80E-03	9.41E-03	2.24E-02	7.87E-03	2.92E-02	7.43E-03	1.14E-02	9.49E-03	7.62E-03	1.18E-02	2.39E-02	mol/mol
Hg+2/Na+ Molar Ratio	1.40E-05	1.31E-05	1.40E-05	2.47E-08	2.87E-08	2.86E-06	6.67E-07	9.64E-07	1.01E-06	2.16E-07	1.83E-07	3.14E-06	1.40E-05	2.49E-07	4.22E-08	mol/mol
TOC Mass Fraction	0.10%	0.04%	0.15%	0.47%	0.52%	0.44%	0.28%	0.03%	0.29%	0.23%	0.04%	0.09%	0.09%	0.19%	0.19%	kg TOC/kg waste
PCB Mass Fraction	3.8	3.2	3.4	0.3	5.8	5.5	27.5	3.5	0.1	1.4	3.7	42.2	3.0	1.9	0.5	mg PCB/kg waste
pH	14.3	14.3	14.0	14.0	14.1	14.1	14.1	14.0	13.9	14.1	14.0	14.0	14.0	14.0	13.9	-
Equivalent Cs-137 Concentration	0.03	0.02	0.04	0.06	0.07	0.07	0.06	0.01	0.02	0.02	0.01	0.01	0.03	0.04	0.01	Ci/L slurry
Am-241 Concentration	7.9E-04	1.4E-03	1.7E-03	4.1E-03	6.4E-03	5.0E-04	2.4E-04	8.9E-04	1.4E-03	3.5E-04	5.0E-05	1.5E-04	6.2E-04	3.4E-04	1.5E-05	Ci/L slurry
Pu-238 Concentration	2.2E-05	2.6E-05	2.8E-05	2.3E-05	3.9E-05	1.6E-05	6.5E-06	1.8E-05	2.1E-05	2.5E-05	1.2E-06	2.3E-06	5.8E-06	4.9E-06	6.5E-07	Ci/L slurry
Pu-239 Concentration	8.6E-04	1.1E-03	4.5E-04	2.4E-04	3.5E-04	4.9E-04	2.6E-04	4.1E-04	1.3E-04	2.3E-04	7.4E-05	9.0E-05	2.0E-04	2.8E-05	1.2E-05	Ci/L slurry
Pu-240 Concentration	2.0E-04	2.3E-04	1.2E-04	6.6E-05	9.1E-05	1.1E-04	4.6E-05	1.0E-04	3.8E-05	5.8E-05	1.3E-05	1.9E-05	4.6E-05	8.6E-06	3.1E-06	Ci/L slurry
Sr-90 Concentration	4.1E-01	5.2E-01	4.3E-01	5.3E-01	5.2E-01	5.2E-01	1.4E-01	5.2E-01	2.0E-01	2.6E-02	2.9E-02	7.7E-02	3.1E-01	5.5E-02	4.3E-03	Ci/L slurry
Pu to Metals Loading Ratio	0.69	0.61	0.35	1.04	0.37	0.58	0.36	0.39	0.22	0.78	0.43	0.27	0.16	0.16	0.15	g Pu Eq/kg Met Eq
U-Fissile to U-Total Ratio	8.07	7.19	8.54	8.10	7.78	6.65	6.71	7.95	7.92	8.66	6.56	6.42	6.99	7.67	7.40	g U-Fis/kg U-Tot
Public ULD	3,789	5,328	4,358	7,712	11,535	2,632	1,146	3,057	2,816	1,164	284	554	1,867	692	62	Sv/L slurry
CLW ULD	2,547	3,563	2,917	5,102	7,561	1,839	783	2,107	1,869	762	193	379	1,290	465	43	Sv/L slurry
UHGRtotal	1.1E-07	1.3E-07	1.1E-07	1.0E-07	1.2E-07	1.1E-07	6.3E-08	9.6E-08	4.6E-08	2.5E-08	1.6E-08	1.5E-08	7.4E-08	1.7E-08	2.6E-09	mol H2/h·L slurry
Concentration of Nitrate in Liquid	0.70	0.75	1.14	1.08	1.04	1.12	1.02	1.29	1.11	1.07	1.27	1.30	1.20	1.27	1.32	mol/L liquid
Concentration of Nitrite in Liquid	0.52	0.59	0.82	0.84	0.82	0.84	0.59	0.91	0.82	0.83	0.83	0.89	0.89	0.93	0.95	mol/L liquid
Concentration of TOC in Liquid	0.02	0.01	0.05	0.01	0.01	0.01	0.05	0.01	0.00	0.03	0.01	0.00	0.02	0.00	0.00	wt%
Concentration of Al in Liquid	0.44	0.41	0.25	0.25	0.30	0.28	0.27	0.26	0.22	0.31	0.27	0.26	0.27	0.27	0.22	wt%
Liquid Mass Fraction	0.81	0.81	0.81	0.81	0.81	0.85	0.85	0.90	0.90	0.90	0.95	0.95	0.95	0.95	0.95	kg Liq/kg Tot
Hα	4.9E-05	7.0E-05	6.1E-05	1.1E-04	1.7E-04	3.0E-05	1.5E-05	3.9E-05	4.5E-05	2.3E-05	3.8E-06	7.4E-06	2.4E-05	1.1E-05	9.8E-07	W/kg
Hβ/γ	2.0E-03	2.4E-03	2.1E-03	2.6E-03	2.6E-03	2.8E-03	8.9E-04	2.7E-03	1.1E-03	1.9E-04	2.1E-04	4.6E-04	1.8E-03	4.3E-04	7.4E-05	W/kg
GO(H2)α	3.5E-01	3.3E-01	2.5E-01	2.5E-01	2.6E-01	2.5E-01	2.7E-01	2.2E-01	2.5E-01	2.6E-01	2.3E-01	2.2E-01	2.4E-01	2.3E-01	2.2E-01	mol H2/100 eV
GO(H2)β/γ	1.1E-01	1.1E-01	8.1E-02	8.3E-02	8.6E-02	8.2E-02	9.0E-02	7.3E-02	8.2E-02	8.4E-02	7.5E-02	7.3E-02	7.7E-02	7.4E-02	7.2E-02	mol H2/100 eV
GTOC(H2)α	1.6E-03	1.3E-03	5.1E-03	6.2E-04	5.5E-04	1.1E-03	4.6E-03	9.6E-04	3.5E-04	2.6E-03	1.4E-03	1.8E-05	1.7E-03	2.5E-04	3.7E-05	mol H2/100 eV
GTOC(H2)β/γ	3.3E-03	2.5E-03	1.0E-02	1.2E-03	1.1E-03	2.1E-03	9.1E-03	1.9E-03	7.0E-04	5.2E-03	2.9E-03	3.5E-05	3.3E-03	5.0E-04	7.4E-05	mol H2/100 eV
G(H2)α	3.5E-01	3.3E-01	2.5E-01	2.6E-01	2.6E-01	2.5E-01	2.8E-01	2.3E-01	2.5E-01	2.6E-01	2.3E-01	2.2E-01	2.4E-01	2.3E-01	2.2E-01	mol H2/100 eV
G(H2)β/γ	1.2E-01	1.1E-01	9.1E-02	8.4E-02	8.7E-02	8.4E-02	9.9E-02	7.5E-02	8.3E-02	8.9E-02	7.8E-02	7.3E-02	8.0E-02	7.5E-02	7.2E-02	mol H2/100 eV
HGRrad	1.8E-06	2.1E-06	1.5E-06	1.8E-06	2.0E-06	1.8E-06	7.0E-07	1.7E-06	8.3E-07	1.9E-07	1.5E-07	3.0E-07	1.3E-06	3.0E-07	4.7E-08	mol H2/d/kg
HGRtherm	1.9E-07	1.4E-07	4.6E-07	5.6E-08	5.4E-08	1.1E-07	4.4E-07	9.7E-08	3.3E-08	2.8E-07	1.6E-07	1.9E-09	1.8E-07	2.7E-08	3.7E-09	mol H2/d/kg
Preferences																
F in Waste Oxide	0.4%	0.8%	12.3%	11.4%	0.5%	0.3%	0.4%	7.8%	8.4%	1.6%	0.4%	0.7%	0.3%	0.7%	4.3%	wt%
Na2O in Waste Oxide	29.2%	30.9%	53.1%	66.7%	40.8%	48.1%	37.4%	61.5%	73.4%	59.4%	66.6%	71.4%	69.9%	76.3%	77.6%	wt%
SO3 in Waste Oxide	0.5%	0.9%	0.6%	10.5%	0.8%	1.0%	1.8%	1.0%	8.0%	1.0%	1.9%	1.7%	1.3%	2.2%	4.7%	wt%
ThO2 in Waste Oxide	0.8%	0.8%	0.0%	0.0%	0.0%	0.0%	0.1%	0.0%	0.0%	1.3%	0.0%	0.0%	0.0%	0.0%	0.0%	wt%
ZrO2 in Waste Oxide	0.4%	0.4%	25.3%	0.4%	0.7%			15.6%	0.1%	2.8%	0.0%	0.3%	0.0%	0.0%	0.0%	wt%
Bulk Density	100%	100%	100%	100%	100%	98%	98%	95%	95%	95%	92%	92%	92%	92%	92%	
Liquid Density	100%	100%	100%	100%	100%	100%	100%	100%	100%	100%	100%	100%	100%	100%	100%	
Na+ Molar Concentration	68%	63%	100%	100%	78%	95%	68%	103%	105%	95%	95%	103%	105%	108%	108%	
NO3- Molar Concentration	37%	40%	60%	57%	55%	59%	54%	68%	59%	56%	67%	69%	63%	67%	69%	
NO2- + NO3- Molar Concentration	58%	64%	93%	92%	89%	93%	77%	105%	92%	91%	100%	105%	100%	105%	108%	
NH3/NH4+ Molar Concentration	0%	0%	0%	0%	0%	0%	0%	0%	0%	0%	0%	0%	0%	0%	0%	
Cl-/OH- Molar Ratio	1%	1%	3%	3%	2%	3%	1%	4%	4%	3%	3%	3%	3%	4%	4%	
Cl-/Na+ Molar Ratio	32%	32%	35%	33%	38%	39%	26%	39%	32%	36%	36%	38%	36%	39%	37%	
F-/Na+ Molar Ratio	26%	33%	50%	50%	16%	14%	17%	41%	47%	25%	9%	12%	8%	12%	37%	
SO4-2/Na+ Molar Ratio	10%	19%	11%	45%	14%	13%	32%	11%	42%	11%	16%	14%	11%	17%	34%	
Hg+2/Na+ Molar Ratio	100%	93%	100%	0%	0%	20%	5%	7%	7%	2%	1%	22%	100%	2%	0%	
TOC Mass Fraction	1%	0%	1%	5%	5%	4%	3%	0%	3%	2%	0%	1%	1%	2%	2%	
PCB Mass Fraction	8%	6%	7%	1%	12%	11%	55%	7%	0%	3%	7%	84%	6%	4%	1%	
pH	119%	119%	117%	117%	118%	118%	118%	117%	116%	118%	117%	117%	117%	117%	116%	
Equivalent Cs-137 Concentration	1%	0%	1%	2%	2%	2%	2%	0%	1%	0%	0%	0%	1%	1%	0%	
Am-241 Concentration	1%	2%	2%	5%	7%	1%	0%	1%	2%	0%	0%	0%	1%	0%	0%	
Pu-238 Concentration	4%	4%	5%	4%	7%	3%	1%	3%	4%	4%	0%	0%	1%	1%	0%	
Pu-239 Concentration	20%	24%	10%	5%	8%	11%	6%	9%	3%	5%	2%	2%	5%	1%	0%	
Pu-240 Concentration	17%	20%	10%	6%	8%	9%	4%	9%	3%	5%	1%	2%	4%	1%	0%	

	3	4	16	17	18	2	12	4	18	21	25	56	58	76	77	Units
	Batch 3	Batch 4	Batch 16	Batch 17	Batch 18	Batch 20	Batch 30	Batch 45	Batch 59	Batch 62	Batch 101	Batch 132	Batch 134	Batch 152	Batch 153	
	SOL20	SOL20	SOL20	SOL20	SOL20	SOL15	SOL15	SOL10	SOL10	SOL10	SOL5	SOL5	SOL5	SOL5	SOL5	
Sr-90 Concentration	55%	70%	57%	70%	70%	70%	19%	70%	27%	3%	4%	10%	42%	7%	1%	
Pu to Metals Loading Ratio	12%	10%	6%	17%	6%	10%	6%	7%	4%	13%	7%	5%	3%	3%	2%	
U-Fissile to U-Total Ratio	87%	78%	92%	88%	84%	72%	73%	86%	86%	94%	71%	69%	76%	83%	80%	
Public ULD	8%	12%	10%	17%	26%	6%	3%	7%	6%	3%	1%	1%	4%	2%	0%	
CLW ULD	24%	33%	27%	48%	71%	17%	7%	20%	17%	7%	2%	4%	12%	4%	0%	
UHGRtotal	11%	13%	11%	10%	12%	11%	6%	10%	5%	2%	2%	2%	7%	2%	0%	
F in Waste Oxide	27%	54%	823%	757%	32%	22%	29%	518%	560%	107%	29%	46%	23%	44%	288%	
Na2O in Waste Oxide	88%	93%	159%	200%	123%	145%	112%	185%	220%	178%	200%	214%	210%	229%	233%	
SO3 in Waste Oxide	31%	54%	38%	616%	47%	60%	107%	60%	471%	59%	112%	98%	79%	127%	277%	
ThO2 in Waste Oxide	24%	23%	1%	0%	1%	0%	2%	0%	2%	39%	0%	0%	1%	0%	0%	
ZrO2 in Waste Oxide	3%	2%	152%	3%	4%	0%	0%	93%	1%	17%	0%	2%	0%	0%	0%	
Tank Layers Passing All WAC																
Tank Layers Failing 1 or more WAC	1	1	1	1	1	1	1	1	1	1	1	1	1	1	1	
																80%
Tank Layers Passing by Margin																
Tank Layers Failing by Margin 1 or More	1	1	1	1	1	1	1	1	1	1	1	1	1	1	1	
Tank Layers Passing All Preferences	1	1														
Tank Layers Failing 1 or More Preferences			1	1	1	1	1	1	1	1	1	1	1	1	1	
	2.696	2.011	0.421	0.725	1.618	1.627	1.480	0.347	0.383	0.875	0.634	0.470	0.457	0.497	0.379	mol/L
	2.696	2.011	0.421	0.725	1.618	0.051	0.024	0.058	0.047	0.048	0.050	0.056	0.055	0.060	0.058	mol/L
	2.696	2.011	0.421	0.725	1.618	0.380	0.194	0.348	0.436	0.315	0.296	0.347	0.434	0.388	0.299	mol/L
	2.696	2.011	0.421	0.725	1.618	0.066	0.006	0.003	0.005	0.017	0.001	0.002	0.008	0.016	0.038	mol/L
	2.696	2.011	0.421	0.725	1.618	0.045	0.057	1.000	1.047	0.185	0.041	0.066	0.033	0.063	0.436	mol/L
	2.696	2.011	0.421	0.725	1.618	0.168	0.179	0.199	0.101	0.037	0.049	0.062	0.193	0.026	0.002	mol/L
	2.696	2.011	0.421	0.725	1.618	0.783	0.551	0.872	0.789	0.799	0.816	0.876	0.873	0.911	0.930	mol/L
	2.696	2.011	0.421	0.725	1.618	1.089	0.995	1.241	1.071	1.026	1.248	1.276	1.186	1.271	1.297	mol/L
	2.696	2.011	0.421	0.725	1.618	1.098	1.123	0.978	0.842	1.180	1.093	1.020	1.030	1.036	0.826	mol/L
	2.696	2.011	0.421	0.725	1.618	0.053	0.264	0.020	0.055	0.168	0.103	0.098	0.024	0.050	0.043	mol/L
	2.696	2.011	0.421	0.725	1.618	0.034	0.056	0.031	0.237	0.027	0.042	0.038	0.031	0.049	0.113	mol/L
	2.696	2.011	0.421	0.725	1.618	0.000	0.001	0.000	0.000	0.011	0.000	0.000	0.000	0.000	0.000	mol/L
	2.696	2.011	0.421	0.725	1.618	0.011	0.061	0.012	0.002	0.009	0.015	0.004	0.001	0.001	0.004	mol/L
	2.696	2.011	0.421	0.725	1.618	0.002	0.003	0.304	0.003	0.048	0.000	0.004	0.000	0.001	0.001	mol/L

Pacific Northwest National Laboratory

902 Battelle Boulevard
P.O. Box 999
Richland, WA 99354
1-888-375-PNNL (7665)

www.pnnl.gov